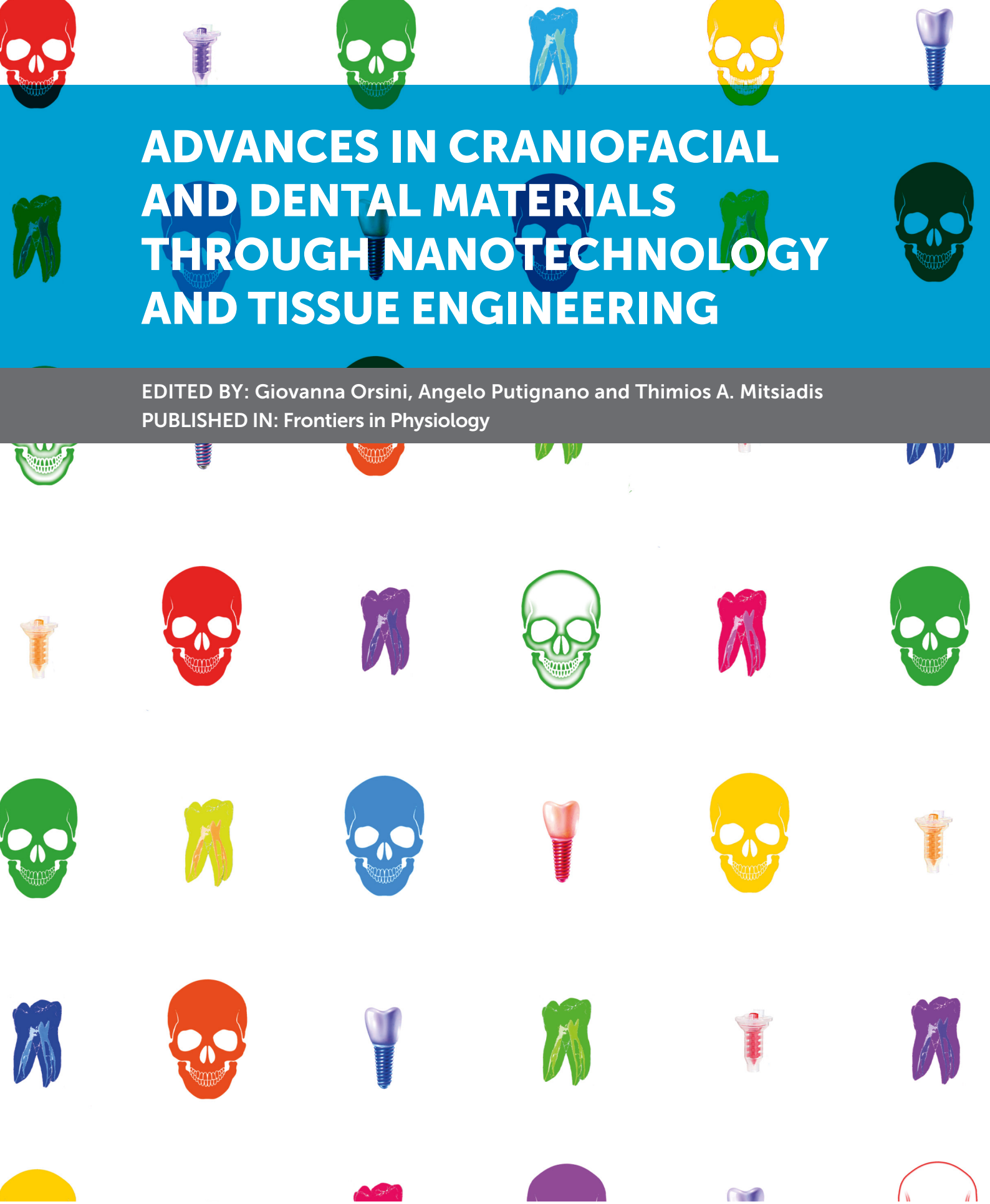

ADVANCES IN CRANIOFACIAL AND DENTAL MATERIALS THROUGH NANOTECHNOLOGY AND TISSUE ENGINEERING

EDITED BY: Giovanna Orsini, Angelo Putignano and Thimios A. Mitsiadis

PUBLISHED IN: Frontiers in Physiology

frontiers Research Topics

ISSN 1664-8714
ISBN 978-2-88945-858-5
DOI 10.3389/978-2-88945-858-5

About Frontiers

Frontiers is more than just an open-access publisher of scholarly articles: it is a pioneering approach to the world of academia, radically improving the way scholarly research is managed. The grand vision of Frontiers is a world where all people have an equal opportunity to seek, share and generate knowledge. Frontiers provides immediate and permanent online open access to all its publications, but this alone is not enough to realize our grand goals.

Frontiers Journal Series

The Frontiers Journal Series is a multi-tier and interdisciplinary set of open-access, online journals, promising a paradigm shift from the current review, selection and dissemination processes in academic publishing. All Frontiers journals are driven by researchers for researchers; therefore, they constitute a service to the scholarly community. At the same time, the Frontiers Journal Series operates on a revolutionary invention, the tiered publishing system, initially addressing specific communities of scholars, and gradually climbing up to broader public understanding, thus serving the interests of the lay society, too.

Dedication to Quality

Each Frontiers article is a landmark of the highest quality, thanks to genuinely collaborative interactions between authors and review editors, who include some of the world's best academicians. Research must be certified by peers before entering a stream of knowledge that may eventually reach the public - and shape society; therefore, Frontiers only applies the most rigorous and unbiased reviews.
Frontiers revolutionizes research publishing by freely delivering the most outstanding research, evaluated with no bias from both the academic and social point of view. By applying the most advanced information technologies, Frontiers is catapulting scholarly publishing into a new generation.

What are Frontiers Research Topics?

Frontiers Research Topics are very popular trademarks of the Frontiers Journals Series: they are collections of at least ten articles, all centered on a particular subject. With their unique mix of varied contributions from Original Research to Review Articles, Frontiers Research Topics unify the most influential researchers, the latest key findings and historical advances in a hot research area! Find out more on how to host your own Frontiers Research Topic or contribute to one as an author by contacting the Frontiers Editorial Office: researchtopics@frontiersin.org

ADVANCES IN CRANIOFACIAL AND DENTAL MATERIALS THROUGH NANOTECHNOLOGY AND TISSUE ENGINEERING

Topic Editors:
Giovanna Orsini, Polytechnic University of Marche, Italy
Angelo Putignano, Polytechnic University of Marche, Italy
Thimios A. Mitsiadis, University of Zurich, Switzerland

Cover by Thimios Mitsiadis, 2019.

Dental and craniofacial treatments are actually based on advances in biomaterials, tissue engineering and nanotechnology sciences. These developments brought considerable improvements on biomaterials commonly used in dental clinics. However, there is still a medical need for innovative techniques and materials for a controllable and efficient regeneration/repair of damaged craniofacial tissues and teeth. The novel biomaterials, imaging techniques, diagnostic and technological tools may offer thrilling perspectives for alternative treatments in dentistry.

Citation: Orsini, G., Putignano, A., Mitsiadis, T. A., eds. (2019). Advances in Craniofacial and Dental Materials Through Nanotechnology and Tissue Engineering. Lausanne: Frontiers Media. doi: 10.3389/978-2-88945-858-5

Table of Contents

frontiers in Physiology

EDITORIAL
published: 27 March 2019
doi: 10.3389/fphys.2019.00303

Editorial: Advances in Craniofacial and Dental Materials Through Nanotechnology and Tissue Engineering

Giovanna Orsini[1,2]*, *Angelo Putignano*[2] *and Thimios A. Mitsiadis*[1]*

[1] Orofacial Development and Regeneration, Centre for Dental Medicine, Institute of Oral Biology, University of Zurich, Zurich, Switzerland, [2] Department of Clinical Sciences and Stomatology, Polytechnic University of Marche, Ancona, Italy

Keywords: tooth, craniofacial, regeneration, stem cells, tissue engineering, nanotechnology, bone, dental

Edited by:
Gianpaolo Papaccio, Second University of Naples, Italy

Reviewed by:
Jean-Christophe Farges, Université Claude Bernard Lyon 1, France
Francesco De Francesco, Azienda Ospedaliero Universitaria Ospedali Riuniti, Italy

***Correspondence:**
Giovanna Orsini
Giovanna.Orsini@zzm.uzh.ch; g.orsini@univpm.it
Thimios A. Mitsiadis
thimios.mitsiadis@zzm.uzh.ch

Specialty section:
This article was submitted to Craniofacial Biology and Dental Research, a section of the journal Frontiers in Physiology

Received: *28 January 2019*
Accepted: *07 March 2019*
Published: *27 March 2019*

Citation:
Orsini G, Putignano A and Mitsiadis TA (2019) Editorial: Advances in Craniofacial and Dental Materials Through Nanotechnology and Tissue Engineering. Front. Physiol. 10:303. doi: 10.3389/fphys.2019.00303

Editorial on the ResearchTopic

Advances in Craniofacial and Dental Materials Through Nanotechnology and Tissue Engineering

The extraordinary recent advances in biomaterials, tissue engineering, and nanotechnology sciences opened new horizons and now offer innovative options to the clinical practitioners for the restoration and/or regeneration of missing and damaged dental and bone tissues (Mitsiadis et al., 2015; Orsini et al., 2018). Dental and craniofacial treatments are commonly based on specific biomaterials. Substantial improvements of such biomaterials have been partly achieved via incorporation of filler elements possessing at least one dimension in the nanometer range for the enhancement of the healing capability of the tissues (Yi et al., 2016). Nanometric surface modifications of biomaterials are constantly applied in order to ameliorate their physical and biological properties, thereby improving the quality and the duration of tissue repair (Variola et al., 2011). The structure and functionality of dental and periodontal tissues are compromised upon traumatic and carious lesions, periodontal diseases and genetic disorders. Therefore, there is a high medical need for the regeneration and/or repair of damaged teeth and the surrounding alveolar bone. Although bone and several of the dental-specific mineralized tissues such as dentin and cementum exhibit a natural regenerative potential, tooth enamel cannot be regenerated in humans (Mitsiadis et al., 2015). In fact, the enamel-producing ameloblastic cells are eliminated soon after the eruption of teeth in the oral cavity and therefore the regeneration of enamel is impossible upon its damage by the various tooth insults. However, in several teeth of other species, such as in incisors of rodents, enamel is continuously regenerated. Studies in rodent incisors allow the collection of precious information fundamental to elucidate the molecular and cellular mechanisms that are involved in the regeneration of enamel. This information might be useful for tooth enamel repair in humans, when combined with the recent technological advances in nanosciences, tissue engineering, and stem cell biology, and it will undoubtedly bring in the near future extremely innovative dental treatments in the clinics.

The present research topic focuses on the use of different modern materials coupled with nanotechnology to improve the clinical performances in all fields of dentistry as well as in bone regeneration procedures. Prominent researchers within the craniofacial and dental fields have contributed with important discoveries and generated exciting results concerning the repair or regeneration of the mineralized tissues using biomaterials.

Tooth specific proteins such as Amelogenin and Enamelin are involved in the initial steps of enamel formation (amelogenesis) that is followed by enamel mineralization, which is a very complex process. The role of Leucine Rich Amelogenin Peptide (LRAP), a product of the amelogenin gene, in enamel mineralization is examined (Le Norcy et al.) As full-length amelogenin, LRAP has been shown to regulate hydroxyapatite (HAP) crystal formation depending on its phosphorylation status. Micro-computed tomography, field emission scanning electron microscopy, transmission electron microscopy, diffraction imaging, and qPCR analysis have been used to elucidate the impact of its phosphorylation status on enamel mineralization. The results showed that LRAP, independently of its phosphorylation status, is able to induce an up-regulation of *Amelogenin* transcription and promote mineral formation in both cells and mouse molar germ cultures. Therefore, LRAP isoforms can be envisioned as potential candidates for the treatment of enamel lesions or defects.

The functions and roles of the extracellular matrix (ECM) molecules in the mineralization process of the various craniofacial tissues are also under intensive investigation. The ECM protein TRIP-1 may play a pivotal role in the organization of the mineralized matrices of bone and dentin (Chen and George). TRIP-1 regulates both osteogenesis and angiogenesis, which are essential biological processes for the elaboration of novel therapeutic approaches focusing on mineralization-related disorders.

Although bone has an amazing ability to heal spontaneously, in several specific cases it fails to heal. Hence, it is important to consider the mechanical conditions affecting its regeneration and the influence of the environment. Since craniofacial morphology is regulated genetically and epigenetically by microenvironmental factors, the effects of food consistency in the mandibular morphology of mice have been assessed (Kono et al.) Micro-3D CT data has been used to detect the 3D quantitative changes occurring in the mandibular skeletal structures and the site-specific bone response to different masticatory activities.

The application of mechano-biological principles such as the significance of fixation and controlled motion (dynamization) for enhancing bone healing is of prime importance (Glatt et al.) The selection of appropriate fixation devices, scaffolds, signaling molecules is mandatory for achieving consistent and predictable bone healing that guarantees the clinical outcome. For instance, the tension that is created by gradual mechanical distraction stimulates the formation of new bone, vessels, nerves, and muscles, thus leading to bone lengthening and regeneration. Although recent research has unraveled the interplay between mechanics and biology, the realization of *in vivo* studies is compromised due to the lack of important tools. Deficiencies in controlling the chemical, physical, and biological environment within the healing defects are still of actuality.

Scaffolds are key elements for the success of tissue regeneration. Dental implantology has benefited from recent advances in bone regeneration, due to the use of many osseous substitutes that can be clinically applied in regenerative approaches, such as sinus augmenting procedures. A biomimetic porous three-dimensional MgHA/collagen-based scaffold could be used for enhancing the poor quantity and/or quality of bone in delicate maxillary areas (e.g., nearby the sinus) where the placement of dental implants is envisaged (Scarano et al.) Tomographic, radiological, histological and histomorphometric analyses have demonstrated the enhancement of bone formation and the complete resorbing of the scaffold after 6 months of treatment.

Various diseases affecting teeth or their supporting tissues lead to their infection and progressive destruction and loss. Guided tissue regeneration is a procedure widely used for the treatment of severe periodontal diseases. This technique involves the placement of an occlusive barrier to facilitate the regeneration of damaged areas by periodontal ligament stem cells (PDLSCs). An ECM-based scaffold has been compared to a Collagen I (COLI) membrane for its ability in providing a suitable microenvironment that will support proliferation and proper differentiation of PDLSCs (Wang et al.) The cementoblastic/osteogenic activity of PDLSCs was characterized by evaluating periodontal tissue differentiation biomarkers, including TNAP enzyme activity, Alizarin red stain, and differential mRNA expression. The ECM membrane exhibited superior biological properties when compared to COLI membrane, and significantly promoted PDLSCs cell proliferation, differentiation and mineral formation. *In vivo* studies are still required to confirm these findings and finally offer new alternatives for the treatment of periodontal diseases using ECM membranes.

A new biomaterial for regenerative purposes has been proposed for endodontic treatment purposes (Hertig et al.) Scanning electron microscopy and spectrophotometry has been used to assess a fibrin hydrogel, a common scaffold employed for filling the pulp chamber, via an iodine-based radiopaque agent. The study has been performed in chick chorioallantoic membranes (CAM) of fertilized eggs and showed that the tested biomaterial is not toxic and allows monitoring of its degradation-related modifications.

The multidisciplinary strategies based on the association of stem cells with advanced tissue engineering products try to tackle a good number of challenges related to regenerative dentistry (Orsini et al.) Novel platforms for tooth modeling and inspired discoveries for diagnostic and therapeutic purposes have been advancing. The employment of nanostructured biomaterials is also decisive in the fine modulation of stem cell behavior in order to drive proper dental and bone tissue regeneration by providing proper tissue innervation and vascularization (Abdal Dayem et al., 2018). Similarly, nanotechnology-related achievements had a tremendous impact on the evolution of biomaterials, thus widening the possibilities for novel and more accurate treatments for the repair or replacement of damaged or lost enamel and dentin. The precise and efficient repair of these tissues has been greatly improved thanks to the introduction of novel and sophisticated composite and ceramic materials, as well as modern adhesive systems that may durably bond these materials to the dental tissues, thus increasing the longevity of tooth crown restorations (Monterubbianesi et al.) Nano-based synthetic resin composite materials, characterized by the employment

of nanocluster fillers that enhance their physical properties, have been introduced over the last decade. This allowed the elaboration of simplified procedures for filling dental cavities in molars. The "bulk -fill composites" have been demonstrated to maintain a high degree of conversion and exhibited an incredible hardness both at the surface and base of any restoration, which is advantageous for numerous clinical cases.

Advanced imaging techniques can verify and quantify the degree of mineralization and vascularization of the implanted scaffolds at the earliest stages of bone regeneration (Giuliani et al.) Synchrotron produces brilliant X-ray photon beams, thus achieving a higher image quality with sub-micrometer spatial resolution. X-ray imaging and holotomography are suitable for detecting both *in vitro* and *ex vivo* the newly formed extracellular matrices, the early phases of hard tissue mineralization and the vascular network in regenerating bones.

Nanotechnological advances have also been largely implemented in diagnostic research, and these innovations could be also used in the field of oral oncology (Mascitti et al.) Non-invasive diagnostic devices constitute great promises for this field and the early treatment of oral cancers. Light-based detection systems have been introduced for earlier detection of oral squamous cell carcinomas and other potentially malignant disorders. Implementing light-based detection systems based on tissue-marking dyes and nanoparticle properties could be exploited for diagnosis and possible cure of several cancers.

The recent progresses in the fields of nanotechnology, tissue engineering, and stem cell biology allowed the generation of novel sophisticated biomaterials that could be successfully used for medical purposes. However, several concerns still exist concerning their applicability in the dental clinics. Therefore, there is an urgent need for clinical trials that will demonstrate the reliability and accuracy of these alternative strategies for tissue regeneration. Nevertheless, all these novel biomaterials and technological tools, combined with the constantly increasing scientific knowledge, offer exciting perspectives for modern alternative therapies in the dental and craniofacial fields.

AUTHOR CONTRIBUTIONS

All authors listed have made a substantial, direct and intellectual contribution to the work, and approved it for publication.

FUNDING

This work was supported by grants of the University of Zurich (UZH) and Polytechnic University of Marche.

REFERENCES

Abdal Dayem, A., Lee, S. B., and Cho, S. G. (2018). The impact of metallic nanoparticles on stem cell proliferation and differentiation. *Nanomaterials* 8:E761. doi: 10.3390/nano8100761

Mitsiadis, T. A., Orsini, G., and Jimenez-Rojo, L. (2015). Stem cell-based approaches in dentistry. *Eur. Cell Mater.* 30, 248–257. doi: 10.22203/eCM.v030a17

Orsini, G., Pagella, P., and Mitsiadis, T. A. (2018). Modern trends in dental medicine: an update for internists. *Am. J. Med.* 131, 1425–1430. doi: 10.1016/j.amjmed.2018.05.042

Variola, F., Brunski, J. B., Orsini, G., Tambasco De Oliveira, P., Wazen, R., and Nanci, A. (2011). Nanoscale surface modifications of medically relevant metals: state-of-the art and perspectives. *Nanoscale* 3, 335–353. doi: 10.1039/c0nr00485e

Yi, H., Ur Rehman, F., Zhao, C., Liu, B., and He, N. (2016). Recent advances in nano scaffolds for bone repair. *Bone Res.* 4:16050. doi: 10.1038/boneres.2016.50

Conflict of Interest Statement: The authors declare that the research was conducted in the absence of any commercial or financial relationships that could be construed as a potential conflict of interest.

frontiers in Physiology

ORIGINAL RESEARCH
published: 08 February 2018
doi: 10.3389/fphys.2018.00055

Phosphorylated and Non-phosphorylated Leucine Rich Amelogenin Peptide Differentially Affect Ameloblast Mineralization

Elvire Le Norcy[1,2], *Julie Lesieur*[1], *Jeremy Sadoine*[1], *Gaël Y. Rochefort*[1], *Catherine Chaussain*[1,2] *and Anne Poliard*[1]*

[1] EA2496 Faculté de Chirurgie Dentaire, Université Paris Descartes USPC, Paris, France, [2] APHP, Hôpital Bretonneau, Service d'Odontologie, Paris, France

The Leucine Rich Amelogenin Peptide (LRAP) is a product of alternative splicing of the *amelogenin* gene. As full length amelogenin, LRAP has been shown, in precipitation experiments, to regulate hydroxyapatite (HAP) crystal formation depending on its phosphorylation status. However, very few studies have questioned the impact of its phosphorylation status on enamel mineralization in biological models. Therefore, we have analyzed the effect of phosphorylated (+P) or non-phosphorylated (−P) LRAP on enamel formation in ameloblast-like cell lines and *ex vivo* cultures of murine postnatal day 1 molar germs. To this end, the mineral formed was analyzed by micro-computed tomography, Field Emission Scanning Electron Microscopy, Transmission Electron Microscopy, Selected Area Electon Diffraction imaging. *Amelogenin* gene transcription was evaluated by qPCR analysis. Our data show that, in both cells and germ cultures, LRAP is able to induce an up-regulation of *amelogenin* transcription independently of its phosphorylation status. Mineral formation is promoted by LRAP(+P) in all models, while LRAP(–P) essentially affects HAP crystal formation through an increase in crystal length and organization in ameloblast-like cells. Altogether, these data suggest a differential effect of LRAP depending on its phosphorylation status and on the ameloblast stage at the time of treatment. Therefore, LRAP isoforms can be envisioned as potential candidates for treatment of enamel lesions or defects and their action should be further evaluated in pathological models.

Keywords: amelogenin, leucine-rich amelogenin peptide, LRAP, phosphorylation, hydroxyapatite, ameloblasts, ameloblastic cell line, tooth germ

OPEN ACCESS

Edited by:
Thimios Mitsiadis, University of Zurich, Switzerland

Reviewed by:
Thomas G. H. Diekwisch, Texas A&M University College of Dentistry, United States
Javier Catón, CEU San Pablo University, Spain
Claudio Cantù, University of Zurich, Switzerland

***Correspondence:**
Anne Poliard
anne.poliard@parisdescartes.fr

Specialty section:
This article was submitted to Craniofacial Biology and Dental Research, a section of the journal Frontiers in Physiology

Received: *12 October 2017*
Accepted: *17 January 2018*
Published: *08 February 2018*

Citation:
Le Norcy E, Lesieur J, Sadoine J, Rochefort GY, Chaussain C and Poliard A (2018) Phosphorylated and Non-phosphorylated Leucine Rich Amelogenin Peptide Differentially Affect Ameloblast Mineralization. Front. Physiol. 9:55. doi: 10.3389/fphys.2018.00055

INTRODUCTION

Dental Enamel is the outermost layer of the teeth and the most mineralized structure in the vertebrates, since it is constituted of at least 95% minerals. Its microstructure is composed of nanorod-like hydroxyapatite (HA) crystals arranged in a highly organized unit called the enamel prism or rod. Prism high organization leads to enamel robust mechanical properties for tissue protection against cariogenic bacteria and mechanical force upon tooth function. Enamel is formed through synthesis, growth, and organization of these rods by specialized cells, the ameloblasts, throughout the process of amelogenesis. In contrast to bone or dentin, it is acellular in its mature

form. Indeed, ameloblasts are once and for all, degraded during the process of tooth eruption and consequently, they cannot regenerate and actively repair by themselves. In view of the high prevalence of dental caries and enamel defects, enamel regeneration, and repair has become a target for developing biomimetic therapeutic approaches (Cao et al., 2014; Ruan and Moradian-Oldak, 2015; Snead, 2015).

The biological processes involved in enamel formation are well characterized (Li et al., 2006). During amelogenesis, ameloblasts undergo a maturation process with a change in appearance from early, elongated secretory cells actively involved in organic extracellular matrix synthesis, to more round, mature cells involved in the degradation of this matrix and deposition of the mineral. Ameloblast extracellular matrix is known to be key for controlling growth and organization of enamel crystals during mineralization (Robinson et al., 1989; Iijima and Moradian-Oldak, 2004). It is essentially synthesized by the secretory stage ameloblasts and is composed of various structural proteins such as amelogenin, ameloblastin, enamelin, and MMP20. Among these proteins, amelogenins are the most abundant (Fincham et al., 1999; Moradian-Oldak, 2012). Native amelogenin, has been shown, in porcine teeth, to be synthesized mostly under a form phosphorylated on the single Serine-16 site. Phosphorylation affects amelogenin function since phosphorylated native porcine amelogenin (P173) inhibits calcium phosphate crystallization and stabilizes amorphous calcium phosphate while its recombinant un-phosphorylated counterpart guides the formation and organization of aligned enamel crystals (Beniash et al., 2005; Wang et al., 2007; Kwak et al., 2009; Wiedemann-Bidlack et al., 2011; Margolis et al., 2014). Different isoforms of amelogenin, mostly resulting from alternative splicing, have been evidenced in bovine and rodent enamel (Shimokawa et al., 1989; Lau et al., 1992). They are translated into amelogenin proteins that vary in length and relative abundance (Bartlett et al., 2006; Yamakoshi, 2011). Among these alternative isoforms, the Leucine Rich Amelogenin Peptide (LRAP) is the second most abundant amelogenin protein (Shimokawa et al., 1989). LRAP was observed in secretory stage ameloblasts (Iacob and Veis, 2008) and shown to be produced throughout amelogenesis (Yuan et al., 1996; Veis et al., 2000). It is a short peptide (56–59 amino acids, depending on the species) identical to the full-length amelogenin except for the majority of the exon-6 coded region that is lacking (Bonass et al., 1994). It contains the two self-assembly domains of the full-length amelogenin form (Paine and Snead, 1997; Pugach et al., 2010) and has been evidenced in mouse, porcine, bovine, and human (Goldberg, 2010). LRAP has been demonstrated to display both signaling and structural properties on dental cells. It is able to promote ameloblast or odontoblast *in vitro* differentiation (Tompkins and Veis, 2002; Sarkar et al., 2014) and can affect *in vitro* calcium phosphate formation in a very similar fashion to the full-length amelogenin (Beniash et al., 2005; Kwak et al., 2009, 2014; Wiedemann-Bidlack et al., 2011). Remarkably, the phosphorylated form of the peptide on serine 16 [LRAP(+P)] stabilized amorphous calcium phosphate (ACP) whereas the non-phosphorylated form [LRAP(–P)] was shown to guide the formation of bundles of well-aligned needle-like apatitic crystals (Le Norcy et al., 2011b). LRAP(–P) has also been recently shown to act as a surface treatment agent to enhance remineralization of altered enamel (Shafiei et al., 2015) and guide the regeneration of acid-etched enamel structure (Kwak et al., 2017).

Despite these recent observations, few studies have addressed the direct role of LRAP, on enamel mineralization in biological models, in relation to its phosphorylation status. Namely, nothing is still known on the ratio of un-phosphorylated to phosphorylated LRAP forms and whether this ratio changes during tooth development and maturation. Indeed, up to now, most researches have been performed with a recombinant non-phosphorylated LRAP peptide although amelogenins are detected *in vivo* under their phosphorylated form (Fincham and Moradian-Oldak, 1993). In a context of future therapeutic applications, the aim of this work was therefore to determine whether the phosphorylation status of LRAP impacts the nature of the mineral formed in biological systems as it does *in vitro*. To this end, the effect of the LRAP (+P) or (–P) on mineral formation was analyzed in two ameloblast-like cellular models mimicking secretory (LS8) and maturation (ALC) stage ameloblasts and in a model of *ex vivo* tooth germ culture (Chen et al., 1992; Nakata et al., 2003; Sarkar et al., 2014).

MATERIALS AND METHODS

Preparation of LRAP

Variations of the porcine LRAP (MPLPPHPGHPGYINFS^{P}YEV LTPLKWYQNMIR HPSLLDLPLEAWPATDKTKREEVD) with and without the phosphate group on Serine-16, were synthesized commercially (NEO Peptide, Cambridge, MA, USA) and re-purified, as previously described (Nagano et al., 2009). Lyophilized peptides were weighed and dissolved in distilled de-ionized water at room temperature to yield a stock solution of 2 mg/mL. Complete solubilization of both peptides in water was verified by dynamic light scattering analyses. LRAP concentrations were confirmed by nanodrop analyses at 280 nm.

Cell Culture

The mouse ameloblastic cell lines LS8 (Chen et al., 1992) and ALC (Nakata et al., 2003) were routinely cultured in Dulbecco's Modified Eagle Medium (DMEM) supplemented with 10% Fetal Bovine Serum (FBS) and 1% Penicillin-Streptomycin (PS). ALC cultures also contained 10 ng/mL mouse Epidermal Growth Factor (mEGF) (Nakata et al., 2003). Control mouse embryonic fibroblast cells (NIH3T3) were cultured in DMEM High Glucose (DMEM HG) supplemented with 10% FBS and 1% PS. For mineralization studies, the cells were then cultured in DMEM (or DMEM HG for NIH3T3 cells) supplemented with 1% FBS, 1% PS, 50 μg/mL ascorbic acid, 5 mM β-glycerophosphate referred as the mineralizing medium. ALC cells were also supplemented with 10 ng/mL mEGF and 10^{-8}M Dexamethasone. One μg/mL LRAP(+P) or LRAP(–P) were added to the mineralization medium. Controls were cultured in the same medium without LRAP peptides. Mineralization was evaluated by alizarin red staining. Cells were rinsed with Phosphate-Buffered Saline (PBS), stained with Alizarin Red Stain (2%) for 2 min then rinsed two times with PBS.

Molar Germ Culture

First mandibular and maxillary molar germs ($n = 125$) were extracted from post-natal day 1 Swiss Webster mice (PND1) after euthanasia. This procedure was carried out in accordance with the French regulations on animal testing (Decree n^r 2013-118 of February 1st 2013 on animal protection used for scientific purposes NOR: AGRG1231951D). Germs were cultured in a mineralizing medium composed of Minimum Essential Medium α (MEM α) supplemented with 10% FBS, 0.18 mg/mL ascorbic acid, 1x Glutamine, 1% Penicillin/streptomycin, and 5 mM β-glycerophosphate. A quantity equivalent to one third of the medium volume of agar was added to each well. Thirty three ng/mL LRAP(+P) or of LRAP(–P) were added to the medium before agar addition (Tompkins et al., 2005). Five mandibular and five maxillary molar germs were separately cultured for 9 days (D9) under each condition and time point and experiments were repeated 4 times ($n = 4$). Germs were fixed on the day of extraction (D0) or after 9 days of culture, by immersion in 4% paraformaldehyde (PFA) for 30 min then rinsed with PBS and stored in 70% ethanol.

RNA Extraction and Quantitative PCR

Total RNAs were extracted from cells at D0, D2, and D7, and also at D14 for ALC cells and from tooth germs at D0 and D9 using respectively RNeasy Mini Kits for the cells and RNeasy Micro Kits (Qiagen) for the molars. Five hundred and fifty nanograms of total RNA were respectively reverse transcribed to first strand cDNA using a Verso cDNA Synthesis Kit (Thermo Fisher Scientific). For quantitative PCR, mouse specific primers for *Amelx* (F: GATGGCTGCACCACCAAATC, R: CTGAAG GGTGTGACTCGGG), Actin (F: GTGGCATCCATGAAACTA CAT, R: GGCATAGAGGTCTTTACGG), GAPDH (F: TGTGTC CGTCGTGGATCTGA, R: TTGCTGTTGAAGTCGCAGGAG) were used. PCR was accomplished in a Lightcycler thermocycler 480R with SYBR® Green Supermix (Bio-Rad) according to the manufacturer's instructions. Values were calculated with the LightCycler® 480 software 1.5.0 (Roche, Applied Science). Results were analyzed by the method of ΔΔCt. All data points were normalized to Actin and/or GAPDH and all samples were run in triplicate. Statistical analyses were conducted with Microsoft Excel 2011 software (Microsoft, Redmond WA, USA). A two-tailed unpaired Student T comparison test was performed ($\alpha = 0.05$, $^*p < 0.05$; $^{***}p < 10^{-4}$). LRAP(–P) and LRAP(+P) treated samples were compared to the control.

Micro-Computed Tomography (Micro-CT) Imaging and Analyses

Germ mineralization was quantified by X-ray Micro Computed Tomography imaging (Micro-CT, Quantum FX Caliper, Life Sciences, Perkin Elmer, Waltham, MA, USA) at 90 kV and 160 μA. Tridimensional images were acquired with an isotropic voxel size of 20 μm and a rotation step of 0.1° (scan time = 3 min). Before each micro-CT acquisition, the lead citrate calibrator was scanned with an HAP phantom to assign an HAP value for each gray level of lead citrate solutions. Reconstructed files were converted into eight-bit images with fixed lower and upper brightness limits using the "CT analyzer" software (Skyscan, release 1.15.4.0, Kontich, Belgium). A binary segmentation process was applied uniformly on each data stack to separate the mineralized and non-mineralized material inside the whole germ volume. The threshold value used for binarization was manually set so that every voxel with an equal or higher value was represented as solid material, and lower values represented as space. Similar gray level values for global germ density and mineral density were set and used for analysis in all samples. In the quantifications, the mineral density corresponded to a mean of the total germ mineral content (addition of dentin and enamel) whereas the enamel volume is reflected by the ratio between the volume occupied by the enamel layer and the whole germ volume.

Transmission Electron Microscope (TEM) Analyses

Ten microliters of aliquots were taken from scraped regions of alizarin red stained cell cultures observed under the light microscope and placed on carbon-coated Cu grids (Electron Microscopy Sciences, Hatfield, PA, USA). Duplicate grids were prepared from a minimum of three different experiments. Images were obtained in bright field and Selected Area Electron Diffraction (SAED) modes with a Tecnai 12BT Transmission Electron Microscope (TEM) at 80 kV.

Field Emission—Scanning Electron Microscopy (FE-SEM) Analyses

PFA fixed germs were analyzed using a Field Emission—Scanning Electron Microscope (Zeiss SUPRA 40). They were air dried and placed on an SEM holder without any preparation. Lateral faces of molar cuspids were observed. Acquisitions were made using the Everhart-Thornley type Secondary Electron detector (SE2) for the first three magnifications (177–226x, 10 kx, 20 kx) and using the In-lens detector for the largest magnification (40 kx).

RESULTS

Effect of LRAP Phosphorylation Status on Ameloblast Cell Line Mineralization

To analyze the effect of LRAP and its phosphorylation status on ameloblast mineralization, we used two murine ameloblast-like cell lines (LS8 and ALC) mimicking different stages of enamel formation as well as control murine embryonic fibroblast NIH3T3 cells. LS8 cells appear to correspond to secretory stage ameloblasts characterized by high expression of *Amelx*, *Ambn*, *Enam*, and *Mmp20* transcripts while ALC cells behave as maturation stage ameloblasts with high expression of *Odam* and *Klk4* transcripts (Sarkar et al., 2014).

Culture in mineralizing medium promoted the formation of macroscopically visible mineralization nodules after alizarin red staining, at day 7 in the LS8 cells but only very scarce and light nodules in the ALC cell cultures. After 2 weeks, ALC cells exhibited small squared mineralization nodules while the LS8 cells started to degenerate (data not shown). In contrast, control culture of NIH3T3 cells in the same medium did

not lead to any mineralization even after 3 weeks of culture (data not shown). Therefore, both ameloblastic cell lines were able to mineralize but with a different kinetics (Supplementary material).

To characterize the structure of the mineral formed in the various conditions, SAED analyses were performed. They showed that the mineral formed under all conditions was HAP (**Figures 1**, **2**). Furthermore, TEM observations revealed that the mineral formed by untreated LS8 cells was composed of dispersed needle shaped HAP crystals (mean length of 43.9 ± 7.8 nm; $n = 24$) (**Figures 1A,B**). Upon LRAP(+P) addition, similarly dispersed but slightly longer needle shaped HAP crystals, (mean length of 56.7 ± 9.2 nm; $n = 35$) were observed (**Figures 1C,D**) while, bundles of fine elongated HAP crystals (mean length of 103 ± 17.8 nm; $n = 34$) were formed with LRAP(–P) (**Figures 1E,F**). Crystal length to width ratio (L/W) was similar in the control and LRAP(+P) treated cells (4.44 ± 0.89 and 4.4 ± 0.73, respectively) whereas it was increased in the presence of LRAP(–P) (7.38 ± 1.26; **Table 1**).

In untreated ALC cells (**Figures 2A,B** and **Table 1**), a mixture of large round mineral particles and few very large elongated HAP crystals (mean length of 342.7 ± 49.5 nm) were predominantly observed with TEM and characterized by SAED although a small quantity of shorter needle-shaped HAP crystals was also present (mean length of 74.9 ± 40.9 nm; $n = 16$). On the whole, mineral structures were much larger than those found in the LS8 control cells. Upon LRAP(+P) treatment, only needle shaped HAP crystals (mean length of 84 ± 33.1 nm; $n = 34$) were observed (**Figures 2C,D** and **Table 1**). LRAP(–P) treatment promoted the formation of bundles of elongated HAP crystals (mean length of 76.2 ± 57.1 nm; $n = 42$) similar to those formed by the LS8 cell (**Figures 2E,F** and **Table 1**). While length to width ratios were similar in untreated, and LRAP(+P) or LRAP(–P) treated cells (9.08 ± 3.46, 9.13 ± 2.97, and 9.15 ± 2.89, respectively; **Table 1**), the mineral organization was very different between LRAP-treated and untreated cultures: large crystals were predominant in controls but absent in the peptide-treated cultures. In addition, needle-shaped crystallites were organized in bundles whereas they were randomly dispersed in the untreated cultures. This organization was more particularly evident after LRAP(-P) treatment (**Figures 2E,F**).

Since the un-phosphorylated form of LRAP had been previously shown to impact *Amelx* gene transcription (Iacob and Veis, 2008), the relative effect of both peptides on *Amelx* expression by the cells was evaluated by qPCR. We observed that both forms of LRAP induced an early (D2) statistically significant up-regulation of *Amelx* transcription in the LS8 cells although more pronounced with LRAP(-P) (**Figure 3A**). In ALC, a similar up-regulation (D7) in *Amelx* transcription was observed with the two peptides, although only statistically significant with LRAP(–P) (**Figure 3B**). This up-regulation was however delayed as compared to LS8 cells in agreement with the mineralization kinetics (**Figures 3A,B**).

Therefore, both peptides affected amelogenin expression and presented an effect on crystal organization.

Effect of LRAP Peptides on Germ Mineralization

To determine the effect of LRAP phosphorylation on mineral formation, in a more integrated biological context, we tested the peptide effect on PND1 molar tooth germs cultured *ex vivo* over a 9 day period (Bègue-Kirn et al., 1992; Tompkins et al., 2005). Growth of the first molar germs was observed in all conditions upon 9 days of *ex vivo* culture on semi-solid medium (**Figure 4A**). Micro-CT imaging allowed quantifying germ mineralization in all samples, as well as determining the mineral density (enamel and dentin combined) and the enamel volume (**Figures 4B,C**). An increase in mineral density was detected in all cultured samples, i.e., treated and untreated, as compared to uncultured D0 germs confirming the germ growth in culture (**Figure 4B**). Peptide treatment did not appear to impact this value. In contrast, germ culture in the presence of LRAP(+P) led to an increase in enamel volume (>50%) as compared to untreated germs, in contrast to LRAP(–P) treatment which did not (**Figure 4C**).

The mineral formed in the PND1 molar tooth germs was further characterized by FE-SEM (**Figure 5**). Ameloblast pits typical of immature enamel were observed in all samples, confirming enamel formation in the culture process (**Figures 5A,D,G**). LRAP(+P) treated germs displayed smaller and more spaced pits (**Figures 5E,F**) than untreated controls (**Figures 5B,C**), while those of LRAP(–P) germs appeared slightly wider (**Figures 5H,I**) than the LRAP+P-treated or control germs. These observations suggested an increased mineralization process in the presence of LRAP(+P) confirming the micro-CT analysis.

The effect of the LRAP peptides on *Amelx* transcription was evaluated in the PND1 molar germs cultures. A statistically significant up-regulation of *Amelx* transcription was observed with both LRAP(+P) and LRAP(–P) treatment relative to untreated germs, with a stronger effect of LRAP(+P) than LRAP(–P) (respectively 3- vs. 1.5-fold relative to the control) (**Figure 3C**).

DISCUSSION

This study shows a differential effect of the LRAP peptide on enamel formation, depending on its phosphorylation status in *in vitro* and *ex vivo* culture models. Mature enamel, in contrast to other mineralized tissues like bone or dentin, cannot be repaired. When the tooth erupts in the oral cavity, ameloblasts are degraded and, consequently, the enamel cannot be re-grown or regenerated. The search for molecules able to restore enamel defects is therefore ongoing. In this context, the LRAP peptide has proven of interest thanks to its signaling properties as well as its apparent effect on crystal growth and structure (Shaw et al., 2004; Beniash et al., 2009; Le Norcy et al., 2011a,b; Wiedemann-Bidlack et al., 2011; Moradian-Oldak, 2012; Kwak et al., 2016, 2017).

In the present study, we first show that both forms of peptide have a differential effect on the mineral formed by ameloblast-like cells in culture. Untreated LS8 cells, a model for secretory stage

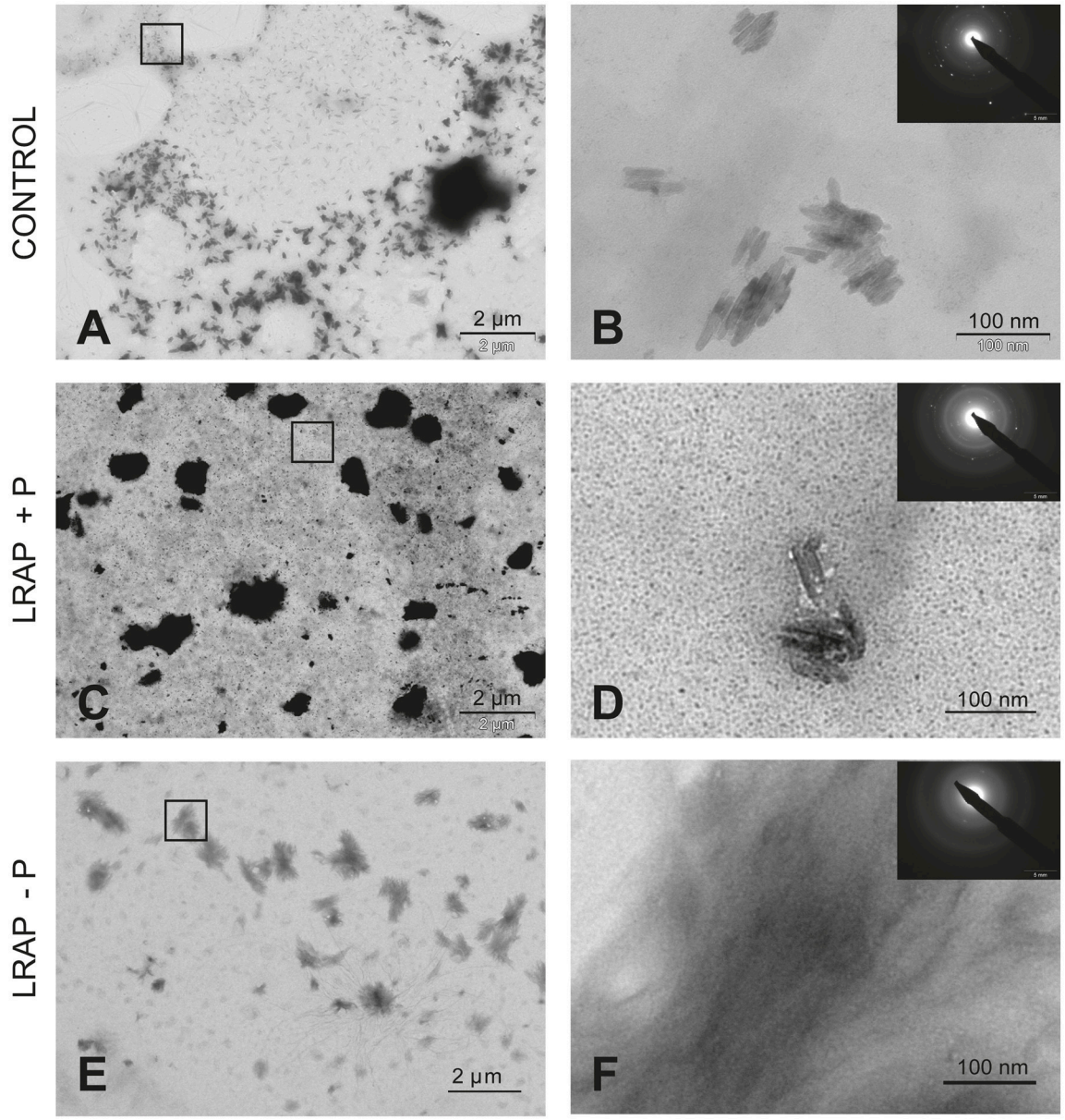

FIGURE 1 | TEM and SAED analyses of mineral phases formed under mineralizing conditions by the LS8 cells in the absence and presence of added peptide. **(A,B)** CONTROL, no added peptide; **(C,D)** LRAP(+P); and **(E,F)** LRAP(–P). In **(A,C,E)**, general crystal distribution can be observed, crystal characterization is presented in **(B,D,F)**. As shown, ordered needle like HAP (based on the observed selected area diffraction patterns) crystals were formed in the control **(A,B)** and in the presence of LRAP(+P) **(C,D)** in the LS8 cells. In the presence of LRAP(–P), the HAP crystals (SAED pattern in inset) appeared thinner, longer, and grouped in bundles **(E,F)**.

ameloblast, thus actively expressing *Amelx*, *Ambn*, and *Enam*, and *Mmp20* mRNAs (Sarkar et al., 2014), synthesize crystals with a very similar structure to those observed in secretory stage tooth enamel. LRAP(-P) treatment potentiates the crystal lengthening and bundle formation whereas LRAP (+P) has little effect on the general crystal shape. Therefore, in the LS8 model, despite the up-regulation of *Amelx* expression promoted by both forms of the peptide, the structure of the mineral appears mainly affected by the LRAP(–P) form, likely through a direct action of the peptide on HAP crystals as previously observed in precipitation experiments (Le Norcy et al., 2011b).

In the ALC cell line, a model for maturation stage ameloblast, characteristically expressing *Amelx*, *Odam,* and *Klk4* transcripts, treatment by both peptides affects crystal formation, favoring bundle formation, as in LS8 cells. This effect is, however, again most evident with LRAP(–P). Remarkably, when measuring the length to width ratio, no significant difference is found between the crystals formed by control or LRAP-treated cells

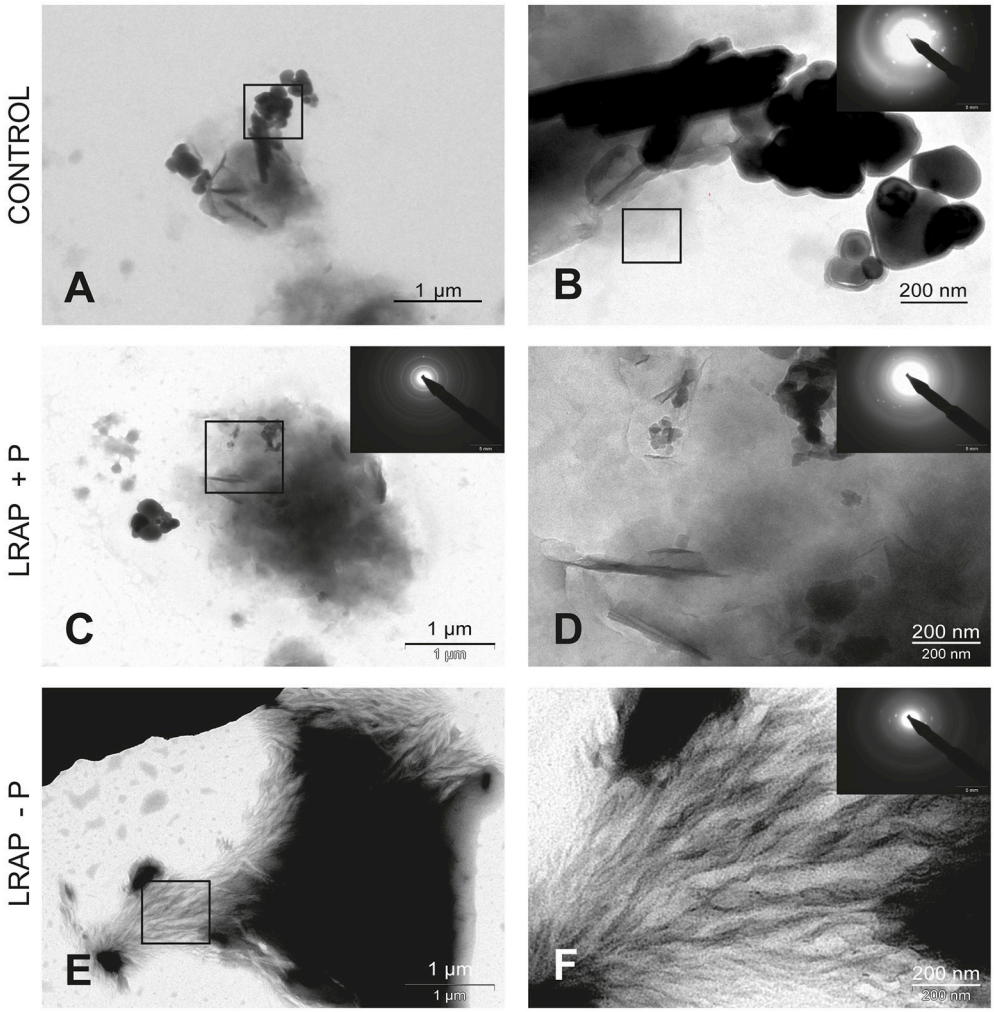

FIGURE 2 | TEM and SAED analyses of mineral phases formed under mineralizing conditions by the ALC cells in the absence and presence of added peptide. **(A,B)** CONTROL, no added peptide; **(C,D)** LRAP(+P); and **(E,F)** LRAP(–P). In **(A,C,E)**, general crystal distribution can be observed, crystal characterization is presented in **(B–D,F)**. Very large round and elongated HAP crystals are present in the control **(A,B)**. Upon addition of LRAP(+P) **(C,D)** and LRAP(–P) **(E,F)**, needle-like HAP crystals were formed with LRAP(–P) potentiating, bundle formation.

which might be related to the fact that this maturation stage is characterized by a crystal growth and no longer elongation (Sarkar et al., 2014). The fact that both peptides stimulate *Amelx* expression in the ALC cell, where it is usually low, could explain the change in crystal morphology and organization through guidance by the potentially newly induced amelogenin protein. The observed LRAP(–P) action could then result from a direct effect of the peptide on crystal shape as observed in LS8 cells and in precipitation experiments (Le Norcy et al., 2011a,b) and recently on acid etched enamel surfaces of human teeth (Kwak et al., 2017).

Molar germs can be cultured *ex vivo* and were shown to develop well-organized layers of polarized ameloblasts and odontoblasts (Tompkins and Veis, 2002). Micro-CT and FE-SEM analyses of the mineral formed by PND1 molar germs after a 9-day culture revealed an increase in enamel volume with LRAP(+P) while it was not increased by LRAP(–P) treatment. Rescue experiments with recombinant plasmid encoding LRAP in amelogenin KO mice, have shown that LRAP contributes to final enamel thickness and prism organization (Gibson et al., 2011; Xia et al., 2016). It can be speculated from our data, that in these mice LRAP is present under its phosphorylated form.

Altogether our results obtained in cell and germ cultures claimed for a differential effect of the phosphorylated and non-phosphorylated LRAP on crystal formation. It is not clear however at this point why LRAP(–P) did not significantly impact the mineral volume in the germ culture while it did so in the cell lines. This observation might be related to the 3D vs. 2D cell organization in both system and to the homogeneous differentiation stage present in the cell cultures as compared to the cultured germs where secretory and mature ameloblasts co-exist.

Our results on the peptide action on ameloblast cell-like culture, strongly suggest that peptide phosphorylation is not essential to achieve an impact on amelogenin gene expression, and likely on differentiation, since LRAP(+P) as well as LRAP(−P) were both able to stimulate amelogenin transcripts in the LS8 and ALC cells. This stimulation is restricted in a time frame since for both cell lines and peptides, it is followed by a decrease in amelogenin expression in agreement with what is observed during the process of differentiation of tooth ameloblasts. Our results with LRAP(–P) are concordant with previous studies showing its action on ameloblastic differentiation (Tompkins and Veis, 2002; Tompkins et al., 2005; Ravindranath et al., 2007). Notably, the two cell lines reacted to the peptide treatment with a different kinetics. The LS8 cell line responded very quickly to LRAP treatment (48 h) by increasing the number of *Amelx* transcripts whereas the ALC cell response was delayed (7 days). This variation in response kinetics is likely linked to the different stage of ameloblastic differentiation mimicked by these cell lines. Amelogenin secretion is very active during the secretory stage (Aoba et al., 1987), but then drops as the cells mature. In the LS8 cells, the peptides appear to potentiate the already active expression of amelogenin and this process appears direct as shown previously for LRAP(–P) (Iacob and Veis, 2008) while in the ALC cells they likely act through indirect more complex processes.

Understanding the potential complementary action of LRAP(+P) and LRAP(–P) on cell mineralization and metabolism is a next step in our analysis. This may further lead to the establishment of differential treatments by

TABLE 1 | Mean crystal length and length to width ratio formed by the LS8 and ALC cells.

	LS8		ALC	
	Mean crystal length (nm)	**L/W ratio**	**Mean crystal length (nm)**	**L/W ratio**
Control	43.9 ± 7.8	4.44 ± 0.89	74.9 ± 40.9	9.08 ± 3.46
LRAP(+P)	56.7 ± 9.2*	4.4 ± 0.73	84 ± 33.1	9.13 ± 2.97
LRAP(–P)	103 ± 17.8***	7.38 ± 1.26	76.2 ± 57.1	9.15 ± 2.89

Mean length of HAP crystals and length to width ratio were measured in TEM images in the control, LRAP(+P) and LRAP(-P) treated cells at D7 for LS8 and D14 for ALC. A statistically significant increase in crystal length was observed under both treatment conditions in the LS8 cells ($p < 0.05$ and ***$p < 10^{-6}$). For the ALC cells, due to the large heterogeneity in crystals observed, statistical analyses of crystal length were not relevant. Similar length to width ratio were observed in the control and the LRAP(+P) treated cells with both cell lines; an increase in the ratio was observed when LS8 cells were treated with LRAP(-P).*

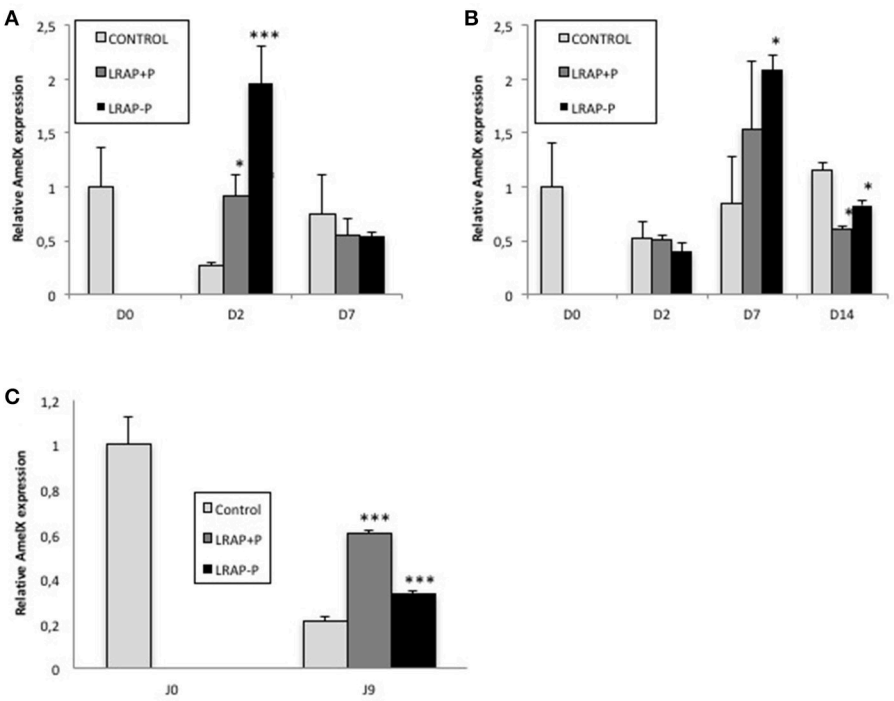

FIGURE 3 | Kinetic of expression of amelogenin gene in LS8 and ALC cells and in the cultured first molar germs. **(A,B)** *Amelx* quantitative PCR analyses for the LS8 **(A)** and ALC **(B)** cell lines at selected time-points. *Amelx* expression was normalized to GAPDH and Actin for each time-point and cell line. Average expression levels and standard deviation error were calculated from 3 different qPCR experiments (each run in triplicate, $n = 3$). At D2, both peptides induced a statistically significant increase in amelogenin transcripts relative to the control in the LS8 [*$p < 0.05$ for LRAP(+P) and ***$p < 10^{-4}$ for LRAP(–P)]. At D7, both peptides induced a similar increase for the ALC, statistically significant for LRAP(–P) (*$p < 0.05$) relative to the control. **(C)** *Amelx* transcripts levels were compared between D0 (PND1 germ) and cultured D9 germs. Inhibition of *Amelx* expression was observed in all conditions relative to the D0 germ. LRAP(+P) and LRAP(–P) treatment induced a statistically significant (*$p < 0.05$) increase in *Amelx* expression relative to the control.

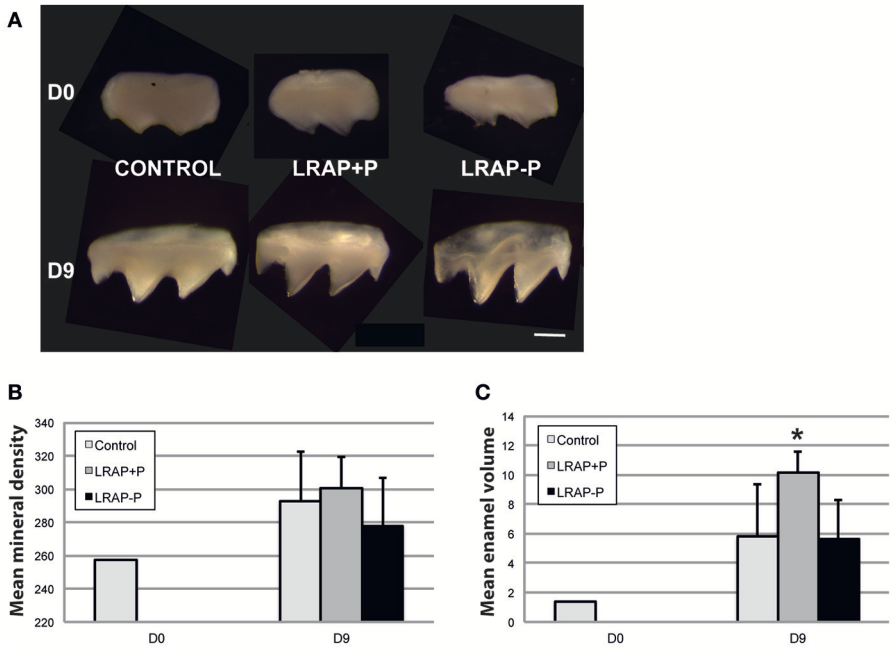

FIGURE 4 | Macroscopic views and mineral density and enamel volume of first molar germs cultured in the absence and presence of added peptide. **(A)** Photographs of first molar germs at D0 and after 9 days of culture in the absence (CONTROL) or presence of LRAP(+P) and LRAP(–P). Scale bar 500 μm. Mean mineral density **(B)** and enamel volume **(C)** were calculated from Micro-CT scans of first molar germs at D0 and after 9 days of culture. Addition of LRAP(+P) peptide lead to a statistically significant increase ($^*p < 0.05$) in enamel volume relative to the D9 control, no difference could be observed between LRAP(–P) treated and control samples. All samples presented an increased mineral density **(B)** and enamel volume **(C)** at D9 relative to D0 confirming tooth germ growth and maturation.

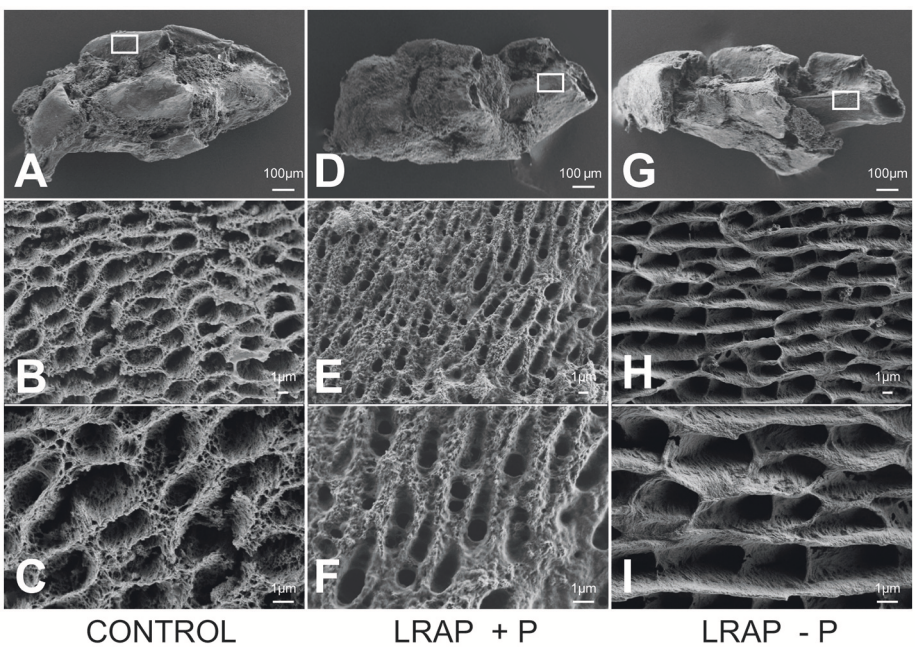

FIGURE 5 | FE-SEM analyses of D9 first molar germs cultured in the absence and presence of added peptide **(A–C)** CONTROL, **(D–F)** LRAP(+P), and **(G–I)** LRAP(–P). Ameloblast pits and mineral organization were clearly observed for all three samples, confirming enamel growth in culture. Ameloblast pits appeared smaller and more spaced in molar germs treated with LRAP(+P) **(E,F)** relative to the control **(B,C)** and slightly wider in molar germs treated with LRAP(–P) **(H,I)** relative to the control.

selected peptide(s) according to the tooth developmental stage.

The present data obtained in biological models parallel those recently described *in vitro* claiming that LRAP(–P) is involved in the modulation of crystal maturation (length, width) (Shafiei et al., 2015; Kwak et al., 2017). Therefore, its topical application can be envisioned for a future repair of enamel lesions. Furthermore, our *ex vivo* observations on LRAP(+P) correlate with the recent *in vitro* findings by Yamazaki and colleagues on the native phosphylated amelogenins during the early stages of enamel formation (Yamazaki et al., 2017). Unraveling the signaling pathways underlying this action is therefore mandatory for a potential use of this peptide as early treatment of inborn disorders of enamel.

AUTHOR CONTRIBUTIONS

ELN: Designed the setup of experiments, performed experiments, and drafted the manuscript; JL: Performed experiments. JS: Performed experiments. GR: Participated in result analysis. CC: Participated in drafting the manuscript. AP: Designed the setup of experiments, and drafted the manuscript.

ACKNOWLEDGMENTS

We want to thank Professor Toshihiro Sugiyama (Akita University School of Medicine, Japan) and Doctor Malcolm L. Snead (Center for Craniofacial Molecular Biology, Division of Biomedical Sciences, Ostrow School of Dentistry of USC, University of Southern California, Los Angeles, United States), for generously sharing their ameloblast cell lines (respectively ALC and LS8) with us. We thank Mr. Ludovic Mouton (Université Paris 7 Diderot—ITODYS) for his help with SEM acquisitions and analyses. We thank Doctor Henry C. Margolis (The Forsyth Institute, Cambridge, MA, USA) for useful discussions and for supplying us with the LRAP peptides.

This work was supported by grants from Paris Descartes University (ELN), Fondation pour la Recherche Médicale (EA2496) and PIV (FRM DGE20111123012), as well as the grant IDEX Sorbonne Paris Cité "Once upon a tooth" (CC).

SUPPLEMENTARY MATERIAL

The Supplementary Material for this article can be found online at: https://www.frontiersin.org/articles/10.3389/fphys.2018.00055/full#supplementary-material

REFERENCES

Aoba, T., Tanabe, T., and Moreno, E. C. (1987). Proteins in the enamel fluid of immature porcine teeth. *J. Dent. Res.* 66, 1721–1726. doi: 10.1177/00220345870660120501

Bartlett, J. D., Ball, R. L., Kawai, T., Tye, C. E., Tsuchiya, M., and Simmer, J. P. (2006). Origin, splicing, and expression of rodent amelogenin exon 8. *J. Dent. Res.* 85, 894–899. doi: 10.1177/154405910608501004

Bègue-Kirn, C., Smith, A. J., Ruch, J. V., Wozney, J. M., Purchio, A., Hartmann, D., et al. (1992). Effects of dentin proteins, Transforming Growth factor Beta 1 (TGF Beta 1) and Bone Morphogenetic Protein 2 (BMP2) on the differentiation of odontoblast *in vitro*. *Int. J. Dev. Biol.* 36, 491–503.

Beniash, E., Metzler, R. A., Lam, R. S., and Gilbert, P. U. (2009). Transient amorphous calcium phosphate in forming enamel. *J. Struct. Biol.* 166, 133–143. doi: 10.1016/j.jsb.2009.02.001

Beniash, E., Simmer, J. P., and Margolis, H. C. (2005). The Effect of recombinant mouse amelogenins on the formation and organization of hydroxyapatite crystals *in vitro*. *J. Struct. Biol.* 149, 182–190. doi: 10.1016/j.jsb.2004.11.001

Bonass, W. A., Kirkham, J., Brookes, S. J., Shore, R. C., and Robinson, C. (1994). Isolation and characterisation of an alternatively-spliced rat amelogenin cDNA: LRAP–a highly conserved, functional alternatively-spliced amelogenin? *Biochim. Biophys. Acta* 1219, 690–692. doi: 10.1016/0167-4781(94)90228-3

Cao, Y., Mei, M. L., Li, Q. L., Lo, E. C., and Chu, C. H. (2014). Enamel prism-like tissue regeneration using enamel matrix derivative. *J. Dent.* 42, 1535–1542. doi: 10.1016/j.jdent.2014.08.014

Chen, L. S., Couwenhoven, R. I., Hsu, D., Luo, W., and Snead, M. L. (1992). Maintenance of amelogenin gene expression by transformed epithelial cells of mouse enamel organ. *Arch. Oral Biol.* 37, 771–778. doi: 10.1016/0003-9969(92)90110-T

Fincham, A. G., and Moradian-Oldak, J. (1993). Amelogenin post-translational modifications: carboxy-terminal processing and the phosphorylation of bovine and porcine "TRAP" and "LRAP" amelogenins. *Biochem. Biophys. Res. Commun.* 197, 248–255. doi: 10.1006/bbrc.1993.2468

Fincham, A. G., Moradian-Oldak, J., and Simmer, J. P (1999). The structural biology of the developing dental enamel matrix. *J. Struct. Biol.* 126, 270–299. doi: 10.1006/jsbi.1999.4130

Gibson, C. W., Li, Y., Suggs, C., Kuehl, M. A., Pugach, M. K., Kulkarni, A. B., et al. (2011). Rescue of the murine amelogenin null phenotype with two amelogenin transgenes: amelogenin null rescue. *Eur. J. Oral Sci.* 119, 70–74. doi: 10.1111/j.1600-0722.2011.00882.x

Goldberg, M. (2010). *Amelogenins: Multifaceted Proteins for Dental & Bone Formation & Repair*, Vol. 1. Paris: Bentham Science Publishers.

Iacob, S., and Veis, A. (2008). Identification of the functional activity of the [A-4] amelogenin gene splice product in newborn mouse ameloblasts. *Bone* 42, 1072–1079. doi: 10.1016/j.bone.2008.01.023

Iijima, M., and Moradian-Oldak, J. (2004). Interactions of amelogenins with octacalcium phosphate crystal faces are dose dependent. *Calcif. Tissue Int.* 74, 522–531. doi: 10.1007/s00223-002-0011-3

Kwak, S. Y., Kim, S., Yamakoshi, Y., Simmer, J. P., Beniash, E., and Margolis, H. C. (2014). Regulation of calcium phosphate formation by native amelogenins *in vitro*. *Connect. Tissue Res.* 55 (Suppl. 1), 21–24. doi: 10.3109/03008207.2014.923853

Kwak, S. Y., Litman, A., Margolis, H. C., Yamakoshi, Y., and Simmer, J. P. (2017). Biomimetic enamel regeneration mediated by leucine-rich amelogenin peptide. *J. Dent. Res.* 96, 524–530. doi: 10.1177/0022034516688659

Kwak, S. Y., Wiedemann-Bidlack, F. B., Beniash, E., Yamakoshi, Y., Simmer, J. P., Litman, A., et al. (2009). Role of 20-kDa Amelogenin (P148) Phosphorylation in calcium phosphate formation *in vitro*. *J. Biol. Chem.* 284, 18972–18979. doi: 10.1074/jbc.M109.020370

Kwak, S. Y., Yamakoshi, Y., Simmer, J. P., and Margolis, H. C. (2016). MMP20 proteolysis of native amelogenin regulates mineralization *in vitro*. *J. Dent. Res.* 95, 1511–1517. doi: 10.1177/0022034516662814

Lau, E. C., Simmer, J. P., Bringas, P. Jr., Hsu, D. D., Hu, C. C., Zeichner-David, M., et al. (1992). Alternative splicing of the mouse amelogenin primary RNA transcript contributes to amelogenin heterogeneity. *Biochem. Biophys. Res. Commun.* 188, 1253–1260. doi: 10.1016/0006-291X(92)91366-X

Le Norcy, E., Kwak, S. Y., Wiedemann-Bidlack, F. B., Beniash, E., Yamakoshi, Y., Simmer, J. P., et al. (2011a). Potential role of the amelogenin N-terminus in the regulation of calcium phosphate formation *in vitro*. *Cells Tissues Organs* 194, 188–193. doi: 10.1159/000324827

Le Norcy, E., Kwak, S. Y., Wiedemann-Bidlack, F. B., Beniash, E., Yamakoshi, Y., Simmer, J. P., et al. (2011b). Leucine-rich amelogenin peptides regulate mineralization *in vitro*. *J. Dent. Res.* 90, 1091–1097. doi: 10.1177/0022034511411301

Li, Y., Yuan, Z. A., Aragon, M. A., Kulkarni, A. B., and Gibson, C. W. (2006). Comparison of body weight and gene expression in amelogenin null and wild-type mice. *Eur. J. Oral Sci.* 114(Suppl. 1), 190–193, discussion: 201–202, 381. doi: 10.1111/j.1600-0722.2006.00286.x

Margolis, H. C., Kwak, S. Y., and Yamazaki, H. (2014). Role of mineralization inhibitors in the regulation of hard tissue biomineralization: relevance to initial enamel formation and maturation. *Front. Physiol.* 5:339. doi: 10.3389/fphys.2014.00339

Nagano, T., Kakegawa, A., Yamakoshi, Y., Tsuchiya, S., Hu, J. C., Gomi, K., et al. (2009). Mmp-20 and Klk4 cleavage site preferences for amelogenin sequences. *J. Dent. Res.* 88, 823–828. doi: 10.1177/0022034509342694

Nakata, A., Kameda, T., Nagai, H., Ikegami, K., Duan, Y., Terada, K., et al. (2003). Establishment and characterization of a spontaneously immortalized mouse ameloblast-lineage cell line. *Biochem. Biophys. Res. Commun.* 308, 834–839. doi: 10.1016/S0006-291X(03)01467-0

Moradian-Oldak, J. (2012). Protein-mediated enamel mineralization. *Front. Biosci.* 17:4034. doi: 10.2741/4034

Paine, M. L., and Snead, M. L. (1997). Protein Interactions during assembly of the enamel organic extracellular matrix. *J. Bone Miner. Res.* 12, 221–227. doi: 10.1359/jbmr.1997.12.2.221

Pugach, M. K., Li, Y., Suggs, C., Wright, J. T., Aragon, M. A., Yuan, Z. A., et al. (2010). The amelogenin c-terminus is required for enamel development. *J. Dent. Res.* 89, 165–169. doi: 10.1177/0022034509358392

Ravindranath, R. M., Devarajan, A., and Bringas, P. (2007). Enamel formation *in vitro* in mouse molar explants exposed to amelogenin polypeptides ATMP and LRAP on enamel development. *Arch. Oral Biol.* 52, 1161–1171. doi: 10.1016/j.archoralbio.2007.06.008

Robinson, C., Kirkham, J., and Fincham, A. (1989). The enamelin/non-amelogenin problem. A brief review. *Connect. Tissue Res.* 22, 93–100. doi: 10.3109/03008208909114124

Ruan, Q., and Moradian-Oldak, J. (2015). Amelogenin and enamel biomimetics. *J. Mater. Chem. B Mater Biol. Med.* 3, 3112–3129. doi: 10.1039/C5TB00163C

Sarkar, J., Simanian, E. J., Tuggy, S. Y., Bartlett, J. D., Snead, M. L., Sugiyama, T., et al. (2014). Comparison of two mouse ameloblast-like cell lines for enamel-specific gene expression. *Front. Physiol.* 5:277. doi: 10.3389/fphys.2014.00277

Shafiei, F., Hossein, B. G., Farajollahi, M. M., Fathollah, M., Marjan, B., and Tahereh, J. K. (2015). Leucine-Rich Amelogenin Peptide (LRAP) as a surface primer for biomimetic remineralization of superficial enamel defects: an *in vitro* study. *Scanning* 37, 179–185. doi: 10.1002/sca.21196

Shaw, W. J., Campbell, A. A., Paine, M. L., and Snead, M. L. (2004). The COOH Terminus of the amelogenin, LRAP, is oriented next to the hydroxyapatite surface. *J. Biol. Chem.* 279, 40263–40266. doi: 10.1074/jbc.C400322200

Shimokawa, H., Tamura, M., Ibaraki, K., Ogata, Y., and Sasaki, S. (1989). "Human amelogenin gene," in *Tooth Enamel V*, ed R. W. Fearnhead (Yokohama: Florence Publishers), 301–305.

Snead, M. L. (2015). Biomineralization of a self-assembled-, soft-matrix precursor: enamel. *JOM* 67, 788–795. doi: 10.1007/s11837-015-1305-z

Tompkins, K., Alvares, K., George, A., and Veis, A. (2005). Two related low molecular mass polypeptide isoforms of amelogenin have distinct activities in mouse tooth germ differentiation *in vitro*. *J. Bone Miner. Res.* 20, 341–349. doi: 10.1359/JBMR.041107

Tompkins, K., and Veis, A. (2002). Polypeptides translated from alternatively spliced transcripts of the amelogenin gene, Devoid of the Exon 6a, B, c Region, have specific effects on tooth germ development in culture. *Connect. Tissue Res.* 43, 224–231. doi: 10.1080/03008200290001096

Veis, A., Tompkins, K., Alvares, K., Wei, K., Wang, L., Wang, X. S., et al. (2000). Specific amelogenin gene splice products have signaling effects on cells in culture and in implants *in vivo*. *J. Biol. Chem.* 275, 41263–41272. doi: 10.1074/jbc.M002308200

Wang, L., Guan, X., Du, C., Moradian-Oldak, J., and Nancollas, G. H. (2007). Amelogenin promotes the formation of elongated apatite microstructures in a controlled crystallization system. *J. Phys. Chem. C Nanomater. Interfaces* 111, 6398–6404. doi: 10.1021/jp0675429

Wiedemann-Bidlack, F. B., Kwak, S. Y., Beniash, E., Yamakoshi, Y., Simmer, J. P., and Margolis, H. C. (2011). Effects of phosphorylation on the self-assembly of native full-length porcine amelogenin and its regulation of calcium phosphate formation *in vitro*. *J. Struct. Biol.* 173, 250–260. doi: 10.1016/j.jsb.2010.11.006

Xia, Y., Ren, A., and Pugach, M. K. (2016). Truncated amelogenin and LRAP transgenes improve amelx null mouse enamel. *Matrix Biol.* 52–54, 198–206. doi: 10.1016/j.matbio.2015.11.005

Yamakoshi, Y. (2011). Porcine amelogenin : alternative splicing, proteolytic processing, protein - protein interactions, and possible functions. *J. Oral Biosci.* 53, 275–283. doi: 10.1016/S1349-0079(11)80011-3

Yamazaki, H., Beniash, E., Yamakoshi, Y., Simmer, J. P., and Margolis, H. C. (2017). Protein phosphorylation and mineral binding affect the secondary structure of the leucine-rich amelogenin peptide. *Front. Physiol.* 8:450. doi: 10.3389/fphys.2017.00450

Yuan, Z. A., Collier, P. M., Rosenbloom, J., and Gibson, C. W. (1996). Analysis of amelogenin mRNA during bovine tooth development. *Arch. Oral Biol.* 41, 205–213. doi: 10.1016/0003-9969(95)00119-0

Conflict of Interest Statement: The authors declare that the research was conducted in the absence of any commercial or financial relationships that could be construed as a potential conflict of interest.

The reviewer CC and handling Editor declared their shared affiliation.

frontiers in Physiology

ORIGINAL RESEARCH
published: 15 August 2018
doi: 10.3389/fphys.2018.01092

TRIP-1 Promotes the Assembly of an ECM That Contains Extracellular Vesicles and Factors That Modulate Angiogenesis

*Yinghua Chen and Anne George**

Brodie Tooth Development Genetics and Regenerative Medicine Research Laboratory, Department of Oral Biology, University of Illinois at Chicago, Chicago, IL, United States

Transforming growth factor beta receptor II interacting protein-1 (TRIP-1) was recently localized in the mineralized matrices of bone and dentin. The function of TRIP-1 in the ECM is enigmatic, as it is known to function as an intracellular endoplasmic reticulum protein during protein synthesis. Based on its localization pattern in bones and teeth, we posited that TRIP-1 must function as a regulatory protein with multiple functions during mineralization. In this study, we determined the *in vivo* function of TRIP-1 by an implantation assay performed using recombinant TRIP-1 and TRIP-1 overexpressing and knocked down cells embedded in a 3D biomimetic scaffold. After 4 weeks, the subcutaneous tissues from TRIP-1 overexpressing cells and scaffolds containing recombinant TRIP-1 showed higher expression levels of several ECM proteins such as fibronectin and collagen I. Picrosirius red and polarized microscopy was used to identify the birefringence of the collagen fibrils in the extracellular matrix (ECM). Interestingly, knockdown of TRIP-1 resulted in lower fibronectin and downregulation of the activation of the ERK MAP kinase. We further demonstrate that TRIP-1 overexpression leads to higher expression of pro-angiogenic marker VEGF and downregulation of anti-angiogenic factors such as pigment epithelium-derived factor and thrombospondin. Field emission scanning electron microscope results demonstrated that TRIP-1 overexpressing cells released large amount of extracellular microvesicles which were localized on the fibrillar matrix in the ECM. Overall, this study demonstrates that TRIP-1 can promote secretion of extracellular vesicles, synthesis of key osteogenic ECM matrix proteins and promote angiogenesis.

Keywords: TRIP-1, ECM, bone, mineralization, microvesicles, angiogenesis, matrix

OPEN ACCESS

Edited by:
Giovanna Orsini,
Università Politecnica delle Marche, Italy

Reviewed by:
Claudio Cantù,
Linköping University, Sweden
Hayato Ohshima,
Niigata University, Japan

***Correspondence:**
Anne George
anneg@uic.edu

Specialty section:
This article was submitted to Craniofacial Biology and Dental Research, a section of the journal Frontiers in Physiology

Received: *02 April 2018*
Accepted: *23 July 2018*
Published: *15 August 2018*

Citation:
Chen Y and George A (2018) TRIP-1 Promotes the Assembly of an ECM That Contains Extracellular Vesicles and Factors That Modulate Angiogenesis. Front. Physiol. 9:1092. doi: 10.3389/fphys.2018.01092

INTRODUCTION

Osteoblasts and odontoblasts are bone and dentin forming cells that synthesize and assemble a specialized extracellular matrix (Gajjeraman et al., 2007; George and Veis, 2008). Biological apatite deposited in the extracellular matrix (ECM) is orchestrated by an organic extracellular matrix that controls mineral nucleation and growth (He et al., 2003). This extracellular matrix is a complex network of collagens, glycoproteins such as fibronectin, SIBLING protein family members, phosphoproteins, proteoglycans, and polysaccharides (He et al., 2005;

Ravindran and George, 2014). During bone development several of these regulatory proteins are expressed at defined stages to perform specific function in maintaining the structure and function of bone (Hao et al., 2004). In hard tissues, the calcified ECM matrix acts as an osteoinductive matrix and influences cell behavior and influences physiological processes such as angiogenesis (Nienhuijs et al., 2011; Ajlan et al., 2015). However, there are yet unidentified proteins in the matrix that may play a regulatory role in initiating physiological processes such as cell differentiation and angiogenesis during the formation of mineralized tissues.

To understand the mechanisms of matrix mineralization, we have identified a potentially new matrix protein, TRIP-1 [transforming growth factor beta (TGF-β) receptor II interacting protein-1] (Ramachandran et al., 2012). Earlier reports show that TRIP-1 is localized in the ER and functions in concert with other subunits of the initiation complex to regulate protein synthesis (Choy and Derynck, 1998; Perez et al., 2011; Herrmannova et al., 2012). Therefore, its localization in the matrix was enigmatic. TRIP-1 expression is regulated spatially and temporally during skeletal development. During intramembranous bone development, predominant localization was seen during mouse development as early as embryo day 20 in preosteoblasts and differentiated osteoblasts. During endochondral ossification process, TRIP-1 expression was observed early during development in the epiphyseal growth plate. Interestingly TRIP-1 was observed in the extracellular matrix of the proliferating chondrocytes (Ramachandran et al., 2012). With the development of the primary spongiosa, TRIP-1 expression shifted from the cartilage and was abundantly expressed in the osteoid of the bony spicules. Within mature bone, TRIP-1 expression persisted in the periosteum, osteoblasts, osteocytes and in the bone matrix. Interestingly, its localization in the primary spongiosa suggests that TRIP-1 might function in the extracellular matrix to regulate mineralization as well as promote angiogenesis. A pivotal role for TRIP-1 in mineralization has been recently demonstrated in an *in vitro* nucleation model (Ramachandran et al., 2016, 2018).

To investigate other potential functions of TRIP-1 in the extracellular matrix, genetically modified cell lines overexpressing (TRIP1-OE) and knocked down TRIP-1 (TRIP1-KD) in preosteoblast MC3T3-E1cells were generated. The morphology of the genetically modified cells, nature of the deposited ECM matrix, osteogenic potential and its influence on neovascularization were studied.

MATERIALS AND METHODS

Expression and Purification of Recombinant TRIP-1

Recombinant TRIP-1 protein was expressed in bacteria using the pQE-30 plasmid (Qiagen) system. Briefly, 973-bp fragment corresponding to the coding region of TRIP-1 was cloned into *Eco*RI/*Xho*I restriction sites in pQE-30 vector. This plasmid was transformed into *E. coli* bacteria BL21-Gold (DE3). The protein expression was induced by the addition of 1 mM IPTG. The expressed protein was purified using Ni-NTA agarose (Qiagen) column under native conditions. The manufacturer's protocol was followed for protein elution. Specifically, the buffer containing 250 mM imidazole, pH 8.0 was used to elute TRIP-1 from the column.

Overexpression and Knock-Down of TRIP-1

Stable overexpression was performed by transfecting the pECFP vector (Clontech Laboratories, Mountain View, CA, United States) containing the rat TRIP-1 cDNA in MC3T3-E1 cells as published earlier (Ramachandran et al., 2016). Cells mock transfected with the empty vector served as the control. For knock-down studies, mission shRNA clones for TRIP-1 (Sigma-Aldrich, St. Louis, MO, United States) was used to generate a stable cell-line. Cells transfected with scrambled shRNA was used as control. Real-time PCR analysis was used to confirm the expression levels of TRIP-1 in the genetically modified MC3T3-E1 cells (Ramachandran et al., 2012).

Isolation of the ECM

MC3T3-TRIP1-OE (overexpression) and MC3T3-TRIP1-KD (knocked-down) cells were grown to confluence on cover glass for ECM isolation. Cells were lysed by incubating for 15 min with 0.5% TritonX-100, 0.01 M sodium phosphate, 0.15 M NaCl, pH 7.4 at 37°C and 5% CO2, followed by incubation for 10 min under the same conditions with 0.25 M ammonium hydroxide. The cover glass were then washed with 0.02 M Tris-HCl, pH 7.4, 0.15 M NaCl and 0.05% Tween-20. A final wash was performed with HBS buffer. The ECM was then fixed in 4% paraformaldehyde and subjected to immunostaining with rabbit anti-DMP1 antibody (1/2000), rabbit anti-GRP-78 (1/500), anti-fibronectin (1/100 Sigma-Aldrich), and rabbit anti-DMP4 antibodies (developed and characterized in our laboratory).

In vivo Assay Using a Subcutaneous Implantation Model in Mice to Determine the Osteogenic and Angiogenic Potential of TRIP-1

Two groups of implantation experiments were conducted in this study. The first group consisted of hydrogel scaffold pretreated with rTRIP-1 and seeded with 2×10^6 MC3T3-E1 cells while the hydrogel containing cells with no treatment served as control. In the second group control and genetically modified cells were seeded at a density of 2×10^6 cells per scaffold. LZ–Control protein at 7% concentration was used to make hydrogel scaffolds. Preparation of the leucine zipper (LZ) hydrogel scaffold was performed as published earlier (Huang et al., 2014; Ravindran et al., 2014). LZ hydrogel scaffold was adsorbed with 100 μg rTRIP-1 protein and LZ hydrogel with no treatment served as control were used. The cell seeded scaffolds were cultured *in vitro* for 48 h and were then implanted subcutaneously on the back of 1 month old athymic nude mice (Charles River Laboratories). Four weeks post implantation, the animals were sacrificed and the scaffolds were retrieved, fixed in 4% neutral buffered formalin, embedded and sectioned into 5 μm thick

sections for histological evaluation. All animal experiments were performed as per protocol approved by the UIC animal care committee (Assurance number A-3460-01).

Histology and Immunohistochemistry

All sections were deparaffinized in xylene, rehydrated in graded ethanol solutions, and hematoxylin and eosin (H&E) staining was performed as per published protocols (Hao et al., 2009). Immunohistochemistry using peroxidase conjugated secondary antibodies or fluorescent probes according to published protocols. The following antibodies were used: Rabbit anti-cluster of differentiation (CD31) antibody (1/100; Abcam), rabbit anti-vascular endothelial growth factor (VEGF) antibody (1/100, Santa Cruz Biotechnology), rabbit anti-pigment epithelium-derived factor (PEDF) antibody (1/500; Millipore), mouse anti-von Willebrand factor (vWF) antibody (1/100; Santa Cruz Biotechnology); rabbit anti fibronectin (FN) antibody (1/100; Sigma-Aldrich), goat alkaline phosphatase (ALP) antibody (1/100; Thermo Fisher Scientific), mouse dentin matrix protein 1 (DMP1) antibody (1/10000; kind gift from Dr. Qin, University of Texas), rabbit type I Collagen (1/100; Abcam) and mouse anti-phospho serine antibody (1/100; Sigma-Aldrich), mouse anti-thrombospondin (1/100; Sigma-Aldrich). For all immunohistochemistry experiments with fluorescent secondary antibody labeling, anti-mouse FITC (1/100; Sigma-Aldrich) and anti-rabbit (TRITC 1/100; Sigma-Aldrich) antibodies were used. All fluorescently stained sections were imaged at the University of Illinois at Chicago Research Resource Center core imaging facility. Imaging was performed using a Zeiss LSM 710 confocal microscope equipped with Zen image analysis software. Peroxidase stained sections were imaged using a Zeiss Axio-observer D1 microscope. All comparative fluorescence images were obtained using the same imaging conditions.

Western Blot Analysis

Total proteins were isolated as published earlier (Ramachandran et al., 2012). The blots were blocked with 5% nonfat milk, probed with rabbit polyclonal fibronectin antibody (1:2000) and rabbit pERK ½ (1:200; Santa Cruz Biotechnology).

Picrosirius Red Staining

Paraffin embedded sections were stained using the dye picrosirius red to demonstrate the presence of collagen in the ECM. Birefringence pattern of collagen fibers was determined using Zeiss polarized light microscope.

Image Processing for Quantification of Collagen Fiber

Representative images from picrosirius red stained sections were processed to obtain collagen fiber metrics at defined regions of interest. Collagen length and diameter were measured using CT-FIRE fiber detection software (LOCI; Madison, WI, United States) (Bredfeldt et al., 2014).

Scanning Electron Microscopy

MC3T3-E1, MC3T3-E1-TRIP1-OE, and MC3T3-E1-TRIP1-KD cells were grown on 12-mm cover glass placed in 12-well tissue culture plates in osteogenic differentiation media, i.e., normal growth medium supplemented with 10 mM β-glycerophosphate, 100 mg/ml ascorbic acid and 10 nM dexamethasone for 14 days. They were then washed twice with PBS and fixed in 1.5% glutaraldehyde in 0.15 M sodium cacodylate buffer for 24 h at 4°C. After washing twice with PBS, the samples were dehydrated in graded ethanol solutions and then completely dehydrated by immersing them in a solution of hexamethyldisilazane (HMDS) for 10 min followed by air–drying inside a tissue culture hood. The samples were coated with 10 μm thickness of platinum/palladium and imaged on a scanning electron microscope (Hitachi S-3000N). Field emission scanning electron microscope (FESEM) JEOL JSM-6320 was used to image collagen fibrils and vesicles in the matrix.

Exosome Isolation and TEM

Media was collected from confluent MC3T3-E1-TRIP1-OE cells and centrifuged at 400 *g* for 5 min to remove debris. The cleared supernatants were processed by sequential ultracentrifugation according to published protocols (Xu et al., 2017). The final pellet was suspended in 200 μl of PBS and processed for transmission electron microscopy (TEM).

Twenty microliters of the resuspended exosomes were added to 300 mesh formvar coated nickel grids and viewed without coating. For immunogold cytochemistry, published protocols were followed (Ramachandran et al., 2016). Briefly, the grids were fixed in 10% neutral formalin, permeabilized with PBS containing 1% Trton-X100 for 30 min and blocked with 3% BSA for 1 h at room temperature. The grids were then incubated with rabbit polyclonal CD63 (1/500) and mouse monoclonal TRIP1 (1/500) antibody. The grids were washed followed by incubation with gold conjugated anti-rabbit IgG (20 nm) and anti-mouse IgG (10 nm) washed and analyzed by TEM.

Statistical Analysis

Data are presented as the mean ± standard deviation of at least three independent experiments. Statistical analysis of the data was calculated using the Student's *t*-test. $P < 0.05$ was considered significant.

RESULTS

Histological Evaluation of the Explant Tissue

Hematoxylin and eosin staining was used to define the cellular and matrix content in the stroma generated by different cell types used in this study. Results in **Figures 1A,B** showed abundant ECM produced in the LZ-rTRIP1 and LZ-TRIP1-OE group. All the four groups showed high cellular content. The control LZ scaffold contained was infiltrated by few host cells.

Picrosirius red staining of the ECM matrix under bright field microscopy showed that the collagen fibrils appeared uniformly dark pink (**Figures 2A–E**) and birefringence colors under polarized light microscopy in all the groups (**Figures 2F–J**). In the groups containing TRIP-1 the collagen fibrils were thick

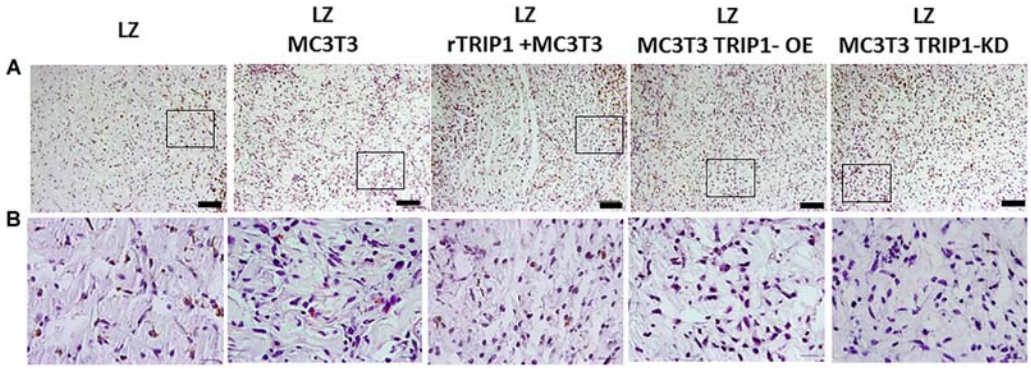

FIGURE 1 | Cellular architecture of *de novo* formed tissue analyzed by histological H&E staining. **(A)** Low power magnification of the tissues from different groups as indicated. Connective tissue stains as light pink and the cell nuclei stains blue. Bar represents 100 microns. **(B)** Higher magnification of the boxed areas from panel **(A)**. Bar represents 20 microns.

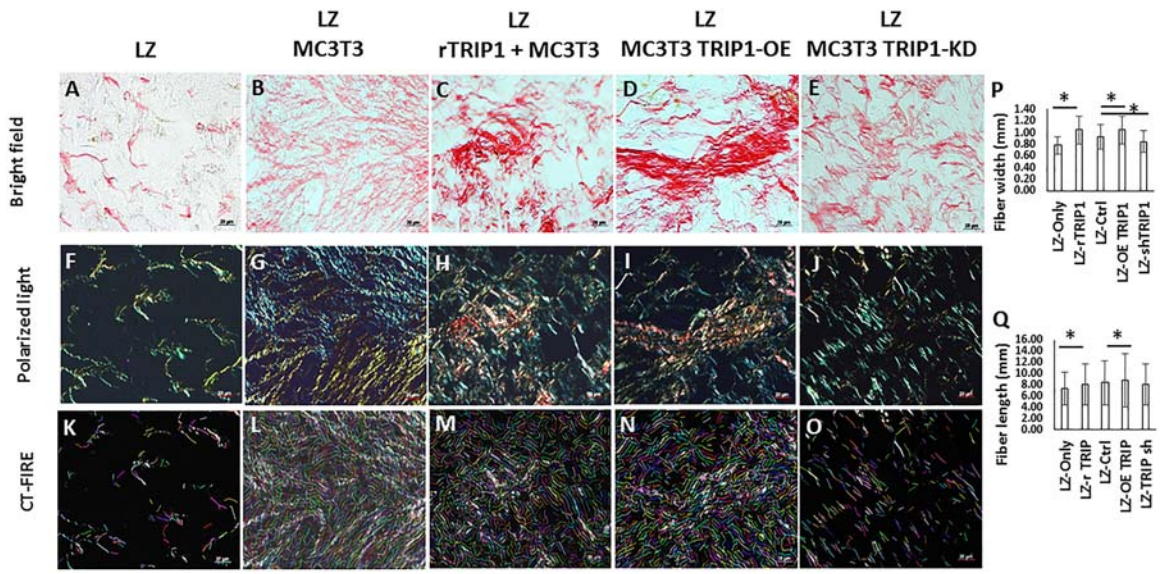

FIGURE 2 | Histology of *de novo* formed tissues stained with picrosirius red to assess the presence of collagen fibrils in the matrix. **(A–E)** Picrosirius red stained tissues obtained from different experimental groups under light microscopy. Bar represents 20 microns. **(F–J)** Picrosirius red stained tissues obtained from different experimental groups under polarized light. Bar represents 20 microns. **(K–O)** CT-FIRE was used to quantify collagen fiber length and diameter in different groups and the quantifications are represented in panels **(P,Q)**. Stastically significant differences are indicated. $^*P \leq 0.05$.

and tightly packed and exhibited yellowish orange birefringent colors (**Figures 2H–I**). In the absence of TRIP-1 loose network of thin fibers, weakly birefringent ranging from greenish blue to yellow were observed (**Figure 2J**). CT-FIRE fiber analysis of images (**Figures 2K–O**) revealed that the collagen fibrils were thicker and longer in groups containing TRIP-1 (**Figures 2P,Q**).

TRIP-1 Overexpressing MC3T3-E1 Cells Produce a Unique Extracellular Matrix Containing Extracellular Vesicles

Genetically-modified cell-lines established earlier were used in this study to investigate the morphology and evaluate the presence of key matrix components in the ECM when cultured under osteogenic conditions for 14 days. SEM analysis showed numerous extracellular vesicles (EV) on the surface of all the three cell types (**Figure 3**). However, TRIP1-OE cells showed highly elongated cellular processes coated with numerous EV (**Figure 3B**) while, TRIP1-KD cells had remarkably low amounts of EV (**Figure 3C**). The control MC3T3-E1 cells which had endogenous levels of TRIP-1 released more microvesicles than the TRIP1-KD cells (**Figure 3A**). High-resolution visualization of the ECM using Field Emission SEM showed the ultrastructure of the heterogeneous matrix. Images in **Figures 4A,B** showed that TRIP1-OE cells secreted a network of fibrillary ECM and the diameter of the fibrils were highly homogeneous (**Figure 4C**). Adhered to the fibrils were

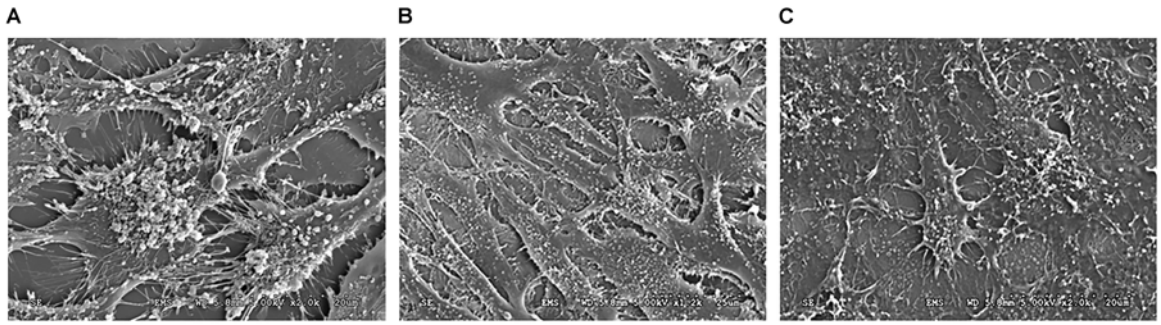

FIGURE 3 | SEM image of the cells and the secreted microvesicles when cultured for 14 days in osteogenic media. The SE micrographs are representative images of MC3T3-E1 cells **(A)**, TRIP1-OE cells **(B)**, and TRIP1-KD cells **(C)** grown in osteogenic media for 14 days. Note the large amount of extracellular vesicles released by TRIP1-OE cells.

numerous vesicles (**Figure 4D**). TEM analysis of the EV isolated by ultracentrifugation showed nanometer sized heterogenous population of exosome-like particles containing electron-dense particles in the core (**Figure 4E**). Analysis of the solubilized exosomes by immunogold labeling show the presence of CD-63 an exosome marker (**Figure 4F**, black arrows) and also contained TRIP-1 (**Figure 4F**, white arrows).

We next isolated the ECM from TRIP1-OE and TRIP1-KD cells and examined for several matrix proteins such as DMP1, FN, GRP78, and DMP4 (Fam20C) by IHC (**Figure 5A**). Interestingly, fibronectin the principal protein of the ECM was present in low amounts in TRIP1-KD cells when compared to TRIP-OE cells. Expression levels of GRP-78 and DMP4 were also modestly reduced, however, higher expression levels of

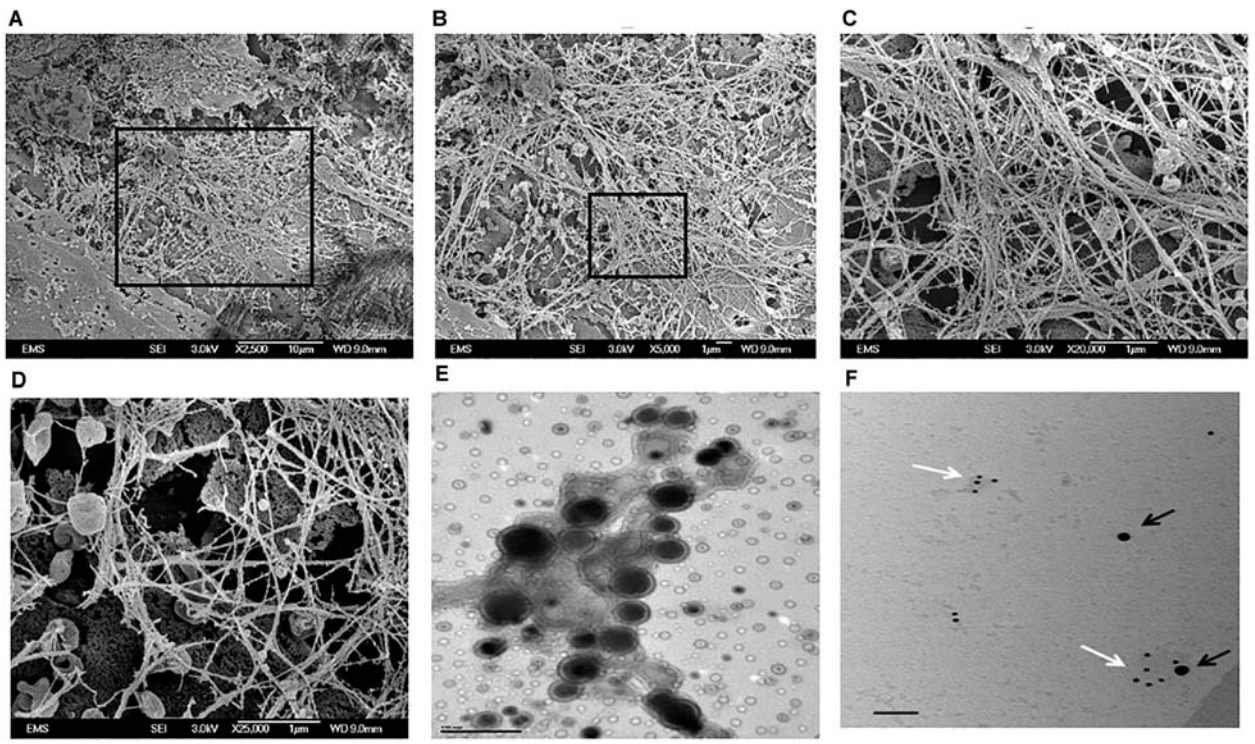

FIGURE 4 | Electron Microscopy images of the secreted ECM by TRIP1 overexpressing cells after 14 days of culture in osteogenic media. Representative low-magnification FESEM images of the secreted ECM from MC3T3-TRIP1-OE cells **(A);** high magnification image of the boxed area in panel **(A)** showing a highly fibrous ECM with embedded extracellular vesicles **(B)**; high magnification from the boxed area in panel **(B)** showing the dense fibrous matrix **(C)**; high magnification image showing the cup-shaped extracellular vesicles localized specifically on the fibrils **(D)**. Magnification as indicated. Representative TEM image of unstained extracellular vesicles showing the morphology of the vesicles isolated from TRIP1-OE cells under mineralization **(E).** Scale bar 100 nm. Representative TEM image of solubilized exosomes showing the presence of immunogold labeled CD-63 (black arrows, 20 nm) and TRIP-1 (white arrows,10 nm) **(F).** Scale bar 100 nm.

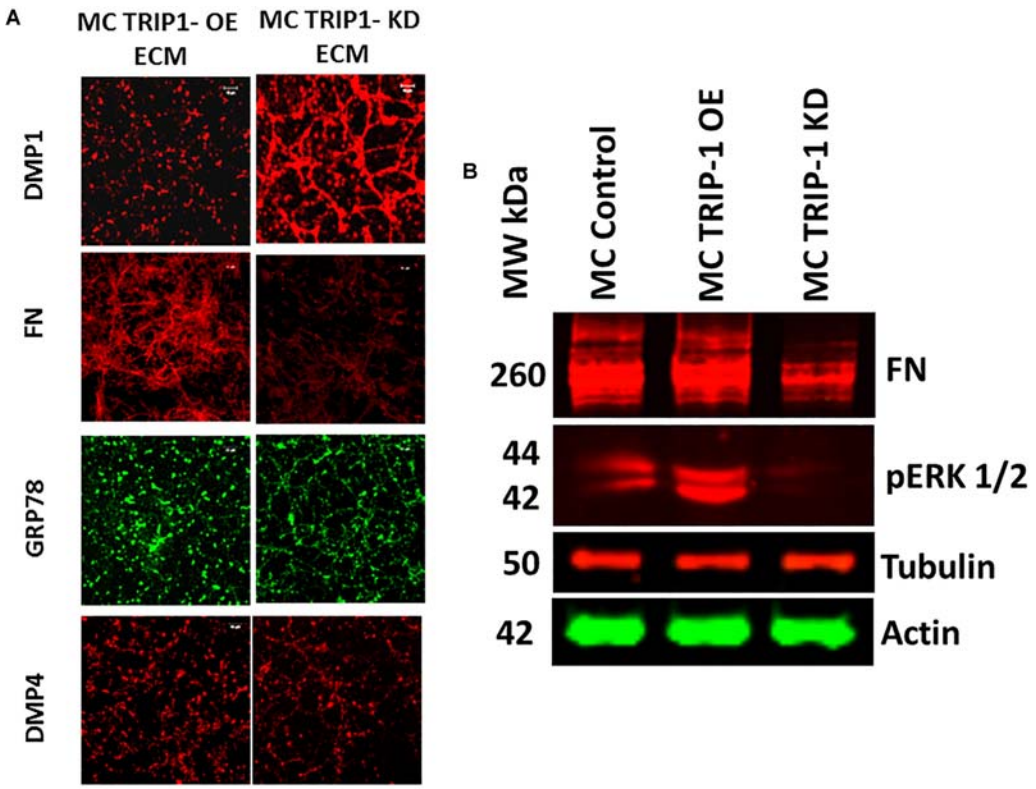

FIGURE 5 | Expression of key extracellular matrix proteins involved in mineralization. Representative confocal micrographs showing the expression of DMP1, FN, GRP-78 and DMP4 in the ECM of MC3T3-TRIP1-OE and MC3T3-TRIP1-KD cells **(A)**. Western blot of total proteins showing the presence of FN, pERK in MC3T3-E1, MC3T3-TRIP1-OE, and MC3T3-TRIP1-KD cells. Note lower expression of FN and pERK1/2 in TRIP1-KD cells. Tubulin and actin were used as loading controls **(B).**

DMP1 was observed with TRIP1-KD cells. Additionally, Western blot analysis in **Figure 5B** confirmed lower expression levels of fibronectin in TRIP1-KD cells. As fibronectin in the matrix is known to activate ERK1/2 MAP kinase, therefore, we sought to determine if TRIP-1 mediated fibronectin expression could regulate cellular differentiation by activating ERK MAP kinase. Western blot results in **Figure 5B** also confirm ERK activation in response to TRIP-1 overexpression and attenuated in TRIP1-KD cells.

TRIP-1 Overexpression Promotes Cellular Differentiation as Assessed by the Presence of Biomineralization Regulators

In vivo function of TRIP-1 in biomineralization was assessed by examining the explants obtained from subcutaneous implantation of 3D-scaffolds containing MC3T3-E1, TRIP1-OE, or TRIP1-KD cells. Use of LZ hydrogel scaffolds for *in vivo* analysis was established and published (Huang et al., 2014). The explants were harvested after 4 weeks and subjected to immunohistochemical analysis. Results show an increase in the expression of the major ECM proteins (**Figure 6A**) such as type I collagen (Col1) (B1–B3), ALP a key enzyme that initiates mineralization (B4–B6) and Glucose regulated protein 78 (GRP-78) that we have recently identified in the matrices of bone and dentin (B10–B12). However, the expression level of dentin matrix protein 1 (DMP1) a key regulatory matrix protein in bone and dentin mineralization was higher in TRIP1-KD cells (B7–B9). Control rabbit and mouse secondary (B13) did not show any staining.

With the scaffolds containing MC3T3-E1 cells adsorbed with rTRIP1 on the LZ scaffold (**Figure 6B**), an increase in ALP expression (a and b), Col1 (c and d), phosphoserine containing proteins (P-serine) (e and f) were observed.

TRIP-1 Overexpression Stimulates the Expression of TGF-β Signaling Modulators

TRIP-1 is a TGF-β receptor II binding protein, therefore, we investigated if TRIP-1 had an effect on the expression levels of TGF-β ligand and type II serine/threonine kinase receptor (**Figure 7A**). Interestingly, TRIP1-OE cells showed abundant expression of type II receptor within the cells and the ligand was highly expressed within the ECM matrix and lower expression in TRIP1-KD cells (**Figure 7A**). As *p*-serine staining showed higher level of phosphoproteins in the matrix,

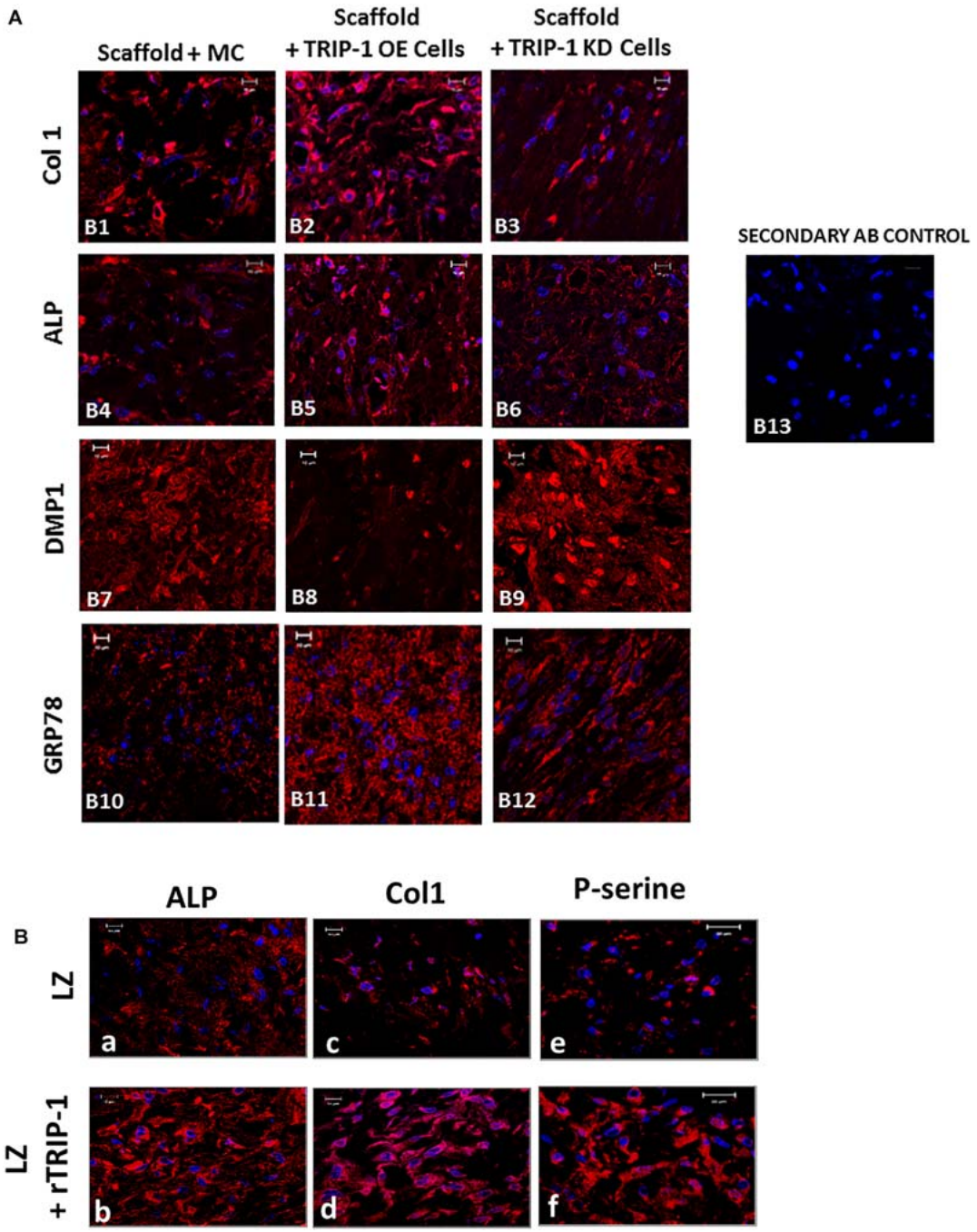

FIGURE 6 | (A) Effect of TRIP-1 overexpression and knock-down and its influence on secretion of matrix proteins *in vivo*. Representative confocal micrographs showing the localization of Col1 **(B1–B3)**, ALP **(B4–B6)**, DMP1 **(B7–B9)**, GRP-78 **(B10–B12)** in implanted scaffold containing control MC3T3-E1, TRIP1-OE, and TRIP1-KD cells, respectively. Scale bar represents 20 μm for all images. **(B)** Effect of rTRIP-1 adsorbed on LZ-scaffold containing MC3T3-E1 cells on matrix proteins *in vivo*. Representative confocal micrographs showing the immunohistochemical localization of ALP **(a,b)**, Col1 **(c,d)**, P-serine **(e,f)** in implanted control scaffold and scaffold +rTRIP-1, respectively. Note increased expression levels of osteogenic markers with rTRIP-1 treatment. Scale bar represents 20 μm for all images.

we sought to examine the levels of Fam20C (initially designated as DMP4 in our initial study) a secretory pathway kinase that phosphorylates proteins in the extracellular matrices of bone and teeth. Interestingly, TRIP1 overexpression showed high levels of Fam20C expression and was downregulated in TRIP1-KD cells (**Figure 7A**). Similar expression pattern was observed with rTRIP1 on LZ scaffold containing MC3T3-E1 cells (**Figure 7B**).

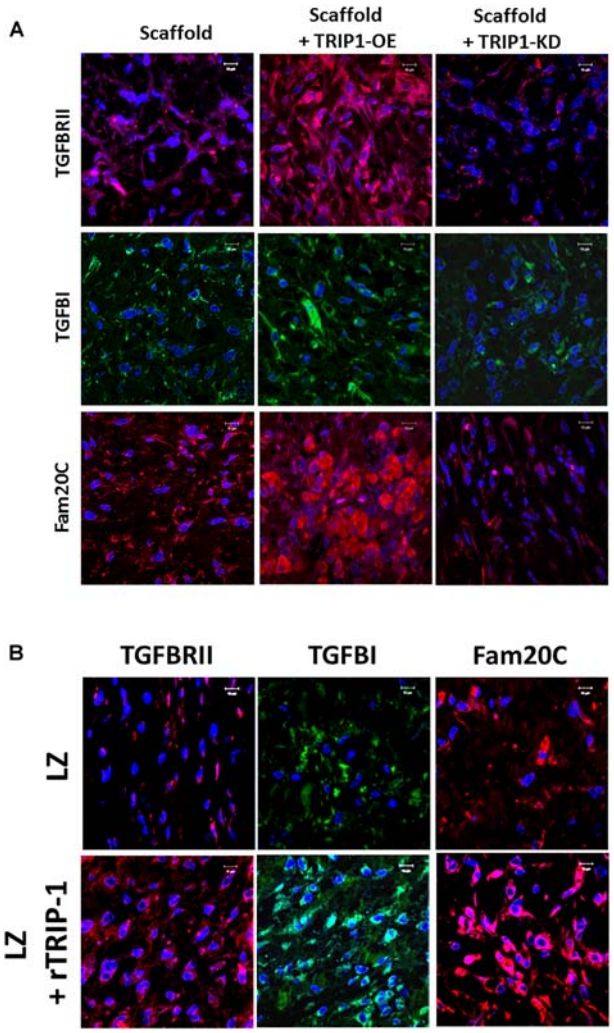

FIGURE 7 | TRIP-1 and its effect on TGF-β signaling members and the secreted kinase of the ECM *in vivo*. **(A)** Effect of TRIP1-OE and TRIP1-KD cells on TGF-β ligand, its receptor and Golgi kinase Fam20C *in vivo*: Representative confocal micrographs showing the expression of TGF-βRII, TGF-β, and Fam20C in implanted scaffold containing control MC3T3-E1, TRIP1-OE, and TRIP1-KD cells, respectively. Scale bar represents 20 μm for all images. **(B)** Effect of rTRIP-1 adsorbed on LZ-scaffold on TGF-β ligand, its receptor and Golgi kinase Fam20C *in vivo*: Representative confocal micrographs showing the expression of TGF-βRII, TGF-β1, and Fam20C. Note increased expression levels of these markers with rTRIP-1 treatment. Scale bar represents 20 μm for all images.

TRIP-1 Overexpression Promotes Angiogenesis *in vivo*

We next explored if TRIP-1 modulated angiogenesis *in vivo*. Immunohistochemical analysis was performed with several pro-angiogenic and anti-angiogenic markers (**Figures 8A,B**). In the experimental group with LZ scaffold adsorbed with rTRIP-1, more staining for VEGF a pro-angiogenic marker was observed when compared with the control (A1–A2). VEGF was highly upregulated in TRIP1-OE cells when compared with the control and reduced expression in TRIP1-KD cells (B1–B3).VEGF staining pattern corroborated well with the number of RBCs in TRIP-OE cells and rTRIP-1 treated scaffolds (**Figure 8C**) implying TRIP1 promoted vascularization. Immunohistochemical analysis with endothelial cell markers CD31 and vWF were carried out to investigate if TRIP-1 aids vasculogenesis by recruiting endothelial cells. Results show CD31 was enhanced with TRIP-1 (A3–A4 and B4–B6). vWF showed a similar pattern of expression with TRIP1-OE cells and LZ-rTRIP-1 treated scaffolds when compared to control LZ containing MC3T3-E1 and MC3T3-KD cells (A5–A6 and B7–B9). Thus, the above results demonstrate that TRIP-1 influences angiogenesis *in vivo*.

Pigment epithelium-derived factor is an anti-angiogenic factor and decreased expression was observed both in recombinant TRIP-1 treated scaffolds and TRIP1-OE cells, however, expression was higher in the absence of TRIP1 (A7–A8 and B10–B12). Similar expression patterns were observed with thrombospondin (TBSP) an anti-angiogenic factor (A9–A10 and B13–B15).

DISCUSSION

The ECM of bone and dentin are unique, as it contains several matrix molecules which provide the structural framework to support cells and it also contains a rich milieu of cytokines and growth factors entrapped within the fibrillar matrix which conveys signals for various cellular functions (Posey et al., 2008; Alford et al., 2015). The signaling function from the ECM to the cells and from the cells to the ECM is a two-way dialog. Unique to bone matrix are several phosphoproteins, notably members of the SIBLING family that aid in hydroxyapatite nucleation and growth. Recently, we have identified TRIP-1 in the ECM of bone and dentin. This suggests that several proteins exist in the ECM that are synthesized by the osteoblasts and odontoblasts that might play a pivotal role in the organization of the mineralized matrices of bone and dentin.

In order to determine other potential functions of TRIP-1 in the ECM, preosteoblast MC3T3-E1 cells were genetically modified to overexpress or silence TRIP-1. Morphological examination by SEM showed that with TRIP-1 overexpression and in the presence of differentiation media the cells were elongated with several prominent cell processes and secreted large amounts of EV. SEM analysis further showed that the EVs were able to penetrate inside the dense fibrous ECM and they were specifically localized on the fibrillary strands. However, the mechanism by which the EVs are transported on the dense network of the ECM are yet to be studied. These EV appeared as functional component of the extracellular matrix. Published reports demonstrate that EVs include exosomes, matrix vesicles, and microvesicles, and carry a multi-molecular cargo of proteins, nucleic acids, lipids metabolites and signaling molecules (Rilla et al., 2017). TEM analysis show that the EV are enveloped by a lipid bilayer with an electron-dense core. Such nano-vesicular structures have been shown to carry calcium phosphate crystals and are transported to the ECM to initiate the process of mineral nucleation (Hasegawa et al., 2017). In cartilage, bone

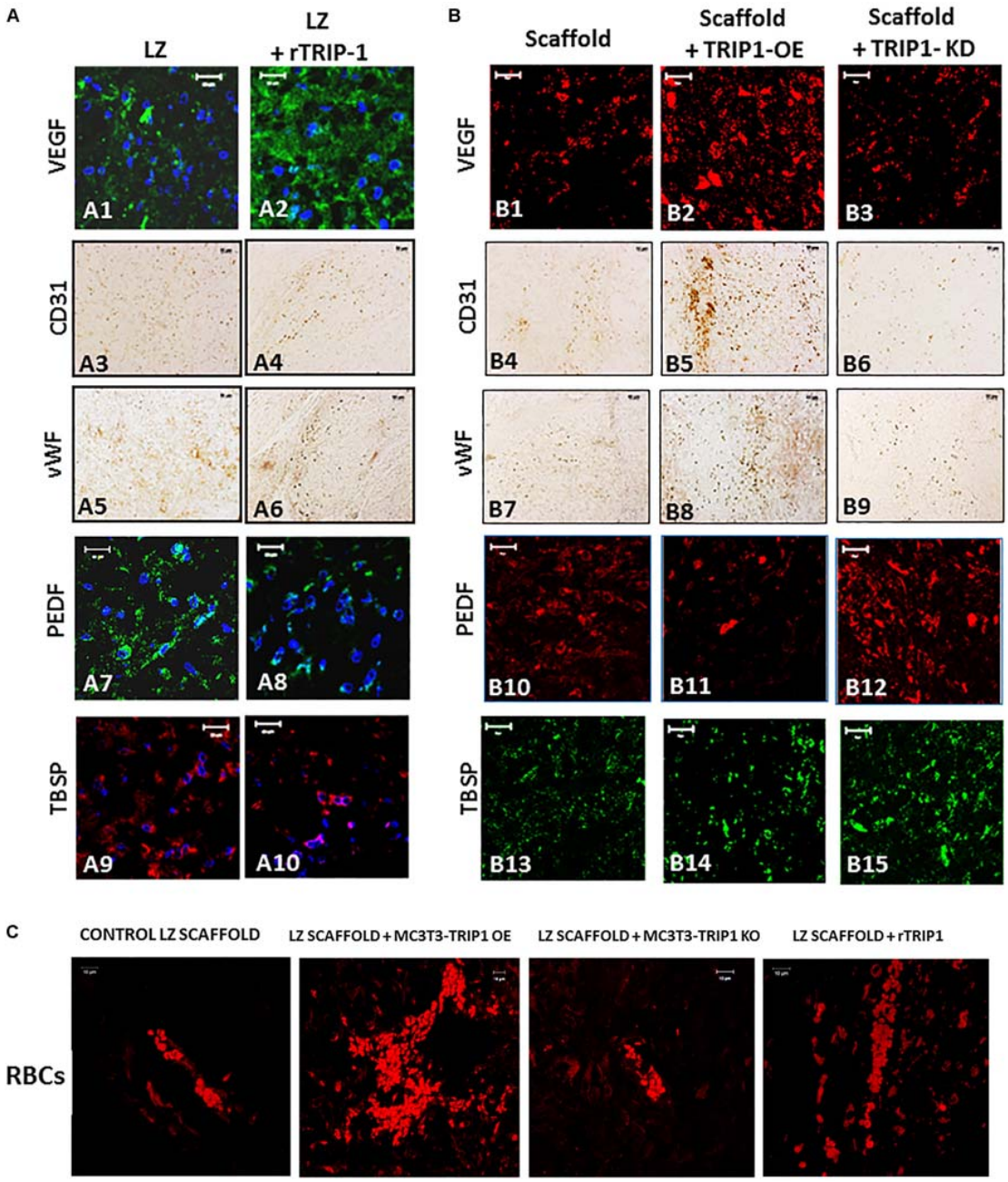

FIGURE 8 | TRIP-1 promotes angiogenesis *in vivo*. **(A)** Effect of rTRIP-1 adsorbed on LZ-scaffold on angiogenesis: Representative confocal micrographs showing the immunohistochemical localization of VEGF **(A1,A2)**, CD31 **(A3,A4)**, vWF **(A5,A6)**, PEDF **(A7,A8)**, TBSP **(A9,A10)** in implanted control scaffold and scaffold +rTRIP-1, respectively. Note increased expression levels of angiogenesis and endothelial cell markers with rTRIP-1 treatment. Scale bar represents 20 μm for all images. **(B)** Effect of TRIP1-OE and TRIP1-KD cells on angiogenesis: Representative confocal micrographs showing the expression levels of VEGF **(B1–B3)**, CD31 **(B4–B6)**, vWF **(B7–B9)**, PEDF **(B10–B12)**, TBSP **(B13–B15)** in implanted scaffold containing control MC3T3-E1, TRIP1-OE, and TRIP1-KD cells, respectively. Scale bar represents 20 μm for all images. **(C)** TRIP-1 promotes the formation of red blood cells: Representative confocal images showing autofluorescence of RBCs in the different groups as stated.

and dentin it has been shown that matrix vesicles also release their bioactive cargo to the ECM changing its properties, rather than to other cells (Chaudhary et al., 2016). TRIP-1 is one such protein that lacks a signal peptide, and we have earlier provided evidence that intracellular TRIP-1 can be packaged and exported to the ECM via exosomes. In this study, we demonstrate that TRIP-1 can be considered to play an important role in modifying the composition of the extracellular matrix by secreting EVs. Interestingly, the amount of EVs on the cell surface increased in the presence of TRIP-1. Knockdown of TRIP-1 attenuates EV

deposition. Therefore, it is possible that TRIP-1 favors biogenesis of EVs and their secretion to the ECM to modulate mineralization and permit communication between different bone cell types, stem cells and endothelial cells in the microenvironment of the secreted vesicles.

ECM components in mineralized matrices not only function as a scaffold and supports mineralization but also influence structural flexibility, promote angiogenesis and other cellular functions to support structure and function. We have observed that overexpression of TRIP-1 and presence of immobilized TRIP-1 in the cellular microenvironment results in increased expression of key matrix proteins of mineralized tissues namely type I collagen and fibronectin. Collagen an important constituent of the connective tissue stroma in mineralized tissues play a vital role in maintaining structural integrity and function as a template in matrix mineralization. As collagen has a natural birefringence which is attributed to the arrangement of fibers and enhanced by picrosirius red staining, therefore, it is an ideal technique to visualize the structure of the *de-novo* collagen synthesized by the various cell types used in this study. Picrosirius red along with polarized light impart different birefringent colors in shades of green-yellow representing immature procollagen to orange-red depicting mature closely packed collagen fibers. Processing of these images with CT-FIRE fiber quantification software showed that TRIP-1 had an influence on the length and width of the collagen fibrils.

Besides providing a structural template for mineralization both fibronectin and collagen play a role in angiogenesis. Recently, it was observed that type I collagen was deposited on the endothelial wall of the blood vessels and served as a template for new bone during endochondral bone formation (Shoham et al., 2016). Specifically, a correlation between Col1A1 expression and vascular development was established in this study. The abundant deposition of fibronectin is interesting as it is required for matrix assembly and vascular morphogenesis. Polymerization of fibronectin is required for endothelial cell survival, proliferation and tube formation (Wijelath et al., 2004). Knockout mice of the splice variants of fibronectin EIIIA and EIIIB show severe vascular defects. Fibronectin-integrin binding is known to initiate a MAP-kinase dependent signaling cascade. Interestingly, TRIP-1 overexpression is able to induce the phosphorylation and activation of ERK1/2 and this would be an important signaling mechanism for cellular differentiation. Specificity of ERK1/2 activation was attenuated with TRIP1-KO cells.

Results show that TRIP-1 promotes higher expression of extracellular phosphoproteins as demonstrated by IHC analysis using phosphoserine antibody. Correspondingly, we have shown that Fam20C a kinase that catalyze the phosphorylation of secreted proteins is also upregulated with TRIP-1 overexpression. Fam20C has been shown to be a single kinase that generates the majority of the secreted phosphoproteome.

TGF-β cytokine can induce a diverse set of responses that is modulated by the cellular context. As TRIP-1 is a TGF-β receptor II interacting protein we investigated if it had an influence on the expression of type II receptor. Interestingly, TRIP-1 overexpression led to an increase in the expression of type-II receptor and higher TGF-β ligand localized in the ECM. It is well established that the TGF-β signaling is activated when the ligand binds to the type II receptor which then phosphorylates serine and threonine residues in the type I receptor, which subsequently propagates the signal through Smad activation (Wrana et al., 1994). The downstream targets of TRIP-1 mediated TGF-β signaling are yet to be identified. However, TGF-β can stimulate angiogenesis depending on the expression levels and the tissue context.

Vasculature in mineralized tissues play a significant role in the ossification process of bone and dentin. It is possible that TRIP-1 can activate TGF-β to promote the expression of a major regulator of angiogenesis VEGF (Yuan et al., 2014). Several studies have shown that matrix-bound VEGF induces prolonged activation of VEGFR2 leading to downstream signaling events (Sivaraj and Adams, 2016). Immobilized VEGF can also induce the association of cell surface integrin β-1 subunit with VEGFR2. Thus matrix-bound VEGF is important for bone angiogenesis. Interestingly, it has previously been demonstrated that vascular patterning directs bone formation (Shoham et al., 2016). Increase in expression of CD31 and vWF with TRIP-1 suggests the presence of endothelial cells in the ECM (Langen et al., 2017). CD31 a membrane glycoprotein is traditionally used as a marker for endothelial cells. It is possible that pre-osteoblasts might transdifferentiate into endothelial cells. In the bone marrow $CD31^+$ cells are reported to be highly angiogenic and vasculogenic cells (Kim et al., 2010). von Willebrand factor is another glycoprotein produced by endothelial cells and is normally used as a marker to identify vessels and vessel density in tissue sections (Shi et al., 1998; Jazayeri et al., 2008; Wang et al., 2017). The presence of abundant RBCs in the scaffolds with TRIP-1 further suggest the ability of ECM from TRIP-1 overexpressing cells to favor formation of blood vessels.

TRIP-1 overexpression lowered the expression of PEDF and TSP (thrombospondin). PEDF, a member of the serine protease inhibitor (serpin) superfamily, has been described as one of the most potent anti-angiogenic factor in the ECM (Tombran-Tink et al., 2005; Chetty et al., 2015). PEDF is not only able to inhibit EC migration and proliferation but can also induce EC apoptosis (Broadhead et al., 2010). PEDF contains collagen-binding site and heparin-binding site, therefore, binding of ECM components can modulate its activity (Meyer et al., 2002; Sekiya et al., 2011). Thrombospondin is another matricellular extracellular matrix protein with an anti-angiogenic function during bone development.

Therefore, the EV from TRIP-1 overexpression might have a role in the transformation of the cells within its microenvironment to form endothelial cells. It is possible that TRIP-1 containing exosomes might contain the ingredients to promote vasculogenesis and angiogenesis.

CONCLUSION

TRIP-1 is a recently identified ECM protein which has the ability to bind calcium and precipitate calcium phosphate polymorphs, therefore can work in concert with other matrix proteins to fine tune matrix mineralization. The mineralized matrix not

only provides the mechanical strength to the tissue but contains several macromolecules embedded within the matrix that provide signaling cues and guides cell differentiation. In this study, we demonstrate that TRIP-1 promotes the secretion of EV and play an important role in modulating the composition of the matrix. Multiple macromolecules such as collagen and fibronectin which functions in the hierarchical organization of the ECM in mineralized tissues are influenced by the overexpression of TRIP-1. Transport of TRIP-1 to the ECM was shown to be facilitated by exosomes. TRIP-1 in the ECM can promote both direct and indirect effects on adhering preosteoblasts and consequently stimulate cell differentiation and angiogenesis. A better understanding of the multifunctional role of TRIP-1 in regulating osteogenesis and angiogenesis is essential for the development of therapeutics for mineralization-related disorders.

AUTHOR CONTRIBUTIONS

YC performed the experiments and assembled the data. AG analyzed the data and wrote the manuscript.

FUNDING

This study was supported by NIH grant DE 11657 and the Brodie Endowment Fund.

ACKNOWLEDGMENTS

We thank Dr. Ravindran for help with the implantation studies and Ms. Ramachandran for immunohistochemical analysis.

REFERENCES

Ajlan, S. A., Ashri, N. Y., Aldahmash, A. M., and Alnbaheen, M. S. (2015). Osteogenic differentiation of dental pulp stem cells under the influence of three different materials. *BMC Oral Health* 15:132. doi: 10.1186/s12903-015-0113-8

Alford, A. I., Kozloff, K. M., and Hankenson, K. D. (2015). Extracellular matrix networks in bone remodeling. *Int. J. Biochem. Cell Biol.* 65, 20–31. doi: 10.1016/j.biocel.2015.05.008

Bredfeldt, J. S., Liu, Y., Pehlke, C. A., Conklin, M. W., Szulczewski, J. M., Inman, D. R., et al. (2014). Computational segmentation of collagen fibers from second-harmonic generation images of breast cancer. *J. Biomed. Opt.* 19:016007. doi: 10.1117/1.JBO.19.1.016007

Broadhead, M. L., Becerra, S. P., Choong, P. F., and Dass, C. R. (2010). The applied biochemistry of PEDF and implications for tissue homeostasis. *Growth Factors* 28, 280–285. doi: 10.3109/08977191003604513

Chaudhary, S. C., Kuzynski, M., Bottini, M., Beniash, T. E., Dokland, T., Mobley, C. G., et al. (2016). Phosphate induces formation of matrix vesicles during odontoblast-initiated mineralization in vitro. *Matrix Biol.* 52-54, 284–300. doi: 10.1016/j.matbio.2016.02.003

Chetty, A., Bennett, M., Dang, L., Nakamura, D., Cao, G. J., Mujahid, S., et al. (2015). Pigment epithelium-derived factor mediates impaired lung vascular development in neonatal hyperoxia. *Am. J. Respir. Cell Mol. Biol.* 52, 295–303. doi: 10.1165/rcmb.2013-0229OC

Choy, L., and Derynck, R. (1998). The type II transforming growth factor (TGF)-beta receptor-interacting protein TRIP-1 acts as a modulator of the TGF-beta response. *J. Biol. Chem.* 273, 31455–31462. doi: 10.1074/jbc.273.47.31455

Gajjeraman, S., Narayanan, K., Hao, J., Qin, C., and George, A. (2007). Matrix macromolecules in hard tissues control the nucleation and hierarchical assembly of hydroxyapatite. *J. Biol. Chem.* 282, 1193–1204. doi: 10.1074/jbc.M604732200

George, A., and Veis, A. (2008). Phosphorylated proteins and control over apatite nucleation, crystal growth, and inhibition. *Chem. Rev.* 108, 4670–4693. doi: 10.1021/cr0782729

Hao, J., Ramachandran, A., and George, A. (2009). Temporal and spatial localization of the dentin matrix proteins during dentin biomineralization. *J. Histochem. Cytochem.* 57, 227–237. doi: 10.1369/jhc.2008.952119

Hao, J., Zou, B., Narayanan, K., and George, A. (2004). Differential expression patterns of the dentin matrix proteins during mineralized tissue formation. *Bone* 34, 921–932. doi: 10.1016/j.bone.2004.01.020

Hasegawa, T., Yamamoto, T., Tsuchiya, E., Hongo, H., Tsuboi, K., Kudo, A., et al. (2017). Ultrastructural and biochemical aspects of matrix-vesicle-mediated mineralization. *Jpn. Dent. Sci. Rev.* 53, 34–35. doi: 10.1016/j.jdsr.2016.09.002

He, G., Dahl, T., Veis, A., and George, A. (2003). Nucleation of apatite crystals in vitro by self-assembled dentin matrix protein 1. *Nat. Mater.* 2, 552–558. doi: 10.1038/nmat945

He, G., Ramachandran, A., Dahl, T., George, S., Schultz, D., Cookson, D., et al. (2005). Phosphorylation of phosphophoryn is crucial for its function as a mediator of biomineralization. *J. Biol. Chem.* 280, 33109–33114. doi: 10.1074/jbc.M500159200

Herrmannova, A., Daujotyte, D., Yang, J. C., Cuchalova, L., Gorrec, F., Wagner, S., et al. (2012). Structural analysis of an eIF3 subcomplex reveals conserved interactions required for a stable and proper translation pre-initiation complex assembly. *Nucleic Acids Res.* 40, 2294–2311. doi: 10.1093/nar/gkr765

Huang, C. C., Ravindran, S., Yin, Z., and George, A. (2014). 3-D self-assembling leucine zipper hydrogel with tunable properties for tissue engineering. *Biomaterials* 35, 5316–5326. doi: 10.1016/j.biomaterials.2014.03.035

Jazayeri, M., Allameh, A., Soleimani, M., Jazayeri, S. H., Piryaei, A., and Kazemnejad, S. (2008). Molecular and ultrastructural characterization of endothelial cells differentiated from human bone marrow mesenchymal stem cells. *Cell Biol. Int.* 32, 1183–1192. doi: 10.1016/j.cellbi.2008.07.020

Kim, H., Cho, H. J., Kim, S. W., Liu, B., Choi, Y. J., Lee, J., et al. (2010). CD31+ cells represent highly angiogenic and vasculogenic cells in bone marrow: novel role of nonendothelial CD31+ cells in neovascularization and their therapeutic effects on ischemic vascular disease. *Circ. Res.* 107, 602–614. doi: 10.1161/CIRCRESAHA.110.218396

Langen, U. H., Pitulescu, M. E., Kim, J. M., Enriquez-Gasca, R., Sivaraj, K. K., Kusumbe, A. P., et al. (2017). Cell-matrix signals specify bone endothelial cells during developmental osteogenesis. *Nat. Cell Biol.* 19, 189–201. doi: 10.1038/ncb3476

Meyer, C., Notari, L., and Becerra, S. P. (2002). Mapping the type I collagen-binding site on pigment epithelium-derived factor. Implications for its antiangiogenic activity. *J. Biol. Chem.* 277, 45400–45407. doi: 10.1074/jbc.M208339200

Nienhuijs, M. E., Walboomers, X. F., Gelinsky, M., Stoelinga, P. J., and Jansen, J. A. (2011). The evaluation of mineralized collagen as a carrier for the osteoinductive material COLLOSS((R))E, in vivo. *Tissue Eng. Part A* 17, 1683–1690. doi: 10.1089/ten.TEA.2009.0349

Perez, R. E., Navarro, A., Rezaiekhaligh, M. H., Mabry, S. M., and Ekekezie, I. I. (2011). TRIP-1 regulates TGF-beta1-induced epithelial-mesenchymal transition of human lung epithelial cell line A549. *Am. J. Physiol. Lung Cell Mol. Physiol.* 300, L799–L807. doi: 10.1152/ajplung.00350.2010

Posey, K. L., Hankenson, K., Veerisetty, A. C., Bornstein, P., Lawler, J., and Hecht, J. T. (2008). Skeletal abnormalities in mice lacking extracellular matrix proteins, thrombospondin-1, thrombospondin-3, thrombospondin-5, and type IX collagen. *Am. J. Pathol.* 172, 1664–1674. doi: 10.2353/ajpath.2008.071094

Ramachandran, A., He, K., Huang, C. C., Shabazian-Yassar, R., Shokuhfar, T., and George, A. (2018). TRIP-1 in the extracellular matrix promotes nucleation of calcium phosphate polymorphs. *Connect. Tissue Res.* 59, 13–19. doi: 10.1080/03008207.2018.1424146

Ramachandran, A., Ravindran, S., and George, A. (2012). Localization of transforming growth factor beta receptor II interacting protein-1 in bone

and teeth: implications in matrix mineralization. *J. Histochem. Cytochem.* 60, 323–337. doi: 10.1369/0022155412436879

Ramachandran, A., Ravindran, S., Huang, C. C., and George, A. (2016). TGF beta receptor II interacting protein-1, an intracellular protein has an extracellular role as a modulator of matrix mineralization. *Sci. Rep.* 6:37885. doi: 10.1038/srep37885

Ravindran, S., and George, A. (2014). Multifunctional ECM proteins in bone and teeth. *Exp. Cell Res.* 325, 148–154. doi: 10.1016/j.yexcr.2014.01.018

Ravindran, S., Zhang, Y., Huang, C. C., and George, A. (2014). Odontogenic induction of dental stem cells by extracellular matrix-inspired three-dimensional scaffold. *Tissue Eng. Part A* 20, 92–102. doi: 10.1089/ten.TEA.2013.0192

Rilla, K., Mustonen, A.-M., Arasu, U. T., Harkonen, K., Matilainen, J., and Nieminen, P. (2017). Extracellular vesicles are integral and functional components of the extracellular matrix. *Matrix Biol.* doi: 10.1016/j.matbio.2017.10.003 [Epub ahead of print].

Sekiya, A., Okano-Kosugi, H., Yamazaki, C. M., and Koide, T. (2011). Pigment epithelium-derived factor (PEDF) shares binding sites in collagen with heparin/heparan sulfate proteoglycans. *J. Biol. Chem.* 286, 26364–26374. doi: 10.1074/jbc.M111.252684

Shi, Q., Rafii, S., Wu, M. H., Wijelath, E. S., Yu, C., Ishida, A., et al. (1998). Evidence for circulating bone marrow-derived endothelial cells. *Blood* 92, 362–367.

Shoham, A. B., Rot, C., Stern, T., Krief, S., Akiva, A., Dadosh, T., et al. (2016). Deposition of collagen type I onto skeletal endothelium reveals a new role for blood vessels in regulating bone morphology. *Development* 143, 3933–3943. doi: 10.1242/dev.139253

Sivaraj, K. K., and Adams, R. H. (2016). Blood vessel formation and function in bone. *Development* 143, 2706–2715. doi: 10.1242/dev.136861

Tombran-Tink, J., Aparicio, S., Xu, X., Tink, A. R., Lara, N., Sawant, S., et al. (2005). PEDF and the serpins: phylogeny, sequence conservation, and functional domains. *J. Struct. Biol.* 151, 130–150. doi: 10.1016/j.jsb.2005.05.005

Wang, C., Li, Y., Yang, M., Zou, Y., Liu, H., Liang, Z., et al. (2017). Efficient differentiation of bone marrow mesenchymal stem cells into endothelial cells in vitro. *Eur. J. Vasc. Endovasc. Surg.* 55, 257–265. doi: 10.1016/j.ejvs.2017.10.012

Wijelath, E. S., Rahman, S., Murray, J., Patel, Y., Savidge, G., and Sobel, M. (2004). Fibronectin promotes VEGF-induced CD34 cell differentiation into endothelial cells. *J. Vasc. Surg.* 39, 655–660. doi: 10.1016/j.jvs.2003.10.042

Wrana, J. L., Attisano, L., Wieser, R., Ventura, F., and Massagué, J. (1994). Mechanism of activation of the TGF-β receptor. *Nature* 370, 341–347.

Xu, R., Simpson, R. J., and Greening, D. W. (2017). A protocol for isolation and proteomic characterization of distinct extracellular vesicle subtypes by sequential centrifugal ultrafiltration. *Methods Mol. Biol.* 1545, 91–116. doi: 10.1007/978-1-4939-6728-5_7

Yuan, Y., Zhang, Y., Yao, S., Shi, H., Huang, X., Li, Y., et al. (2014). The translation initiation factor eIF3i up-regulates vascular endothelial growth factor a, accelerates cell proliferation, and promotes angiogenesis in embryonic development and tumorigenesis. *J. Biol. Chem.* 289, 28310–28323. doi: 10.1074/jbc.M114.571356

Conflict of Interest Statement: The authors declare that the research was conducted in the absence of any commercial or financial relationships that could be construed as a potential conflict of interest.

frontiers in Physiology

METHODS
published: 14 August 2017
doi: 10.3389/fphys.2017.00567

A Novel Method to Detect 3D Mandibular Changes Related to Soft-Diet Feeding

Kana Kono[1], *Chihiro Tanikawa*[2], *Takeshi Yanagita*[1], *Hiroshi Kamioka*[3] *and Takashi Yamashiro*[2]*

[1] Department of Orthodontics, Okayama University Hospital, Okayama, Japan, [2] Department of Orthodontics and Dentofacial Orthopedics, Graduate School of Dentistry, Osaka University, Osaka, Japan, [3] Graduate School of Medicine, Dentistry and Pharmaceutical Sciences, Okayama University, Okayama, Japan

Craniofacial morphology varies among individuals, which is regulated by the interaction between genes and the environment. Soft-diet feeding is a widely-used experimental model for studying the association between the skeletal morphology and muscle-related loading on the bone. Traditionally, these studies have been based on linear and angular measurements provided on two-dimensional (2D) radiographs in the lateral view. However, 2D observation is based on simplification of the anatomical structures and cannot detect three-dimensional (3D) changes in detail. In this study, we newly developed a modified surface-based analysis with micro-3D computed tomography (CT) to examine and detect the 3D changes in the mandible associated with soft-diet feeding. Mice at 3 weeks of age were fed a powdered soft-diet (SD) or hard-diet (HD) of regular rodent pellets until 9 weeks of age. Micro-CT images were taken at age 9 weeks to reconstruct the anatomical architecture images. A computer-generated averaged mandible was superimposed to directly visualize the morphological phenotypes. Gross observation revealed the apparent changes at the posterior body of the mandible, the angular process and the condyle between HD and SD mice. Significant differences in the mapping indicated the regions of significant displacement in the SD mice over the averaged 3D image of the HD mice. This map revealed that vertical displacement was most evident in 3D changes. We also noted a combination of vertical, transverse and anteroposterior directions of displacement in the condylar growth, resulting in complicated shape changes in the whole condylar process in SD mice. In contrast, transverse displacement was more significant in the coronoid process. The map analysis further showed the significant outward displacement of the inner surface of the alveolar process, which consequently resulted in thinning of the alveolar process.

Keywords: 3D, CT, soft food, mice, mandible, morphological change

OPEN ACCESS

Edited by:
Thimios Mitsiadis,
University of Zurich, Switzerland

Reviewed by:
Nenad Filipovic,
University of Kragujevac, Serbia
Alexandros Efthimis Tsouknidas,
University of Western Macedonia, Greece
David P. Rice,
University of Helsinki, Finland
Heleni Vastardis,
National and Kapodistrian University of Athens, Greece

***Correspondence:**
Takashi Yamashiro
yamashiro@dent.osaka-u.ac.jp

Specialty section:
This article was submitted to Craniofacial Biology and Dental Research, a section of the journal Frontiers in Physiology

Received: *08 June 2017*
Accepted: *20 July 2017*
Published: *14 August 2017*

Citation:
Kono K, Tanikawa C, Yanagita T, Kamioka H and Yamashiro T (2017) A Novel Method to Detect 3D Mandibular Changes Related to Soft-Diet Feeding. Front. Physiol. 8:567. doi: 10.3389/fphys.2017.00567

INTRODUCTION

Craniofacial morphology is the result of a complex network of interactions between the genotype and the environment and the mandibular structure adapts according to the physiological loading during mastication (Klingenberg and Leamy, 2001). Malocclusion is more prevalent in modern populations than in ancient ones. The modern diet, characterized by softer and/or processed foods,

may contribute to reduced chewing activity and a decreased masticatory function have been linked with an increased prevalence of malocclusion and craniofacial deficiency in humans (Corruccini, 1984; Larsson et al., 2005).

Previous studies have shown that a soft-food diet resulted in a posteriorly rotated mandible, reduced ramus size, more posteriorly directed growth of the condyle, and a shorter vertically angular process (Bouvier and Hylander, 1984; Kiliaridis et al., 1985; Yamada and Kimmel, 1991; Maki et al., 2002; Anderson et al., 2014). Soft diet leads to reduced masticatory muscle strength and decreased loading applied to the mandible, which can affect the bone modeling specifically in the regions where the masticatory muscle attaches (Mavropoulos et al., 2004; Hichijo et al., 2014, 2015). These findings provided solid evidence that the masticatory muscle function influences the mandibular growth pattern and thus the morphology of the mandible. However, these studies were based on linear and angular measurements obtained on two-dimensional (2D) radiographs. The rodent and human craniofacial structure is complicated in shape, and 2D observations insufficiently display the anatomical structures by representing them as sets of landmarks.

In addition, a 2D radiograph analysis in smaller animals, e.g., young mice, is difficult due to unstable head positioning and mandible orientation in comparison to rats or larger animals. Indeed, in the aforementioned 2D studies identifying the bone phenotypes associated with soft-diet feeding, they used mice 6 months old, or rats only 8 weeks old. Young mice have advantages over other mammals, as genetically modified mice are commonly used as animal models of human diseases.

These limitations are currently overcome by acquiring three-dimensional (3D) micro-computed tomography (CT) images, which permits capturing the shapes of the subjects with high resolution and provide methods to visualize, quantify and compare the surface morphology of the materials in 3D (Nakano et al., 2003). Micro-CT generates reconstructed 3D models in voxels for qualitative 3D morphological observation, and then the bone surface voxel can be extracted and converted to coordinates for quantitative morphometric analysis (Swain and Xue, 2009). However, most previous studies using 3D micro-CT performed 2D observation on a reconstructed slice or measurement among the reference points placed on reconstructed models (Mavropoulos et al., 2004; Swain and Xue, 2009; Enomoto et al., 2010; Saito et al., 2011; Goto et al., 2015). While 3D observation using micro-CT provided more accurate data than previous 2D studies had, a conventional 3D analysis did not show any additional advantages for evaluating any possible deviations in the mandibular shape.

3D volumetric images are first converted into 3D surface models, and then the Standard Tessellation Language software program (STL; a triangulated mesh representation of 3D images) makes it possible to parameterize the entire curved surface (Gelaude et al., 2008). In our previous studies, wire mesh fitting based on the anatomical landmarks were applied to the STL data, which allowed for the detection of deviations in the parameters describing the facial morphological phenotypes among males and females (Tanikawa et al., 2016). In the present study, we first applied wire mesh fitting for a 3D analysis of micro-CT data to evaluate how food consistency influences the whole mandibular morphology. A wire mesh fitting analysis using approximately 10,000 points of wire mesh on the mandibular surface was applied to assess the quantitative topographic variation in the bony surface of the mandible. Our approach clearly visualized the 3D distribution of significant changes on the mandibular surface in response to changes in food consistency.

MATERIALS AND METHODS

Animals

Sixteen ICR mice (body weight 7 g, all obtained from Crea Japan, Tokyo, Japan), weaned at postnatal 3 weeks, were randomly divided into groups. The control group was fed a hard diet (HD) of regular rodent pellets (CE-2, Crea Japan) with tap water, and the soft-diet (SD) group was given a powdered diet of the same nutritional value (powdered CE-2) until postnatal 9 weeks. All aspects of animal care and experiments were approved by the Okayama University Committee for Animal Care and Use. All animals, housed three or four to a cage, were fed and watered *ad libitum* and maintained at 23 ± 1°C with a 12-h day/night cycle.

The animal experiments were performed under the research protocol approved by the Animal Research Committee at Okayama University (OKU-2014520). To minimize animal suffering, the number of animals used was based on the minimum required to obtain statistically valid results.

Micro-CT

Nine mice with SD and 7 with HD were sacrificed and decapitated at postnatal 9 weeks. The heads were fixed in 4% paraformaldehyde (PFA) for 12 h. Micro-CT images were taken with a Ratheta LCT-200 In Vivo Micro-CT Scanner for Small Lab Animals (HITACHI-Aloka, Tokyo, Japan) at 90 kV and 110 mA with a 96 μm slice width, and 1-voxel size at 96 × 96 × 96 μm.

Segmentation

Surface generation from micro-CT data was performed with 3D Slicer (version 4.5.0-1, http://www.slicer.org) (Kikinis and Pieper, 2011), which is an open-source software platform for the analysis and visualization of CT data. Following data preparation, such as painting, erosion, and dilation, to obtain a mandibular 3D model, semiautomatic segmentation was performed on this platform using a region-growing algorithm called GrowCut (Supplementary Figure 1).

Identification of the Landmarks

The positions of 69 landmarks [36 landmarks were defined in previous studies (Kiliaridis et al., 1985; Odman et al., 2008; Boell and Tautz, 2011) and 33 landmarks were newly defined in the present study (See Supplementary Figure 2)] were identified by a visual inspection of the image and digitized using a computer mouse cursor and HBM-Rugle (Medic Engineering Co, Kyoto, Japan). For the reliability of the identification of the landmarks, please see Supplementary Figure 1. The 3D images were imported into the new coordinate system for standardization based on the aforementioned landmarks (Supplementary Figure 2).

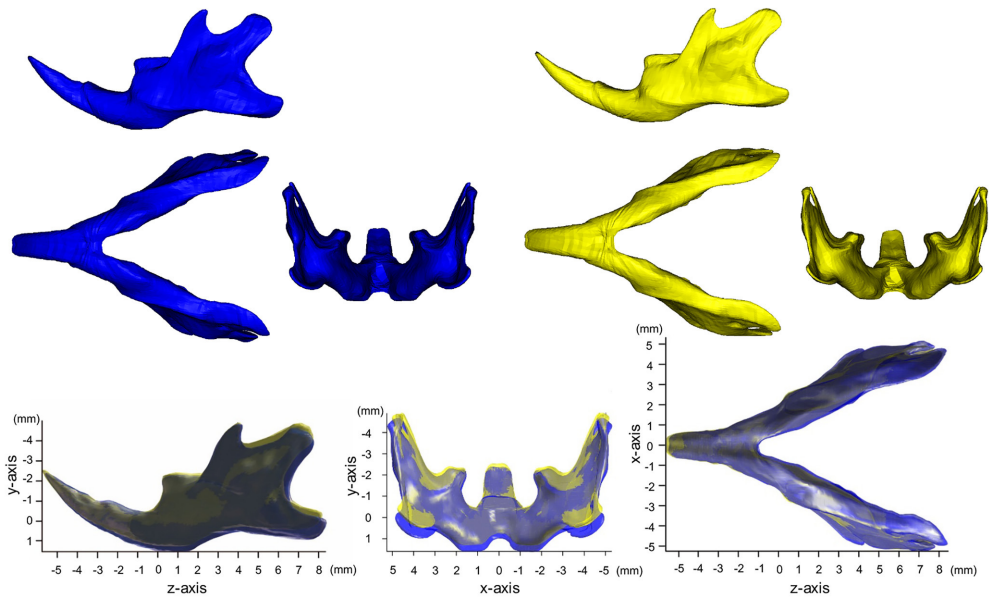

FIGURE 1 | Averaged mandibular surface computed for the SD (Yellow, $n = 9$) and HD groups (Blue, $n = 7$).

Homogeneous Modeling

For each mandibular model, fitting of high-resolution template meshes (Brett et al., 2003) was performed using HBM-Rugle, based on the landmarks assigned to each 3D image. This method automatically generated a homogeneous model consisting of 12,186 points (i.e., nodes of the fitted mesh) on the wire mesh for each model. This technique permits the extraction of relevant surface anatomy from micro-CT data while removing and/or smoothing out non-relevant data, yielding high-resolution, 3D surface data that provide enough detail to facilitate a quantitative assessment while maintaining small file sizes that are easily manipulatable and portable to a range of visualization technologies. The average distance between the points on the meshes was 32 ± 24 μm, which is less than the slice thickness of 96 μm. Thus, the mesh resolution employed was considered adequate for representing the original mandibular shape. The arithmetic means of the coordinate values of each corresponding point on the wire mesh were computed and used to generate the averaged 3D mandibular images for each subject group.

The surface displacement was quantitatively evaluated in each x-, y-, and z-axis in two different ways. The actual displacement and significance of differences were calculated for the 12,186 points on each mesh between the HD and SD groups. The calculated values in millimeters were visualized with color-coding on the computed 3D models of HD mice. Thereafter, the arithmetic means of the coordinate values of each corresponding point on the wire mesh were statistically analyzed for significant differences between the HD and SD groups using a two-sample t-test. A significance probability map (Duffy et al., 1981) of the x-, y-, and z-values was generated to visualize these significant differences.

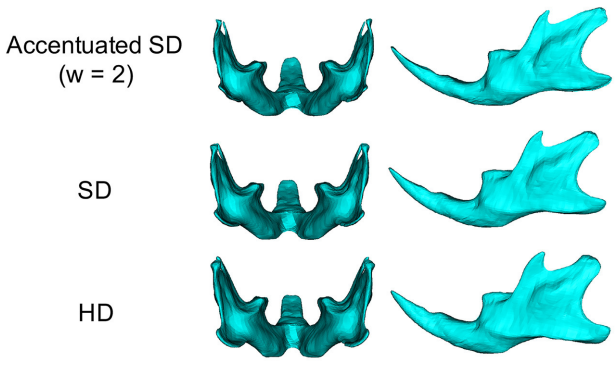

FIGURE 2 | Accentuated SD mandibular surface (**Top**), SD group (**middle**), HD group (**bottom**).

Accentuated Images on SD Feeding

To facilitate the quantitative understanding of the 3D phenotypes associated with SD feeding, accentuated averaged mandibles were computed for SD mice to highlight the site-specific impact on these animals (Tanikawa et al., 2016). For details of the calculations, please see Supplementary Figure 2.

RESULTS

Average and Accentuated Average Images in SD Mice

Figure 1 shows the averaged mandibular surface computed for the SD (Yellow in **Figure 1**) and HD groups (Blue in **Figure 1**) and superimposed at the mental foramen parallel to the occlusal plane (Kiliaridis et al., 1985; Odman et al., 2008) (For more

TABLE 1 | Result summary of the right halves of the mandible for SD when compared with HD.

	Surfaces	X-axis (Transverse direction)		Y-axis (Vertical direction)		Z-axis (Antero-posterior direction)	
		Displacement	*p*-value	Displacement	*p*-value	Displacement	*p*-value
Coronoid process	Lateral (Outer)	Inward	****	NS		NS	
	Medial (Inner)		**				
	Anterior		***				
	Posterior		***				
	Superior		****				
Condyle	Lateral (Outer)	Inward	**	Upward	**	NS	
	Medial (Inner)	NS			*		
	Anterior	Inward	*		**		
	Posterior		*		*		
	Superior		*		*		
Alveolar process	Lateral (Outer)	NS		Upward	*	NS	
	Medial (Inner)	Outward	****		**		
	Anterior	NS			**		
	Posterior	Outward	****		**		
Inferior part of the mandibular body	Lateral (Outer)	NS		Upward	****	NS	
	Medial (Inner)	Inward	*		****		
	Inferior		*		****		
Angular process	Lateral (Outer)	Inward	*	Upward	****	Forward	**
	Medial (Inner)	NS			****		*
	Posterior	Inward	*		****		*
	Superior		*		***		**
	Inferior		*		****		*
Antegonial notch	Lateral (Outer)	NS		Upward	***	Forward	**
	Medial (Inner)				**		**
	Posterior				***		***
Molars	Labial	Inward	**	Upward	***	NS	
	Lingual		***		**		
	Occlusal		**		**		

*NS indicates P > 0.05; *, P ≤ 0.05; **, P ≤ 0.01; ***, P ≤ 0.001; ****, P ≤ 0.0001.*

details, please see Supplementary Figure 3). **Figure 2** shows the accentuated images. These images clearly reveal the manner in which SD mandible differs from the HD in 3D. Details of the x-, y-, and z-axis are shown below and in **Table 1**.

Map of Significant Differences for the X-Axis: Transverse Direction

The most significant changes in the x-axis were observed in the coronoid process (**Figures 3**, **4**, **Table 1**). The outer surface of the coronoid process was displaced significantly in the inward direction in the SD group, with less-marked displacement also observed in the inner surface. Consequently, the transverse distance between the coronoid process and the width of the coronoid process decreased significantly in comparison to the HD group. Since greater inward displacement of the process was noted at the tip than in other areas, the coronoid process became significantly tipped in the inward direction, as revealed by the significant reduction in the angle of the coronoid process. Like the coronoid process, the outer surface of the condyle was also displaced in the inward direction, whereas the inner surface was not significantly displaced. Consequently, the condyle became significantly thinner in the SD group than in the HD group (Supplementary Figures 4, 5).

In contrast, the inner surface of the alveolar process and of the basal bone supporting the alveolar process was significantly displaced in the outward direction, while the outer surface of these bones was not displaced, leading to a reduction in the transverse width of the alveolar bone and the basal bone at the alveolar bone regions (Supplementary Figure 4C).

Map of Significant Differences for the Y-Axis: Vertical Direction

The significance probability map clearly showed that shape changes associated with SD feeding were most prominently

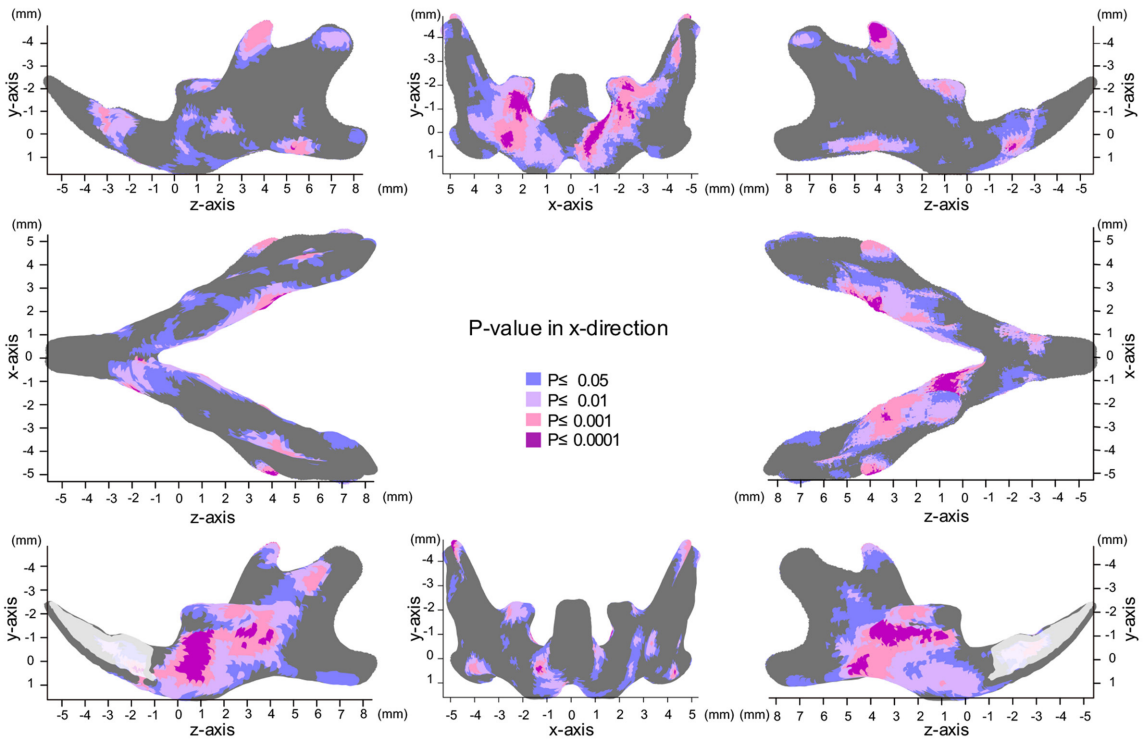

FIGURE 3 | Significance probability map in the x-axis. Blue designates $P \leq 0.05$; Pale pink, $P \leq 0.01$; Dark pink, $P \leq 0.001$; Purple, $P \leq 0.0001$. Top left indicates left lateral view; top middle, posterior view; top right, right lateral view; middle left, inferior view; middle right, superior view; bottom left, medial view of the right halve of the mandible, and bottom right, medial view of the left halve of the mandible.

observed in the y-axis among the three dimensions (**Figures 5**, **6**, **Table 1**). The areas showing significant differences were widely distributed along the inferior surface of the mandible, where remarkable upward displacement was observed due to SD feeding. This led to an apparent decrease in the vertical height of the mandibular corpus (Supplementary Figures 4, 5).

In the angular process, upward displacement was more significant in the inferior surface than in the superior surface, resulting in significant reduction in the vertical width of the angular process (Supplementary Figure 4A). Along the inferior surface of the mandible, upward displacement was most significant at the angular process, causing the mandibular plane angle to steepen. Furthermore, along the inferior border, upward displacement was much less drastic at the antegonial notch, resulting in a relatively flat mandibular surface. In contrast, such upward displacement was not observed in the coronoid process, and less so in the condylar regions. In the condylar process, upward displacement was greater and more significant at the anterior surface than at the posterior surface, resulting in a shallower condyle from the lateral view. These findings can be ascertained more clearly in the accentuated averaged mandibles (**Figure 2**).

Regarding the vertical positon of the molars, the mean displacement was quite small (less than 0.05 mm), but significant upward displacement, i.e., elongation of the molars, was observed ($P \leq 0.05$).

Map of Significant Differences for the Z-Axis: Anterior-Posterior Direction

In the z-axis, significant displacement toward the anterior direction of the angular process and ramus were observed, while the condyle did not show any anterior-posterior displacement (**Figures 7**, **8**, **Table 1**). These results suggest an anterior-posteriorly smaller angular process and greater gonial angle in the SD group than in the HD group.

DISCUSSION

In the present study, we applied a surface-based analysis of micro-CT to evaluate the 3D shape changes in the mandible associated with different food consistencies. The present micro-CT data provide highly accurate 3D imaging data, and 12,186 points on the triangulated mesh were fitted to the curved mandibular surface, which enabled the quantitative topographic assessment of the bony surface and reconstruction of the anatomical architecture images with high resolution. In most previous studies, the distance and/or the angle between the corresponding landmarks were measured after the 3D differences in the superimposed models were usually translated into 2D (Mavropoulos et al., 2004; Swain and Xue, 2009; Enomoto et al., 2010; Saito et al., 2011; Goto et al., 2015). In contrast, in our present approach, a computer-generated averaged mandible

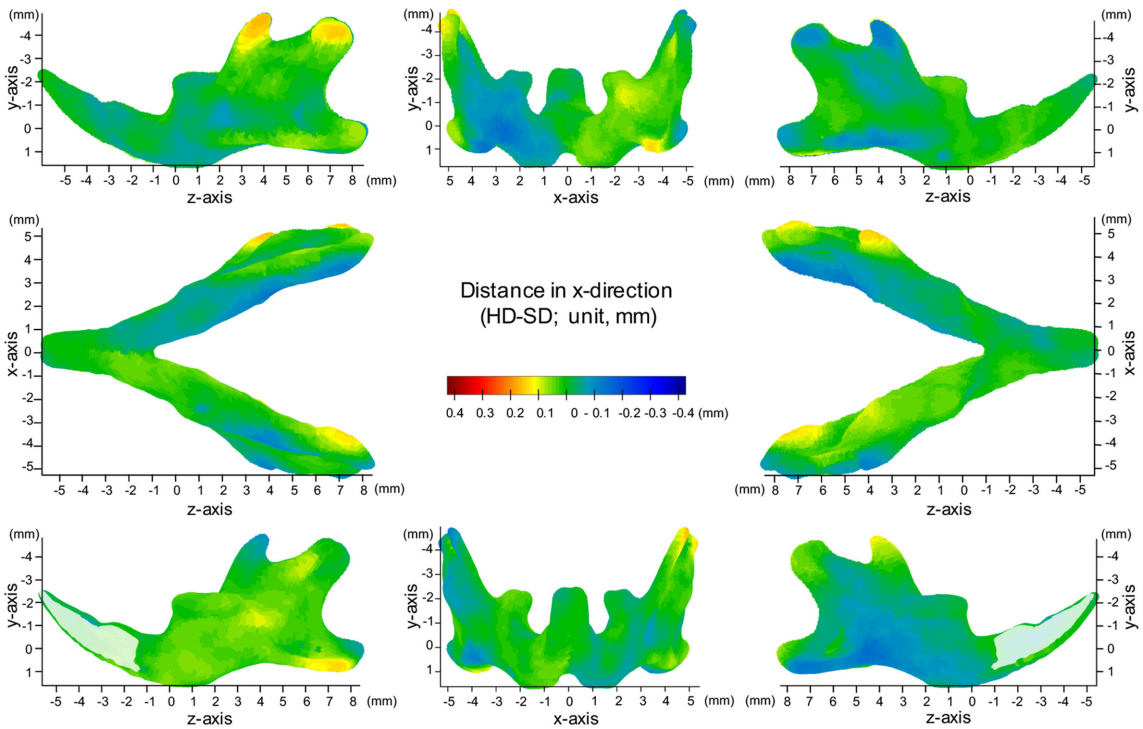

FIGURE 4 | Difference (HD minus SD) in the x-axis. Units: mm. Red indicates that the HD group is greater than the SD group, while blue indicates that the SD group is greater than the HD group.

was superimposed to describe the morphological phenotypes in the mandibular shape, and then variations in the surface morphology were directly visualized and quantified using a 3D image with a map of points of significant difference. In addition, an accentuated averaged SD mandible was developed to confirm and highlight the site-specific skeletal phenotypes associated with SD feeding. This study has shown the novel application of a surface-based analysis for studying the 3D phenotypes of the complicated shapes of the craniofacial structures.

Manipulating raw data using a computer software program carries a risk of possible loss of anatomical detail. A previous study has already validated the procedure for extracting high-resolution surface meshes from micro-CT voxel data (Norman et al., 2014). Another study also verified the absolute 3D accuracy of CT-based bone outer surface meshes using STL (Almukhtar et al., 2014). In our study, micro-CT images were taken with high resolution and a 96 μm slice width. Our experimental conditions in our micro-CT surface-based data analysis using STL format can be used to evaluate the skeletal shape of the rodent mandible.

The craniofacial anatomical changes associated with food consistency have been examined using various experimental animal models, such as monkey (Corruccini and Beecher, 1982), pig (Dias et al., 2011), minipigs (Ciochon et al., 1997) and rats (Kiliaridis et al., 1985, 1999; Kiliaridis, 2006). Mice carry advantages over other mammals because they are less expensive to maintain and genetically modified mice are readily available. However, mice also have disadvantages due to their small size. The smaller size of their experimental samples requires high accuracy in data sampling, especially in the evaluation of topographical changes. In previous 2D analyses using cephalograms, landmarks were difficult to locate compared using CT, and head positioning and mandibular orientation were critical. In addition, 2D cephalometric analyses provided linear and angular measurements, which explains why only a fraction of the changes in the complicated shapes of the mandible were noted. The present combination of micro-CT and an STL analysis overcomes these problems in quantitative morphometric analyses. In the present study, we were able to identify significant shape changes 6 weeks after the start of SD feeding. The duration of the experimental period was also much shorter than in similar previous studies, in which the experimental period lasted about 6 months (Renaud et al., 2010; Anderson et al., 2014). Our novel approach involving a surface-based analysis provided advantages over 2D approaches with respect to the non-destructive and 3D visualization and quantification of the morphology of the experimental materials.

Craniofacial dental and skeletal changes were better detected by superimposing the cephalograms on the stable natural reference structures. The superimposition of the CBCT images of the growing mandible makes it possible to determine the regions of bone apposition and resorption. The reference plane and/or points should be stable, especially when growing experimental animals are used. Previous studies have suggested that the mental foramen and lingual foramen are relatively stable landmarks on

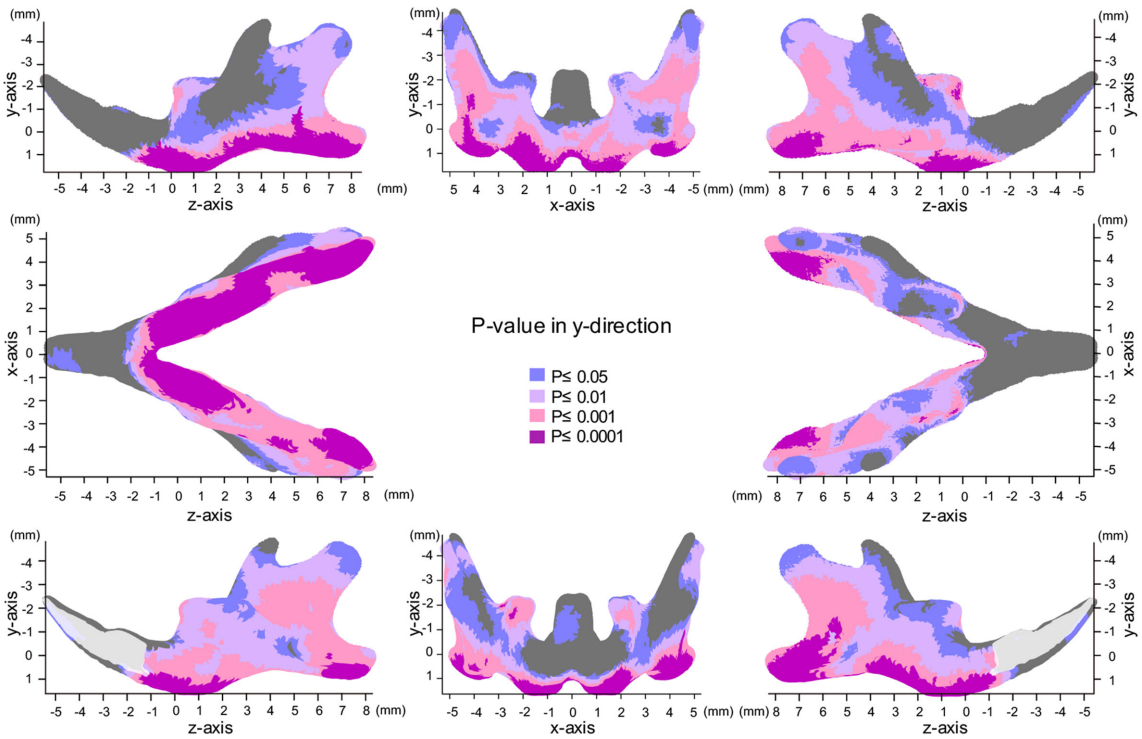

FIGURE 5 | Significance probability map in the y-axis. Blue designates $P \leq 0.05$; Pale pink, $P \leq 0.01$; Dark pink, $P \leq 0.001$; Purple, $P \leq 0.0001$. Top left indicates left lateral view; top middle, posterior view; top right, right lateral view; middle left, inferior view; middle right, superior view; bottom left, medial view of the right halve of the mandible, and bottom right, medial view of the left halve of the mandible.

the growing mandible because no muscles are attached there (Mavropoulos et al., 2004). However, we found that the bone surface around the lingual foramen was actively modeled and the changes associated with SD in its vertical position were significant. Therefore, only the mental foramen was selected as the point of origin for morphological comparison, and the occlusal plane was additionally used to define the x-z plane.

The patients with hypofunctioning muscles often showed an anterior open bite due to significant posterior tooth eruption, possibly because the reduced mechanical loading on the molars due to SD allows these teeth to further erupt (Lieberman et al., 2004). In our present experiments, the bone surface modeling resulted from a combination of normal growth and the effect of SD. In a previous animal study evaluating the effects of SD on molar eruption, the findings were inconclusive (Maki et al., 2002; Odman et al., 2008). In contrast, our present analysis clearly detected significant elongation of the molars due to SD when evaluated using our reference plane.

The present significance difference map clearly indicated where the SD-induced skeletal shape changes appear on the averaged 3D mandibular images in the x-, y-, and z-axis. The present maps for the x-, y-, and z-axis showed that the y-axis displacement was most evident and the regions showing significant differences in the y-axis were the most widely distributed on the averaged mandibular images, indicating that mandibular growth in the vertical direction was most affected by SD among the 3D changes. The present findings are reasonable because the masticatory muscle runs in the vertical direction, and the direct effect of an SD appears first in the vertical direction.

The present surface map analysis provided for the first time quantitative and comparable 3D data, thereby explaining how the previous findings in the mandibular shape changes were associated with SD. A previous study described SD-induced morphological phenotypes, such as a decreased gonial process, decreased posterior height of the corpus, a steep mandibular plane, a vertically reduced angular process and a shallower antegonial notch (Kiliaridis et al., 1985; Kiliaridis, 2006). Such anatomical changes were clearly explained by region-specific vertical bone modeling on the bone surface, as demonstrated by the significance difference map of y-axis. In other words, our surface-based analysis provided quantitative evidence of how the masticatory activity affects the site-specific response on the bone surface and consequently the 3D complicated growth of the mandible.

With respect to the association between feeding style and craniofacial evolution, our conclusions are consistent with those drawn through mathematical simulations using Finite Element models (Cox et al., 2012; Tsouknidas et al., 2017). For example, it has been shown that rodents have a mechanically efficient morphology of masticatory musculature and skulls to their feeding style, i.e., gnawing or chewing (Cox et al., 2012). Feeding style was also proven to result in varying loading patterns

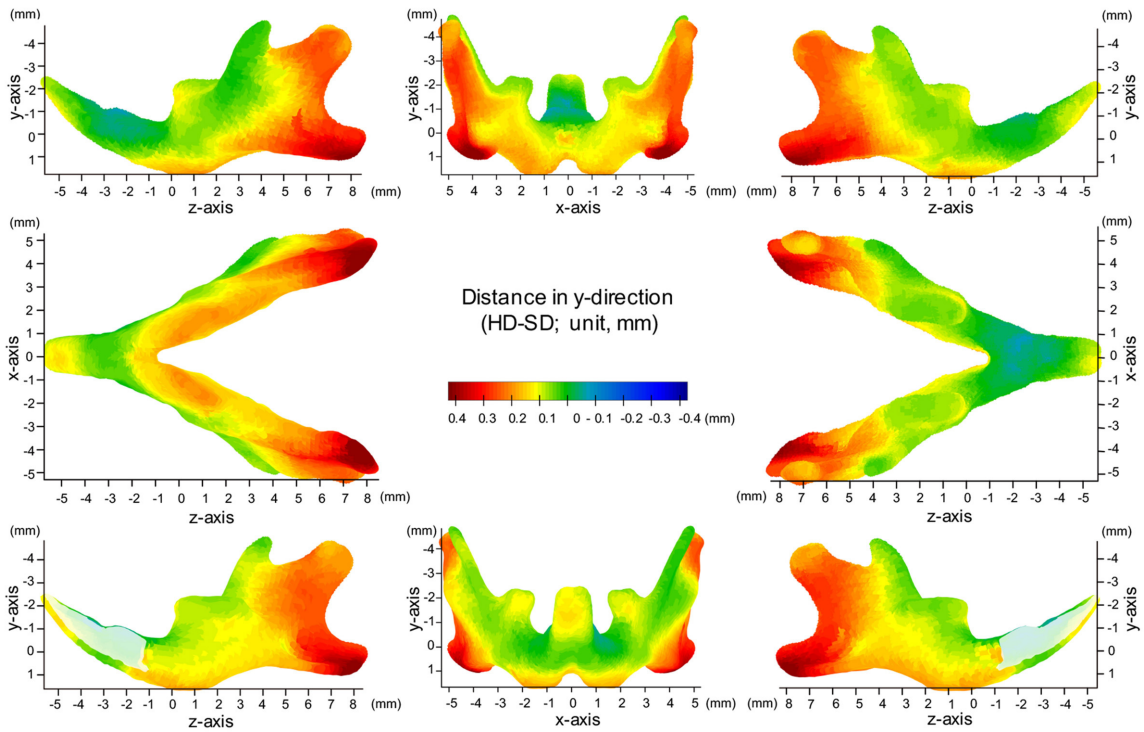

FIGURE 6 | Difference (HD minus SD) in the y-axis. Units: mm. Red indicates that the HD group is greater than the SD group, while blue indicates that the SD group is greater than the HD group.

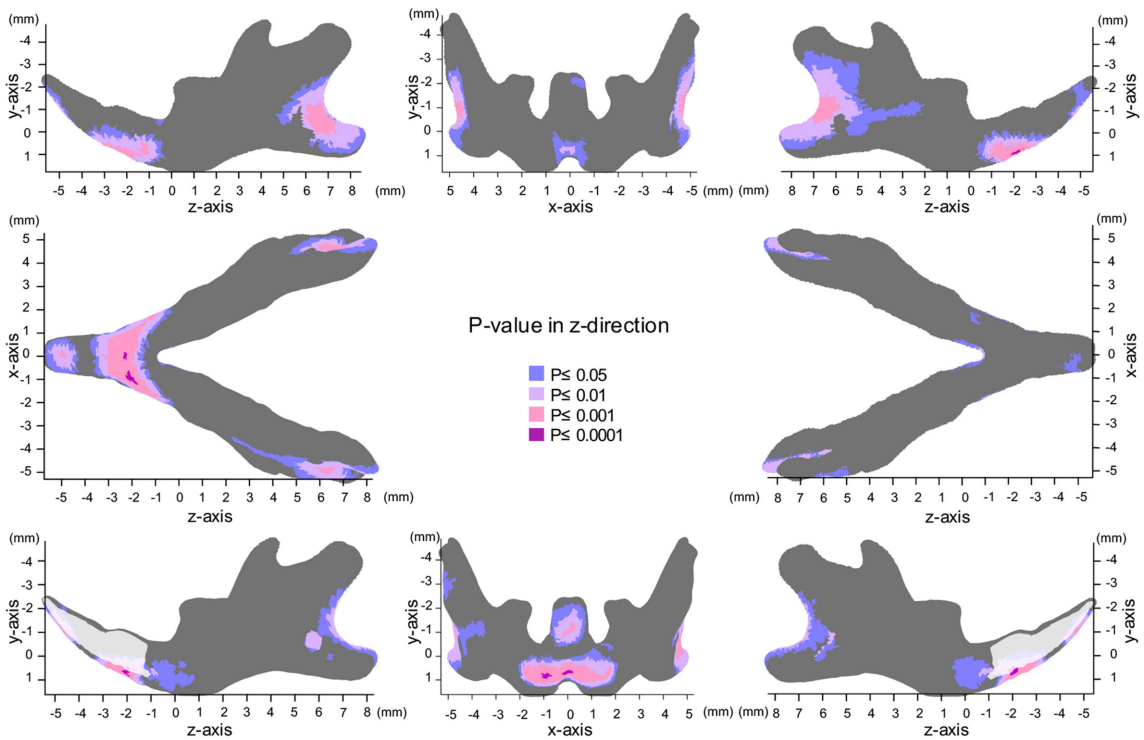

FIGURE 7 | Significance probability map in the z-axis. Blue designates $P \leq 0.05$; Pale pink, $P \leq 0.01$; Dark pink, $P \leq 0.001$; Purple, $P \leq 0.0001$. Top left indicates left lateral view; top middle, posterior view; top right, right lateral view; middle left, inferior view; middle right, superior view; bottom left, medial view of the right halve of the mandible, and bottom right, medial view of the left halve of the mandible.

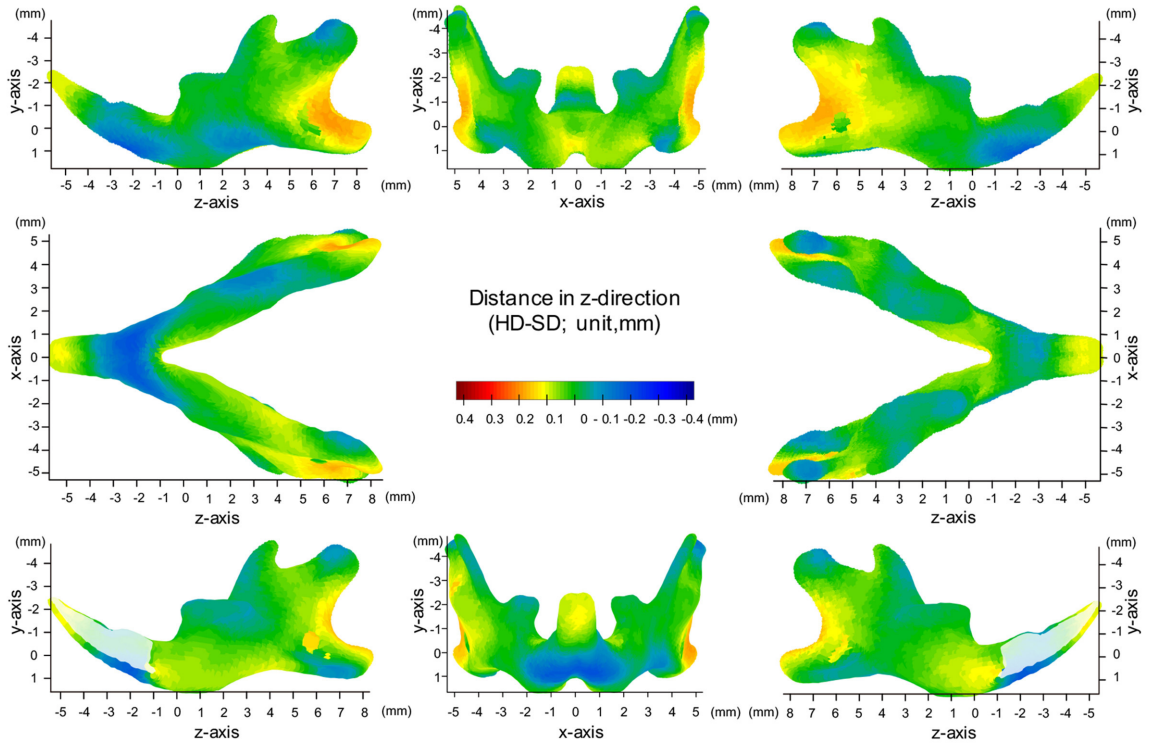

FIGURE 8 | Difference (HD minus SD) in the z-axis. Units: mm. Red indicates that the HD group is greater than the SD group, while blue indicates that the SD group is greater than the HD group.

on the mandibles (Tsouknidas et al., 2017), e.g., loads to the masseter ridge, the mental foramen of the mandible, and the temporomandibular joints. As food texture is known to change the feeding style (Peyron et al., 1997), it would be reasonable to state that the food consistency of SD or HD can influence microevolutionary divergence patterns in mandible shape.

The present study additionally suggested that the shape of the condylar process was also modulated by the masticatory muscle in a complicated manner. It has been established that an SD results in a decreased inclination of the condylar process from the lateral view (Kiliaridis, 2006). The present significance map showed that such angular changes in the condylar process were site-specific displacements between the anterior and posterior surface of the condyle.

Furthermore, a previous study demonstrated a reduction in the transverse width of the condyle in SD mice (Kiliaridis et al., 1999). The present significance map showed that such a reduction was caused by the inward displacement of the outer surface of the condyle. Our analysis therefore demonstrated for the first time the inward tipping of the condyle.

As mentioned above, an SD allowed for the elongation of the molars (Odman et al., 2008). The present significance map showed that the outer surface of the alveolar bone or of the basal bone supporting the alveolar process was not affected, while their inner surface was displaced laterally in the outward direction. Thus far, due to the complicated inner surface morphology, it has been quite difficult to accurately measure its distances and/or angles. The findings of our surface-based analysis, however, clearly suggested that the width of the alveolar process and the basal bone significantly decreased with the elongation of the molars.

Our study has several limitations. Firstly, the sample size for our analysis was relatively small; therefore, it is possible that our results would have differed with a larger sample. Secondly, the age and duration of the SD feeding might have an influence on the morphological variety. Therefore we need further research on the impact of the time-related changes of SD feeding. There is also a limitation in our experimental protocol. In original CT images, the internal structure of the craniofacial bone can be visualized, however, only the bony surface information is extracted and evaluated as STL data in our protocol. Hence, the soft diet-induced changes in cortical bone or cartilage thickness, which was demonstrated in the previous study, were excluded from our interest.

CONCLUSION

In this study, we presented a novel, accurate superimposition protocol for micro-CT data of the mandibular skeletal structures. Our surface-based analysis detected and visualized the areas showing significant deviation associated with SD on averaged 3D images. The present findings provided 3D quantitative evidence supporting previous findings regarding shape changes with additional novel phenotypes in SD mice. Furthermore, its

high accuracy with respect to the quantitative measurement of the bone surface enabled the identification of the anatomical phenotypes in mice in a relatively short period of 6 weeks. In conclusion, our surface-based analysis provided quantitative evidence of how the masticatory activity affects the site-specific response on the bone surface and consequently affects the 3D complicated growth of the mandible in mice.

AUTHOR CONTRIBUTIONS

KK performed experiments. CT developed analytical methods and analyzed the 3D data. TYan performed experiments. HK gave technical support and conceptual advice. TYam supervised its analysis and edited the manuscript. All authors discussed the results and implications and commented on the manuscript at all stages.

ACKNOWLEDGMENTS

The present study was partially supported by JSPS KAKENHI Grant Numbers JP17K17325, JP15H02577, JP25862008, and JP26463093.

SUPPLEMENTARY MATERIAL

The Supplementary Material for this article can be found online at: http://journal.frontiersin.org/article/10.3389/fphys.2017.00567/full#supplementary-material

REFERENCES

Almukhtar, A., Ju, X., Khambay, B., McDonald, J., and Ayoub, A. (2014). Comparison of the accuracy of voxel based registration and surface based registration for 3D assessment of surgical change following orthognathic surgery. *PLoS ONE* 9:e93402. doi: 10.1371/journal.pone.0093402

Anderson, P. S., Renaud, S., and Rayfield, E. J. (2014). Adaptive plasticity in the mouse mandible. *BMC Evol. Biol.* 14, 85. doi: 10.1186/1471-2148-14-85

Boell, L., and Tautz, D. (2011). Micro-volutionary divergence patterns of mandible shapes in wild house mouse (*Mus musculus*) populations. *BMC Evol. Biol.* 11:306. doi: 10.1186/1471-2148-11-306

Bouvier, M., and Hylander, W. L. (1984). The effect of dietary consistency on gross and histologic morphology in the craniofacial region of young rats. *Am. J. Anat.* 170, 117–126. doi: 10.1002/aja.1001700109

Brett, A., Brian, C., and Zoran, P. (2003). The space of all body shapes: reconstruction and parameterization from range scans. *ACM Trans. Graph.* 22, 587–594. doi: 10.1145/1201775.882311

Ciochon, R. L., Nisbett, R. A., and Corruccini, R. S. (1997). Dietary consistency and craniofacial development related to masticatory function in minipigs. *J. Craniofac. Genet. Dev. Biol.* 17, 96–102.

Corruccini, R. S. (1984). An epidemiologic transition in dental occlusion in world populations. *Am. J. Orthod.* 86, 419–426. doi: 10.1016/S0002-9416(84)90035-6

Corruccini, R. S., and Beecher, R. M. (1982). Occlusal variation related to soft diet in a nonhuman primate. *Science* 218, 74–76. doi: 10.1126/science.7123221

Cox, P. G., Rayfield, E. J., Fagan, M. J., Herrel, A., Pataky, T. C., and Jeffery, N. (2012). Functional evolution of the feeding system in rodents. *PLoS ONE* 7:e36299. doi: 10.1371/journal.pone.0036299

Dias, G. J., Cook, R. B., and Mirhosseini, M. (2011). Influence of food consistency on growth and morphology of the mandibular condyle. *Clin. Anat.* 24, 590–598. doi: 10.1002/ca.21122

Duffy, F. H., Bartels, P. H., and Burchfiel, J. L. (1981). Significance probability mapping: an aid in the topographic analysis of brain electrical activity. *Electroencephalogr. Clin. Neurophysiol.* 51, 455–462. doi: 10.1016/0013-4694(81)90221-2

Enomoto, A., Watahiki, J., Yamaguchi, T., Irie, T., Tachikawa, T., and Maki, K. (2010). Effects of mastication on mandibular growth evaluated by microcomputed tomography. *Eur. J. Orthod.* 32, 66–70. doi: 10.1093/ejo/cjp060

Gelaude, F., Vander Sloten, J., and Lauwers, B. (2008). Accuracy assessment of CT-based outer surface femur meshes. *Comput. Aided Surg.* 13, 188–199. doi: 10.3109/10929080802195783

Goto, S., Fujita, Y., Hotta, M., Sugiyama, A., and Maki, K. (2015). Influence of differences in the hardness and calcium content of diets on the growth of craniofacial bone in rats. *Angle Orthod.* 85, 969–979. doi: 10.2319/102214-765.1

Hichijo, N., Kawai, N., Mori, H., Sano, R., Ohnuki, Y., Okumura, S., et al. (2014). Effects of the masticatory demand on the rat mandibular development. *J. Oral Rehabil.* 41, 581–587. doi: 10.1111/joor.12171

Hichijo, N., Tanaka, E., Kawai, N., Ruijvan, L., and Langenbach, G. J. (2015). Effects of decreased occlusal loading during growth on the mandibular bone characteristics. *PLoS ONE* 10:e0129290. doi: 10.1371/journal.pone.0129290

Kikinis, R., and Pieper, S. (2011). 3D Slicer as a tool for interactive brain tumor segmentation. *Conf. Proc. IEEE Eng. Med. Biol. Soc.* 2011, 6982–6984. doi: 10.1109/IEMBS.2011.6091765

Kiliaridis, S. (2006). The importance of masticatory muscle function in dentofacial growth. *Semin. Orthod.* 2, 110–119. doi: 10.1053/j.sodo.2006.01.004

Kiliaridis, S., Engstrom, C., and Thilander, B. (1985). The relationship between masticatory function and craniofacial morphology. I. A cephalometric longitudinal analysis in the growing rat fed a soft diet. *Eur. J. Orthod.* 7, 273–283. doi: 10.1093/ejo/7.4.273

Kiliaridis, S., Thilander, B., Kjellberg, H., Topouzelis, N., and Zafiriadis, A. (1999). Effect of low masticatory function on condylar growth: a morphometric study in the rat. *Am. J. Orthod. Dentofacial Orthop.* 116, 121–125. doi: 10.1016/S0889-5406(99)70207-6

Klingenberg, C. P., and Leamy, L. J. (2001). Quantitative genetics of geometric shape in the mouse mandible. *Evolution* 55, 2342–2352. doi: 10.1111/j.0014-3820.2001.tb00747.x

Larsson, E., Ogaard, B., Lindsten, R., Holmgren, N., Brattberg, M., and Brattberg, L. (2005). Craniofacial and dentofacial development in pigs fed soft and hard diets. *Am. J. Orthod. Dentofacial Orthop.* 128, 731–739. doi: 10.1016/j.ajodo.2004.09.025

Lieberman, D. E., Krovitz, G. E., Yates, F. W., Devlin, M., and St Claire, M. (2004). Effects of food processing on masticatory strain and craniofacial growth in a retrognathic face. *J. Hum. Evol.* 46, 655–677. doi: 10.1016/j.jhevol.2004.03.005

Maki, K., Nishioka, T., Shioiri, E., Takahashi, T., and Kimura, M. (2002). Effects of dietary consistency on the mandible of rats at the growth stage: computed X-ray densitometric and cephalometric analysis. *Angle Orthod.* 72, 468–475. doi: 10.1043/0003-3219(2002)072<0468:EODCOT>2.0.CO;2

Mavropoulos, A., Kiliaridis, S., Bresin, A., and Ammann, P. (2004). Effect of different masticatory functional and mechanical demands on the structural adaptation of the mandibular alveolar bone in young growing rats. *Bone* 35, 191–197. doi: 10.1016/j.bone.2004.03.020

Nakano, H., Watahiki, J., Kubota, M., Maki, K., Shibasaki, Y., Hatcher, D., et al. (2003). Micro X-ray computed tomography analysis for the evaluation of asymmetrical condylar growth in the rat. *Orthod Craniofac Res.* 6 (Suppl. 1), 168–172; discussion: 179–182. doi: 10.1034/j.1600-0544.2003.252.x

Norman, D. G., Getgood, A., Thornby, J., Bird, J., Turley, G. A., Spalding, T., et al. (2014). Quantitative topographic anatomy of the femoral ACL footprint: a micro-CT analysis. *Med. Biol. Eng. Comput.* 52, 985–995. doi: 10.1007/s11517-014-1196-0

Odman, A., Mavropoulos, A., and Kiliaridis, S. (2008). Do masticatory functional changes influence the mandibular morphology in adult rats. *Arch. Oral Biol.* 53, 1149–1154. doi: 10.1016/j.archoralbio.2008.07.004

Peyron, M. A., Maskawi, K., Woda, A., Tanguay, R., and Lund, J. P. (1997). Effects of food texture and sample thickness on mandibular movement

and hardness assessment during biting in man. *J. Dent. Res.* 76, 789–795. doi: 10.1177/00220345970760031201

Renaud, S., Auffray, J. C., and de la Porte, S. (2010). Epigenetic effects on the mouse mandible: common features and discrepancies in remodeling due to muscular dystrophy and response to food consistency. *BMC Evol. Biol.* 10:28. doi: 10.1186/1471-2148-10-28

Saito, F., Kajii, T. S., Sugawara-Kato, Y., Tsukamoto, Y., Arai, Y., Hirabayashi, Y., et al. (2011). Morphological evaluation of cranial and maxillary shape differences of the brachymorphic mouse with spontaneous malocclusion using three-dimensional micro-computed tomography. *Orthod. Craniofac. Res.* 14, 100–106. doi: 10.1111/j.1601-6343.2011.01513.x

Swain, M. V., and Xue, J. (2009). State of the art of Micro-CT applications in dental research. *Int. J. Oral Sci.* 1, 177–188. doi: 10.4248/IJOS09031

Tanikawa, C., Zere, E., and Takada, K. (2016). Sexual dimorphism in the facial morphology of adult humans: A three-dimensional analysis. *Homo* 67, 23–49. doi: 10.1016/j.jchb.2015.10.001

Tsouknidas, A., Jimenez-Rojo, L., Karatsis, E., Michailidis, N., and Mitsiadis, T. A. (2017). A bio-realistic finite element model to evaluate the effect of masticatory loadings on mouse mandible-related tissues. *Front. Physiol.* 8:273. doi: 10.3389/fphys.2017.00273

Yamada, K., and Kimmel, D. B. (1991). The effect of dietary consistency on bone mass and turnover in the growing rat mandible. *Arch. Oral Biol.* 36, 129–138. doi: 10.1016/0003-9969(91)90075-6

Conflict of Interest Statement: The authors declare that the research was conducted in the absence of any commercial or financial relationships that could be construed as a potential conflict of interest.

APPENDIX

Reliability of the Identification of Landmarks

To determine the intra-observer reliability of the identification of landmarks, the 3D images of 10 subjects were randomly selected, and the coordinate values of the landmarks were determined by the experimenter (KK). The digitization process was then repeated a week later, and the two sets of results were compared. The results showed a mean absolute difference of $45.7 \pm 37.4\,\mu$m. These values were small compared to the slice thickness ($96\,\mu$m) of the micro-CT.

Accentuated Images on SD Feeding

To quantitatively facilitate our instantaneous and intuitive understanding of the skeletal changes in the mandible associated with SD, accentuated averaged mandibular forms, $\overline{AccA(SD_w)}$, were calculated for the SD and HD groups to highlight the differences between the two subject groups, where

$$\overline{AccA(SD_w)} = \overline{A(HD)} + w\left(\overline{A(SD)} - \overline{A(HD)}\right)(w = 2)$$

and $\overline{A(HD)}$ and $\overline{A(SD)}$ are the arithmetic means of the coordinate values for the HD and SD group, respectively, and w is the weight value.

Selection of an Appropriate Reference Plane

The selection of an appropriate reference plane directly affects the interpretation of the 3D skeletal changes associated with different food consistencies. SD results in a decreased occlusal load and masticatory muscle activity, which affects the bone activity directly or indirectly. In a previous 2D study, the occlusal plane was used as reference plane for superimposition in growing experimental animals, and such superimposition clearly demonstrated differences in the shape changes of the mandible between SD and HD rats (Kiliaridis et al., 1985). However, the reference anatomical points should be less influenced by mastication activity during in mandibular growth. Previous studies have used reference planes connecting the mental foramen and lingual foramen (Odman et al., 2008). These landmarks are known to be relatively stable on the growing mandible. In this study, we found that the occlusal plane was significantly displaced upward when evaluated from the mental foramen in SD rats. We also found that the vertical position of the mandibular foramen was unstable in our experimental protocol (Supplementary Figure 3B). Therefore, the averaged 3D images were superimposed at the mental foramen parallel to the occlusal plane (Supplementary Figure 3A)

frontiers in Physiology

REVIEW
published: 24 January 2017
doi: 10.3389/fphys.2016.00678

A Concert between Biology and Biomechanics: The Influence of the Mechanical Environment on Bone Healing

Vaida Glatt[1,2]*, *Christopher H. Evans*[3] and *Kevin Tetsworth*[2,4]

[1] Department of Orthopaedic Surgery, University of Texas Health Science Center San Antonio, San Antonio, TX, USA, [2] Orthopaedic Research Centre of Australia, Brisbane, QLD, Australia, [3] Rehabilitation Medicine Research Center, Mayo Clinic, Rochester, NY, USA, [4] Department of Orthopaedic Surgery, Royal Brisbane and Women's Hospital, Herston, QLD, Australia

In order to achieve consistent and predictable fracture healing, a broad spectrum of growth factors are required to interact with one another in a highly organized response. Critically important, the mechanical environment around the fracture site will significantly influence the way bone heals, or if it heals at all. The role of the various biological factors, the timing, and spatial relationship of their introduction, and how the mechanical environment orchestrates this activity, are all crucial aspects to consider. This review will synthesize decades of work and the acquired knowledge that has been used to develop new treatments and technologies for the regeneration and healing of bone. Moreover, it will discuss the current state of the art in experimental and clinical studies concerning the application of these mechano-biological principles to enhance bone healing, by controlling the mechanical environment under which bone regeneration takes place. This includes everything from the basic principles of fracture healing, to the influence of mechanical forces on bone regeneration, and how this knowledge has influenced current clinical practice. Finally, it will examine the efforts now being made for the integration of this research together with the findings of complementary studies in biology, tissue engineering, and regenerative medicine. By bringing together these diverse disciplines in a cohesive manner, the potential exists to enhance fracture healing and ultimately improve clinical outcomes.

Keywords: bone repair/regeneration, dynamyzation/reverse dynamization, mechanical environment, fixation stability, large bone defects, fracture fixation, external/internal fracture fixation, bone healing/biomechanics

OPEN ACCESS

Edited by:
Thimios Mitsiadis, University of Zurich, Switzerland

Reviewed by:
Denitsa Docheva, University Regensburg Medical Centre, Germany
Vicki Rosen, Harvard University, USA
Claudio Cantù, University of Zurich, Switzerland

***Correspondence:**
Vaida Glatt
glatt@uthscsa.edu

Specialty section:
This article was submitted to Craniofacial Biology and Dental Research, a section of the journal Frontiers in Physiology

Received: *08 November 2016*
Accepted: *20 December 2016*
Published: *24 January 2017*

Citation:
Glatt V, Evans CH and Tetsworth K (2017) A Concert between Biology and Biomechanics: The Influence of the Mechanical Environment on Bone Healing. Front. Physiol. 7:678. doi: 10.3389/fphys.2016.00678

INTRODUCTION

Fracture healing generally occurs on a routine basis and is therefore easily dismissed and often overlooked, but the process is no less remarkable. This involves a spectrum of growth factors and other stimuli interacting with one another in an organized response, and is in many ways analogous to the performance of a symphony. When an orchestra appears in concert, many musicians playing different types of instruments can create an auditory masterpiece through a carefully coordinated, and exquisitely timed performance. The same is true with fracture healing, where a wide variety of biological factors and their products must also perform in a highly coordinated fashion. To achieve

the desired outcome, each individual component must fulfill a specific and equally important function. The role of the various biological factors, the timing and spatial relationship of their introduction, and how the mechanical environment influences this activity are all critical aspects to consider. The best results require the concerted activity of each modulator in the correct amounts at the proper times, many working in harmony with other factors and their products to produce robust callus resulting in fracture union. The critical role of coordinating the complex interaction of factors characteristic of this biological orchestra is filled by the mechanical environment, and one could consider this the conductor of fracture healing. Most significantly, understanding how this process normally occurs is vitally important in managing those instances when the performance is sub-optimal and a fracture fails to unite.

While the biological basis of bone healing has been well studied, less is known about the mechanical factors that play unique and key roles in the success of the repair process. It has been known since the time of Wolff (1892) that bone is exquisitely responsive to its mechanical environment. The general principal of Wolff's Law (1892) states that skeletal elements are strategically placed to optimize strength in relation to the distribution of applied loading, and that the mass of the skeletal elements is directly related to the magnitude of the applied loads (Wolff, 1986). Even earlier, Roux (1881) proposed the idea that cells within tissues engage in "a competition for the functional stimulus," and it is this competition that determines cell survivorship and therefore tissue phenotype (Roux, 1881). He hypothesized that the mechanical environment has a very specific relationship with phenotype, where tension results in fibrous connective tissue, shear forms cartilage, and compression produces bone. Roux called this phenomenon *Entwicklungsmechanik* (developmental mechanics). He postulated that structural adaptation of tissue to mechanical loads is a direct consequence of competition between cells. Years later, the discoveries of Pauwels refined the concept that the differentiation of mesenchymal progenitor cells into chondrocytes and osteoblasts is regulated by mechanical forces (**Figure 1**). Since then, many researchers have investigated this notion and have shown the differential effects of the type and magnitude of mechanical forces on tissue formation (Pauwels, 1960).

This review discusses the current state of the art concerning the application of these mechano-biological principles to enhance bone healing, by controlling the mechanical environment under which bone regeneration takes place. PubMed served as the main search engine to identify relevant articles. Keyword combinations included variations of the following phrases: mechanical environment; fracture healing; bone healing; fixation stability; dynamization; large bone defects; tissue regeneration; animal models; growth factors; bone morphogenetic proteins;

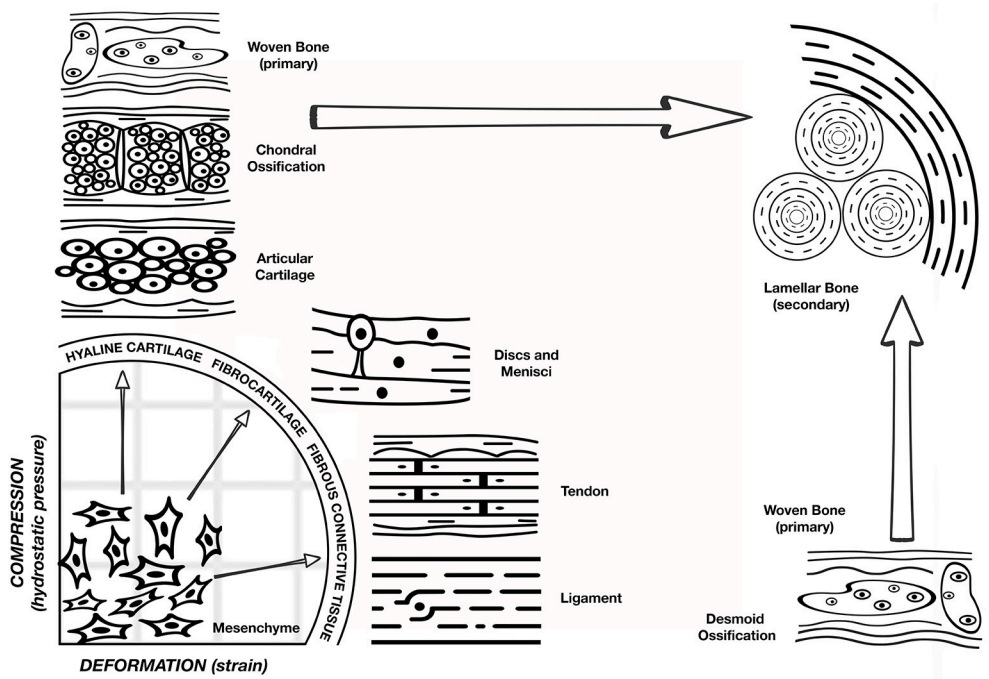

FIGURE 1 | Pauwel's concept of tissue differentiation: a schematic representation of the hypothesized influence of the biophysical stimuli on tissue phenotype. Deformation of shape strain is on the x axis and the hydrostatic compression is on the y axis. A combination of these stimuli will act on the multipotent progenitor cells leading to hyaline cartilage, fibrocartilage, or fibrous connective tissue as shown on the quadrant perimeter. Depending on the response of the mechanical environment to the presence of these tissues, osteoblast proliferation and ossification can occur. However, bone regeneration occurs only after stabilization of the mechanical environment by the formation of soft tissue. (Figure adapted from Weinans and Prendergast, 1996).

mechanical signals; mesenchymal stem cells; intramedullary nails; external fixators; internal fixators; orthopedics; fracture fixation.

BASIC PRINCIPLES

Bone is a mechanosensitive organ and has the ability to respond to the mechanical stimuli placed upon it. After skeletal maturation, it continues to remodel throughout life and is reshaped in response to the mechanical forces acting upon it. The role of physical factors on bone regeneration cannot be addressed without mention of mechano-biology, which is the study of how mechanical and physical conditions regulate biological processes (Carter et al., 1998). Much of our present day understanding about the effects of mechanical forces on tissue differentiation comes from Pauwels (1960). Building on the earlier developmental mechanics of Roux, he was one of the first to recognize that physical factors cause stress and deformation of mesenchymal progenitors, including what we now refer to as mesenchymal stem cells (MSCs), and that such mechanical stimuli could determine cell fate. Pauwels (1960) compared the mechanical environment of cells in a fracture callus with fracture repair patterns, and proposed that deformation (strain) of shape is a specific stimulus for the formation of collagenous fibers, and hydrostatic compression is the specific stimulus for the formation of cartilage. Osteogenesis, however, requires that the mechanical environment first becomes stabilized by the presence of fibrous tissue (Perren and Cordey, 1980). Therefore, Pauwels' hypothesis, as shown in **Figure 1**, is that the mechanical environment determines tissue phenotype. Carter (Carter et al., 1988) further developed this concept as a function of shear and hydrostatic stress, called the osteogenic index.

It is possible to use such concepts to help explain the cellular events occurring during fracture healing. A study by Lacroix and Prendergast showed that local tissue stresses and strains not only alter the pressure on bone cells, but also influence cell differentiation (Lacroix and Prendergast, 2002). For instance, in the fracture gap after fixation hydrostatic pressure is relatively low, but intrafragmentary strains (IFS) are relatively high. However, when callus becomes larger the stiffness in the fracture increases, while at the same time rising hydrostatic pressure decreases the matrix permeability, and this in turn reduces the shear strains in the fracture gap. In this environment, increasing numbers of chondrocytes are formed, and endochondral ossification begins. As more collagen matrix is produced the strain declines further, more osteoblasts accumulate, and ossification predominates. It is plausible that mesenchymal progenitors cannot differentiate into bone cells or chondrocytes unless a suitable biophysical environment for tissue differentiation is present. Therefore, for bone healing to occur the fracture environment has to be exposed to the strain rates that elicit bridging callus, increasing collagen synthesis, and rising hydrostatic pressures.

In fact, it is widely accepted that the molecular and cellular responses to the spatiotemporally specific mechanical stimuli applied at the osteotomy site will guide the migration, proliferation, and differentiation of endogenous skeletal progenitor cells. Collaborative research efforts in the fields of molecular and cell biology, bioengineering, and the material sciences expanded our understanding of the molecular pathways involved in the process of bone regeneration including mechanotransduction, progenitor cells homing and differentiation, and neovascularization. From these studies specific molecular pathways have been identified as being the critical contributors to the tissue regeneration process including those involving growth factors, morphogens, cytokines, signal transduction, and epigenetic changes, among others (Carter et al., 1998; Kelly and Jacobs, 2010; Wang et al., 2011, 2012; Thompson et al., 2012). However, exactly how the bone cell population is influenced by the mechanical environment when responding to mechanical signals to regenerate and remodel a successful structure is still uncertain. Nevertheless, it is certain that it occurs at various levels including organ, tissue, cellular, and molecular contributions. For instance, exposure to the physical factors at the organ level such as force, displacement, and deformation at the fracture site will have an effect on the behavior of bone cells, which in turn will determine the type of tissue formed. At the tissue level, the mechanical stimulus characterized by stress and strain parameters will determine different patterns of tissue formation. Moreover, the influence of mechanical signals at the cellular level would take into account changes of cell shape, cell pressure, as well as oxygen tension, and this will determine the patterns and production of extracellular matrix components. And finally, mechanical signals sensed at the molecular level will determine changes in the cytoskeleton, resulting in intracellular signaling that promotes specific cell activities. While the specifics of these processes are beyond the scope of this review article, details can be found in the review articles by Rubin, Chen, and many others (Rubin and Hausman, 1988; Uhthoff et al., 1994; Carter et al., 1998; Morgan et al., 2008; Huang and Ogawa, 2010; Kelly and Jacobs, 2010; Thompson et al., 2012).

Understanding the nature of these mechanical cues, and the biological responses to them at various levels is very important as this will determine the quality, the type of tissue formed, and the rate of the healing process. For example, at the organ level, instability of fracture fixation will result in fibrous and cartilaginous tissue formation, that will most likely lead to a delayed union or a non-union. At the cellular level, excessive mechanical stimulation will influence cells to proliferate and differentiate toward specific lineages, and this will be dependent upon the flexibility of the fracture fixation. Likewise, at the molecular level, specific pathways will be activated to produce a specific type of tissue, reflecting mechanical cues at the organ level. The aforementioned clearly shows how a stimulus initiated at the organ level (fixation stability) would lead to changes at the molecular level which determine the rate, type, and the quality of the tissue regeneration process. Numerous studies have also shown that bone regeneration and remodeling are sensitive to changes in strain magnitude (Rubin and Lanyon, 1984), the number of loading cycles (Rubin and Lanyon, 1984), the distribution of loading, and the rate of strain. Findings from these studies suggest that cells respond not only to mechanical

deformation (hydrostatic pressure) (Qin et al., 2003) but also to fluid flow (Meinel et al., 2004; Jekir and Donahue, 2009; Stiehler et al., 2009; Qin and Hu, 2014), and in an *in vivo* setting both of these biomechanical stimuli are present (Pacicca et al., 2002; Huang and Ogawa, 2010). Furthermore, the cellular response from biomechanical loading is heavily dependent upon the magnitude of strain (Yanagisawa et al., 2007, 2008; Luu et al., 2009; Klein-Nulend et al., 2013; Uzer et al., 2015), the type of loading conditions (Tanno et al., 2003; Haasper et al., 2008), and on the differentiation stage of the progenitor cells (Weyts et al., 2003; Jansen et al., 2004).

INFLUENCE OF MECHANICAL FORCES ON BONE HEALING: FRACTURES, OSTEOTOMIES, AND SEGMENTAL DEFECTS

Many articles describe the effects of mechanical stimulation on the healing of fractures in both laboratory animals and human subjects. The work of Perren, Carter, Claes, Kenwright, Goodship, and others have shown convincingly that manipulation of the ambient mechanical forces around a fracture site can determine whether a fracture heals or not, and will determine both the rate of healing and whether healing occurs via intramembranous or endochondral pathways (Carter and Wong, 1988a,b; Grundnes and Reikerås, 1993; Utvåg and Reikerås, 1998; Augat et al., 2005). The mechanical environment is determined by the stiffness of fracture fixation and weight bearing; if fixation is either too flexible or too rigid the healing might fail. For instance, as long as high strain forces exist at a fracture site (inadequate stability), fibrous tissue will remain, and stabilizing bony callus will be unable to form. If such conditions continue for long enough, a fibrous non-union will result (Carter et al., 1988; Claes et al., 1997). Earlier studies agreed that rigid fixation provided the best clinical outcome, and this has led to the wide use of nailing and plating to provide rigid internal fixation (Grundnes and Reikerås, 1993). However, some studies have also demonstrated that excessively rigid fixation may paradoxically impair fracture healing (Goodship and Kenwright, 1985; Aalto et al., 1987; Chao et al., 1989). Major concerns raised are the possible inhibition of external callus formation, maintenance of a fracture gap aggravated by bone-end resorption, and the excessive protection of the healing bone from normal stresses (stress shielding), producing adverse remodeling. Consequently, based on the results from these studies, many mechanical factors have been identified as having an influence on fracture healing, including the magnitude and direction of interfragmentary movement (IFM), the type of fracture, and fracture geometry (Aro and Chao, 1993; Augat et al., 1998, 2003).

IFM is the movement occurring between fracture fragments in response to physiological and external loading of the fractured limb. When the fractured bone is loaded, the fracture fragments displace relative to each other, producing a multiaxial strain that varies spatially throughout the fracture gap (Perren and Cordey, 1980). Depending on the external load phase and muscle activity, any combination of axial forces and bending or torsional moments can occur. There are two main factors that influence IFM; the rigidity of the implant used to stabilize the fracture and the surface area of the fracture fragments, which determine the tissue strain and the cellular reaction in the fracture gap. The amplitude and the direction of IFMs in the fracture gap also depend upon the load applied through weight bearing, muscle forces, and the stiffness of the chosen device (Klein et al., 2003; Augat et al., 2005; Epari et al., 2006). Strain resulting from IFM is distributed over the fracture surface and will differ depending on the fracture geometry. For instance, comminuted fractures will be able to tolerate relatively greater motion since the strain is applied over a larger surface area of fracture fragments. The size of callus formed during the healing process will depend on the magnitude of IFM (McKibbin, 1978; Goodship and Kenwright, 1985; Claes et al., 1997, 1998; Wu, 1997). If IFM exceeds a critical level, the blood vessels formed at the fracture site will be subjected to repeated disruption and would not become established, preventing the development of stable tissues (Carter et al., 1988; Claes et al., 1997). For example, a certain amount of mechanical instability leads to greater IFM with the formation of cartilage, and thus to endochondral healing by which the majority of fractures heal (Augat et al., 2005). Interfragmentary strain (IFS) did not influence healing of osteotomy gaps of 1 mm or smaller in a sheep model. However, decreased bone formation and inferior mechanical properties of healed bone were evident when larger IFS were applied to 2 and 6 mm fractures gaps (Augat et al., 1998). This leads to the conclusion that larger gaps require stable fixation that is still flexible enough to stimulate initial callus formation. This is preferable to fixation that is very unstable or too rigid. Moreover, both the quality of the tissue along the osteotomy line and the width of the osteotomy gap help to determine the mechanical quality of the healed bone (Augat et al., 1998).

Numerous experimental studies have been conducted to isolate the type of loading (axial, shear, torsion) and the effect it has on bone healing (Yamagishi and Yoshimura, 1955; Kenwright and Goodship, 1989; Park et al., 1999; Duda et al., 2002; Augat et al., 2003; Klein et al., 2004; Bishop et al., 2006). Moderate compressive axial IFMs enhanced periosteal callus formation and increased the rate of fracture healing in both animal models (Yamagishi and Yoshimura, 1955; Kenwright and Goodship, 1989; Klein et al., 2003; Augat et al., 2005) and clinical studies (Noordeen et al., 1995). However, both shear and tensile IFMs of similar magnitude appeared to inhibit fracture repair (Yamagishi and Yoshimura, 1955; Augat et al., 2003; Klein et al., 2004). In fact, shear movement considerably delayed the healing of experimental fractures, and in most instances produced only partial bridging and less persiosteal callus formation, resulting in significantly delayed healing (Augat et al., 2003, 2005). Although these studies clearly demonstrate the impact of IFM on bone healing, more research remains to be done to understand fully the biological processes involved.

Many computational models have also been developed to study the effect of the mechanical environment on fracture healing. These again confirm that the stiffness of fixation influences fracture healing. Gómez-Benito et al. (2006) developed a finite element model of a simple transverse mid-diaphyseal

fracture of an ovine metatarsus fixed with bilateral external fixators of three different stiffnesses. Their calculations predicted that a low stiffness external fixator would delay fracture healing and cause a larger callus than a more rigid external fixator. Carter et al. (1998) examined the importance of cyclic motion and local stresses and strains on bone tissue formation. They confirmed the basic mechanobiologic concepts that bone formation is promoted in the areas of low to moderate tensile strain, fibrous tissue is promoted in the areas of moderate to high tensile strains, and chondrogenesis is promoted in areas of hydrostatic compressive stress (pressure). On the other hand, Claes et al. (1998), using a sheep model, investigated the influence of the osteotomy gap size and IFM on fracture healing. They hypothesized that gap size and the amount of strain and hydrostatic pressure along the calcified surface in the fracture gap are the fundamental mechanical factors involved in bone healing. They proposed that intramembranous bone formation would occur for strains smaller than approximately 5% and hydrostatic pressure of no more than 0.15 MPa. On the contrary, strains up to 15% and hydrostatic pressure of more than 0.15 MPa would stimulate endochondral ossification. As expected, they found that there was a significant decrease in the rate of healing with an increasing osteotomy gap size. Furthermore, they found that a 2 mm gap led to greater IFM, more periosteal callus, and an increased amount of connective tissue in the fracture gap compared to osteotomies 1 mm or smaller. In fact, large critical sized gaps of 6 mm never healed during a period of 9 weeks, and they mainly produced fibrous connective tissue in the osteotomy gap regardless of the amount of IFM.

Kenwright and Gardner (1998) summarized studies that measured interfragmentary displacement in six degrees of freedom throughout healing in patients with tibial diaphyseal fractures treated by external fixation, and developed a finite element analysis model of healing tibial fractures. The model predicted that tissue damage might occur in the later (hard callus) phase of healing, even while the fixation device is still in place, because of very high stresses and strains. This study also indicated that the mechanical environment should be better controlled to provide amplitudes of movement in the first weeks of healing, and that the rigidity of fixation should then be increased to optimize the fracture healing process until the fixator is removed.

DYNAMIZATION

Many authors have suggested that the delayed introduction of controlled motion ("dynamization") as healing progresses may lead to faster maturation of bone (De Bastiani et al., 1984; Wu, 1997; Arazi et al., 2002), but this remains controversial and has not greatly influenced clinical practice (Gorman et al., 2005; Tigani et al., 2005; Claes et al., 2009). Dynamization is a word used when the IFM is increased by changing from a stable fixation to a more flexible fixation. It is often used when an implant allows axial shortening of a bone through a telescoping mechanism incorporated into the fixation device (De Bastiani et al., 1984). This regimen of treatment was only implemented after recognizing that IFM between the fracture ends is beneficial to the healing process, provided it is controlled. External fixation devices can readily be changed from a stable to a dynamic configuration, thereby allowing for more axial movement between the fracture fragments. Surprisingly, there have not been many fracture fixation devices specifically developed that actively incorporate dynamization in the clinical treatment of fractures. At this time it remains unclear when during the healing process dynamization should be applied, and whether it helps fractures repair more efficiently. For example, there have been a few clinical studies that have attempted to determine the optimal axial IFM or the effect of dynamization at the various stages of fracture repair, and it is unclear whether this accelerates bone repair in an efficient and timely manner (Marsh et al., 1991; Siguier et al., 1995; Domb et al., 2002). There are no clinical studies to our knowledge that have attempted to determine the effects of dynamization on the healing of large segmental bone defects.

The results of animal studies on the effects of dynamization on bone healing are inconsistent. A study by Larsson et al. (2001) investigated the effect of early axial dynamization (1 week post-op) on tibial bone healing in a canine model. They used a rigid external fixator to stabilize a 2 mm transverse osteotomy on both tibias of each dog to allow paired comparison of the results. They found that early dynamization resulted in accelerated callus formation and maturation, with increased remodeling of endosteal and periosteal callus tissue. Moreover, the dynamized side showed significantly higher torsional stiffness after 5 weeks of treatment than did the controls. A study by Aro and Chao (1993) also investigated bone healing patterns affected by loading, fracture fragment stability, fracture type, and fracture compression in a canine osteotomy model. This study had three different groups: transverse and oblique fractures were fixed with a rigid unilateral external fixator, with bone fragments separated by a distance of 1 mm, 2 mm, or in contact. Dynamization with uniform axial loading and motion was performed at either 2 or 4 weeks. They found that, for a given rigidity of external fixation, the amount of physiological stress and the presence of a significant gap proved to be the most significant factors in determining the pattern of fracture repair. Motion with loading tended to promote external callus maturation and secondary bone healing.

On the contrary, two studies using a rat model found that neither early nor late dynamization was beneficial to fracture healing. These two studies used very different fixation devices, including a rigid IM nail (Utvag et al., 2001) and an external fixator (Claes et al., 2009). Both groups found that dynamization increased callus formation, but reduced the quality of healed bone. These findings are not surprising, given that the evidence in the literature shows that increased IFM resulting from a flexible fixation device leads to greater callus formation, a prolonged chondral phase, and delayed healing by disrupting the vascular supply needed for bone tissue to repair and remodel (Rand et al., 1981; Ozaki et al., 2000). In fact, a study by Cullinane et al. (2002) attempted to influence cell fate decisions through precisely controlled motion using a custom made external fixator that introduced IFM bending strain. This was compared to a

rigidly fixed segmental defect. The results of this study showed that they were able to direct formation of cartilage and bone during fracture repair by inducing controlled motion. They also demonstrated that the spatial organization of the collagen fiber architecture within the newly formed tissue was influenced by the local mechanical environment, and noted that bone did not form when the IFM was too high.

These clinical (Wiss et al., 1986; Brumback et al., 1988; Meléndez and Colón, 1989) and experimental (Wolf et al., 1998; Hente et al., 1999; Claes et al., 2009) studies have been inconclusive and contradictory, and have failed to convincingly demonstrate any benefit of dynamization to bone healing (**Table 1**). Yet one thing is clear, the mechanical environment surrounding the fracture gap plays a very important role and largely determines how and if the fracture will heal. Although, in principle, dynamization is a sound strategy to attempt to accelerate the healing process its main clinical drawback is the early loss of frame stability, potentially leading to delayed union, refracture, or the development of a secondary deformity. Regardless, early dynamization has shown favorable healing outcomes as long as the treatment was applied after a bridging callus has formed (Acker et al., 1985; Kempf et al., 1985; Foxworthy and Pringle, 1995; Basumallick and Bandopadhyay, 2002).

REVERSE DYNAMIZATION

Based upon data from the healing of fractures and sub-critical size osteotomies, large segmental defects are subjected clinically to rigid internal fixation. However, there is little evidence to justify such an action, and few studies can be found that investigate the influence of the mechanical environment in healing large segmental bone defects. In response to this, for the past several years we have used a rat model to investigate the effects of fixator stiffness on the healing of large bone defects treated with BMP-2. We hypothesized that the healing of large, osseous defects can be enhanced by manipulating the mechanical environment as healing progresses. Specifically, we suggested that healing would be accelerated by first stabilizing the defect under conditions of low stiffness, and then imposing high stiffness once healing was underway, a strategy we call reverse dynamization. The results of this study were remarkable, confirming that the healing of large bone defects is highly responsive to the ambient mechanical environment (**Figure 2**), allowing the rate and quality of healing to be manipulated by altering fixation stability (Glatt et al., 2012b). Moreover, this study was the first to introduce the concept of reverse dynamization, and demonstrated its superiority as a means of accelerating the healing and maturation of bone (**Figure 2**). Based on these observations, a subsequent study determined whether the dose of BMP-2 could be reduced without compromising the healing process when using this enhanced mechanical environment (Glatt et al., 2016a). This study has shown that while the initial healing was slightly delayed, forming a smaller callus thoughout the healing period, the quality of healing bone was similar or slightly superior to that treated with the higher dose of BMP-2 (**Figure 2**). Interestingly, the same study also showed that if the dose of BMP-2 was insufficient, healing did not occur no matter which stiffness fixation device was used.

A study by Boerckel et al. (2011) reported that the application of early mechanical loading significantly inhibited vascular invasion and reduced bone formation in an 8 mm rat femoral defect when compared to stiff plate controls using two different doses of BMP-2 (0.2 and 2.5 μg). On the other hand, delaying mechanical loading by 3 weeks significantly enhanced bone formation. In a different study, using a 6 mm rat model, they demonstrated that the functional transfer of axial loads by modulation of fixation plate stiffness at 4 weeks significantly enhanced BMP-mediated large bone defect repair (Boerckel et al., 2012). Similar results to those of Boerckel et al. were reported by Claes's group who demonstrated superior results when mechanical modulation, from rigid to more flexible fixation, was applied at 3 and 4 weeks (Claes et al., 2011) after surgery compared to 1 week (Claes et al., 2009). However, for those studies a 1 mm osteotomy model stabilized with an external fixator was used. Results from these studies are not surprising and are consistent with the literature suggesting that extremely rigid fixation is detrimental to bone healing (Chao et al., 1989), and allowing increased flexibility during the later stages of healing is beneficial. Furthermore, this is attributed to the tissues occupying the fracture gap as was demonstrated by both Gardner et al. (1996) and Glatt et al. (2012a). They demonstrated if there is no material present in the fracture gap, which simulates conditions immediately post-surgery, the fixator frame provided stability at the fracture site with no contribution from the gap itself to support the fracture site. On the contrary, when they interposed material with low stiffness, which represents the early stages of healing, they found that the mechanical properties of the fixator were as important as those of the fracture material in influencing axial IFM at around 2–4 weeks post fixation. In contrast, with stiff intra-fracture materials, simulating the remodeling stage of healing, axial movement was influenced only by the stiffness of these materials, with little contribution from the fixation devices. Fracture movement arises from the combined flexibility of the fixation devices and the compliance of tissue material in the fracture gap, and is a consequence of weight-bearing and any loads applied. For dynamization implemented at the later stages of healing, accelerated bone healing is more likely a consequence of bone adaptation following Wolff's law rather than fixator dynamization itself. In fact, this hypothesis was confirmed using the reverse dynamization regimen in the same 1 mm osteotomy

TABLE 1 | Comparison of reverse dynamization to dynamization.

Reverse dynamization	Dynamization
Decreases IFM	Increases IFM
Early reverse dynamization accelerates union	Early dynamization leads to non-union
Late reverse dynamization of no benefit	Late dynamization of no benefit
Has not yet been the subject of any large scale study to determine if there is any clinical benefit	Limited or no proven clinical benefit despite multiple studies attempting to do so

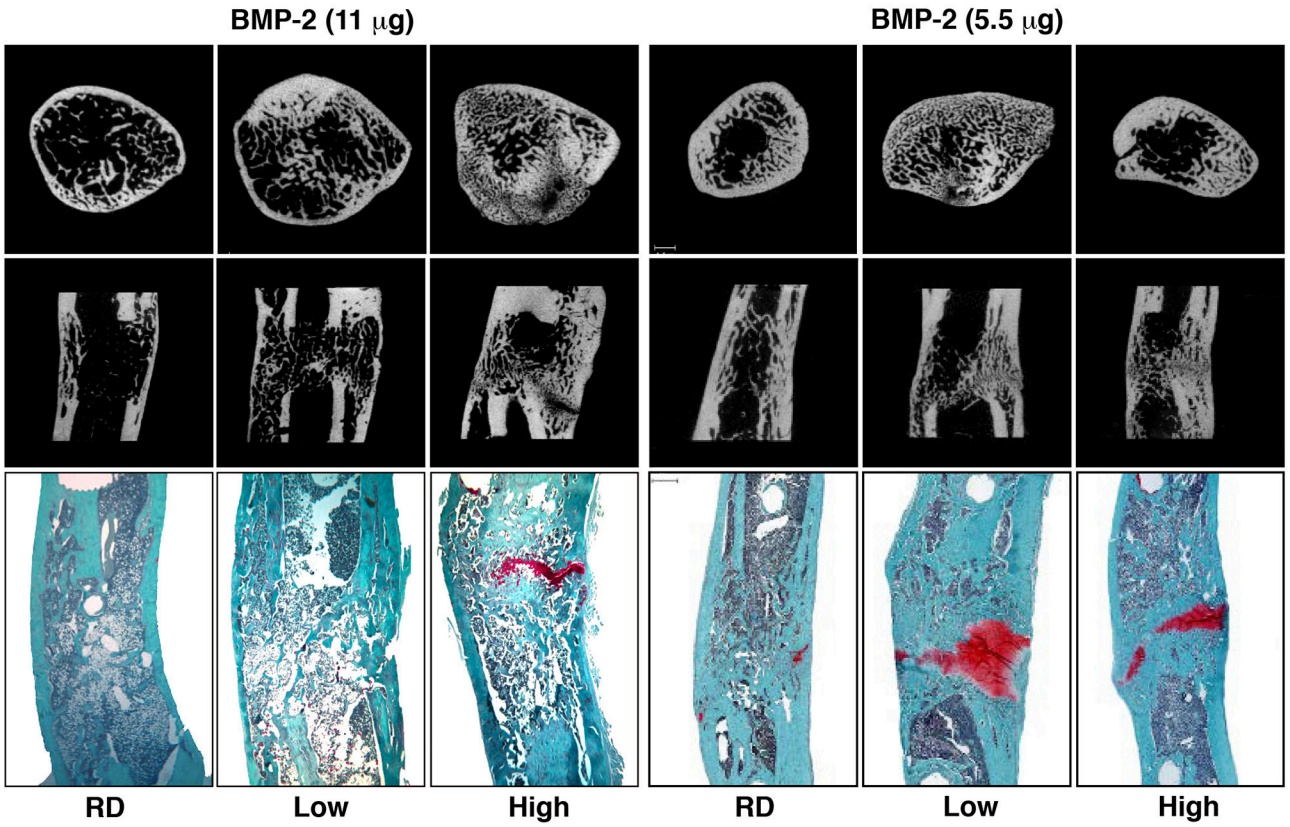

FIGURE 2 | Micro-computed tomography (μCT) and histology images illustrating healing of segmental defects with 11 and 5.5 μg doses of BMP-2, high and low stiffness external fixator groups as well as a Reverse Dynamization group (RD) after 8 weeks of treatment. μCT images of cross-sectional distal part of the defect (top row) and coronal plane of the defect (middle row). Histological sections were stained with safranin orange-fast green (bottom row, Scale bar = 1 mm). Low = low stiffness fixator (114 N/mm); High = high stiffness fixator (254 N/mm); RD = low to high stiffness fixation at 2 weeks (from Glatt et al., 2012b, 2016a).

rat model as was used by Claes' group (Bartnikowski et al., 2016). In this study we showed that when reverse dynamization, from flexible to rigid fixation, was applied at 3 weeks the healing outcome at the end of the treatment period was the same as the dynamization regimen (Claes et al., 2011; Bartnikowski et al., 2016). However, when reverse dynamization was applied at 1 week the healing outcome was exceedingly superior to that of the dynamized group (**Table 1**), constant rigid and flexible fixation groups (Bartnikowski et al., 2016). On the contrary, the dynamization regimen at 1 week was detrimental to bone healing when compared to any of the other groups tested (Claes et al., 2009).

Suprisingly, only one study can be found that investigated a reverse dynamization regimen in humans. A study by Howard et al. (2013) found that allowing initial axial macromovement from 2 to 4 weeks after surgery followed by more rigid stabilization accelerated fracture healing. Faster healing was associated with a reduction in the average time to removal of the fixator in the dynamization group (∼11 weeks), compared to the standard of care (∼22 weeks) when treating isolated closed or open grade I tibial fractures.

Such studies are only beginning to provide knowledge about the influence of modulating the mechanical environment and the effects it has on bone repair. The data from these studies appear to suggest there is no single set of mechanical circumstances that suits all stages of fracture repair, and that healing might be enhanced by changing the stiffness of fixation systematically during different phases. Selecting the specific mechanical conditions, as well as determining the most appropriate time to modulate this environment, will be critical to achieve the optimal conditions for bone repair. This is particularly true for reverse dynamization, where initially flexible conditions are followed by more rigid fixation, as this new concept requires further investigation to better define its role clinically (Glatt et al., 2016b).

HOW THIS KNOWLEDGE HAS INFLUENCED CLINICAL PRACTICE

Physicians and healers have managed fractures non-operatively for thousands of years, using splints and other simple devices. Over the course of the past century, orthopedic implants have revolutionized the treatment of bone injuries based on new discoveries combining basic and clinical research, advances in implant technology, materials science, and improved surgical techniques. The main purpose of fracture fixation is to provide

more anatomical alignment to the fragments of broken bone, and to achieve sufficient mechanical stability so that the biological process of bone healing is not disturbed. The link between mechanical and biological processes of bone regeneration and repair has been investigated for many decades. Knowledge gained from empirical, experimental, and clinical studies has tremendously changed and improved how fractures are treated today. Possible fixation strategies to treat bone fractures range from splints to external and internal fixators, and the decision to use a particular device depends on the specific bone involved, the fracture location, and the type of fracture, either "closed" or "open." The rigidity of the fixation device used determines the degree of movement of fracture ends relative to each other that occurs through weight-bearing (external loading) and muscle contractions, and will govern the formation of specific tissues in the fracture gap. The following sections will outline the types of fixation methods used for load bearing bones, and how those methods have been influenced by our greater appreciation of the contributions of mechanobiology to fracture healing.

Splinting

Management of a wide variety of orthopedic injuries requires the use of a splint. Splinting is used for acute fractures where swelling is anticipated, or for the initial stabilization of reduced, displaced, or unstable fractures before surgical intervention. No one knows when the first splint was used, but injured limbs have been bandaged or immobilized in some fashion since ancient times. Interestingly, despite its name, Arabians were reported to be the first ones to use the technique of pouring a plaster-of-paris mixture around the injured limb. This technique was brought to the attention of European practitioners in the early nineteenth century. Malgaigne recorded in detail the various techniques of its use, but was not keen to use it himself after having problems with swelling within a rigid cast (Malgaaigne, 1859). He subsequently abandoned the technique in favor of albuminated and starched bandages, as recommended by Seutin (Browner et al., 2008).

Different types of splints are used for various circumstances; they differ in their construction and indication. For example, a long bone fracture immobilized by a splint will be subjected to an intermittent compressive axial force imposed at the fracture site as a result of muscle activity and partial weight bearing. This allows a large degree of IFM and will typically induce healing through abundant callus formation (McKibbin, 1978; Sarmiento and Latta, 1981). The greatest disadvantage of prolonged immobilization of the limb is that the patient is often confined to bedrest until the fracture heals, which is subject to risks and complications. Modern surgeons now agree this is generally contrary to the overall health of the patient, and is avoided or minimized whenever possible. Seutin should be credited as one of the first physicians to appreciate that complete immobilization of the limb should be avoided, and in the mid nineteenth century was already promoting the benefits of fracture massage and early mobilization (Browner et al., 2008). Seutin gained many followers, but others still believed that total immobilization was a better choice. However, he continued to emphasize the importance of joint motion and one of his advocates, Lucas-Championniere, later confirmed these benefits in animal experiments (Lucas-Championniere, 1881). He went so far as to recommend massage of the injured limb to encourage motion between the fragments, generating more robust callus. This controversy between mobilizers and immobilizers resulted in the development of new splinting techniques such as the Thomas splint, various designs of traction devices, and functional braces. Perkin, Russell, Dowden, and many others were major advocates of movement, both active and passive, as the most important factor for the optimal functional outcome of the involved limb (Russell, 1924; Browner et al., 2008). The widespread use of functional bracing minimized hospitalization and permitted an earlier return to work and daily activities. However, despite historical evidence demonstrating that the influence of the mechanical environment on bone healing was already recognized in the nineteenth century, the significance of its role and its potential benefits are still actively debated today.

Open Reduction Internal Fixation (ORIF)

Splinting, casting, and traction techniques are suitable for many fractures, and the vast majority of these will unite spontaneously when adequately reduced and immobilized. However, closed (non-operative) methods are not suitable in many circumstances, and the prolonged immobilization or bedrest often required is associated with its own set of risks and complications. Pneumonia, contractures, ulcers, and loss of motion are not uncommon; thromboembolic phenomena, including both deep vein thrombosis and pulmonary embolism, are more serious possibilities. Because of these issues, and driven by patient expectations and the economic realities of prolonged hospitalization, modern fracture care has become far more dependent on operative stabilization. Progress in medicine and surgery over the course of the past 150 years now allows surgeons to intervene in a tremendous variety of pathological conditions, both acute and chronic. Advances in metallurgy, the development of biocompatible alloys, and improvements in the production quality of implants have paralleled the evolution of surgical science over this period. These elements have all conspired to provide orthopedic surgeons with unprecedented abilities to consider operative stabilization of many fractures, for a wide variety of indications.

For instance, when a fracture has an open soft tissue wound or is potentially infected, external or internal fixation devices are more often used. Internal fixation of fractures dates back to the mid 1800s when Lister introduced the concept of ORIF for patella fractures. Since then, internal metal plates to stabilize fractures have been used for over 100 years. While internal fixation devices are available in various sizes and shapes for different bones and anatomical sites (**Figure 3**), initially, internal fixation methods were complicated by many hurdles such as infection, insufficient strength, poor surgical techniques, and corrosion, which were a consequence of limited biological and mechanical knowledge of fracture healing. Over the past several decades, advances in these sciences have significantly improved internal fixation designs and techniques, although some problems still exist. An ideal plate

FIGURE 3 | Radiographic and intra-operative images illustrating internal fixation using plates: (A) Intra-operative image showing distal tibial fracture fixation with two small plates; **(B)** AP radiograph showing distal tibial fracture fixation with two plates, and a single plate for the associated fibular fracture; **(C)** Corresponding lateral radiograph demonstrating stabilization using these three small plates; **(D)** Comminuted distal tibial/fibular fracture; **(E)** AP radiograph of relatively rigid distal tibial/fibula fracture fixation with a long medial locked plate; **(F)** Corresponding lateral radiograph of this distal tibial/fibular fracture fixation; **(G)** Comminuted distal femoral fracture; **(H)** AP radiograph of relatively flexible distal femoral fracture fixation with a lateral locked plate that bridges the zone of comminution; **(I)** Corresponding lateral radiograph of this distal femoral fracture stabilized with a lateral locked plate.

should accelerate fracture healing while not interfering with bone physiology. After their preliminary introduction, Lane (1895), Lambotte (1909), and Sherman (1912) subsequently abandoned metal internal fixation plates due to problems with corrosion and insufficient strength. Eggers (1948) then designed a plate that had two long slots, allowing the screw heads to slide thereby compensating for the resorption of the fragment ends. However, the use of this plate was limited and eventually also abandoned, because its structural weakness resulted in unstable fixation.

Danis first recognized the virtue of compression between the fracture fragments (Danis, 1949). He achieved this using an internal plate that suppressed IFM and increased fixation stability, resulting in primary bone healing. The compression plate underwent further design modifications when oval holes were created to provide interfragmentary compression during screw tightening, while another strategy achieves interfragmentary compression by tightening a tensioner that was temporarily anchored between the bone and plate. These design changes set the stage for the rigid plating of bone fractures, where healing advances without periosteal callus formation. In fact, any appearance of callus formation was thought to indicate fracture instability (Perren et al., 1988). The dynamic compression plate (DCP) was developed after improved designs to the rigid plate. The advantages of the DCP system were related to the low incidence of malunion, stable fixation, and the lack of any need for external immobilization. However, despite being superior to prior plate designs the DCP had some disadvantages, including delayed union and cortical bone loss under the plate. Furthermore, it was difficult to assess the progress of fracture healing radiologically due to the absence of callus formation. To avoid cortical porosity at the bone-plate interface, a new plate was designed called the limited contact-dynamic compression plate (LC-DCP), intended to have a 50% reduced contact area (Uhthoff et al., 2006). However, independent studies confirmed that the LC-DCP plating system was not advantageous in fracture healing, and did not restore cortical bone perfusion to the devascularized cortex. These studies agreed that cortical porosity was related to stress shielding induced by rigid fixation, and was not due to the remodeling of necrotic bone under the plate (Uhthoff and Dubuc, 1971; Akeson et al., 1976; Uhthoff et al., 1981, 1994; Uhthoff and Finnegan, 1983). Most importantly, the initial hypothesis stating that rigid fixation was necessary for fractures to heal uneventfully was abandoned with the introduction of biological osteosynthesis (Gerber et al., 1990). With this new concept the appearance of callus formation was actually a favorable sign suggesting rapid fracture healing, thereby refuting earlier statements that promoted rigid internal fixation. The desire to provide more biologically responsive stabilization then led to the development of point-contact fixation (PC-Fix), which eliminated interfragmentary compression and bicortical fixation. Unfortunately, a new plate design with very minimal plate-bone contact failed to prove beneficial clinically (Eijer et al., 2001; Haas et al., 2001; Uhthoff et al., 2006) and did not solve the problem of delayed union. However, this new plating system did improve fixation strength, especially for osteoporotic bone, and encouraged fracture healing through periosteal callus formation.

The current school of thought for successful fracture healing using internal fixation adheres to two fundamental principles. The first is to achieve the optimal anchoring of the implant to the bone surface which maintains the fracture reduction during the healing process. The second involves simultaneously reducing the amount of soft tissue damage during the surgery, thereby maintaining local vascularity. To accomplish this the type of plate, the number of screws, and their positions should

be carefully considered and must be suitable for each fracture situation. Rigid fixation with stiff compression plates following anatomical reduction is still an established method with excellent clinical results for many fractures (**Figures 3D–F**; Ruedi et al., 2007). However, when the fracture is highly comminuted and anatomic reduction would require extensive exposure that would devitalize the fragments, it is now considered preferable to employ "bridge" plating using less invasive techniques that preserve local vasculature (Chrisovitsinos et al., 1997; Farouk et al., 1998, 1999; Stoffel et al., 2003). This required the development of locked screw and plate designs, to achieve functional unity of the various elements of the construct. Locked plating and fixed-angle devices have become increasingly common over the past decade, and the altered mechanical environment can result in improvements in fracture healing when applied correctly in appropriate cases (**Figures 3G–I**; Gautier and Sommer, 2003; Stoffel et al., 2003). However, in some circumstances the constructs are considered too rigid and fracture healing can be delayed, resulting in implant failure and subsequent non-union (**Figure 4**; Gautier and Sommer, 2003; Lujan et al., 2010). Further research to address this issue has led to the development of modified designs that limit the stiffness of the implant-fracture construct, including far-cortical locking screws (Bottlang et al., 2009) and the recently proposed "active" plate (Bottlang et al., 2016). It is far too soon to know whether either of these developments will demonstrate sufficient advantages clinically, or will instead lead to further modifications to internal fixation.

Intramedullary Nails

The design of intramedullary nails has advanced considerably since the first attempts during ancient times using wooden dowels, and later with ivory pegs in the 1800's (Gluck, 1890; Konig, 1913; Hippocrates, 1938). In fact, autologous bone was even suggested and used as an intramedullary implant in an effort to fix fractured bone. This technique involved cutting out a section of cortical bone, which was then passed up the medullary canal across the fracture site (Hoglund, 1917). In 1939 Gerhard Kuntscher (Kuntscher, 1958), an orthopedic surgeon from Kiel, Germany, was primarily responsible for the development of the current day intramedullary nail. However, his method was not initially well received by fellow surgeons around the world, and it was considered an atrocity when it was discovered intramedullary nails were used to stabilize femur fractures in injured US pilots downed over Germany during World War II. Since its inception, this technique has been modified and applied with numerous improvements for the treatment of a diverse range of long bone fractures (**Figure 5**). Fracture healing following intramedullary nailing is very similar to what occurs during spontaneous, unsupported healing in nature, and as with cast or splint fixation, is accompanied by bridging callus formation.

The cross section of the first intramedullary nail was V-shaped, but was later modified to a cloverleaf pattern to improve resistance to torsional loads. In the 1950's, Lottes (1954, 1974) developed a flexible, unreamed, triflanged tibial nail, which was different from the cloverleaf shaped nail designed by Kuntscher (1958). This design was chosen to conform to the shape of the tibia, and gave it a markedly different flexibility and stiffness. In theory, at the time of insertion the nail would conform to the shape of the tibial medullary canal, and through elasticity would then revert to its original shape, while both reducing and stabilizing the fracture. Nevertheless, despite reports from

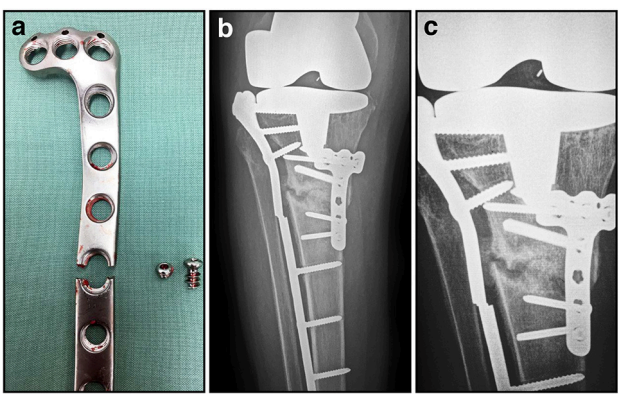

FIGURE 4 | Post-operative and radiographic images illustrating fatigue failure of an internal fixation locking plate. (A) Appearance of broken locking plate having failed, as expected, through a screw hole; **(B)** AP radiograph showing proximal tibial non-union and failed implant; **(C)** Close-up of AP radiograph showing non-union and failed implant. The lateral plate has characteristically broken through a screw hole at the same level as the non-union.

FIGURE 5 | Radiographic intramedullary nail images. (A) Statically locked tibial nail to stabilize a mid-diaphyseal fracture; **(B)** Statically locked femoral nail to stabilize a mid-diaphyseal short oblique fracture.

a decade earlier noting an approximately 90% success rate was achieved using straight Kuntscher nails depending on the fracture configuration (Zucman and Maurer, 1969; d'Aubigne et al., 1974), perforation of the posterior tibial cortex was the main complication associated with straight Kuntschner nails. Herzog addressed this problem by adding a 20° apex posterior curve, with an additional 5° apex posterior curve of the distal nail (Donald and Seligson, 1983). These curves allowed easier insertion of the nail into the medullary canal, and this proximal curve remains an integral part of the design of contemporary nails. Although the nail design was improved by adding curvature, fracture outcomes were not significantly improved. A report by d'Aubigne et al. (1974) suggested that tibial fracture stabilization with intramedullary nailing offered poor fixation at the upper and lower ends of the bone. Grosse et al. (1978) later added interlocking screws that could be inserted through the nail and the bone on both sides of the fracture. The use of interlocking screws prevented rotational movement and telescoping (**Figure 5**), which improved fracture stability and allowed for earlier weight bearing (Kempf et al., 1985). Furthermore, interlocking nails had either dynamic holes allowing fracture compression during weight bearing, or static holes providing greater stability without allowing fracture compression. Since then the main design elements of nails have not changed significantly, although different insertion approaches have been used to improve surgical outcomes (Tornetta and Collins, 1996; Court-Brown et al., 1997; Keating et al., 1997; Tornetta et al., 1999; Toivanen et al., 2002). Titanium was introduced as an alternative because its material properties more closely replicate the modulus of elasticity of normal bone, in an effort to promote more uniform and rapid union. However, the transition from stainless steel to titanium nails over the past two decades has resulted in implants with thicker walls that behave nearly the same biomechanically, and with negligible clinical benefits (Bong et al., 2007). Before a nail is inserted, the medullary canal is generally reamed to allow a larger nail to be used, and to improve the fit between the surface of the nail itself and endosteal bone, which maximizes contact and limits instability that might eventually result in implant failure (Bong et al., 2007). Although a large prospective randomized clinical study demonstrated reamed nailing was mildly superior to unreamed nailing for closed tibial shaft fractures, this was not true for open fractures where reaming provided no apparent benefit (Bhandari et al., 2008).

Typical intramedullary nails are passive devices with biomechanical advantages that encourage the spontaneous union of diaphyseal fractures. However, nail technology became much more sophisticated when these devices were introduced as active elements to achieve limb lengthening by Bliskunov (1983). Distraction histogenesis is most commonly employed for limb length equalization and deformity correction, or when lengthening for stature. As remarkable as this process is, it has become commonplace in the realm of limb lengthening and reconstruction (Ilizarov, 1989a,b; Fischgrund et al., 1994; Tetsworth and Paley, 1995). Lengthening nails are generally telescopic in design (**Figure 6**), with a slightly smaller tube gradually extruded from within a slightly larger tube. The

FIGURE 6 | Radiographic images illustrating the process of gradual femoral lengthening using a telescopic nail: (A) AP radiograph of a femoral lengthening nail obtained early post-operative, following only limited distraction; **(B)** AP radiograph of a telescopic lengthening nail after completing distraction of 2.7 cm; **(C)** Radiographic image illustrating lengthening gap at 6 weeks, demonstrating early regenerate bone formation; **(D)** Radiographic image at 12 weeks, as the regenerate gradually matures and consolidates; **(E)** Radiographic image illustrating lengthening gap at 24 weeks, as the regenerate bone matures further and hypertrophies; **(F)** Radiographic image illustrating fully consolidated gap at 52 weeks, following removal of the telescopic nail.

various implants available use different strategies to provide the necessary distraction force, including mechanical, motorized, or magnetic devices (Betz et al., 1990; Baumgart et al., 1997; Cole et al., 2001; Thaller et al., 2014; Kucukkaya et al., 2015; Paley, 2015; Paley et al., 2015). These adjustable intramedullary nails are a less invasive alternative to external fixators, and are therefore more attractive to both patients and surgeons. Yet both types of device achieve exactly the same objective, controlled gradual mechanical distraction to produce bone growth when desired (**Figures 6A–F**; Hasler and Krieg, 2012).

The latest iteration of these implants relies on an external rotating magnet inducing motion in an internal magnet, that in turn drives a gearbox to achieve lengthening (Thaller et al., 2014; Kucukkaya et al., 2015; Paley, 2015; Paley et al., 2015). This technology was originally introduced by Verkerke in 1989, for use in an expandable endoprosthesis following tumor resection in pediatric patients (Verkerke et al., 1989). Powered devices, either motorized or magnetically driven, offer unprecedented control over the implant, and provide the ability to modulate the process of distraction and directly influence the growth of bone (Betz et al., 1990; Thaller et al., 2014; Kucukkaya et al., 2015;

Paley, 2015; Paley et al., 2015). It is now possible to increase or decrease the rate of distraction, and to discontinue or even reverse the process if necessary. Gaining popularity at this time, magnetically powered lengthening nails have been successfully employed in over 1000 cases globally (Paley, 2015). Fully implanted distraction devices like these decrease the risk of pin site infection associated with external fixation, but lengthening still exposes the patient to the other associated risks of nerve injury, contracture, subluxation, or secondary deformity (Thaller et al., 2014; Kucukkaya et al., 2015; Paley, 2015; Paley et al., 2015).

External Fixators

Despite the inconvenience to the patient and the high likelihood of superficial pin site infections, external fixators fill a clinical niche when other methods of fracture stabilization are unsuitable. Following high energy trauma with open injuries, plates and intramedullary nails are sometimes considered an unacceptable risk for deep infection. Occasionally the extent of comminution and the breadth of involvement results in a fracture configuration inherently unstable, but external fixators can even span joints to better control the fracture mechanically (**Figure 7**). Significantly, unlike plates and most intramedullary nails, external fixators provide opportunites for postoperative modification. The adjustability of external fixators has, until recently, been unique, and in part explains why they continue to play an important role in musculoskeletal trauma care. External fixation has transitioned from being a last resort fixation method to becoming the method of choice when treating some of the most challenging bone pathology encountered clinically. Although alternative treatment strategies are available, it continues to be an essential element in limb salvage during both early and late bone reconstruction of serious extremity injuries. It is currently the only system that allows the surgeon to control the flexibility of the fixation during the course of bone healing. External fixators have evolved dramatically from the most primitive designs incorporating wooden splints, to contemporary designs where a wide array of metals and composite materials are used. Unfortunately, with the evolution of these devices

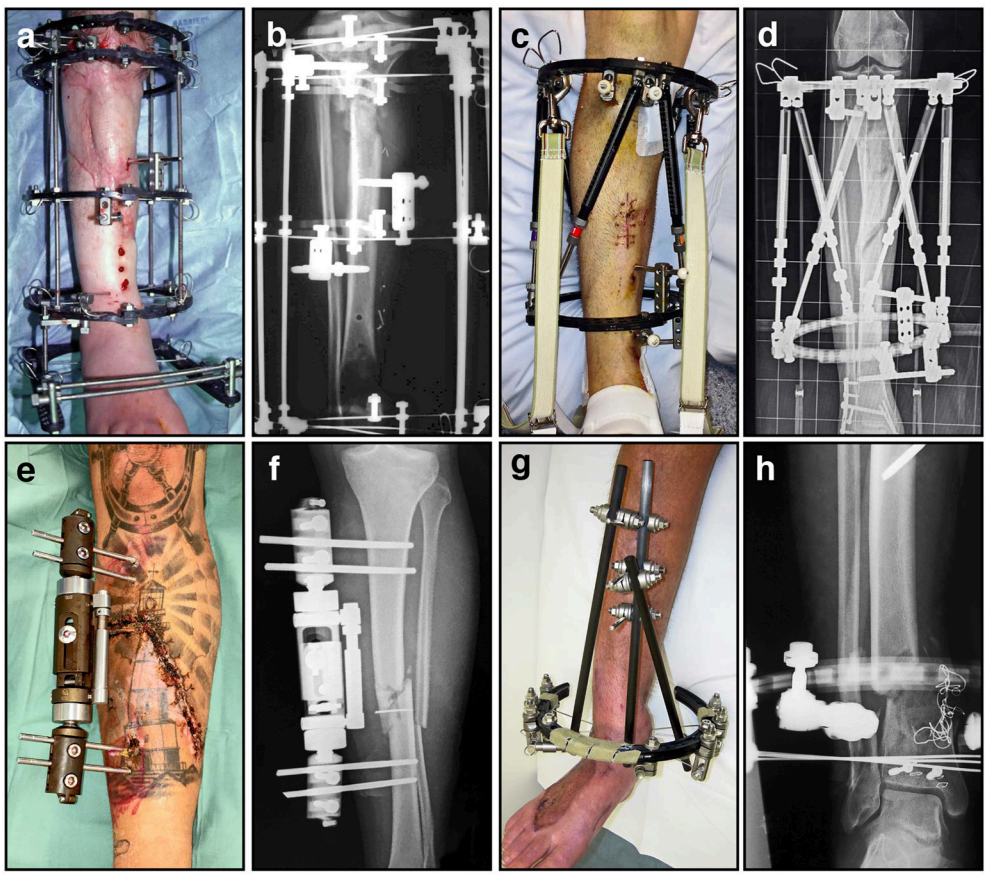

FIGURE 7 | A variety of external fixators are used for fracture fixation, most often for tibia fractures as demonstrated here. (A) Clinical image of an Ilizarov external fixator applied to a fractured leg, with multiple rings and tensioned wires; **(B)** Corresponding radiograph illustrating proximal tibial fracture fixation with this circular frame; **(C)** Clinical image of a hexapod-based external fixator applied to a fractured limb, using a pair of rings; **(D)** Corresponding radiograph illustrating stabilization of a comminuted segmental tibia fracture; **(E)** Clinical image of a unilateral fixator in position; **(F)** Corresponding radiograph demonstrating mid-tibial open fracture fixation using this device; **(G)** Clinical image of a hybrid (cantilever) external fixator, incorporating a single juxta-articular ring and unilateral diaphyseal elements; **(H)** Corresponding radiograph demonstrating a distal tibial fracture stabilized using this device.

came many complications, and it has become a more technically demanding procedure. Despite these factors, many surgeons worldwide continue to use external fixators to treat complex fractures, segmental defects, and congenital deformities.

The work of many clinicians, researchers, and engineers from around the world are responsible for the current design of external fixation devices. For example, the distraction and compression mechanisms of modern devices are credited to Lambret from 1911 (LaBianco et al., 2001). In 1931 Pitkin and Blackfield were the first surgeons to advocate bi-cortical pins attached to two external fixation clamps, as a bilateral frame to improve fracture healing. Anderson et al. presented a series of papers from 1933–1945 (Anderson, 1935, 1938; Anderson and Burgess, 1943), outlining the use of both half-pins and transfixation pins for the treatment of various long bone fractures, arthrodesis, and limb lengthening procedures (Christian, 1998). These gradual incremental improvements have resulted in the designs currently available today, providing external fixators that come in three major configurations (**Figure 7**): circular (A–D), monorail (unilateral) (E–F) and hybrid (G–H).

Professor Gavril A. Ilizarov must be acknowledged not only for his contributions to the modern design of unilateral and circular external fixators, but also for inventing limb salvage and bone lengthening procedures through distraction osteogenesis (Ilizarov, 1988; Ilizarov and Frankel, 1988). Clinically, distraction osteogenesis is the perfect example of using a fixation device to apply mechanical forces to stimulate the process of bone regeneration. This is achieved with a specialized form of external fixation known as a ring or circular fixator (**Figures 7A,B**). Ilizarov found these external frames invaluable for multiple applications including post-traumatic and congenital limb reconstruction, management of osteomyelitis, regeneration of bone defects, deformity correction,

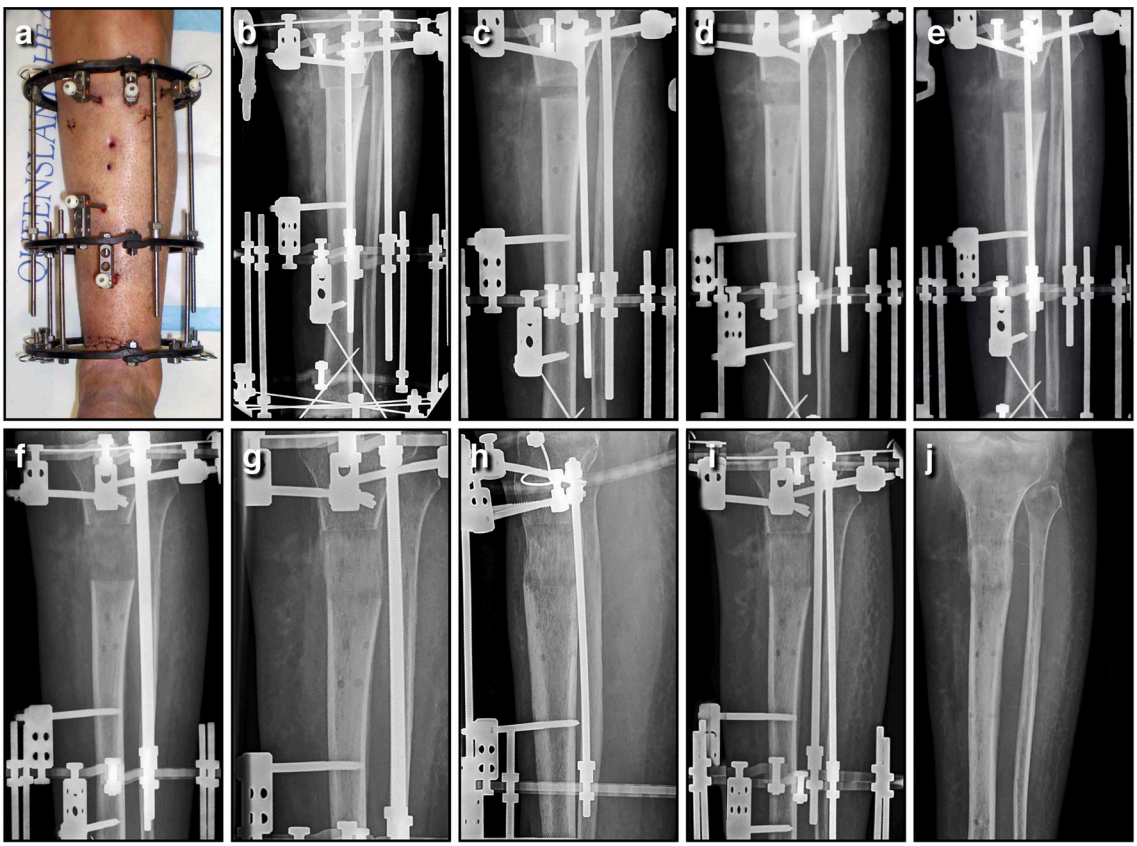

FIGURE 8 | Bone lengthening can be achieved through distraction osteogenesis using an Ilizarov external fixator. In this instance, an open distal tibial fracture resulted in a 3.7 cm segmental defect; the limb was acutely shortened, the wound closed primarily, and length gradually restored through a proximal corticotomy. This panel features a series of AP tibial radiographs demonstrating the 6 month process, and the final result a full year later; **(A)** Clinical image of the fractured limb stabilized with a circular frame after acute shortening of 3.7 cm; **(B)** AP radiograph immediately post-operative, with the proximal corticotomy minimally displaced; **(C)** AP radiograph of proximal tibia lengthening after 2 weeks of distraction; **(D)** AP radiograph of a proximal tibia lengthening at 4 weeks, with regenerate bone visible in the distraction gap; **(E)** AP radiograph of a proximal tibia lengthening at 6 weeks, as the gap slowly increases in size; **(F)** AP radiograph of a proximal tibia lengthening at 8 weeks, after length has been restored; **(G)** AP radiograph of a proximal tibia lengthening at 12 weeks, as the new bone gradually matures; **(H)** AP radiograph of a proximal tibia lengthening at 18 weeks, as the bone continues to consolidate; **(I)** AP radiograph of a proximal tibia lengthening at 26 weeks, shortly before the regenerate bone was solid enough to allow removal of the frame; **(J)** AP radiograph of the lengthened proximal tibia at 52 weeks, as the bone continues to strengthen and remodel. This regenerate bone will eventually become indistinguishable from surrounding normal bone.

and complex arthrodesis. These devices utilize Ilizarov's principle of distraction histogenesis, and rely on a special type of low energy osteotomy that preserves local vasculature (Ilizarov, 1989b). Ideally, only the cortical bone is fractured, leaving the medullary vessels and the periosteum intact in the metaphyseal region. After an initial latency period to allow the osteotomy to begin to heal, the fixator is adjusted on a regular basis to achieve controlled gradual mechanical distraction (Ilizarov, 1989a). As the fixator is slowly lengthened, new bone forms in the gap created at the osteotomy by the now familiar process of distraction osteogenesis (Ilizarov, 1989a,b). For example, this proces allows for skeletal reconstruction across segmental defects through bone transport, using small tensioned Kirschner wires (K-wires) and circumferential ring supports (**Figure 8**). As new bone growth occurs in the metaphyseal region, a segment of healthy bone is gradually translocated into the defect. The tension that is created by gradual mechanical distraction stimulates the formation of new bone, skin, blood vessels, peripheral nerves, and muscle during the analogous process of distraction histogenesis (**Figures 8C–J**). Through this remarkable process, bone lengthening and regeneration can occur at a rate of approximately one centimeter per month. Ilizarov techniques have come a long way in treating non-unions by the mechanical stimulation and modulation of callus for the reconstruction of segmental defects well in excess of what iliac crest bone graft can reliably fill. More importantly, this has resulted in this technique giving rise to limb salvage having the superior quality of regenerated normal bone.

The basic components of the circular frame are rings, tensioned wires, and connecting threaded rods. The stability of the frame depends upon the configuration of the basic components (Calhoun et al., 1992; Kummer, 1992; Podolsky and Chao, 1993; Lenarz et al., 2008), and this will influence the local mechanical environment around the regenerated bone, thereby determining the type, rate, and quality of the tissue formed. For instance, depending on the type and size of the rings (full, partial, or arches) the stability of the construct will change. Full rings provide the most stability, partial intermediate, and arches the least. The diameter of the rings is also very important, and smaller rings are inherently more stable than larger ones of the same thickness (Calhoun et al., 1992; Kummer, 1992; Podolsky and Chao, 1993; Lenarz et al., 2008). Frame stability will also be dependent upon the distance between rings, and the type and quantity of ring connectors such as wires, rods, and Shantz pins. In clinical practice, various combinations of the circular frame components are used, depending on the intended application and required stability.

FUTURE PERSPECTIVES

Bone has an amazing ability to heal spontaneously without forming scar tissue. When bone fails to heal, from either a large defect or non-union of a fracture, it is necessary to consider morphogenetic signals, cells, scaffolds and the precise mechanical conditions in order to achieve successful union. This review, focusing on the last of these, has summarized the decades of work and acquired knowledge that has been used to develop new treatments and technologies for the regeneration of bone. Research has now shown how the precise mechanical environment provided by the fixation stability around the bone lesion significantly influences the way bone heals. Future convergence of this research with the findings of complementary studies in biology, tissue engineering, and regenerative medicine promises important synergies. Bringing together these diverse disciplines in a productive manner remains a challenge for the future.

An important goal of mechano-biology is to determine which biological signals can be successfully manipulated through modulating the local mechanical environment, for instance, by adjusting fixation stability. Identifying these molecular signals will allow them to be targetted in novel ways to initiate, maintain, and accelerate the repair process. Unraveling the interplay between mechanics and biology in this setting is a problem for the emerging field of systems biology (Bizzarri et al., 2013; Giorgi et al., 2016). The levels and types of complexity are massive, and their understanding will require a big data approach. Moreover, we currently lack the experimental tools for a comprehensive investigation of the problem. Although *in vitro* experiments can be performed with sophistication, *in vivo* studies lack the tools for precise, controlled experiments. In particular, there is a need for non-invasive sensors that permit controlled, spatially defined, real-time analysis of the chemical, physical, and biological environment within defects as they heal. Such deficiencies are compounded by the lack of sophisticated ways to control the mechanical environment of a healing defect with precision at a cellular level. Contemporary plates, fixators, and rods are clumsy and imprecise in this regard. Furthermore, the informed and appropriate selection of scaffolds and growth factors for specific purposes, and insights into how these factors interact with mechanical cues, will require additional research.

Finally, there is a need to incorporate this new information into clinical practice. Little consideration of mechanical factors is often given when choosing the type of fixation device to stabilize a fracture. Compounding this deficit is the lack of *in vivo* monitoring tools with which to inform decisions of this type. New methods of non-invasive monitoring of bone healing are being developed that will allow us to address this issue. These should allow for the selection of the appropriate fixation device for any given circumstance, optimize decisions concerning the removal of the device, and encourage an early return to normal weight bearing.

AUTHOR CONTRIBUTIONS

All authors listed have made substantial and direct intellectual contribution to the work, and approved it for publication.

ACKNOWLEDGMENTS

We would like to thank Michael Glatt for his assistance with the design of **Figure 1**.

REFERENCES

Aalto, K., Holmström, T., Karaharju, E., Joukainen, J., Paavolainen, P., and Slatis, P. (1987). Fracture repair during external fixation. Torsion tests of rabbit osteotomies. *Acta Orthop. Scand.* 58, 66–70. doi: 10.3109/17453678709146345

Acker, J. H., Murphy, C., and D'Ambrosia, R. (1985). Treatment of fractures of the femur with the Grosse-Kempf rod. *Orthopedics* 8, 1393–1401.

Akeson, W. H., Woo, S. L., Rutherford, L., Coutts, R. D., Gonsalves, M., and Amiel, D. (1976). The effects of rigidity of internal fixation plates on long bone remodeling. A biomechanical and quantitative histological study. *Acta Orthop. Scand.* 47, 241–249.

Anderson, R. (1935). A new method of treating fractures in the distal third of the femur. *Can. Med. Assoc. J.* 32, 625–629.

Anderson, R. (1938). Ambulatory method of treating femoral shaft fractures, utilizing fracture table for reduction. *Am. J. Surg.* 39, 538–551.

Anderson, R., and Burgess, E. (1943). Delayed union and nonunion. *J. Bone Joint Surg. Am.* 25, 427–445.

Arazi, M., Yalcin, H., Tarakcioglu, N., Dasci, Z., and Kutlu, A. (2002). The effects of dynamization and destabilization of the external fixator on fracture healing: a comparative biomechanical study in dogs. *Orthopedics* 25, 521–524. doi: 10.3928/0147-7447-20020501-20

Aro, H. T., and Chao, E. Y. S. (1993). Bone-healing patterns affected by loading, fracture fragment stability, fracture type, and fracture site compression. *Clin. Orthop. Relat. Res.* 293, 8–17. doi: 10.1097/00003086-199308000-00003

Augat, P., Burger, J., Schorlemmer, S., Henke, T., Peraus, M., and Claes, L. (2003). Shear movement at the fracture site delays healing in a diaphyseal fracture model. *J. Orthop. Res.* 21, 1011–1017. doi: 10.1016/S0736-0266(03)00098-6

Augat, P., Margevicius, K., Simon, J., Wolf, S., Suger, G., and Claes, L. (1998). Local tissue properties in bone healing: influence of size and stability of the osteotomy gap. *J. Orthop. Res.* 16, 475–481. doi: 10.1002/jor.1100160413

Augat, P., Simon, U., Liedert, A., and Claes, L. (2005). Mechanics and mechano-biology of fracture healing in normal and osteoporotic bone. *Osteoporos. Int.* 16(Suppl. 2), S36–S43. doi: 10.1007/s00198-004-1728-9

Bartnikowski, N., Claes, L. E., Koval, L., Glatt, V., Bindl, R., Steck, R., et al. (2016). Modulation of fixation stiffness from flexible to stiff in a rat model of bone healing. *Acta Orthop*. doi: 10.1080/17453674.2016.1256940. [Epub ahead of print].

Basumallick, M. N., and Bandopadhyay, A. (2002). Effect of dynamization in open interlocking nailing of femoral fractures. A prospective randomized comparative study of 50 cases with a 2-year follow-up. *Acta Orthop. Belg.* 68, 42–48.

Baumgart, R., Betz, A., and Schweiberer, L. (1997). A fully implantable motorized intramedullary nail for limb lengthening and bone transport. *Clin. Orthop. Relat. Res.* 343, 135–143. doi: 10.1097/00003086-199710000-00023

Betz, A., Baumgart, R., and Schweiberer, L. (1990). [First fully implantable intramedullary system for callus distraction–intramedullary nail with programmable drive for leg lengthening and segment displacement. Principles and initial clinical results]. *Chirurg* 61, 605–609.

Bhandari, M., Guyatt, G., Tornetta, P. III., Schemitsch, E. H., Swiontkowski, M., Sanders, D., et al. (2008). Randomized trial of reamed and unreamed intramedullary nailing of tibial shaft fractures *J. Bone Joint Surg. Am.* 90, 2567–2578. doi: 10.2106/JBJS.G.01694

Bishop, N. E., van Rhijn, M., Tami, I., Corveleijn, R., Schneider, E., and Ito, K. (2006). Shear does not necessarily inhibit bone healing. *Clin. Orthop. Relat. Res.* 443, 307–314. doi: 10.1097/01.blo.0000191272.34786.09

Bizzarri, M., Palombo, A., and Cucina, A. (2013). Theoretical aspects of Systems Biology. *Prog. Biophys. Mol. Biol.* 112, 33–43. doi: 10.1016/j.pbiomolbio.2013.03.019

Bliskunov, A. I. (1983). [Intramedullary distraction of the femur (preliminary report)]. *Ortop. Travmatol. Protez*. 59–62.

Boerckel, J. D., Kolambkar, Y. M., Stevens, H. Y., Lin, A. S., Dupont, K. M., and Guldberg, R. E. (2012). Effects of *in vivo* mechanical loading on large bone defect regeneration. *J. Orthop. Res.* 30, 1067–1075. doi: 10.1002/jor.22042

Boerckel, J. D., Uhrig, B. A., Willett, N. J., Huebsch, N., and Guldberg, R. E. (2011). Mechanical regulation of vascular growth and tissue regeneration *in vivo*. *Proc. Natl. Acad. Sci. U.S.A.* 108, E674–E680. doi: 10.1073/pnas.1107019108

Bong, M. R., Kummer, F. J., Koval, K. J., and Egol, K. A. (2007). Intramedullary nailing of the lower extremity: biomechanics and biology. *J. Am. Acad. Orthop. Surg.* 15, 97–106. doi: 10.5435/00124635-200702000-00004

Bottlang, M., Doornink, J., Fitzpatrick, D. C., and Madey, S. M. (2009). Far cortical locking can reduce stiffness of locked plating constructs while retaining construct strength. *J. Bone Joint Surg. Am.* 91, 1985–1994. doi: 10.2106/JBJS.H.01038

Bottlang, M., Tsai, S., Bliven, E. K., von Rechenberg, B., Klein, K., Augat, P., et al. (2016). Dynamic stabilization with active locking plates delivers faster, stronger, and more symmetric fracture-healing. *J. Bone Joint Surg. Am.* 98, 466–474. doi: 10.2106/JBJS.O.00705

Browner, B. D., Jupiter, J. B., Levine, A. M., Trafton, P. G., and Krettek, C. (2008). "Skeletal trauma: basic science management and reconstruction," in *The History of Fracture Treatment*, *4th Edn.*, ed C. L. Colton (Philadelphia, PA: W. B. Saunders Company), 3–30.

Brumback, R. J., Uwagie-Ero, S., Lakatos, R. P., Poka, A., Bathon, G. H., and Burgess, A. R. (1988). Intramedullary nailing of femoral shaft fractures. Part II: f*racture-healing with static interlocking fixation.* J. Bone Joint Surg. Am. 70, 1453–1462.

Calhoun, J. H., Li, F., Ledbetter, B. R., and Gill, C. A. (1992). Biomechanics of the Ilizarov fixator for fracture fixation. *Clin. Orthop. Relat. Res.* 280, 15–22. doi: 10.1097/00003086-199207000-00004

Carter, D. R., Beaupré, G. S., Giori, N. J., and Helms, J. A. (1998). Mechanobiology of skeletal regeneration. *Clin. Orthop. Relat. Res.* 355(Suppl.), S41–S55. doi: 10.1097/00003086-199810001-00006

Carter, D. R., Blenman, P. R., and Beaupré, G. S. (1988). Correlations between mechanical stress history and tissue differentiation in initial fracture healing. *J. Orthop. Res.* 6, 736–748. doi: 10.1002/jor.1100060517

Carter, D. R., and Wong, M. (1988a). Mechanical stresses and endochondral ossification in the chondroepiphysis. *J. Orthop. Res.* 6, 148–154.

Carter, D. R., and Wong, M. (1988b). The role of mechanical loading histories in the development of diarthrodial joints. *J. Orthop. Res.* 6, 804–816.

Chao, E. Y., Aro, H. T., Lewallen, D. G., and Kelly, P. J. (1989). The effect of rigidity on fracture healing in external fixation. *Clin. Orthop. Relat. Res.* 241, 24–35.

Chrisovitsinos, J. P., Xenakis, T., Papakostides, K. G., Skaltsoyannis, N., Grestas, A., and Soucacos, P. N. (1997). Bridge plating osteosynthesis of 20 comminuted fractures of the femur. *Acta Orthop. Scand. Suppl.* 275, 72–76. doi: 10.1080/17453674.1997.11744750

Christian, C. A. (1998). "General principles of fracture treatment," in *Campbell's Operative Orthopaedics*, ed S. T. Canale (St. Louis, MO: Mosby), 1993–2041.

Claes, L., Augat, P., Suger, G., and Wilke, H. J. (1997). Influence of size and stability of the osteotomy gap on the success of fracture healing. *J. Orthop. Res.* 15, 577–584. doi: 10.1002/jor.1100150414

Claes, L., Blakytny, R., Besse, J., Bausewein, C., Ignatius, A., and Willie, B. (2011). Late dynamization by reduced fixation stiffness enhances fracture healing in a rat femoral osteotomy model. *J. Orthop. Trauma* 25, 169–174. doi: 10.1097/BOT.0b013e3181e3d994

Claes, L., Blakytny, R., Gockelmann, M., Schoen, M., Ignatius, A., and Willie, B. (2009). Early dynamization by reduced fixation stiffness does not improve fracture healing in a rat femoral osteotomy model. *J. Orthop. Res.* 27, 22–27. doi: 10.1002/jor.20712

Claes, L. E., Heigele, C. A., Neidlinger-Wilke, C., Kaspar, D., Seidl, W., Margevicius, K. J., et al. (1998). Effects of mechanical factors on the fracture healing process. *Clin. Orthop. Relat. Res.* 355(Suppl.), S132–S147. doi: 10.1097/00003086-199810001-00015

Cole, J. D., Justin, D., Kasparis, T., DeVlught, D., and Knobloch, C. (2001). The intramedullary skeletal kinetic distractor (ISKD): first clinical results of a new intramedullary nail for lengthening of the femur and tibia. *Injury* 32(Suppl. 4), SD129–SD139. doi: 10.1016/s0020-1383(01)00116-4

Court-Brown, C. M., Gustilo, T., and Shaw, A. D. (1997). Knee pain after intramedullary tibial nailing: its incidence, etiology, and outcome. *J. Orthop. Trauma* 11, 103–105. doi: 10.1097/00005131-199702000-00006

Cullinane, D. M., Fredrick, A., Eisenberg, S. R., Pacicca, D., Elman, M. V., Lee, C., et al. (2002). Induction of a neoarthrosis by precisely controlled motion in an experimental mid-femoral defect. *J. Orthop. Res.* 20, 579–586. doi: 10.1016/S0736-0266(01)00131-0

Danis, R. (1949). *Theorie et Pratique de L'osteosynthese*. Paris: Masson.

d'Aubigne, R. M., Maurer, P., Zucman, J., and Masse, Y. (1974). Blind intramedullary nailing for tibial fractures. *Clin. Orthop. Relat. Res.* 105, 267–275.

De Bastiani, G., Aldegheri, R., and Renzi Brivio, L. (1984). The treatment of fractures with a dynamic axial fixator. *J. Bone Joint Surg. Br.* 66, 538–545.

Domb, B. G., Sponseller, P. D., Ain, M., and Miller, N. H. (2002). Comparison of dynamic versus static external fixation for pediatric femur fractures. *J. Pediatr. Orthop.* 22, 428–430. doi: 10.1097/01241398-200207000-00003

Donald, G., and Seligson, D. (1983). Treatment of tibial shaft fractures by percutaneous Kuntscher nailing. Technical difficulties and a review of 50 consecutive cases. *Clin. Orthop. Relat. Res.* 64–73.

Duda, G. N., Sollmann, M., Sporrer, S., Hoffmann, J. E., Kassi, J.-P., Khodadadyan, C., et al. (2002). Interfragmentary motion in tibial osteotomies stabilized with ring fixators. *Clin. Orthop. Relat. Res.* 396, 163–172. doi: 10.1097/00003086-200203000-00025

Eggers, G. W. (1948). Internal contact splint. *J. Bone Joint Surg. Am.* 30A, 40–52. doi: 10.2106/00004623-194830010-00006

Eijer, H., Hauke, C., Arens, S., Printzen, G., Schlegel, U., and Perren, S. M. (2001). PC-Fix and local infection resistance–influence of implant design on postoperative infection development, clinical and experimental results. *Injury* 32(Suppl. 2), B38–B43. doi: 10.1016/s0020-1383(01)00124-3

Epari, D. R., Schell, H., Bail, H. J., and Duda, G. N. (2006). Instability prolongs the chondral phase during bone healing in sheep. *Bone* 38, 864–870. doi: 10.1016/j.bone.2005.10.023

Farouk, O., Krettek, C., Miclau, T., Schandelmaier, P., Guy, P., and Tscherne, H. (1999). Minimally invasive plate osteosynthesis: does percutaneous plating disrupt femoral blood supply less than the traditional technique? *J. Orthop. Trauma* 13, 401–406.

Farouk, O., Krettek, C., Miclau, T., Schandelmaier, P., and Tscherne, H. (1998). Effects of percutaneous and conventional plating techniques on the blood supply to the femur. *Arch. Orthop. Trauma Surg.* 117, 438–441. doi: 10.1007/s004020050288

Fischgrund, J., Paley, D., and Suter, C. (1994). Variables affecting time to bone healing during limb lengthening. *Clin. Orthop. Relat. Res.* 301, 31–37. doi: 10.1097/00003086-199404000-00006

Foxworthy, M., and Pringle, R. M. (1995). Dynamization timing and its effect on bone healing when using the Orthofix Dynamic Axial Fixator. *Injury* 26, 117–119. doi: 10.1016/0020-1383(95)92189-H

Gardner, T. N., Evans, M., and Kenwright, J. (1996). The influence of external fixators on fracture motion during simulated walking. *Med. Eng. Phys.* 18, 305–313. doi: 10.1016/1350-4533(95)00056-9

Gautier, E., and Sommer, C. (2003). Guidelines for the clinical application of the LCP. *Injury* 34(Suppl. 2), B63–B76. doi: 10.1016/j.injury.2003.09.026

Gerber, C., Mast, J. W., and Ganz, R. (1990). Biological internal fixation of fractures. *Arch. Orthop. Trauma Surg.* 109, 295–303. doi: 10.1007/BF00636165

Giorgi, M., Verbruggen, S. W., and Lacroix, D. (2016). *In silico* bone mechanobiology: modeling a multifaceted biological system. *Wiley Interdiscip. Rev. Syst. Biol. Med.* 8, 485–505. doi: 10.1002/wsbm.1356

Glatt, V., Bartnikowski, N., Quirk, N., Schuetz, M., and Evans, C. (2016a). Reverse Dynamization: influence of fixator stiffness on the mode and efficiency of large-bone-defect healing at different doses of rhBMP-2. *J. Bone Joint Surg. Am.* 98, 677–687. doi: 10.2106/JBJS.15.01027

Glatt, V., Evans, C. H., and Matthys, R. (2012a). Design, characterisation and *in vivo* testing of a new, adjustable stiffness, external fixator for the rat femur. *Eur. Cell Mater* 23, 289–298. discussion: 299. doi: 10.22203/eCM.v023a22

Glatt, V., Miller, M., Ivkovic, A., Liu, F., Parry, N., Griffin, D., et al. (2012b). Improved healing of large segmental defects in the rat femur by reverse dynamization in the presence of bone morphogenetic protein-2. *J. Bone Joint Surg. Am.* 94, 2063–2073. doi: 10.2106/JBJS.K.01604

Glatt, V., Tepic, S., and Evans, C. (2016b). Reverse dynamization: a novel approach to bone healing. *J. Am. Acad. Orthop. Surg.* 24, e60–e61. doi: 10.5435/JAAOS-D-16-00239

Gluck, T. (1890). Autoplastic transplantation. Implantation von fremdkorpern. *Berl. Klin. Wochenschr.* 19, 421–427.

Gómez-Benito, M. J., García-Aznar, J. M., Kuiper, J. H., and Doblaré, M. (2006). A 3D computational simulation of fracture callus formation: influence of the stiffness of the external fixator. *J. Biomech. Eng.* 128, 290–299. doi: 10.1115/1.2187045

Goodship, A. E., and Kenwright, J. (1985). The influence of induced micromovement upon the healing of experimental tibial fractures. *J. Bone Joint Surg. Br.* 67, 650–655.

Gorman, S. C., Kraus, K. H., Keating, J. H., Tidwell, A. S., Rand, W. M., Parkington, J. D., et al. (2005). *In vivo* axial dynamization of canine tibial fractures using the Securos external skeletal fixation system. *Vet. Comp. Orthop. Traumatol.* 18, 199–207.

Grosse, A., Kempf, I., and Lafforgue, D. (1978). [Treatment of fragments, loss of bony substance and pseudarthrosis of femur and tibia using screw fixation (40 cases)]. *Rev. Chir. Orthop. Reparatrice Appar. Mot.* 64(Suppl. 2), 33–35.

Grundnes, O., and Reikerås, O. (1993). Effects of instability on bone healing. Femoral osteotomies studied in rats. *Acta Orthop. Scand.* 64, 55–58. doi: 10.3109/17453679308994529

Haas, N., Hauke, C., Schütz, M., Kääb, M., and Perren, S. M. (2001). Treatment of diaphyseal fractures of the forearm using the Point Contact Fixator (PC-Fix): results of 387 fractures of a prospective multicentric study (PC-Fix II). *Injury* 32(Suppl. 2), B51–B62. doi: 10.1016/s0020-1383(01)00126-7

Haasper, C., Drescher, M., Hesse, E., Krettek, C., Zeichen, J., and Jagodzinski, M. (2008). [Osteogenic differentiation of human bone marrow stromal cells (hBMSC) by cyclic longitudinal mechanical strain and dexamethasone]. *Z. Orthop. Unfall.* 146, 636–643. doi: 10.1055/s-2008-1038578

Hasler, C. C., and Krieg, A. H. (2012). Current concepts of leg lengthening. *J. Child. Orthop.* 6, 89–104. doi: 10.1007/s11832-012-0391-5

Hente, R., Cordey, J., Rahn, B. A., Maghsudi, M., von Gumppenberg, S., and Perren, S. M. (1999). Fracture healing of the sheep tibia treated using a unilateral external fixator. *Comp. Static Dyn. Fixat. Injury* 30(Suppl. 1), A44–A51.

Hippocrates (1938). *Works of Hippocrates*. Baltimore, MA: Williams and Wilkins.

Hoglund, E. J. (1917). New method of applying autogenous intramedullary bone transplants and of making autogenous bone-screws. *Surg. Gynecol. Obstet.* 24, 243–246.

Howard, C. B., Leibergal, M., Elishoov, O., Matan, Y., Segal, D., and Porat, S. (2013). Can changing the mechanical environment increase the speed of fracture healing? A pilot study in tibial fractures. *J. Trauma Treat* 2, 1–5. doi: 10.4172/2167-1222.1000176

Huang, C., and Ogawa, R. (2010). Mechanotransduction in bone repair and regeneration. *FASEB J.* 24, 3625–3632. doi: 10.1096/fj.10-157370

Ilizarov, G. A. (1988). The principles of the Ilizarov method. *Bull. Hosp. Jt. Dis. Orthop. Inst.* 48, 1–11.

Ilizarov, G. A. (1989a). The tension-stress effect on the genesis and growth of tissues: Part II. The influence of the rate and frequency of distraction. *Clin. Orthop. Relat. Res.* 263–285.

Ilizarov, G. A. (1989b). The tension-stress effect on the genesis and growth of tissues. Part I. The influence of stability of fixation and soft-tissue preservation. *Clin. Orthop. Relat. Res.* 249–281.

Ilizarov, G. A., and Frankel, V. H. (1988). The Ilizarov External Fixator, a physiologic method of orthopaedic reconstruction and skeletal correction. A conversation with Prof. G. A. Ilizarov and Victor H. Frankel. *Orthop. Rev.* 17, 1142–1154.

Jansen, J. H., Weyts, F. A., Westbroek, I., Jahr, H., Chiba, H., Pols, H. A., et al. (2004). Stretch-induced phosphorylation of ERK1/2 depends on differentiation stage of osteoblasts. *J. Cell. Biochem.* 93, 542–551. doi: 10.1002/jcb.20162

Jekir, M. G., and Donahue, H. J. (2009). Gap junctions and osteoblast-like cell gene expression in response to fluid flow. *J. Biomech. Eng.* 131:011005. doi: 10.1115/1.3005201

Keating, J. F., O'Brien, P. J., Blachut, P. A., Meek, R. N., and Broekhuyse, H. M. (1997). Locking intramedullary nailing with and without reaming for open fractures of the tibial shaft. A prospective, randomized study. *J. Bone Joint Surg. Am.* 79, 334–341. doi: 10.2106/00004623-199703000-00003

Kelly, D. J., and Jacobs, C. R. (2010). The role of mechanical signals in regulating chondrogenesis and osteogenesis of mesenchymal stem cells. *Birth Defects Res. C Embryo Today* 90, 75–85. doi: 10.1002/bdrc.20173

Kempf, I., Grosse, A., and Beck, G. (1985). Closed locked intramedullary nailing. Its application to comminuted fractures of the femur. *J. Bone Joint Surg. Am.* 67, 709–720. doi: 10.2106/00004623-198567050-00005

Kenwright, J., and Gardner, T. (1998). Mechanical influences on tibial fracture healing. *Clin. Orthop. Relat. Res.* 355(Suppl.), S179–S190. doi: 10.1097/00003086-199810001-00019

Kenwright, J., and Goodship, A. E. (1989). Controlled mechanical stimulation in the treatment of tibial fractures. *Clin. Orthop. Relat. Res.* 241, 36–47. doi: 10.1097/00003086-198904000-00006

Klein, P., Opitz, M., Schell, H., Taylor, W. R., Heller, M. O., Kassi, J. P., et al. (2004). Comparison of unreamed nailing and external fixation of tibial diastases–mechanical conditions during healing and biological outcome. *J. Orthop. Res.* 22, 1072–1078. doi: 10.1016/j.orthres.2004.02.006

Klein, P., Schell, H., Streitparth, F., Heller, M., Kassi, J. P., Kandziora, F., et al. (2003). The initial phase of fracture healing is specifically sensitive to mechanical conditions. *J. Orthop. Res.* 21, 662–669. doi: 10.1016/S0736-0266(02)00259-0

Klein-Nulend, J., Bakker, A. D., Bacabac, R. G., Vatsa, A., and Weinbaum, S. (2013). Mechanosensation and transduction in osteocytes. *Bone* 54, 182–190. doi: 10.1016/j.bone.2012.10.013

Konig, F. (1913). Uber die Implantation von Elfenbein zum Ersatz von Knochen und Gelenken. Nach experimentellen und klinischen Beobachtungen. *Berl. Klin. Chir.* 85, 91–114.

Kucukkaya, M., Sokucu, S., and Thaller, P. H. (2015). Surgical techniques for lengthening and deformity correction of the femur with lengthening nails. *Tech. Orthop.* 30, 183–188. doi: 10.1097/BTO.0000000000000137

Kummer, F. J. (1992). Biomechanics of the Ilizarov external fixator. *Clin. Orthop. Relat. Res.* 280, 11–14. doi: 10.1097/00003086-199207000-00003

Kuntscher, G. B. (1958). The Kuntscher method of intramedullary fixation. *J. Bone Joint Surg. Am.* 40-A, 17–26. doi: 10.2106/00004623-195840010-00002

LaBianco, G. J., Rush, S. M., and Vito, G. R. (2001). "External fixation," in *McGlamry's Comprehensive Textbook of Foot and Ancle Surgery, 3rd Edn.*, eds A. S. Banks, M. S. Downey, D. E. Martin, and S. J. Miller (Philadelphia, PA: Wiliams and Wilkins), 107–138.

Lacroix, D., and Prendergast, P. J. (2002). A mechano-regulation model for tissue differentiation during fracture healing: analysis of gap size and loading. *J. Biomech.* 35, 1163–1171. doi: 10.1016/S0021-9290(02)00086-6

Lane, W. A. (1895). Some remarks on the treatment of fractures. *Br. Med. J.* 1, 861–863.

Larsson, S., Kim, W., Caja, V. L., Egger, E. L., Inoue, N., and Chao, E. Y. S. (2001). Effect of early axial dynamization on tibial bone healing: a study in dogs. *Clin. Orthop. Relat. Res.* 388, 240–251. doi: 10.1097/00003086-200107000-00033

Lenarz, C., Bledsoe, G., and Watson, J. T. (2008). Circular external fixation frames with divergent half pins: a pilot biomechanical study. *Clin. Orthop. Relat. Res.* 466, 2933–2939. doi: 10.1007/s11999-008-0492-0

Lambotte, A. (1909). A technique et indication des protheses dans le traitement des fractures. *Presse Med.* 17:321.

Lottes, J. O. (1954). Blind nailing technique for insertion of the triflange medullar nail: report of three hundred nailing for fractures of the shaft of the tibia. *J. Am. Med. Assoc.* 155, 1039–1042. doi: 10.1001/jama.1954.03690300017004

Lottes, J. O. (1974). Medullary nailing of the tibia with the triflange nail. *Clin. Orthop. Relat. Res.* 105, 253–266. doi: 10.1097/00003086-197411000-00017

Lucas-Championniere, J. (1881). *Antiseptic Surgery: The Principles, Modes of Application, and Results of Lister Dressing*. Portland, OR: University Press.

Lujan, T. J., Henderson, C. E., Madey, S. M., Fitzpatrick, D. C., Marsh, J. L., and Bottlang, M. (2010). Locked plating of distal femur fractures leads to inconsistent and asymmetric callus formation. *J. Orthop. Trauma* 24, 156–162. doi: 10.1097/BOT.0b013e3181be6720

Luu, Y. K., Pessin, J. E., Judex, S., Rubin, J., and Rubin, C. T. (2009). mechanical signals as a non-invasive means to influence mesenchymal stem cell fate, promoting bone and suppressing the fat phenotype. *Bonekey Osteovis.* 6, 132–149. doi: 10.1138/20090371

Malgaaigne, J. F. (1859). *A Treatise on Fractures*. Philadelphia, PA: JB Lippincott and Co.

Marsh, J. L., Nepola, J. V., Wuest, T. K., Osteen, D., Cox, K., and Oppenheim, W. (1991). Unilateral external fixation until healing with the dynamic axial fixator for severe open tibial fractures. *J. Orthop. Trauma* 5, 341–348. doi: 10.1097/00005131-199109000-00014

McKibbin, B. (1978). The biology of fracture healing in long bones. *J. Bone Joint Surg. Br.* 60-B, 150–162.

Meinel, L., Karageorgiou, V., Fajardo, R., Snyder, B., Shinde-Patil, V., Zichner, L., et al. (2004). Bone tissue engineering using human mesenchymal stem cells: effects of scaffold material and medium flow. *Ann. Biomed. Eng.* 32, 112–122. doi: 10.1023/B:ABME.0000007796.48329.b4

Meléndez, E. M., and Colón, C. (1989). Treatment of open tibial fractures with the Orthofix fixator. *Clin. Orthop. Relat. Res.* 241, 224–230.

Morgan, E. F., Gleason, R. E., Hayward, L. N., Leong, P. L., and Palomares, K. T. (2008). Mechanotransduction and fracture repair. *J. Bone Joint Surg. Am.* 90(Suppl. 1), 25–30. doi: 10.2106/JBJS.G.01164

Noordeen, M. H., Lavy, C. B., Shergill, N. S., Tuite, J. D., and Jackson, A. M. (1995). Cyclical micromovement and fracture healing. *J. Bone Joint Surg. Br.* 77, 645–648.

Ozaki, A., Tsunoda, M., Kinoshita, S., and Saura, R. (2000). Role of fracture hematoma and periosteum during fracture healing in rats: interaction of fracture hematoma and the periosteum in the initial step of the healing process. *J. Orthop. Sci.* 5, 64–70. doi: 10.1007/s007760050010

Pacicca, D. M., Moore, D. C., and Ehrlich, M. G. (2002). Physiologic weight-bearing and consolidation of new bone in a rat model of distraction osteogenesis. *J. Pediatr. Orthop.* 22, 652–659. doi: 10.1097/01241398-200209000-00016

Paley, D. (2015). PRECICE intramedullary limb lengthening system. *Expert Rev. Med. Devices* 12, 231–249. doi: 10.1586/17434440.2015.1005604

Paley, D., Debiparshad, K., Balci, H., Windisch, W., and Lichtblau, C. (2015). Stature lengthening using the PRECICE Intramedullary lengthening nail. *Tech. Orthop.* 30, 167–182. doi: 10.1097/BTO.0000000000000140

Park, S. H., O'Connor, K., Sung, R., McKellop, H., and Sarmiento, A. (1999). Comparison of healing process in open osteotomy model and closed fracture model. *J. Orthop. Trauma* 13, 114–120. doi: 10.1097/00005131-199902000-00008

Pauwels, F. (1960). [A new theory on the influence of mechanical stimuli on the differentiation of supporting tissue. The tenth *contribution to the functional anatomy and causal morphology of the supporting structure.*]. Z Anat. Entwicklungsgesch. 121, 478–515. doi: 10.1007/BF00523401

Perren, S. M., and Cordey, J. (1980). "The concept of interfragmentary strain," in *Internal Fixation of Fractures*, ed H. K. Uhthoff (Berlin: Springer-Verlag), 63–77.

Perren, S. M., Cordey, J., Rahn, B. A., Gautier, E., and Schneider, E. (1988). Early temporary porosis of bone induced by internal fixation implants a reaction to necrosis, not to stress protection? *Clin. Orthop. Relat. Res.* 232, 139–151.

Podolsky, A., and Chao, E. Y. S. (1993). Mechanical performance of Ilizarov circular external fixators in comparison with other external fixators. *Clin. Orthop. Relat. Res.* 293, 61–70. doi: 10.1097/00003086-199308000-00009

Qin, Y. X., and Hu, M. (2014). Mechanotransduction in musculoskeletal tissue regeneration: effects of fluid flow, loading, and cellular-molecular pathways. *Biomed. Res. Int.* 201:863421. doi: 10.1155/2014/863421

Qin, Y. X., Kaplan, T., Saldanha, A., and Rubin, C. (2003). Fluid pressure gradients, arising from oscillations in intramedullary pressure, is correlated with the formation of bone and inhibition of intracortical porosity. *J. Biomech.* 36, 1427–1437. doi: 10.1016/S0021-9290(03)00127-1

Rand, J. A., An, K. N., Chao, E. Y., and Kelly, P. J. (1981). A comparison of the effect of open intramedullary nailing and compression-plate fixation on fracture-site blood flow and fracture union. *J. Bone Joint Surg. Am.* 63, 427–442. doi: 10.2106/00004623-198163030-00018

Roux, W. (1881). "Der Zuchtende Kampf der Teile, oder die" "Teilauslese im Organismus," in *Abhandlungen über Entwickelungsmechanik der Organismus*, ed E. von Krosigk (Leipzig: Wilhelm Engelmann), 135–422.

Rubin, C. T., and Hausman, M. R. (1988). The cellular basis of Wolff's law. Transduction of physical stimuli to skeletal adaptation. *Rheum Dis. Clin. North Am.* 14, 503–517.

Rubin, C. T., and Lanyon, L. E. (1984). Regulation of bone formation by applied dynamic loads. *J. Bone Joint Surg. Am.* 66, 397–402. doi: 10.2106/00004623-198466030-00012

Ruedi, T. P., Buckley, R. E., and Moran, C. G. (2007). *AO Principles of Fracture Managment*. Stuttgart: Thieme.

Russell, R. H. (1924). Fracture of the femur. A clinical study. *Br. J. Surg.* 11:491.

Sarmiento, A., and Latta, L. L. (1981). *Closed Functional Treatment of Fractures*. Berlin; New York, NY: Springer-Verlag.

Sherman, W. O. (1912). Vanadium steel bone plates and screws. *Surg. Gynecol. Obstet.* 14, 629–634.

Siguier, T., Glorion, C., Langlais, J., Rouvreau, P., and Pouliquen, J. C. (1995). [External fixation in fractures of the lower limb in children]. *Rev. Chir. Orthop. Reparatrice Appar. Mot.* 81, 157–162.

Stiehler, M., Bünger, C., Baatrup, A., Lind, M., Kassem, M., and Mygind, T. (2009). Effect of dynamic 3-D culture on proliferation, distribution, and osteogenic differentiation of human mesenchymal stem cells. *J. Biomed. Mater. Res. A* 89, 96–107. doi: 10.1002/jbm.a.31967

Stoffel, K., Dieter, U., Stachowiak, G., Gächter, A., and Kuster, M. S. (2003). Biomechanical testing of the LCP–how can stability in locked internal fixators be controlled? *Injury* 34(Suppl. 2), B11–B19. doi: 10.1016/j.injury.2003.09.021

Tanno, M., Furukawa, K. I., Ueyama, K., Harata, S., and Motomura, S. (2003). Uniaxial cyclic stretch induces osteogenic differentiation and synthesis of bone morphogenetic proteins of spinal ligament cells derived from patients with ossification of the posterior longitudinal ligaments. *Bone* 33, 475–484. doi: 10.1016/S8756-3282(03)00204-7

Tetsworth, K., and Paley, D. (1995). Basic science of distraction histogenesis. *Curr. Opin. Orthop.* 6, 61–68. doi: 10.1097/00001433-199512000-00012

Thaller, P. H., Wolf, F., and Kucukkaya, M. (2014). Surgical Techniques for lengthening and deformity correction of the Tibia with lengthening nails. *Tech. Orthop.* 29, 150–157. doi: 10.1097/BTO.0000000000000074

Thompson, W. R., Rubin, C. T., and Rubin, J. (2012). Mechanical regulation of signaling pathways in bone. *Gene* 503, 179–193. doi: 10.1016/j.gene.2012.04.076

Tigani, D., Fravisini, M., Stagni, C., Pascarella, R., and Boriani, S. (2005). Interlocking nail for femoral shaft fractures: is dynamization always necessary? *Int. Orthop.* 29, 101–104. doi: 10.1007/s00264-004-0627-1

Toivanen, J. A., Vaisto, O., Kannus, P., Latvala, K., Honkonen, S. E., and Jarvinen, M. J. (2002). Anterior knee pain after intramedullary nailing of fractures of the tibial shaft. A prospective, randomized study comparing two different nail-insertion techniques. *J. Bone Joint Surg. Am.* 84-A, 580–585. doi: 10.2106/00004623-200204000-00011

Tornetta, P. III, and Collins, E. (1996). Semiextended position of intramedullary nailing of the proximal tibia. *Clin. Orthop. Relat. Res.* 185–189. doi: 10.1097/00003086-199607000-00029

Tornetta, P. III., Riina, J., Geller, J., and Purban, W. (1999). Intraarticular anatomic risks of tibial nailing. *J. Orthop. Trauma* 13, 247–251. doi: 10.1097/00005131-199905000-00004

Uhthoff, H. K., Bardos, D. I., and Liskova-Kiar, M. (1981). The advantages of titanium alloy over stainless steel plates for the internal fixation of fractures. An experimental study in dogs. *J. Bone Joint Surg. Br.* 63-B, 427–484.

Uhthoff, H. K., Boisvert, D., and Finnegan, M. (1994). Cortical porosis under plates. Reaction to unloading or to necrosis? *J. Bone Joint Surg. Am.* 76, 1507–1512. doi: 10.2106/00004623-199410000-00010

Uhthoff, H. K., and Dubuc, F. L. (1971). Bone structure changes in the dog under rigid internal fixation. *Clin. Orthop. Relat. Res.* 81, 165–170. doi: 10.1097/00003086-197111000-00026

Uhthoff, H. K., and Finnegan, M. (1983). The effects of metal plates on post-traumatic remodelling and bone mass. *J. Bone Joint Surg. Br.* 65, 66–71.

Uhthoff, H. K., Poitras, P., and Backman, D. S. (2006). Internal plate fixation of fractures: short history and recent developments. *J. Orthop. Sci.* 11, 118–126. doi: 10.1007/s00776-005-0984-7

Utvåg, S. E., Korsnes, L., Rindal, D. B., and Reikerås, O. (2001). Influence of flexible nailing in the later phase of fracture healing: strength and mineralization in rat femora. *J. Orthop. Sci.* 6, 576–584. doi: 10.1007/s007760100015

Utvåg, S. E., and Reikerås, O. (1998). Effects of nail rigidity on fracture healing. Strength and mineralisation in rat femoral bone. *Arch. Orthop. Trauma Surg.* 118, 7–13. doi: 10.1007/s004020050301

Uzer, G., Thompson, W. R., Sen, B., Xie, Z., Yen, S. S., Miller, S., et al. (2015). Cell mechanosensitivity to extremely low-magnitude signals is enabled by a LINCed Nucleus. *Stem Cells* 33, 2063–2076. doi: 10.1002/stem.2004

Verkerke, G. J., Schraffordt Koops, H., Veth, R. P., Oldhoff, J., Nielsen, H. K., van den Kroonenberg, H. H., et al. (1989). Design of a lengthening element for a modular femur endoprosthetic system. *Proc. Inst. Mech. Eng. H* 203, 97–102. doi: 10.1243/PIME_PROC_1989_203_017_01

Wang, L., Li, J. Y., Zhang, X. Z., Liu, L., Wan, Z. M., Li, R. X., et al. (2012). Involvement of p38MAPK/NF-κB signaling pathways in osteoblasts differentiation in response to mechanical stretch. *Ann. Biomed. Eng.* 40, 1884–1894. doi: 10.1007/s10439-012-0548-x

Wang, Q., Huang, C., Xue, M., and Zhang, X. (2011). Expression of endogenous BMP-2 in periosteal progenitor cells is essential for bone healing. *Bone* 48, 524–532. doi: 10.1016/j.bone.2010.10.178

Weinans, H., and Prendergast, P. J. (1996). Tissue adaptation as a dynamical process far from equilibrium. *Bone* 19, 143–149. doi: 10.1016/8756-3282(96)00143-3

Weyts, F. A., Bosmans, B., Niesing, R., van Leeuwen, J. P., and Weinans, H. (2003). Mechanical control of human osteoblast apoptosis and proliferation in relation to differentiation. *Calcif. Tissue Int.* 72, 505–512. doi: 10.1007/s00223-002-2027-0

Wiss, D. A., Fleming, C. H., Matta, J. M., and Clark, D. (1986). Comminuted and rotationally unstable fractures of the femur treated with an interlocking nail. *Clin. Orthop. Relat. Res.* 212, 35–47. doi: 10.1097/00003086-198611000-00006

Wolf, S., Janousek, A., Pfeil, J., Veith, W., Haas, F., Duda, G., et al. (1998). The effects of external mechanical stimulation on the healing of diaphyseal osteotomies fixed by flexible external fixation. *Clin. Biomech.* 13, 359–364. doi: 10.1016/S0268-0033(98)00097-7

Wolff, J. (1892). *Das Gesetz der Transformation der Knochen*. Berlin: Verlag von August Hirschwald.

Wolff, J. (1986). *The Law of Bone Remodeling (Translation of the German 1892 Edn)*. Berlin: Springer.

Wu, C. C. (1997). The effect of dynamization on slowing the healing of femur shaft fractures after interlocking nailing. *J. Trauma* 43, 263–267. doi: 10.1097/00005373-199708000-00010

Yamagishi, M., and Yoshimura, Y. (1955). The biomechanics of fracture healing. *J. Bone Joint Surg. Am.* 37-A, 1035–1068. doi: 10.2106/00004623-195537050-00013

Yanagisawa, M., Suzuki, N., Mitsui, N., Koyama, Y., Otsuka, K., and Shimizu, N. (2007). Effects of compressive force on the differentiation of pluripotent mesenchymal cells. *Life Sci.* 81, 405–412. doi: 10.1016/j.lfs.2007.06.004

Yanagisawa, M., Suzuki, N., Mitsui, N., Koyama, Y., Otsuka, K., and Shimizu, N. (2008). Compressive force stimulates the expression of osteogenesis-related transcription factors in ROS 17/2.8 cells. *Arch. Oral Biol.* 53, 214–219. doi: 10.1016/j.archoralbio.2007.08.012

Zucman, J., and Maurer, P. (1969). Two-level fractures of the tibia. Results in thirty-six cases treated by blind nailing. *J. Bone Joint Surg. Br.* 51, 686–693.

Conflict of Interest Statement: The authors declare that the research was conducted in the absence of any commercial or financial relationships that could be construed as a potential conflict of interest.

The reviewer CC and handling Editor declared their shared affiliation, and the handling Editor states that the process nevertheless met the standards of a fair and objective review.

frontiers in Physiology

ORIGINAL RESEARCH
published: 03 August 2017
doi: 10.3389/fphys.2017.00565

Sinus Augmentation with Biomimetic Nanostructured Matrix: Tomographic, Radiological, Histological and Histomorphometrical Results after 6 Months in Humans

Antonio Scarano[1], Felice Lorusso[1], Giorgio Staiti[2], Bruna Sinjari[1], Anna Tampieri[3] and Carmen Mortellaro[4]*

[1] Department of Medical, Oral and Biotechnological Sciences and CeSi-MeT, University of Chieti-Pescara, Chieti, Italy, [2] Private Practice, Torino, Italy, [3] Bioceramics and Bio-hybrid Composites Senior Affiliated Member Methodist Hospital Research Institute, Houston, TX, United States, [4] Department of Health Sciences Oral Surgery Unit, University of Eastern Piedmont, Novara, Italy

OPEN ACCESS

Edited by:
Giovanna Orsini, Università Politecnica delle Marche, Italy

Reviewed by:
Pablo Santos De Oliveira, University Center Inga (UNINGÁ), Brazil
Angelo Putignano, Università Politecnica delle Marche, Italy
Victor E. Arana-Chavez, University of São Paulo, Brazil

***Correspondence:**
Antonio Scarano
ascarano@unich.it

Specialty section:
This article was submitted to Craniofacial Biology and Dental Research, a section of the journal Frontiers in Physiology

Received: *27 January 2017*
Accepted: *20 July 2017*
Published: *03 August 2017*

Citation:
Scarano A, Lorusso F, Staiti G, Sinjari B, Tampieri A and Mortellaro C (2017) Sinus Augmentation with Biomimetic Nanostructured Matrix: Tomographic, Radiological, Histological and Histomorphometrical Results after 6 Months in Humans. Front. Physiol. 8:565. doi: 10.3389/fphys.2017.00565

Background: Many bone substitutes have been applied for sinus regeneration procedures, such as autogenous bone, inorganic bovine bone, porous and resorbable hydroxyapatite, tricalcium phosphate, bioactive glass, and blood clots. The aim of the present study was a tomographic, histological and histomorphometrical evaluation in humans, of specimens retrieved from sinuses augmented with MgHA/collagen-based scaffolds, after a healing period of 6 months.

Materials and Methods: Eleven healthy patients and a total of 15 sinuses were included in this study. The maxillary sinuses were filled with commercial MgHA/collagen-based scaffolds (RegenOss) with a porous three-dimensional (3D) structure (Fin-Ceramica Faenza S.p.A., Faenza, Italy). These grafts have a composite design, that replicate the organization of bone structure, obtained by a technique in which a specific hybrid organic–inorganic composite is spontaneously built by a biological mechanism. The CBCT scans were done before the procedure, after the surgical protocol (T1), and 6 months after sinus surgery (T2) for implantology. Bone specimens were stored in 10% formalin solution, embedded in a glycolmethacrylate resin and sectioned by a high-precision diamond disc. Histologic and histomorphometric analysis were carried out to evaluate the graft reabsorption and bone healing.

Results: The mean volume after graft elevation, calculated for each of the 15 sinuses, was 2,906 mm^3 in the immediate postoperative period (5–7 days), ranging from 2,148.8 to 3,146.4 mm^3. In the late postoperative period (6 months) it was 2,806.7 mm^3, ranging from 2,010.9 to 3,008.9 mm^3. The sinuses were completely healed and no residual MgHA/collagen-based scaffolds were visible. Osteoblasts appeared actively secreting bone matrix and marrow spaces contained moderate numbers of stromal cells and vascular network. Osteoblasts were observed actively secreting osteoid matrix. The

tissues present in the samples were composed of 1.9 ± 1.9% of lamellar bone, 36 ± 1% of woven bone and 58 ± 3.8% of marrow spaces.

Conclusion: Mg-MgHA/collagen-based scaffolds can successfully be used for sinus augmentation procedures.

Keywords: biomimetic, Mg-MgHA/collagen, sinus augmentation, biomaterials, bone healing

INTRODUCTION

Insufficient bone height, following tooth extractions and the pneumatization of the maxillary sinus in the lateral part of the maxilla, is an impediment to dental implant primary stability and a contraindication for implant surgery. In fact, in this situation oral rehabilitation with dental implants is often difficult and there is a high risk of implant displacement/migration into the maxillary, as has previously been reported. The augmentation of bone volume in posterior maxilla atrophy can be performed using a sinus lifting technique described by Tatum in 1986 (Tatum, 1986), allowing for about 6–8 months healing before implant insertion (Del Fabbro et al., 2004). Different biomaterials are currently used in bone regeneration and can be classified into four groups according to their origin: autogenic (bone originating from the same patient), allogenic (bone originating from another person), xenogenic (bone originating from another species) and synthetic (with no biological origin) (Scarano et al., 2006). The features of a bone substitute are critical factors for the success of bone augmentation.

Autogenous bone is considered ideal (Hallman et al., 2002; Samartzis et al., 2005). Donor sites for these techniques are usually the iliac crest for bilateral procedure and the oral cavity for unilateral sinus regeneration. Patients may evaluate the second surgical intervention in the donor area uncomfortable and may prefer the use of bone substitutes for the procedure. Biomaterial is a key component for the success of implants inserted into the grafted maxillary sinus. There is concern that some biomaterials may cause a foreign body reaction and the ideal material for sinus augmentation is still under debate (Scarano et al., 2017a).

Nevertheless, the application of xenografts has been associated with the permanency of residual material, due to their slow rate of reabsorption (Scarano et al., 2006) and the waiting time necessary for the bone to heal after biomaterial application, limiting their use in surgery. These results may be caused by the fact that structural and composition properties of these materials do not resemble those of natural bone. For this reason, many researchers have studied new synthetic grafting materials that promote bone formation with faster resorption processes and new combinations of osteoinductive scaffolds and stem cell-based protocol. Tissue engineering in the field of bone regeneration requires:

- biocompatible scaffold adhesion, diapedesis, proliferation, and differentiation of stem cells;
- an appropriate stem cell source for the deposition of new bone.

In an attempt to increase graft resorption and reduce healing time before implantation, while avoiding autologous bone harvesting, biomimetic Mg-MgHA/collagen-based scaffolds with a sinus augmentation procedure were used in this study. Hydroxyapatite (HA) is an osteoconductive, synthetic bioactive material, without osteoinductive properties, which limits its clinical use. The collagen has been added because it is present in the extracellular matrix of bone, performing the function of support by giving structural support to resident cells, osteoconductivity, biocompatibility, and ductility to the bone. Since Collagen type I is one of the proteins that play critical roles in bone mineralization, it can be the prime candidate material for realizing tissue-engineered grafts. The association of Hydroxyapatite and collagen type I (HA/Collagen) were used to improve osteoblast differentiation (Ramírez-Rodríguez et al., 2016). Magnesium (Mg) was added to HA for its positive role in bone healing. Its role is critical in the metabolism and turnover of bone (Toba et al., 2000).

These grafts have a composite architecture, mimicking the complex hierarchically organized bone structure, obtained through a proprietary technique in which a specific hybrid organic–inorganic composite is spontaneously built, driven by a biological mechanism. We hypothesize that this biomaterial is completely resorbable. In fact, many biomaterials act only as passive scaffolding, so insufficient bone remodeling occurs when bone regeneration mixes with grafts that do not resemble those of natural bone. Various studies have shown the osteoregenerative properties of Mg-MgHA/collagen in bone regeneration, but data on its use in maxillary sinus lifts in humans are not available yet (Berardinelli et al., 2013; Ramírez-Rodríguez et al., 2016). The aim was a radiologic, histological and histomorphometrical evaluation of a biomimetic nanostructure applied for sinus augmentation after a healing period of 6 months.

MATERIALS AND METHODS

Biomaterial

For the present research, a commercial MgHA/collagen-based scaffold, the RegenOss® (Fin-Ceramica Faenza S.p.A., Faenza, Italy), was used. The device is a commercially available, porous, three-dimensional composite bone substitute made of type I collagen fibers, in which nano-sized (10–20 nm) crystals of biomimetic Mg-doped hydroxyapatite (Mg-HA) are nucleated in a 40/60 wt ratio.

The composite material was produced following a biomineralization approach allowing for the formation of a bio inspired nanostructure consisting of nano-apatite crystals (Mg-HA) uniformly distributed in the bio-polymeric collagen

matrix. The device is manufactured being capable of reproducing the composition and the anatomical structure of the bone tissue, as it occurs in the biological process of neo-ossification. The organic component, working as a matrix mediating the mineralization process, was type I collagen extracted from equine Achille's tendon and was supplied by OPOCRIN Spa (Corlo di Formigine (MO), Italy) in a 1wt % suspension in an acetate buffer solution, pH 3.5. The apatitic phase (Mg-HA) was synthetized directly on the collagen molecules by a neutralization process where an acid solution containing suspended type I collagen in phosphoric acid (H_3PO_4, purity $\geq$ 85 wt%; Sigma Aldrich) was added drop-wise to a basic solution containing calcium hydroxide ($Ca(OH)_2$, purity $\geq$ 95 wt%; Sigma Aldrich) and magnesium chloride hexahydrate ($MgCl_2 \cdot 6H_2O$, purity $\geq$ 99 wt%; Sigma Aldrich). This method enables the manufacture of hybrid composites Mg-HA/Coll with a composition of 40/60 wt % obtained in form of a gel that was freeze-dried to achieve a porous device.

The device has a high safety profile highlighted by toxicological studies carried out in accordance with the laws and regulations in force concerning Class III medical devices. Once the tissue regeneration process has been completed, the device is able to undergo resorption. The mineralized structure is manufactured by nucleating bonelike nanostructured nonstoichiometric hydroxyapatite into self-assembling collagen fibers, as it occurs in the biological process of neo-ossification (Palarie et al., 2012).

These grafts have a composite architecture, mimicking the complex hierarchically organized bone structure, obtained through a proprietary technique in which a specific hybrid organic–inorganic composite is spontaneously built, driven by a biological mechanism. In particular, the biomaterial consists of a combination of type I collagen (30%) and MgHA (70%). It is synthesized using a standardized procedure that begins from an atelocollagen aqueous solution in acetic acid (1%, w/w), obtained from equine tendon (Opocrin S.p.A., Modena, Italy).

Surgical Procedure

This study was performed following the principles of the Declaration of Helsinki regarding research on humans; all patients gave a written informed consent to the treatment

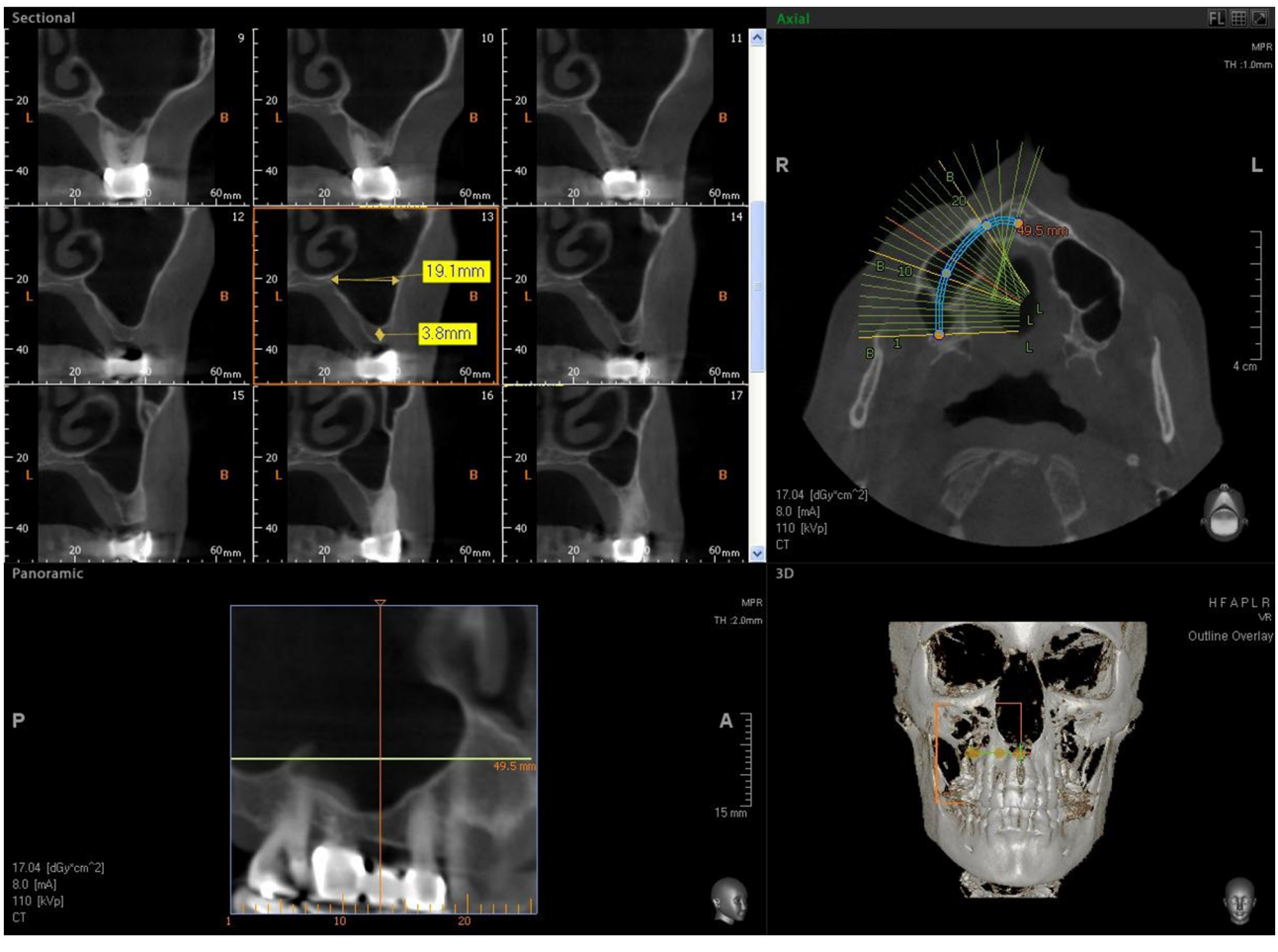

FIGURE 1 | CBCT image showing reduced bone height in the sinus area with a residual alveolar ridge height between 2 and 3 mm.

and study recruiting. The study was approved by the Inter Institutional Ethics Committee of University of Chieti-Pescara, Chieti, Italy. Eleven healthy patients (mean age: 52 years; range 48–65 years) without significant medical anamnesis, 7 women and 4 men, all non-smokers, were recruited as candidates for sinus augmentation and implant rehabilitation. They were treated in the Outpatient Department of Medical, Oral and Biotechnological Sciences of the University of Chieti-Pescara, Chieti, Italy. All sinus lifts were performed by a single surgeon. The inclusion criteria were:

- totally or partially edentulous
- unilateral or bilateral tooth loss (premolar or molar)
- severe atrophy (bone height: between 2 and 3 mm) (**Figure 1**).

The exclusion criteria were:

- severe disease, uncontrolled diabetes and smoking,
- head and neck radio or chemotherapy,
- uncontrolled periodontal disease, sinus pathology, or the presence of any dental roots in the sinus area.

At the initial visit, all subjects were clinically examined and radiographs were carried out for diagnostic evaluation; then the patients were scheduled for surgery procedures including sinus augmentation and implant insertion. They were informed about the surgical protocols and full cooperation was requested during the procedures. Before surgery the patients were subjected to applications of chlorhexidine digluconate solution 0.2% for 2 min to obtain lower bacterial load and local anesthesia was given with Articaine® (Ubistesin 4%—Espe Dental AG Seefeld, Germany) associated with epinephrine (1:100.000). A modified triangular flap, without anterior release, recently described by Scarano et al.

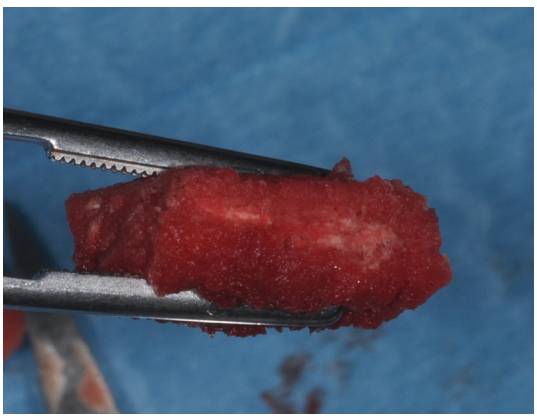

FIGURE 2 | During graft placement the blood molecules and cells promoting bone formation are quickly absorbed.

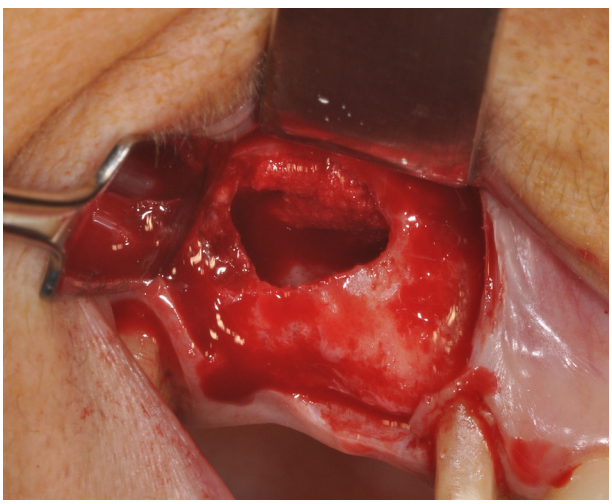

FIGURE 3 | The maxillary sinus lateral wall is exposed and a bone window is cut out.

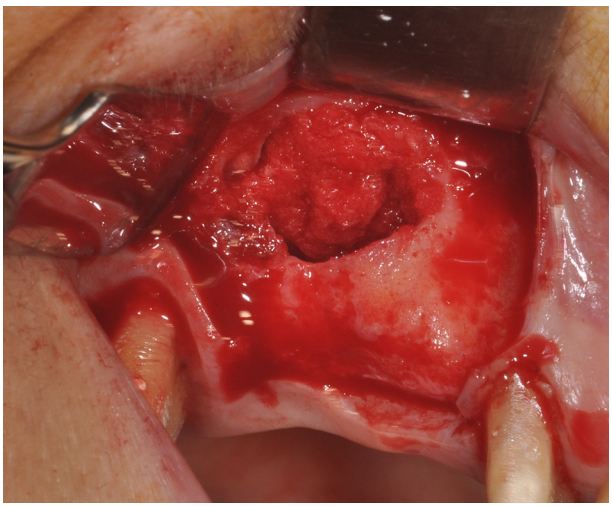

FIGURE 4 | The maxillary sinus filled with commercial MgHA/collagen-based scaffold.

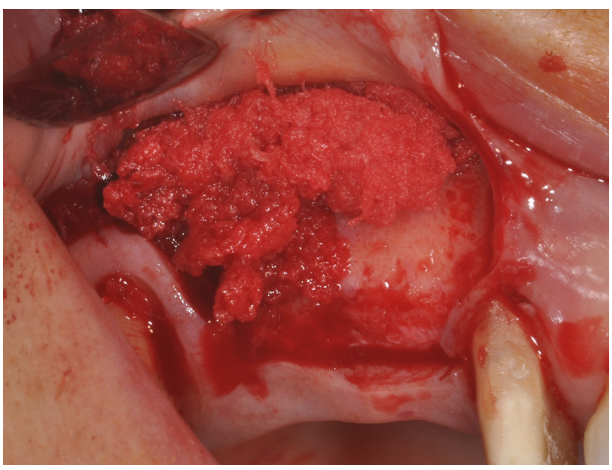

FIGURE 5 | During sinus filling, the scaffold can be easily adapted to the dimension and shape of the sinus, saving time, and improving sinus filling.

was used. The incision was made horizontally on the top of the alveolar ridge extending mesially if the patient was edentulous, in the presence of teeth the incision was continued by a sulcular incision starting near the mesiobuccal edge of the teeth extending up to the midpoint of the buccal sulcus of the canine, without cutting the interdental papilla. Full thickness flaps were detached to expose the bone ridge and the lateral wall of the sinus. A trap door was made in the lateral sinus wall with a piezoelectric device (Piezosurgery, Mectron, Carasco, Italy) under cold (4–5°C) sterile saline irrigation solution and the bone door was rotated inward and upward with a top hinge to a horizontal position. The detachment and elevation of the sinus membrane was accomplished by initially exposing and mobilizing by ultrasonic device, followed by hand instrumentation to further elevate it along the medial bone wall.

Seven patients were treated for unilateral sinus augmentation, while in 4 patients the procedure was bilateral for a total 15 maxillary sinuses. The maxillary sinuses were filled with commercial MgHA/collagen-based scaffold (RegenOss®) (**Figures 2–5**) with a porous three-dimensional structure (3D) (Fin-Ceramica Faenza S.p.A., Faenza, Italy). Thirty-three implants (Bone System, Milano, Italy) were positioned in the treated sinuses after a healing phase of 6 months. Cone Beam Computed Tomography evaluation (CBCT) (VatechIpax 3D PCH-6500, Fort Lee, NJ USA) was performed for preoperative and post-surgical sinus augmentation. DICOM data were elaborated with Ez3D Plus Software (EZ3D Plus, VATECH Global Fort Lee, NJ USA) to elaborate 3D model specimens and find the perfect position and alignment of sinus and biomaterial scaffolds with the bone itself. The CBCT scans were conducted before surgery (**Figure 1**), to diagnose the bone, immediately after surgery (T1), and 6 months after sinus grafting (T2) (**Figure 6**) since this period was recommended by the manufacturer for implant insertion. The CBCT scans were obtained with 1.0 mm in thickness and 0.2 mm interval under 110 kVp and 8 mA with a very low dosage. After selection of the appropriate area, using a specific tool and 3D reconstruction by an experienced radiologist, the software measured the volume.

Undecalcified Specimen Preparation and Histomorphometry

Bone specimens were obtained by a trephine bur with a 2 mm internal diameter and 13 mm length, stored in 10% formalin solution and treated to obtain thin sections (**Figure 7**); the next phase consisted in processing the samples by Precise 1 Automated System (Assing, Rome, Italy). The samples were dehydrated in a graduated

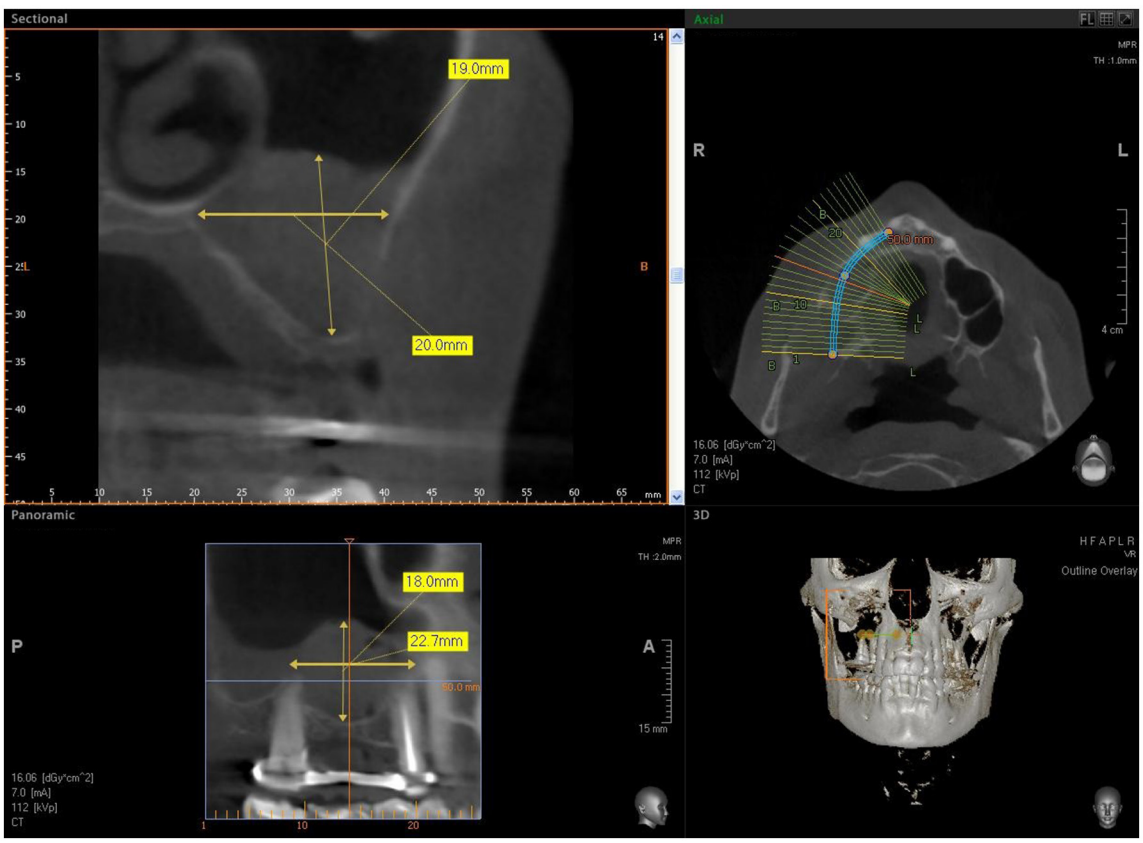

FIGURE 6 | CBCT after sinus augmentation, the grafted biomaterial is clearly distinguishable from the remaining original bone in regard to its density and structure. The biomaterial is well circumscribed with no scattered particles in the sinus.

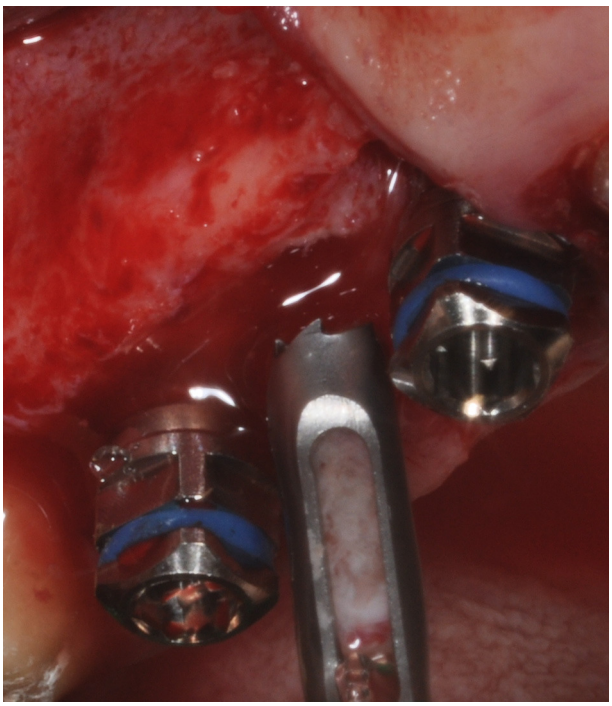

FIGURE 7 | After 6 months of healing: Maxillary sinus augmentation performed with biomaterial. During implant placement, the maxillary sinus lateral wall is completely filled by new bone and bone core retrieval with a trephine bur.

TABLE 1 | Volume graft at T0 and at 6 months from the surgery.

N° sinus	Volume after graft elevation (mm^3)	Volume after 6 months (mm^3)
#1	2,800	2,810
#2	3,120	2,806
#3	2,148	2,011
#4	2,253	2,220
#5	3,001	2,890
#6	3,147	2,960
#7	2,974	2,930
#8	3,101	3,040
#9	3,010	2,820
#10	2,980	2,890
#11	2,909	2,890
#12	3,103	2,992
#13	3,120	2,813
#14	3,010	2,901
#15	2,929	2,830
Mean volume	2,907 mm^3	2,806 mm^3
Range	2,148.8 to 3,146.4 mm^3	2,010.9–3,008.9 mm^3

series of ethanol, embedded in a glycolmethacrylate resin (Technovit 7200 VLC, Kulzer, Wehrheim, Germany) and sectioned longitudinally at about 150 μm by a high-precision diamond disc. The sections were also thinned to 30 μm by a grinding machine (Precise 1 Automated System, Assing, Rome, Italy). Three slides were collected for each specimen and stained with toluidine blue for transmitted light microscopy examination (Leitz Laborlux, Leitz, Wetzlar, Germany).

Histomorphometry was used to evaluate the residual graft material, the percentages of newly-formed bone and marrow spaces. This evaluation was carried out by observation through a microscope (Laborlux S, Leitz, Wetzlar, Germany), connected to a high definition camera (3CCD, JVC KY-F55B, JVC®, Yokohama, Japan) and Personal Computer interface (Intel Pentium III 1200 MMX, Intel®, Santa Clara, CA, USA). This equipment was linked to a digitizing pad (Matrix Vision GmbH, Oppenweiler, Germany) and a histometry software with image capturing applications (Image-Pro Plus 4.5, Media Cybernetics Inc., Immagini & Computer Snc Milano, Italy). Two separate histologists evaluated the results and found few differences.

RESULTS

The biomaterial shapes perfectly to fit the anatomic curvature of the graft sinus. During surgery, this osteostimulative and biodegradable scaffold can be easily adapted to the dimension and shape of the sinus, saving time and improving sinus filling. During graft placement, it can quickly adsorb the blood molecules and cells, promoting bone formation. Its architecture favors cell attachment and proliferation. The grafted biomaterial was clearly distinguishable from the remaining original bone, due to its density and structure (**Figures 3**–**5**). The mean volume after graft elevation, calculated for each of the 15 sinuses, was 2,906 mm^3in the immediate postoperative period (5–7 days), ranging from 2,148.8 to 3,146.4 mm^3. In the late postoperative period (6 months) it was 2,806.7 mm^3, ranging from 2,010.9 to 3,008.9 mm^3 (**Figure 6**). A total of 45 CT scans of the sinus augmentation of the 15 sinuses were evaluated (**Table 1**). No perforation of the sinus membrane was evident in 12 sinuses, while in 3 sinuses a small perforation was evident. No acute infection, nor pain nor fever were observed.

In all cases, bone augmentation showed hyper density in the immediate postoperative period and late postoperative period, with more density than native bone at both times. The statistical analysis demonstrated a significant difference of volume change ($P = 0.001229$). At low magnification, trabecular mature bone was observed. Osteoid material was found only around some of the particles. In all specimens, no pathological inflammatory cell infiltrate was present. No foreign body reactions were present. The biomaterials were completely resorbed. No epithelial cells or connective tissue were found in the retrieved specimens. Prominent woven and mature bone was observed. Mature bone deriving from the endosteal surface filled the external portion of the bone sinus. The periphery and central portion of the cavities showed mineralized new bone formation. The sinuses were completely healed and no particles or MgHA/collagen-based scaffolds were visible (**Figures 8**, **9**). Osteoid matrix actively secreted by osteoblasts (**Figure 10**) andmoderate numbers of

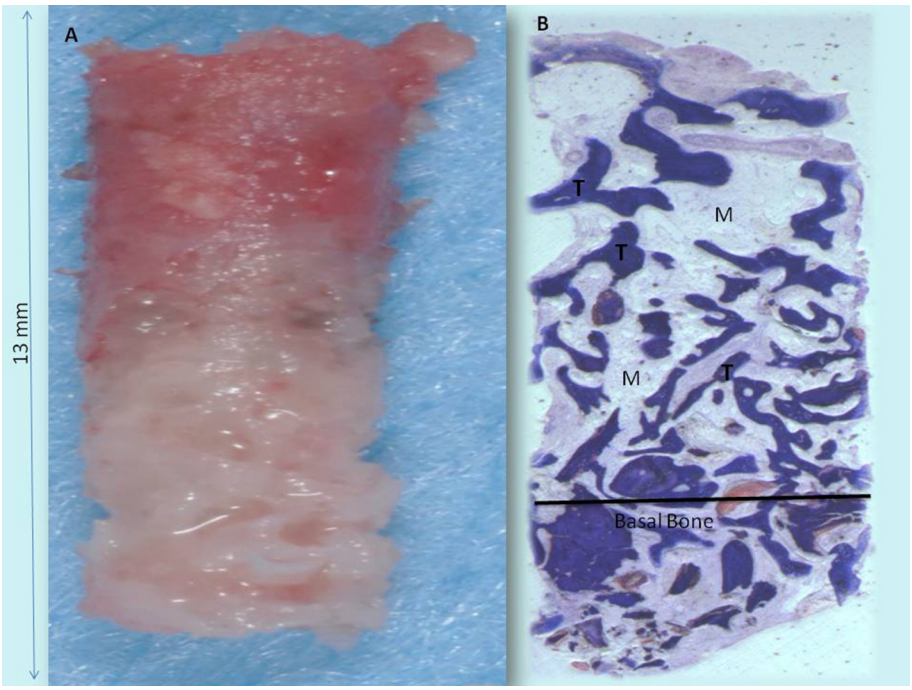

FIGURE 8 | (A) Bone core biopsy carried out with a small trephine. **(B)** The sinus is filled by the newly formed trabecular bone (T) with wide marrow spaces (M), while lamellar bone and haversian system were not present. No residual biomaterials were present. Toluidine blue 3X.

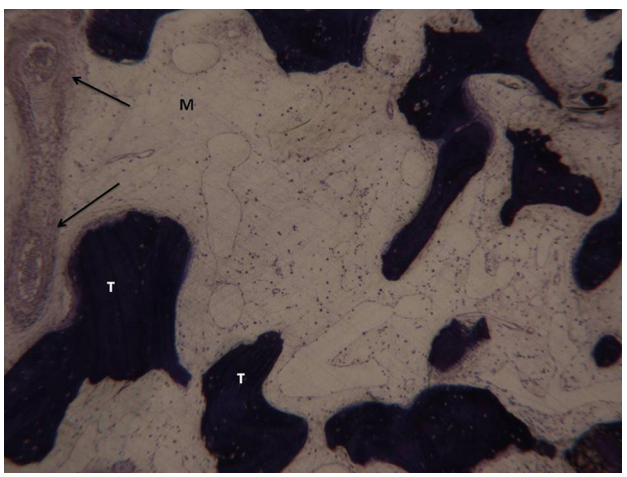

FIGURE 9 | In the marrow space no pathological inflammatory cell infiltrate is present. Neither foreign body reaction cells nor multinucleated giant cells were observed. A small trabecular bone (T) with a large marrow space (M) and vessels is present (arrows). Toluidine blue 100X.

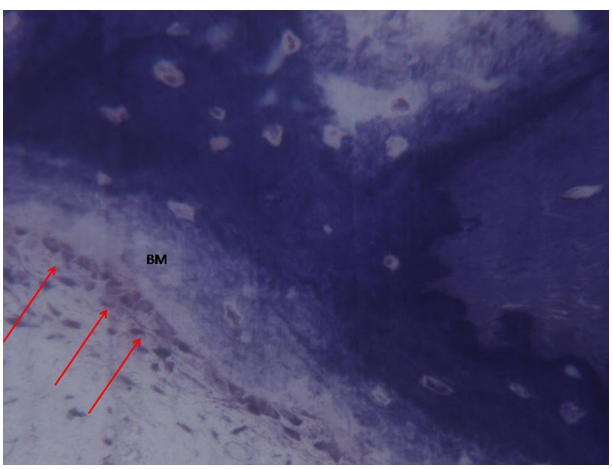

FIGURE 10 | A higher magnification of the previous image. Osteoblasts (arrows) appeared actively secreting bone matrix (BM). Toluidine blue 200X.

marrow stromal cells and vascular network contained in marrow spaceswere observed. In particular, seams of osteoblasts and unmineralized matrix with collagen fibrils in areas of new bone apposition were observed. The tissues present in the sample were composed of 1.9 ± 1.9% of lamellar bone, 36 ± 1% of woven bone and 58 ± 3.8% of marrow spaces (**Table 2**).

DISCUSSION

The most interesting finding of the present study is that new osteogenesis was observed in the grafted sites without showing remnants of the material. In all specimens no foreign body reaction or inflammatory infiltrate were present, thus confirming the high osteoconductivity of this biomaterial (Berardinelli et al., 2013). Indeed, the used biomaterial shows an almost complete

TABLE 2 | Percentage of lamellar bone, woven bone and marrow space.

N° sinus	Lamellar bone	Woven bone	Marrow spaces
1	4	35	61
2	3	35	54
3	3	34	61
4	2	35	59
5	0	37	57
6	2	34	62
7	0	36	62
8	0	35	58
9	2	35	57
10	2	39	61
11	7	35	62
12	0	38	57
13	2	34	63
14	0	36	51
15	2	37	52
Percentage	1.9%	36%	58%
SD	1.9	1.5	3.8

resorption and a gradual apposition of newly formed bone (Grigolo et al., 2011; Berardinelli et al., 2013; Mozzati et al., 2017), while, 6 months after surgery, the use of other graft materials may show the presence of high quantity of residual graft particles (Scarano et al., 2012). In the early stages of healing, serving as a scaffold to guide effective bone regeneration, MgHA/collagen is resorbed by enzymes and cellular action over a period of 6–8 months (Scarano et al., 2017a). Usually, the bone graft is incorporated into the host site by means of interdigitation of the new bone deposited by the native bone (Scarano et al., 2006).

The ideal bone substitute should not evoke any adverse inflammatory response and be biocompatible, osteoconductive, osteoinductive and completely resorbable. Different osteoconductive biomaterials have been tested for maxillary sinus regeneration but, due to the absence of a complete resorption, local osteoprogenitor cells and poor wettability, months are required in order to have complete bone regeneration at the site of sinus floor elevation (Scarano, 2017). Clinical success has been obtained by grafting the maxillary sinus with different bone replacement materials before or simultaneously with implants placement. All surgical treatments in the maxillary region require detailed knowledge of anatomy and possible anatomical variations in order to avoid pitfalls, as well as an accurate preoperative diagnosis. Equally important is knowledge of the biological behavior of the biomaterials used to fill the maxillary sinus.

In fact, the nature of graft materials plays important roles in bone healing and regeneration. A biomaterial used in bone regeneration should have the following characteristics:

1) optimized structure for bone integration;
2) congruous pore volume to receive cells involved in tissue repairing;
3) enough pore interconnectivity with larger pore dimension for continuous tissue growth;
4) mechanical properties similar to the missing tissue;
5) facility in placement into the bone defect within a short setting time.

Bone substitute materials are available in different shapes and sizes, but they require major healing periods in comparison to autologous bone due to the reduced biological potential, as they are cell-free (Scarano et al., 2006).

Tissue engineering has allowed to successfully use osteoconductive biomaterials as carriers for growth factors and mesenchymal stem cells to increase tissue regeneration, accelerate osseointegration of dental implants and bone formation. Recently, the synergic effect of bone marrow stromal stem cells have been incorporated into a scaffold of porcine bone block, showing bone formation in surgical bone defects of the edentulous mandible in mini-pigs (Scarano et al., 2017b). However, these techniques have not been used yet in clinical practice, since bone substitute materials are cell-free and usually used in bone regeneration. On the other hand, the MgHA/collagen association represents a collagen-hydroxyapatite composite bone substitute, structured for bone regeneration on macro, micro and nano-scales, which increases the wettability. Indeed, this biomaterial graft quickly adsorbs the blood molecules and cells (**Figure 2**), thus promoting bone formation. The platelet growth factors and the combination of biomaterials were used with success for bone regeneration (Ohayon et al., 2016) and soft tissue augmentation (Scarano et al., 2016). The platelets imbibed in the MgHA/collagen lead to the activation and development of pseudopod aggregation and, ultimately, platelet degranulation. Alpha granules within the platelets release, via exostosis, a multitude of GFs which act as chemo attractants and mitogenic agents. The growth factors released by platelets within the biomaterial lead to appropriate wound healing. Absorption of the blood subsequent to bleeding, ending with the formation of fibrin or a blood clot, may stimulate cells with osteogenic, and probably angiogenic, potential to migrate to the surgical site. Also hydroxyapatite and collagen type I (HA/Collagen) have been used as a composite material and are found to enhance osteoblast differentiation (Geissler et al., 2000; Xie et al., 2004) and to accelerate osteogenesis (Serre et al., 1993).

Many biomaterials used for bone regeneration, a mixed bone/graft is obtained with a different metabolism for the turnover of native bone.

The outcome of the present study showed that an MgHA/collagen-based scaffold is completely resorbable. The combination of type I collagen (30%) and MgHA (70%) based scaffold mimicked the complex, hierarchically organized bone structure and improved bone formation.

Histologic evaluation of the newly formed tissues in sinus augmentation procedures is very helpful in understanding issues such as the nature and amount of newly formed bone and remnants of graft material. The tomograph showed the cortication of the buccal window in 13 sinuses, while in the 2 remaining sinuses, bone consolidation on the buccal aspect was evident, but no evidence of cortication was seen. Bone

cortication in the wall window confirms the good healing of the entire bone graft. All sinuses healed without complications or clinical signs of sinusitis. The mean volume immediately after graft elevation and after 6 months remained stable and there were no significant differences. This outcome confirms that the bone regeneration obtained is stable up to 6 months, but a long-term follow-up is necessary. The outcome of the present study showed that the MgHA/collagen-based scaffold is a highly biocompatible biomaterial and completely resorbable (Babiker et al., 2012).

In the present study the percentage of marrow spaces was higher than that reported (Scarano et al., 2006) with other biomaterials, in which 40 ± 3.8% was found after 6–8 months. These differences could be related to the complete resorption of the biomaterial used in this study. Probably, the dimension of the particles of HA and Mg, and even the collagen, are beneficial for bone healing and graft resorption.

The shape and complete resorption of a biomaterial has many advantages: absence of foreign body reaction in case of perimplantis; facilitation of the repair of the Schneiderian membrane in case of drilling; production of only native bone and not bone/graft mix; easily adaptation to the dimension and shape of the sinus without risk of perforating the Schneiderian membrane. Our study also shows that grafted sites lead to woven bone and a large marrow space with the ability to adapt to the implant load. In this case, the dental implant placement will come into contact with only the native bone and not with the biomaterial, i.e., assuring an interface with physiological adaptation and bone remodeling, and improved peri-implant bone volume and interfacial loading strength. This is the first clinical study to document bone regeneration with MgHA/collagen-based scaffold in sinus lifting procedure.

However, the characteristics of design and methodology of this study have limitations that mean that the results cannot be considered conclusive. Nevertheless, these results help to set practice parameters that will assure a comparative study with a large number of patients in future research.

Short term histological and histomorphometrical evaluations with a larger number of patients will be necessary for a better comprehension of the resorption phase of this biomaterial. The main advantages of the combination of type I collagen (30%) and MgHA (70%) based scaffold is the complete resorption, also the mechanical properties allow it to be shaped and adapted, thus promoting bone regeneration in non-space maintaining defects.

In conclusion, this first clinical study found that MgHA/collagen-based scaffold can be successfully used for sinus augmentation procedures.

AUTHOR CONTRIBUTIONS

AS Wrote paper and surgery. FL, GS, AT, BS performed data analysis. CM reviewed the manuscript.

REFERENCES

Babiker, H., Ding, M., Sandri, M., Tampieri, A., and Overgaard, S. (2012). The effects of bone marrow aspirate, bone graft, and collagen composites on fixation of Tit0061nium Implants. *J. Biomed. Mater. Res. B Appl. Biomater.* 100, 759–766. doi: 10.1002/jbm.b.32509

Berardinelli, P., Valbonetti, L., Muttini, A., Martelli, A., Peli, R., Zizzari, V., et al. (2013). Role of amniotic fluid mesenchymal cells engineered on MgHA/collagen-based scaffold allotransplanted on an experimental animal study of sinus augmentation. *Clin. Oral Invest.* 17, 1661–1675. doi: 10.1007/s00784-012-0857-3

Del Fabbro, M., Testori, T., Francetti, L., and Weinstein, R. (2004). Systematic review of survival rates for implants placed in the grafted maxillary sinus. *Int. J. Periodontics Restorative Dent.* 24, 565–577.

Geissler, U., Hempel, U., Wolf, C., Scharnweber, D., Worch, H., and Wenzel, K. (2000). Collagen type i-coating of ti6al4v promotes adhesion of osteoblasts. *J. Biomed. Mater. Res.* 51, 752–760. doi: 10.1002/1097-4636(20000915)51:4<752::AID-JBM25>3.0.CO;2-7

Grigolo, B., Fiorini, M., Manferdini, C., Cavallo, C., Gabusi, E., Zini, N., et al. (2011). Chemical-Physical properties and *in vitro* cell culturing of a novel biphasic bio-mimetic scaffold for osteo-chondral tissue regeneration. *J. Biol. Regul. Homeost. Agents* 25(2 Suppl.), S3–S13.

Hallman, M., Sennerby, L., and Lundgren, S. (2002). A clinical and histologic evaluation of implant integration in the posterior maxilla after sinus floor augmentation with autogenous bone, bovine hydroxyapatite, or a 20:80 mixture. *Int. J. Oral Maxillofac. Implants* 17, 635–643.

Mozzati, M., Gallesio, G., Staiti, G., Iezzi, G., Piattelli, A., Mortellaro, C., et al. (2017). Preservation using a biomimetic nanostructured matrix and atraumatic surgical extraction technique. *J. Craniofac. Surg.* 28, 1042–1045. doi: 10.1097/SCS.0000000000003496

Ohayon, L., Taschieri, S., Corbella, S., and Del Fabbro M. (2016). Maxillary sinus floor augmentation using biphasic calcium phosphate and a hydrogel polyethylene glycol covering membrane: an histological and histomorphometric evaluation. *Implant Dent.* 25, 599–605. doi: 10.1097/ID.0000000000000435

Palarie, V., Bicer, C., Lehmann, K. M., Zahalka, M., Draenert, F. G., and Kämmerer, P. W. (2012). Early outcome of an implant system with a resorbable adhesive calcium-phosphate coating–a prospective clinical study in partially dentate patients. *Clin. Oral Invest.* 16, 1039–1048. doi: 10.1007/s00784-011-0598-8

Ramírez-Rodríguez, G. B., Delgado-López, J. M., Iafisco, M., Montesi, M., Sandri, M., Sprio, S., et al. (2016). Biomimetic mineralization of recombinant collagen type i derived protein to obtain hybrid matrices for bone regeneration. *J. Struct. Biol.* 196, 138–146. doi: 10.1016/j.jsb.2016.06.025

Samartzis, D., Shen, F. H., Goldberg, E. J., and An, H. S. (2005). Is autograft the gold standard in achieving radiographic fusion in one-level anterior cervical discectomy and fusion with rigid anterior plate fixation? *Spine* 30, 1756–1761. doi: 10.1097/01.brs.0000172148.86756.ce

Scarano, A. (2017). Maxillary sinus augmentation with decellularized bovine compact particles: a radiological, clinical, and histologic report of 4 cases. *BioMed. Res. Int.* 2017:2594670. doi: 10.1155/2017/2594670

Scarano, A., Cholakis, A. K., and Piattelli, A. (2017a). Histologic evaluation of sinus grafting materials after peri-implantitis-induced failure: a case series. *Int. J. Oral Maxillofac. Implants* 32, e69–e75. doi: 10.11607/jomi.5303

Scarano, A., Crincoli, V., Di Benedetto, A., Cozzolino, V., Lorusso, F., Podaliri Vulpiani, M., et al. (2017b). Bone regeneration induced by bone porcine block with bone marrow stromal stem cells in a minipig model of mandibular 'critical size' defect. *Stem Cells Int.* 2017:9082869. doi: 10.1155/2017/9082869

Scarano, A., Degidi, M., Iezzi, G., Pecora, G., Piattelli, M., Orsini, G., et al. (2006). Maxillary sinus augmentation with different biomaterials: a comparative histologic and histomorphometric study in man. *Implant Dent.* 15, 197–207. doi: 10.1097/01.id.0000220120.54308.f3

Scarano, A, Degidi, M., Perrotti, V., Piattelli, A., and Iezzi, G. (2012). Sinus augmentation with phycogene hydroxyapatite: histological and histomorphometrical results after 6 months in humans. A case

series. *Oral Maxillofac. Surg.* 16, 41–45. doi: 10.1007/s10006-011-0296-3

Scarano, A., Valbonetti, L., Marchetti, M., Lorusso, F., and Ceccarelli, M. (2016). Soft tissue augmentation of the face with autologous platelet-derived growth factors and tricalcium phosphate. microtomography evaluation of mice. *J. Craniofac. Surg.* 27, 1212–1214. doi: 10.1097/SCS.0000000000002712

Serre, C. M., Papillard, M., Chavassieux, P., and Boivin, G. (1993). *In vitro* induction of a calcifying matrix by biomaterials constituted of collagen and/or hydroxyapatite: an ultrastructural comparison of three types of biomaterials. *Biomaterials* 14, 97–106. doi: 10.1016/0142-9612(93)90217-P

Tatum, H. (1986). Maxillary and sinus implant reconstructions. *Dent. Clin. North Am.* 30, 207–229.

Toba, Y., Kajita, Y., Masuyama, R., Takada, Y., Suzuki, K., and Aoe, S. (2000). Dietary magnesium supplementation affects bone metabolism and dynamic strength of bone in ovariectomized rats. *J. Nutr.* 130, 216–220.

Xie, J., Baumann, M. J., and McCabe, L. R. (2004). Osteoblasts respond to hydroxyapatite surfaces with immediate changes in gene expression. *J. Biomed.Mater. Res. A* 71, 108–117. doi: 10.1002/jbm.a.30140

Conflict of Interest Statement: The authors declare that the research was conducted in the absence of any commercial or financial relationships that could be construed as a potential conflict of interest.

The reviewer AP and handling Editor declared their shared affiliation, and the handling Editor states that the process met the standards of a fair and objective review.

frontiers in Physiology

ORIGINAL RESEARCH
published: 18 July 2018
doi: 10.3389/fphys.2018.00942

Extracellular Matrix Membrane Induces Cementoblastic/Osteogenic Properties of Human Periodontal Ligament Stem Cells

Yuanyuan Wang[1], Silvana Papagerakis[2,3], Denver Faulk[4], Stephen F. Badylak[4,5,6], Yuming Zhao[1], Lihong Ge[1], Man Qin[1†] and Petros Papagerakis[7,8†]*

[1] Department of Pediatric Dentistry, School and Hospital of Stomatology, Peking University, Beijing, China, [2] Department of Surgery, College of Medicine, University of Saskatchewan, Saskatoon, SK, Canada, [3] Department of Otolaryngology, Medical School, University of Michigan, Ann Arbor, MI, United States, [4] McGowan Institute for Regenerative Medicine, University of Pittsburgh, Pittsburgh, PA, United States, [5] Department of Surgery, University of Pittsburgh, Pittsburgh, PA, United States, [6] Department of Bioengineering, University of Pittsburgh, Pittsburgh, PA, United States, [7] Colleges of Dentistry and Biomedical Engineering, Toxicology, Pharmacy, Nutrition, Anatomy and Cell Biology, University of Saskatchewan, Saskatoon, SK, Canada, [8] Department of Orthodontics and Pediatric Dentistry, School of Dentistry, University of Michigan, Ann Arbor, MI, United States

OPEN ACCESS

Edited by:
Pierfrancesco Pagella, Universität Zürich, Switzerland

Reviewed by:
Alessandra Pisciotta, Università degli Studi di Modena e Reggio Emilia, Italy
Jean-Christophe Farges, Claude Bernard University Lyon 1, France
Uwe Baumert, Ludwig-Maximilians-Universität München, Germany

****Correspondence:***
Yuanyuan Wang
cwyyd@126.com

[†]Co-equal senior authors.

Specialty section:
This article was submitted to Craniofacial Biology and Dental Research, a section of the journal Frontiers in Physiology

Received: *13 March 2018*
Accepted: *26 June 2018*
Published: *18 July 2018*

Citation:
Wang Y, Papagerakis S, Faulk D, Badylak SF, Zhao Y, Ge L, Qin M and Papagerakis P (2018) Extracellular Matrix Membrane Induces Cementoblastic/Osteogenic Properties of Human Periodontal Ligament Stem Cells. Front. Physiol. 9:942. doi: 10.3389/fphys.2018.00942

Objective: Periodontitis affects nearly 90% of adults over the age of 70, resulting to periodontal tissue infection, destruction, and ultimately tooth loss. Guided tissue regeneration (GTR) is a method widely used to treat severe periodontal disease, and involves placement of an occlusive barrier to facilitate regeneration of the damaged area by periodontal ligament stem cells (PDLSCs). In this study, we evaluate natural extracellular matrix (ECM) as a scaffold material to provide a suitable microenvironment to support the proliferation, differentiation, and tissue-regenerating properties of PDLSCs.

Design: The viability, proliferation, apoptosis, and migration of PDLSCs cultured on ECM membrane, that was isolated from porcine urinary bladders, were compared with those cultured on type I collagen membrane, a commonly used scaffold in GTR. To evaluate the effects of ECM vs. type I collagen on the tissue-regenerating properties of PDLSCs, the bio-attachment and cementoblastic/osteogenic differentiation of PDLSCs were evaluated.

Results: Incubation of PDLSCs with ECM resulted in increased viability, proliferation, and reduced apoptosis, compared with type I collagen treated PDLSCs. Co-culture with ECM membrane also increased the migration and bio-attachment of PDLSCs. Incubation of PDLSCs with ECM membrane increased expression of the cementoblastic/osteogenic differentiation markers BSP, RUNX2, ALP, OPN, OCN, and periostin.

Conclusion: ECM membrane enhances the proliferation and regenerative properties of PDLSCs, indicating that ECM membrane can serve as a suitable scaffold in the application of GTR to treat periodontal disease.

Keywords: periodontal ligament stem cells, periodontal diseases, extracellular matrix, scaffolds, tissue regeneration

INTRODUCTION

Periodontitis is a major dental public health issue that results to periodontal tissues destruction and tooth loss (Haffajee and Socransky, 1994; Slots et al., 1999; Pihlstrom et al., 2005) affecting the majority of older adult population in the United States (Nakashima and Reddi, 2003; Pihlstrom et al., 2005; Nanci and Bosshardt, 2006).

Guided tissue regeneration (GTR) (Gottlow et al., 1986, 1990) is a widely used regenerative procedure for severe periodontal tissue destruction. GTR success relies on stem cell migration from the periodontal ligament (PDLSCs) into the damaged area and subsequent periodontal tissue regeneration.

Collagen Type I membranes (COLI) are often used as a barrier in GTR therapy, and have shown to facilitate PDLSCs migration, proliferation, and differentiation while inducing minimal cytotoxicity (Gentile et al., 2011) and enhancing hemostasis and wound healing (Postlethwaite et al., 1978). COLI membranes have been extensively used in clinical trials (Hämmerle et al., 1992; Mundell et al., 1993; Alarrayed et al., 1995; Bornstein et al., 2007; Zubery et al., 2007; Tal et al., 2008; Friedmann et al., 2011; Ivanovski et al., 2015). However, the fast COLI membrane degradation rate observed in many studies can produce loss of cell attachment (Rothamel et al., 2004) resulting in difficulties to retain structural integrity necessary for tissue regeneration. Therefore, appropriate alternative membranes that can enhance and sustain periodontal tissue regeneration under inflammatory conditions remains to be discovered.

To address this challenge, natural extracellular matrix (ECM) scaffolds are considered excellent alternatives to COLI membranes because of their regenerative and anti-inflammatory properties (Currie et al., 2001; Patino et al., 2002). The binding of ECM proteins to cell surface integrins and other receptors promotes cell survival, proliferation, and migration (Nelson and Bissell, 2006; Geiger and Yamada, 2011) resulting in successful tissue regeneration in clinical trials. ECM proteins have also been shown to successfully guide the differentiation of stem cells both *in vitro* (Li et al., 2004; Brennan et al., 2008) and *in vivo* (Beattie et al., 2009; Agrawal et al., 2011) while enhancing tissue regeneration in skeletal muscle (Marelli et al., 2010; Mase et al., 2010), esophagus (Nieponice et al., 2009), and urinary bladder (Boruch et al., 2010). ECM scaffolds are extracted and prepared from dermis, small intestine, urinary bladder, and pericardium (Gilbert et al., 2006). The shape and mechanical strength of ECM scaffolds can be customized by different processing techniques (Jadhav et al., 2006). We have recently showed that ECM scaffolds from bladder promote dental pulp mesenchymal stem cells differentiation and dental tissue regeneration (Wang et al., 2015).

Here, we comparatively evaluated the effects of natural ECM membranes and COLI membranes on the PDLSCs proliferation rate, osteogenic/cementoblastic differentiation, migration, and attachment. Our data suggests that ECM membranes could provide niche-like signals to PDLSCs and also that ECM membranes are superior in stimulating and accelerating the growth, attachment, and differentiation of human PDLSCs when compared to type I collagen membranes.

MATERIALS AND METHODS

Cell Culture

Normal human impacted third molars (n = 5) were collected from adult patients (20–25-year-old man) at the oral surgery clinic of the University of Michigan School of Dentistry. All extracted teeth were used for isolating human PDLSCs. Totally five different teeth were collected and five different PDLSC primary cell lines were generated and examined following the exact same procedures and methods. Results obtained from the five different PDLSCs cultures were similar.

This study was performed under an ethics protocol previously approved by the Institutional Review Board Ethics Committee of the University of Michigan. All patients that donated their extracted teeth were provided written informed consent and all samples were collected without any identification.

Periodontal ligament stem cells were isolated according to a previously described method (Seo et al., 2004). Briefly, periodontal ligament tissue was gently separated from the surface of the tooth root, and subsequently digested in a solution of 3 mg/mL collagenase type I (Sigma, St. Louis, MO, United States) and 4 mg/mL dispase (Sigma, St. Louis, MO, United States) for 1 h at 37°C. Single-cell suspensions were obtained by passing the cells through a 70 μm strainer (Falcon). Single-cell suspensions ($0.5–1.0 \times 10^3$ cells/well) were seeded onto six-well plates (Costar) containing alpha modification of Eagle's medium (REF:12571, GIBCO/BRL, Grand Island, NY, United States) supplemented with 15% fetal bovine serum (FBS; Hyclone), 100 U/mL penicillin and 100 mg/mL streptomycin (Sigma, St. Louis, MO, United States). Cultures were incubated at 37°C in 5% CO_2. Human dental pulp stem cells (DPSCs) were kindly provided by the laboratory of Dr. Kaigler at the University of Michigan. We used DPSCs as a negative control for scleraxis expression. Scleraxis is a specific maker of tendon tissue and PDL and it was only expressed in PDLSCs but not in DPSCs. The PDLSCs used in this study were cells either from passage 2 or passage 3 after the primary culture initiation.

ECM and Collagen Membrane Materials

Extracellular matrix membrane used in this study was provided by professor Badylak, and isolated from porcine urinary bladders as it has been descripted (Freytes et al., 2008). Type I collagen membranes were obtained from Zimmer Dental (Zimmer Dental, Carlsbad, CA, United States). First, cells were plated and attached on the bottom of the plates. Then, equal size of ECM or collagen I membranes were placed into each well and slowly emerged toward to bottom of each well.

Evaluation of Human PDLSC Marker Expression

RT-PCR

Total RNA was isolated from PDLSCs and DPSCs using TRIzol reagent (Invitrogen, Carlsbad, CA, United States), and 2 μg of total RNA was reverse transcribed into cDNA with TaqMan reverse transcription reagents (Applied Biosystems, Branchburg, NJ, United States), following the manufacturer's

recommendations. The resulting cDNA was amplified by RT-PCR, using AmpliTaq Gold DNA Polymerase (Applied Biosystems). RT-PCR amplifications were performed the following thermal conditions: 95°C for 30 s, 60°C for 30 s, and 72°C for 30 s. The cycle number is 40. The reactions were performed using an ABI PRISM 7500 Sequence Detection System (Applied Biosystems, Foster City, CA, United States), using specific primers. Primers specific for scleraxis gene were used to evaluate the specificity of PDLSCs cultures since scleraxis is considered as PDLSCs lineage marker. Specific primers for bone sialoprotein (*IBSP*), runt-related transcription factor 2 (*RUNX2*), alkaline phosphatase (*ALPL*), osteopontin (*SPP1*), osteocalcin (*BGLAP*), and periostin (*POSTN*) were used for evaluating the cementoblastic/osteogenic differentiation of PDLSCs in our study. Relative RNA expression levels were normalized against Glyceraldehyde 3-phosphate dehydrogenase (GAPDH) reference gene. The design of the primers was based on published human cDNA sequences (**Table 1**). RT-PCR products were sub-cloned into pGEM-T Easy vector (Promega, Madison, WI, United States) and PCR product identity was confirmed by sequencing. Melting curve analysis was performed for all PCR reactions. Each experiment was repeated five times for each separate PDLSCs clone.

Immunohistochemical Staining

Periodontal ligament stem cells (2.0×10^4/well, second passage) were sub-cultured on 12-chamber slides (Costar; Corning Life Sciences, Tewksbury, MA, United States) and grown to 80% confluence. Cells were then fixed in 4% paraformaldehyde and blocked with phosphate buffered saline (PBS) containing 10% normal equine serum (Gibco; New Zealand) for 45 min at room temperature. Cells were then incubated with diluted primary antibody against scleraxis (1:500 dilution; D-14, Santa Cruz Biotechnology, United States) at 4°C overnight. Afterward, cells were washed with PBS, then incubated with fluorescein-conjugated goat anti-mouse polyclonal secondary antibody (Zenon Alexa Fluor 488, Life Technologies, United States) at room temperature in the dark for 45 min. DAPI (Invitrogen, United States) staining was then performed in the dark for 5 min. Slides were washed with PBS, and were analyzed using fluorescence microscopy (Nikon ECLIPSE TS-100; Tokyo, Japan). The scleraxis staining was done for all five PDLSC clones.

Flow Cytometry

In order to evaluate the mesenchymal phenotype in PDLSCs and the potential changes of the PDLSCs after being exposed to ECM membrane for 24 h, the surface antigens of PDLSCs were analyzed by flow cytometry. Cells were trypsinised and incubated in PBS for 60 min with fluorescein conjugated antibodies against CD45 (PerCP/Cy5.5, Biolegend), CD73 (Brilliant Violet421, Biolegend), CD90 (FITC, BD Pharmingen), and CD105 (PE, Biolegend). The flow cytometry analysis of cells was carried out using a Beckman Coulter MoFlo® Astrios™ flow cytometry system, with 500,000 events being counted for each case. Each procedure was repeated three times for each separate PDLSCs clone. PDLSCs co-cultured with ECM and PDLSCs alone underwent FACS separately to evaluate their immunophenotype and identify if ECM changed the expression of mesenchymal stem cell (MSC) phenotypic markers in PDLSCs.

Determination of Cell Viability, Proliferation, and Cell Apoptosis

Viability

Periodontal ligament stem cells (5×10^3 cells/well, second passage) were expanded *ex vivo* in 96-well plates and covered with ECM or type I collagen membranes, at 37°C for 24 h. PDLSCs viability was evaluated using the cell counting kit-8 (CCK-8) assay (Dojindo, Kumamoto, Japan); The assay was repeated for all five PDLSC clones separately as previously described (Wang et al., 2015).

TABLE 1 | Semi-quantitative Real-Time PCR primers.

Gene name	5′-sequence-3′	Product size (bp)	GenBank number
GAPDH	**Forward:** GCAAATTCCATGGCACCGTC	819	XM_003273723.2
	Reverse: GGTCCACCACCCTGTTGCTA		
scleraxis	**Forward:** CTCCAGCTACATCTCGCACC	220	NM_001008271.1
	Reverse: GCGGTCCTTGCTCAACTTTC		
ALP	**Forward:** GCGCAGGACAGGATTAAAGC	246	NM_014476.5
	Reverse: TCCACTGCCACAGTCAATCC		
BSP	**Forward:** AATGCAGAAGGCACCACAGA	241	NM_004967.3
	Reverse: AATTGTCCCCACGAGGTTCC		
OPN	**Forward:** GAAGTTCTGAGGAAAAGCAGC	161	NM_001040058.1
	Reverse: GGACTTACTTGGAAGGGTCTCT		
OCN	**Forward:** ATGAGAGCCCTCACACTCCT	180	NM_199173.4
	Reverse: TGGGGCTCCCAGCCATT		
RUNX2	**Forward:** CACTGGCGCTGCAACAAGA	157	NM_001024630.3
	Reverse: CATTCCGGAGCTCAGCAGAATAA		
Periostin	**Forward:** AAGCGCTTTAGCACCTTCCT	930	NM_006475.2
	Reverse: CTTCCTCACGGGTGTGTCTC		

Proliferation

Periodontal ligament stem cells (5×10^3 cells/well, second passage) were expanded *ex vivo* in 96-well plates and covered with ECM or type I collagen membranes, at 37°C. At days 1, 3, 5, and 7 after cell seeding, cell viability was evaluated using the CCK-8 assay (Dojindo, Kumamoto, Japan), according to the manufacturer's instructions. The assay was repeated five times for each sample to evaluate the number of viable cells.

Apoptosis

Hoechst 33342 staining

The DNA-specific fluorochrome Hoechst 33342 (Cell Signaling Technology) was used to analyze the nuclear morphology of cells following incubation on ECM and type I collagen membranes at 37°C. 24 h after incubation with the membranes, PDLSCs were seeded onto glass slides and fixed in 4% paraformaldehyde at room temperature for 30 min. Afterward, cells were stained with 10 μM Hoechst 33342 dye at room temperature for 20 min. Apoptotic nuclei were counted under a fluorescent microscope (Olympus BX-51, Tokyo, Japan). As a positive control for induction of apoptosis, 500 nM staurosporine (Sigma-Aldrich) was added to some samples and incubated for 5 h. Untreated cells were used as a negative control. Apoptotic cells (fragmented nuclei) were scored manually; at least 200 cells/time point were analyzed.

Flow cytometry

The rate of cellular apoptosis rate was observed by flow cytometry. PDLSCs were cultured with the ECM and type I collagen membranes at 37°C for 24 h. The rate of apoptosis was evaluated using a FITC Annexin V Apoptosis Detection Kit (BD Pharmingen), following standard protocols using the Beckman Coulter MoFlo® Astrios™ flow cytometry system. Cells negative for both PI and annexin V-FITC were considered viable. Cells positive for annexin V-FITC and negative for PI were considered apoptotic. Apoptosis progress was followed over four time points. Cells with a direct increase in Annexin V + /PI + staining without an intermediate

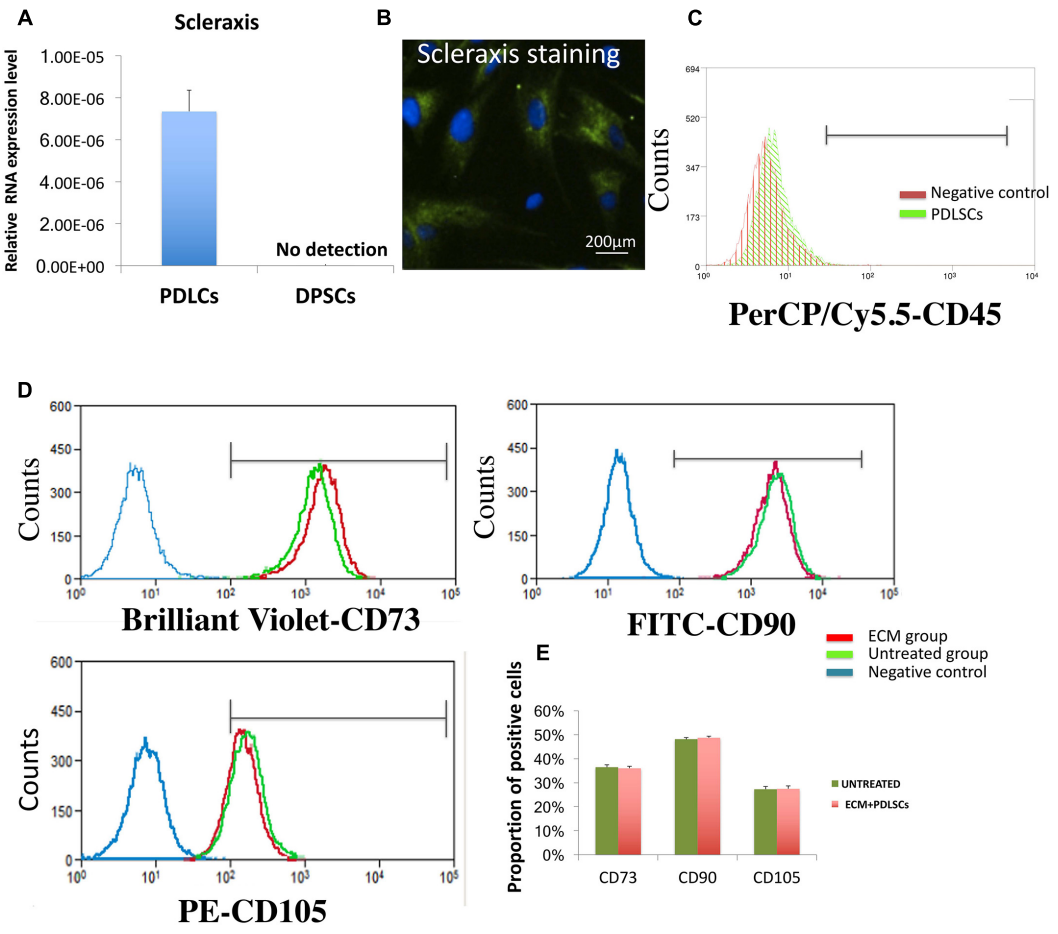

FIGURE 1 | Biomarker characterization of PDLSCs. **(A,B)** RT-PCR and immune-histochemical staining in PDLSCs showing expression of scleraxis, a marker for PDL tissues. DPSCs have been used as a negative control. **(C)** Flow cytometry analysis revealed that PDLSCs lack expression the blood cell marker CD45. **(D)** Flow cytometry analysis revealed that PDLSCs express the MSC markers CD73, CD90, and CD105. No significant difference in the percentage of cells positive for MSCs markers between the ECM group and the untreated group. **(E)** Statistical analysis of the flow cytometry results.

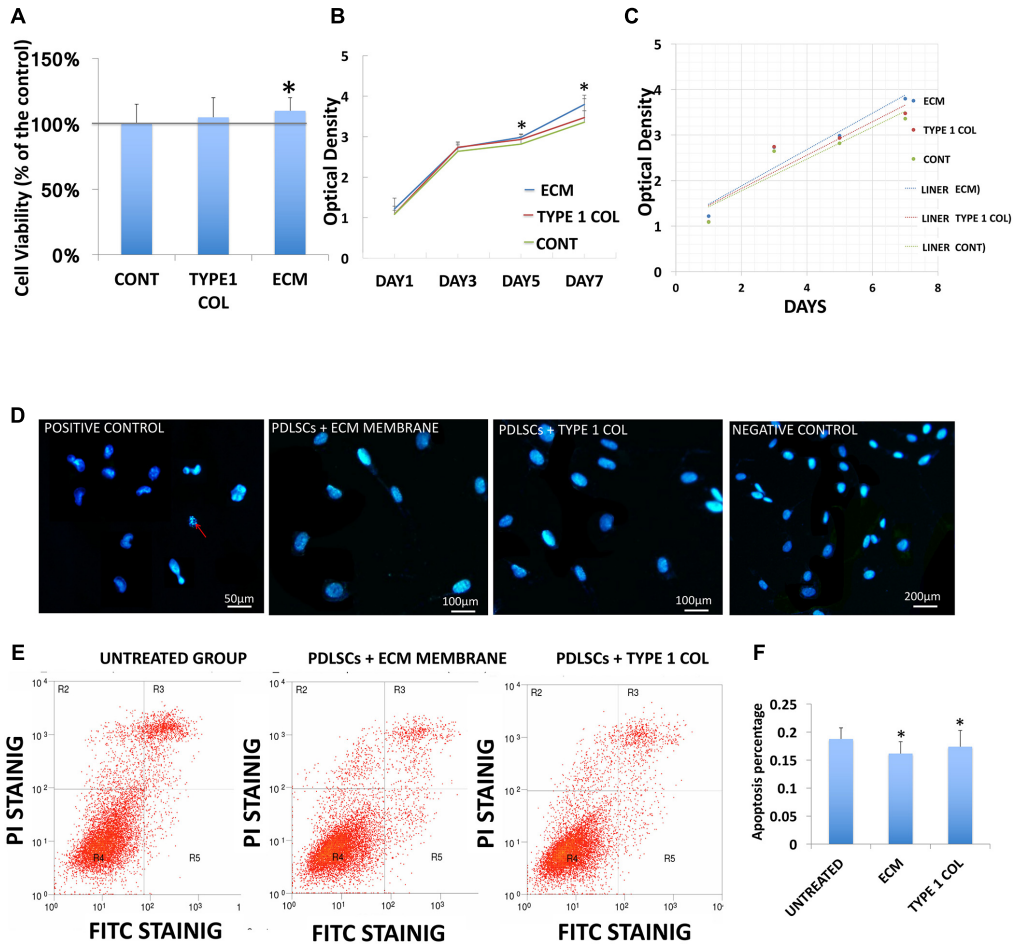

FIGURE 2 | PDLSCs viability and apoptosis. **(A)** The viability of PDLSCs after 24 h of cell culture with ECM or type I collagen, is measured here as a percentage of live cells for the experimental groups and control group. This data shows statistically significant differences between ECM group and control group (*$P < 0.05$). **(B)** The growth curve of PDLSCs after 1, 3, 5, and 7 days in culture with ECM, type I collagen membrane, or control show higher proliferation for ECM group at day 5 and 7. **(C)** The liner fit of the growth curve show a higher proliferation rate in ECM group. **(D)** Evaluation of cellular apoptosis by Hoechst staining 24 h. after incubation Hoechst staining was performed with ECM or type I collagen membrane to evaluate nuclear condensation (red arrow). No obvious apoptosis was observed in any of the three experiment groups. **(E)** FITC/PI staining detected by flow cytometric study showed the apoptosis rate derived from flow cytometric analysis. **(F)** The apoptosis rate was quantified by calculating the areas R2 + R3 + R5 in **D**, statistical analysis revealed that PDLSCs treated with ECM or type I collagen membrane have significantly lower apoptosis rates than the control group (* = statistically significant difference between control and experimental groups ECM and type I collagen membrane, $P < 0.05$).

step of Annexin V + /PI- were considered necrotic. The experiment was repeated three times for each separate PDLSCs clone.

Determination of Cell Migration

Periodontal ligament stem cells (2.0×10^4/well, second passage) were sub-cultured on six-chamber plates and grown to 90% confluence. A scratch experiment was carried out as the following steps: (1) scratch across the cells in each well diagonally; (2) rinse on half of the cells with PBS to wash them or to remove them from one of the halfs of each well; (3) placement of membranes to the washed area and were co-cultured with the cells for 24 h. The distance between the membranes and the cells edges were measured at five different sites at immediately after placement (0 h) and after 24 h co-culture by ImageJ software [National Institutes of Health (NIH), Bethesda, MD, United States].

Determination of Cell Bio-Attachment

Periodontal ligament stem cells were covered with the surface of ECM or type I collagen membranes, and cultured for 24 h. Membranes were fixed with 4% paraformaldehyde for 30 min, and embedded using O.C.T compound (Tissue-Tek), serial 5 μm longitudinal sections of the ECM membrane and absorbable collagen membrane were cut and stained with hematoxylin-eosin (H&E) and DAPI (Invitrogen). Briefly, for H&E staining, the sections were placed on slides, dried at 37°C overnight, then rehydrated using a graded alcohol series, and then stained with hematoxylin for 3 min. Sections were rinsed in running tap water for 10 min until they turned blue and then stained with eosin

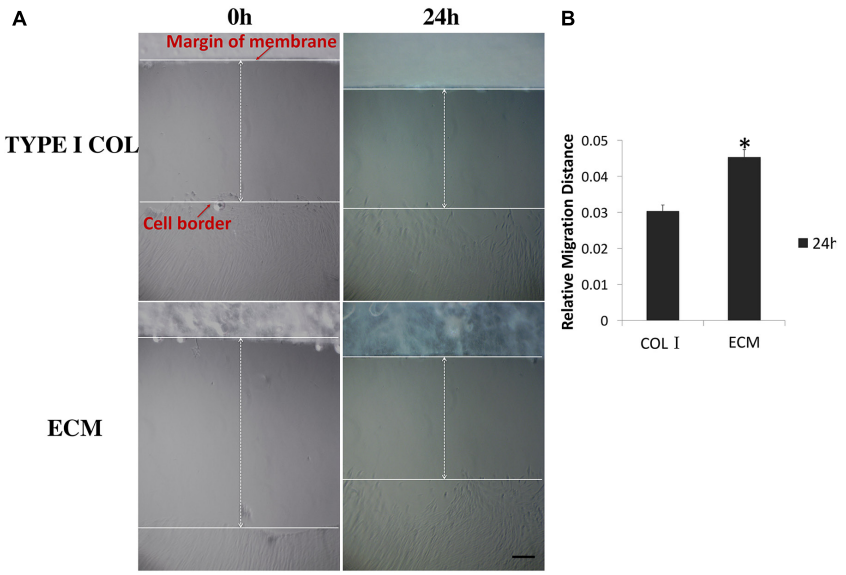

FIGURE 3 | Measurement of PDLSCs cell migration. **(A)** Measurements of the relative migration distance at 0 and 24 h after wound scratching in the presence of ECM or type I collagen membrane were taken and representative photographs are shown here. **(B)** Differential relative migration distance, which is indicative of wound closure, is calculated between the two groups as mean ± SEM ($n = 5$) (* = statistically significant difference in migration distance between ECM and type I collagen membrane group, $P < 0.05$).

for 3 min. For DAPI staining, sections were loaded DAPI solution for 5 min in the dark, washed with PBS and then were analyzed using fluorescence microscopy (Nikon ECLIPSE TS-100; Tokyo, Japan). The experiment was repeated for all five PDLSC clones separately.

Cementoblastic/Osteogenic Differentiation of PDLSCs

Periodontal ligament stem cells (2.0×10^4/well, second passage) were sub-cultured on six-chamber plates and grown for 5 days in α-minimum essential medium containing 15% fetal bovine serum, 50 μg/ml ascorbate, 100 U/mL penicillin and 100 mg/mL streptomycin. Mineralization medium was induced by supplementation of culture media with 10 mM β-glycerophosphate, media was replaced daily. ECM membrane and type I collagen membrane were added to the osteogenic medium separately. Cells cultured in mineralization medium but untreated with ECM membrane or type I collagen membrane were used as the control group. After induction for 7 days, alkaline phosphatase enzyme activity assay, Alizarin Red staining, and RT-PCR for gene expression analysis were performed.

Alkaline Phosphatase Enzyme Activity Assay

TNAP enzyme activity was evaluated using the colorimetric substrate, nitro blue tetrazolium/5-bromo-4-chloro-3-indolyl phosphate (Sigma). Cells were fixed in 70% ethanol for 10–15 min at room temperature, air-dried and incubated with substrate for 1 h at 37°C. Cells were then rinsed with distilled water, air-dried, and visualized macroscopically for evidence of staining. For quantification, the plates were scanned, and the staining intensity was measured using the ImageJ software [National Institutes of Health (NIH), Bethesda, MD, United States].

Alizarin Red Staining

Cells were rinsed with phosphate-buffered saline, fixed for 30 min in 100% ethanol, air-dried and then incubated with 0.5% Alizarin Red-S for 30 min. Cells were then washed with 70% ethanol and air-dried. The plates were scanned, quantification of the staining intensity was measured using the ImageJ software [National Institutes of Health (NIH), Bethesda, MD, United States].

Statistical Analysis

Data are expressed as means ± SD. Between-group differences were compared using one-way ANOVA using SPSS software (version 13.0; SPSS, Chicago, IL, United States; statistical significance was at $P < 0.05$).

RESULTS

Isolation and Characterization of PDLSCs

RT-PCR and immuno-histochemical analysis confirmed that PDLSCs, but not DPSCs, were positive for scleraxis, a marker for tendon tissue which is also considered as a phenotypic marker of PDL cells (**Figures 1A,B**). Flow cytometric results showed a lack expression of CD45 which is a marker of hematopoietic cells (**Figure 1C**). In addition, PDLSCs expressed the MSC markers CD73, CD90, and CD105 after 24 h of culture with ECM membrane. No significant difference in the percentage of cells positive for MSCs markers between the ECM group

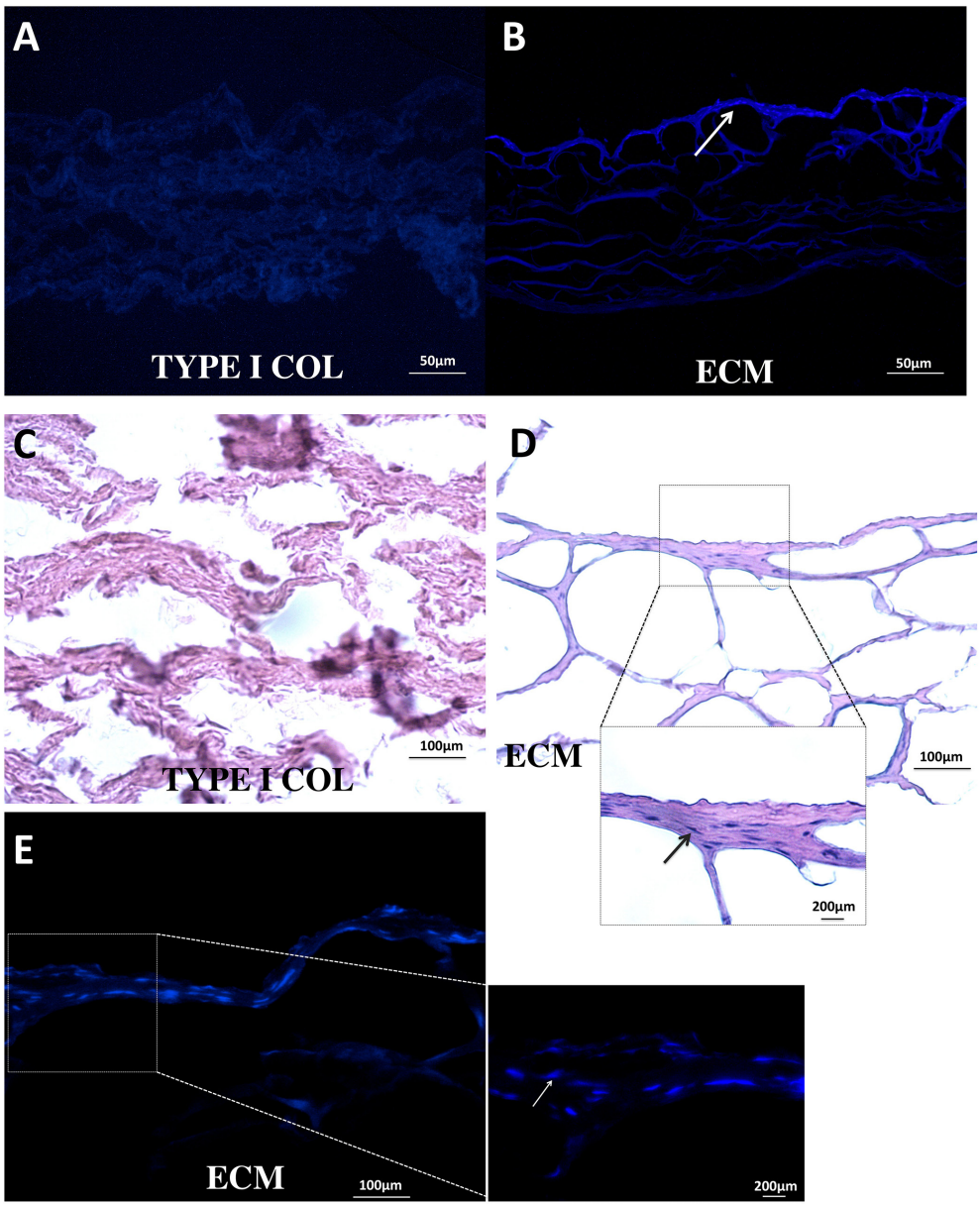

FIGURE 4 | Bio-attachment of PDLSCs. After 24 h, ECM membrane showed a stronger bio-attachment capacity for PDLSCs than type I collagen membrane. PDLSCs were found distributed in the ECM membrane **(B–E)**; in contrast, no typical cell morphology was observed in the type I collagen membrane **(A,C)**.

and the untreated group was found and the flow cytometric analysis indicated that the characteristics of ECM-cultured cells remained unchanged in comparison to the control group (**Figures 1D,E**).

Cell Viability, Proliferation, and Apoptosis

The viability of PDLSCs cultured with ECM membrane or type I collagen membrane was evaluated. Both ECM and type I collagen membranes promoted cell growth but PDLSCs demonstrated significantly higher cell viability after incubation with ECM membrane compared to PDLSCs incubated with type I collagen membrane or the control group (**Figure 2A**).

Cell proliferation increased linearly from day one to day seven of culture in cells co-cultured with either type of membrane materials, and in the control group as well. However, the proliferation rate in cells co-cultured with ECM membrane was higher compared to the type I collagen membrane (**Figures 2B,C**).

The appearance of fragmented nuclei was used as an indicator of apoptosis. Hoechst 33342 staining showed no obvious apoptosis after cells were exposed to the culture media and ECM membrane or type I collagen membrane for 24 h (**Figure 2D**). The results of FITC/PI staining detected by flow cytometric study showed the overall apoptotic rate of PDLSCs cultured with ECM

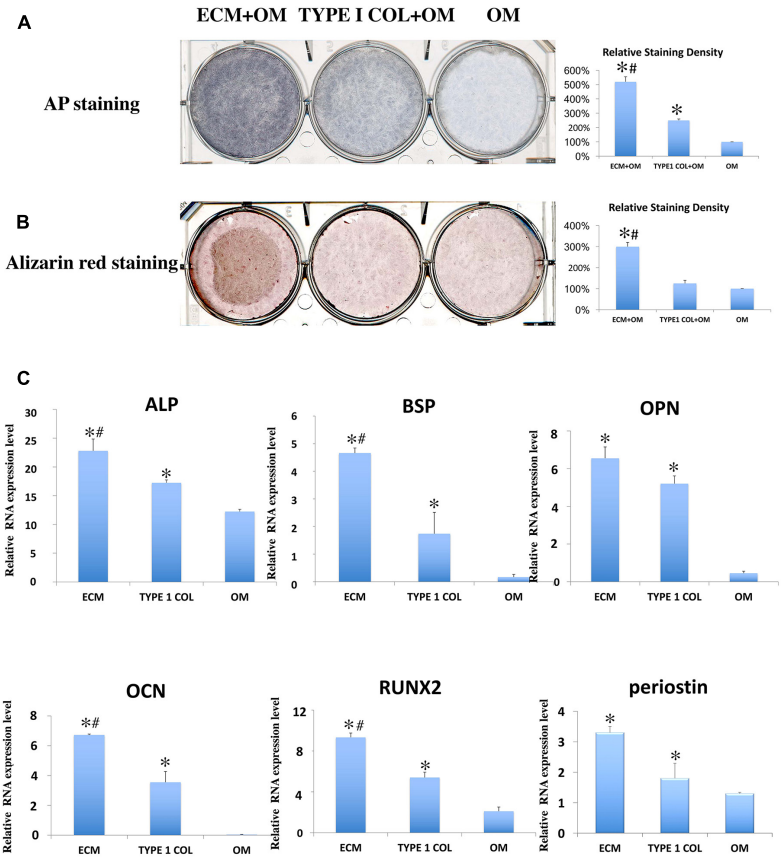

FIGURE 5 | Cementoblastic/osteogenic differentiation of PDLSCs. Cementoblastic/osteogenic differentiation was evaluated by TNAP enzyme activity **(A)** and Alizarin Red **(B)** staining. The relative staining density was calculated between PDLSCs alone (OM: Osteoblastic medium) group and the two experimental groups (ECM + OM; TYPE 1 COL + OM) and was found statistically different being the highest in the ECM + OM group **(A,B)** (* = statistically significant difference found when compared to the control; # = statistically significant difference found between ECM and type I collagen membrane groups). **(C)** RT-PCR was also performed using primers for cementoblastic/osteogenic biomarkers ALP, BSP, OPN, OCN, and RUNX2 and relative RNA expression levels were analyzed by statistics (* = statistically significant difference were found between the PDLSCs alone group and the two experimental groups; # = statistically significant difference found between ECM and type I collagen membrane groups; $P < 0.05$).

membrane or type I collagen membrane was significantly lower ($P < 0.05$) than the control group (**Figures 2E,F**).

Cell Migration

In a 24 h scratch assay, culture with ECM membrane promoted significantly greater cell migration of PDLSCs compared to incubation with type I collagen membrane (**Figures 3A,B**).

Bio-Attachment of PDLSCs

Extracellular matrix membrane showed a significantly stronger capacity to induce PDLSC bio-attachment than type I absorbable collagen membrane (**Figures 4A–D**). PDLSCs were clearly observed in the ECM membrane (**Figure 4E**).

Cementoblastic/Osteogenic Differentiation of PDLSCs

After incubation for 7 days, ECM membrane with osteogenic differentiation medium, showed increased TNAP enzyme activity of PDLSCs when compared to incubation with type I collagen/osteogenic differentiation medium or to incubation with osteogenic differentiation medium alone (**Figure 5A**). ECM membrane also significantly promoted calcium deposition compared to type I collagen/osteogenic differentiation medium group or to the osteogenic differentiation medium alone (**Figure 5B**). The cementoblastic/osteogenic differentiation markers BSP, RUNX2, ALP, OPN, OCN, and periostin were also significantly Up-Regulated in the ECM (**Figure 5C**).

DISCUSSION

Periodontitis is a widespread dental infection disease affecting 47.2 percent of American adults (Eke et al., 2012) and causing severe periodontal defects in the root area of teeth. GTR using biodegradable membranes is a commonly used therapeutic approach that aims to enhance periodontal tissue regeneration. Although the exact mechanism of periodontal tissue regeneration under GTR remains unclear, is it hypothesized that the barrier provided by the Collagen I (COLI) membranes allows PDLSCs

cell migration and regeneration of the infected periodontal tissues (Nyman et al., 1982; Gottlow et al., 1986). These COLI membranes are bio-inert supporting cell proliferation while minimizing cellular inflammation (Gentile et al., 2011) and are routinely used under well documented clinical protocols (Hämmerle et al., 1992; Alarrayed et al., 1995; Bornstein et al., 2007; Zubery et al., 2007; Friedmann et al., 2011). Studies suggest that COLI membranes also promote hemostasis, allowing early wound stabilization, nutrient passage, and fibroblasts recruitment through chemotaxis (Postlethwaite et al., 1978). However, the disadvantages of native collagen type I are primarily in the duration of barrier function, which cannot be strictly controlled, as loss of structural integrity and solubilization of the membrane via phagocytosis may precede the complete healing of the defect (Tal et al., 2008).

The research on dental tissue regeneration (Chatzistavrou et al., 2012) and on bactericidal and bioactive dental materials (Chatzistavrou et al., 2014; Kattan et al., 2015) is being largely explored in the recent years. In particular, the use of natural ECM as a biologic scaffold for dental tissue engineering applications has been suggested as a viable choice for a variety of clinical applications (Wang et al., 2015). In this study, we describe the effects of ECM membrane in PDLSCs cell behavior.

Periodontal ligament stem cells isolated from periodontal tissue were found to expresses scleraxis, a marker of PDL cells (Seo et al., 2004). *Ex vivo* expanded PDLSCs also expressed the MSC-related proteins CD73, CD90, CD105, and lacked expression of the CD45 which is considered a marker of hematopoietic cell lineage (Horwitz et al., 2005; Dominici et al., 2006). These characteristics indicated that the PDLSCs isolated and used in this study retained qualities of PDL mesenchymal stem cells (PDLSCs).

Therapeutic periodontal tissue regeneration relies on migration and differentiation of PDLSCs at the site of injury. Compared to type I collagen membrane, ECM membrane induced higher cell viability, more rapid proliferation rates, lower apoptosis percentage, and an improved capacity for bio-attachment of PDLSCs. These activities are important in facilitating the cementoblastic/osteogenic function of PDLSCs. Follow up studies will further evaluate ECM in clinical relevant scenarios using animal models of periodontal diseases.

The cementoblastic/osteogenic activity of PDLSCs was characterized by evaluating periodontal tissue differentiation biomarkers including TNAP enzyme activity, Alizarin red stain, and differential mRNA expression. Both TNAP and Alizarin red are commonly used stains to measure cementoblastic/osteogenic activity in bone and dentin-forming tissues (Hong et al., 2010; Nam et al., 2011) and ECM strongly enhanced PDLSCs TNAP activity and Alizarin staining. Furthermore, RT-PCR analysis showed that PDLSCs incubated with ECM membrane showed significant Up-Regulated mRNA expression of all these markers when compared to incubation with type I collagen membrane or to untreated cells. These data confirm that ECM membrane has superior biological properties compared to COLI membrane that significantly promote PDLSCs cell proliferation, differentiation, and mineral formation. We propose that these enhanced properties are the result of released growth factors from ECM into the periodontal tissues micro-environment as it has been shown previously in other systems (Voytik-Harbin et al., 1997; Hodde et al., 2001), the generation of bioactive cryptic peptides (Agrawal et al., 2011), or signaling molecules contained within recently identified matrix bound nano-vesicles (Huleihel et al., 2016).

The molecular composition of ECM includes several structural proteins such as collagen type I, glycosaminoglycans, proteoglycans, glycoproteins as well as numerous cytokines and growth factors which are shown to guide cell behavior (Timpl, 1996; Li et al., 2004). Among molecular factors, and biologic peptides found in ECM several have been investigated for bone healing and epithelial tissue regeneration. Furthermore, ECM displays a large degree of conservation among species (Constantinou and Jimenez, 1991; Exposito et al., 1992). These similarities in ECM molecular composition and the conservation among species highlight the fundamental importance of the ECM in cell homeostasis and tissue repair mechanisms (Badylak, 2005).

Type I collagen is widely used as a biologic scaffold for therapeutic applications, including in GTR therapy. In this study, we showed that ECM has a better bio-activity compared to type I collagen membrane alone due potentially to the complex components present in ECM in addition to Collagen I as discussed above. Therefore, the advantage of tissue-extracted ECM for tissue regeneration may come from the presence of molecular factors in amounts and forms similar to the ones that exist in nature. We therefore hypothesize that these distinct characteristics of ECM make it a more suitable material for use in periodontal tissue regeneration than traditional type I collagen membrane.

In conclusion, our study demonstrates that ECM membrane enhances PDLSCs proliferation and cell viability, and cell differentiation suggesting that ECM scaffolds has enhanced periodontal tissues regenerative properties when compared to COLI membranes. Additional *in vivo* studies are required to further confirm this hypothesis and provide a strong foundation for follow up clinical trials. Our study expands the field of regenerative dentistry and provides the foundation for future studies on the clinical application of ECM material membranes.

AUTHOR CONTRIBUTIONS

YW, PP, SP, and LG provided the design of the study. YW carried out the experiment and analyzed the data. SB and DF provided expertise with ECM. YW and YZ drafted the article and revised it critically for important intellectual content. MQ and PP made the final approval of the version to be submitted. MQ and PP were equally contributed senior authors.

FUNDING

This study has been partially funded by a grant from the National Natural Science Youth Foundation of China (No. 81500837) to YW.

REFERENCES

Agrawal, V., Tottey, S., Johnson, S. A., Freund, J. M., Siu, B. F., and Badylak, S. F. (2011). Recruitment of progenitor cells by an extracellular matrix cryptic peptide in a mouse model of digit amputation. *Tissue Eng. Part A* 17, 2435–2443. doi: 10.1089/ten.TEA.2011.0036

Alarrayed, F., Adam, S., Moran, J., and Dowell, P. (1995). Clinical trial of cross-linked human type I collagen as a barrier material in surgical periodontaltreatment. *J. Clin. Periodontol.* 22, 371–379. doi: 10.1111/j.1600-051X.1995.tb00163.x

Badylak, S. F. (2005). Regenerative medicine and developmental biology: the role of the extracellular matrix. *Anat. Rec. B New Anat.* 287, 36–41. doi: 10.1002/ar.b.20081

Beattie, A. J., Gilbert, T. W., Guyot, J. P., Yates, A. J., and Badylak, S. F. (2009). Chemoattraction of progenitor cells by remodeling extracellular matrix scaffolds. *Tissue Eng. Part A* 15, 1119–1125. doi: 10.1089/ten.tea.2008.0162

Bornstein, M. M., Bosshardt, D., and Buser, D. (2007). Effect of two different bioabsorbable collagen membranes on guided bone regeneration: a comparative histomorphometric study in the dog mandible. *J. Clin. Periodontol.* 78, 1943–1953. doi: 10.1902/jop.2007.070102

Boruch, A. V., Nieponice, A., Qureshi, I. R., Gilbert, T. W., and Badylak, S. F. (2010). Constructive remodeling of biologic scaffolds is dependent on early exposure to physiologic bladder filling in a canine partial cystectomy model. *J. Surg. Res.* 161, 217–225. doi: 10.1016/j.jss.2009.02.014

Brennan, E. P., Tang, X.-H., Stewart-Akers, A. M., Gudas, L. J., and Badylak, S. F. (2008). Chemoattractant activity of degradation products of fetal and adult skin extracellular matrix for keratinocyte progenitor cells. *J. Tissue Eng. Regen. Med.* 2, 491–498. doi: 10.1002/term.123

Chatzistavrou, X., Fenno, J. C., Faulk, D., Badylak, S., Kasuga, T., Boccaccini, A. R., Papagerakis, P., et al. (2014). Fabrication and characterization of bioactive and antibacterial composites for dental applications. *Acta Biomater.* 10, 3723–3732. doi: 10.1016/j.actbio.2014.04.030

Chatzistavrou, X., Papagerakis, S., Ma, P. X., and Papagerakis, P. (2012). Innovative approaches to regenerate enamel and dentin. *Int. J. Dent.* 2012:856470. doi: 10.1155/2012/856470

Constantinou, C. D., and Jimenez, S. A. (1991). Structure of cDNAs encoding the triple-helical domain of murine α2 (VI) collagen chain and comparison to human and chick homologues. Use of polymerase chain reaction and partially degenerate oligonucleotides for generation of novel cDNA clones. *Matrix* 11, 1–9. doi: 10.1016/S0934-8832(11)80221-0

Currie, L. J., Sharpe, J. R., and Martin, R. (2001). The use of fibrin glue in skin grafts and tissue-engineered skin replacements: a review. *Plast. Reconstr. Surg.* 108, 1713–1726. doi: 10.1097/00006534-200111000-00045

Dominici, M., Le Blanc, K., Mueller, I., Slaper-Cortenbach, I., Marini, F., Krause, D., et al. (2006). Minimal criteria for defining multipotent mesenchymal stromal cells. The international society for cellular therapy position statement. *Cytotherapy* 8, 315–317. doi: 10.1080/14653240600855905

Eke, P. I., Dye, B. A., Wei, L., Thornton-Evans, G. O., and Genco R. J. (2012). Prevalence of periodontitis in adults in the United States: 2009 and 2010. *J. Dent. Res.* 91, 914–920. doi: 10.1177/0022034512457373

Exposito, J. Y. D., Alessio, M., Solursh, M., and Rameriz, F. (1992). Sea urchin collagen evolutionarily homologous to vertebrate Pro-α2(I) collagen. *J. Biol. Chem.* 267, 15559–15562.

Freytes, D. O., Martin, J., Velankar, S. S., Lee, A. S., and Badylak, S. F. (2008). Preparation and rheological characterization of a gel form of the porcine urinary bladder matrix. *Biomaterials* 29, 1630–1637. doi: 10.1016/j.biomaterials.2007.12.014

Friedmann, A., Gissel, K., Soudan, M., Kleber, B. M., Pitaru, S., and Dietrich, T. (2011). Randomized controlled trial on lateral augmentation using two collagen membranes: morphometric results on mineralized tissue compound. *J. Clin. Periodontol.* 38, 677–685. doi: 10.1111/j.1600-051x.2011.01738.x

Geiger, B., and Yamada, K. M. (2011). Molecular architecture and function of matrix adhesions. *Cold Spring Harb. Perspect. Biol.* 3:a005033. doi: 10.1101/cshperspect.a005033

Gentile, P., Chiono, V., Tonda-Turo, C., Ferreira, A. M., and Ciardelli, G. (2011). Polymeric membranes for guided bone regeneration. *Biotechnol. J.* 6, 1187–1197. doi: 10.1002/biot.201100294

Gilbert, T. W., Sellaro, T. L., and Badylak, S. F. (2006). Decellularization of tissues and organs. *Biomaterials* 27, 3675–3683. doi: 10.1016/j.biomaterials.2006.02.014

Gottlow, J., Karring, T., and Nyman, S. (1990). Guided tissue regeneration following treatment of recession-type defects in the monkey. *J. Clin. Periodontol.* 61, 680–685. doi: 10.1902/jop.1990.61.11.680

Gottlow, J., Nyman, S., Lindhe, J., Karring, T., and Wennström, J. (1986). New attachment formation in the human periodontium by guided tissue regeneration. Case reports. *J. Clin. Periodontol.* 13, 604–616. doi: 10.1111/j.1600-051X.1986.tb00854.x

Haffajee, A. D., and Socransky, S. S. (1994). Microbial etiological agents of destructive periodontal diseases.*Periodontol. 2000* 5, 78–111. doi: 10.1111/j.1600-0757.1994.tb00020.x

Hämmerle, C. H., Schmid, J., Olah, A. J., and Lang, N. P. (1992). Osseous healing of experimentally created defects in the calvaria of rabbits using guided bone regeneration. A pilot study. *Clin. Oral Implants Res.* 3, 144–147.

Hodde, J. P., Record, R. D., Liang, H. A., and Badylak, S. F. (2001). Vascular endothelial growth factor in porcine-derived extracellular matrix. *Endothelium* 8, 11–24. doi: 10.3109/10623320109063154

Hong, S. J., Yu, H. S., Noh, K. T., Oh, S. A., and Kim, H. W. (2010). Novel scaffolds of collagen with bioactive nanofiller for the osteogenic stimulation of bone marrow stromal cells. *J. Biomater. Appl.* 24, 733–750. doi: 10.1177/0885328209338956

Horwitz, E. M., Blanc, K. L., Dominici, M., Mueller, I., Slapercortenbach, I., Marini, F. C., et al. (2005). Clarification of the nomenclature for MSC: the international society for cellular therapy position statement. *Cytotherapy* 7, 393–395. doi: 10.1080/14653240500319234

Huleihel, L., Hussey, G. S., Naranjo, J. D., Zhang, L., Dziki, J. L., Turner, N. J., et al. (2016). Matrix bound nano vesicles within ECM bioscaffolds. *Sci. Adv.* 10:e1600502. doi: 10.1126/sciadv.1600502

Ivanovski, S., Hamlet, S., Retzepi, M., Wall, I., and Donos, N. (2015). Transcriptional profiling of "guided bone regeneration" in a critical-size calvarial defect. *Clin. Oral Implants Res.* 22, 382–389. doi: 10.1111/j.1600-0501.2010.02104.x

Jadhav, A. P., Mason, H. A., and Cepko, C. L. (2006). Notch 1 inhibits photoreceptor production in the developing mammalian retina. *Development* 133, 913–923. doi: 10.1242/dev.02245

Kattan, H., Chatzistavrou, X., Boynton, J., Dennison, J., Yaman, P., Papagerakis, P., et al. (2015). Physical properties of an ag-doped bioactive flowable composite resin. *Materials* 24, 4668–4678. doi: 10.3390/ma8084668

Li, F., Li, W., Johnson, S., Ingram, D., Yoder, M., and Badylak, S. (2004). Low-molecular-weight peptides derived from extracellular matrix as chemoattractants for primary endothelial cells. *Endothelium* 11, 199–206. doi: 10.1080/10623320490512390

Marelli, B., Ghezzi, C. E., Barralet, J. E., Boccaccini, A. R., and Nazhat, S. N. (2010). Three-dimensional mineralization of dense nanofibrillar collagen-bioglass hybrid scaffolds. *Biomacromolecules* 11, 1470–1479. doi: 10.1021/bm1001087

Mase, V. J. Jr., Hsu, J. R., Wolf, S. E., Wenke, J. C., Baer, D. G., Owens, J., Badylak, S. F., et al. (2010). Clinical application of an acellular biologic scaffold for surgical repair of a large, traumatic quadriceps femoris muscle defect. *Orthopedics* 33:511. doi: 10.3928/01477447-20100526-24

Mundell, R. D., Mooney, M. P., Siegel, M. I., and Losken, A. (1993). Osseous guided tissue regeneration using a collagen barrier membrane. *J. Oral Maxillofac. Surg.* 51, 1004–1012. doi: 10.1016/S0278-2391(10)80045-X

Nakashima, M., and Reddi, A. H. (2003). The application of bone morphogenetic proteins to dental tissue engineering. *Nat. Biotechnol.* 21, 1025–1032. doi: 10.1038/nbt864

Nam, S., Won, J. E., Kim, C. H., and Kim, H. W. (2011). Odontogenic differentiation of human dental pulp stem cells stimulated by the calcium phosphate porous granules. *J. Tissue Eng.* 2011:812547. doi: 10.4061/2011/812547

Nanci, A., and Bosshardt, D. D. (2006). Structure of periodontal tissues in health and disease. *Periodontol. 2000* 40, 11–28. doi: 10.1111/j.1600-0757.2005.00141.x

Nelson, C. M., and Bissell, M. J. (2006). Of extracellular matrix, scaffolds, and signaling: tissue architectureregulates development, homeostasis, and cancer. *Annu. Rev. Cell Dev. Biol.* 22, 287–309. doi: 10.1146/annurev.cellbio.22.010305.104315

Nieponice, A., Mcgrath, K., Qureshi, I., Beckman, E. J., Luketich, J. D., Gilbert, T. W., et al. (2009). An extracellular matrix scaffold for esophageal stricture prevention after circumferential EMR. *Gastrointest. Endosc.* 69, 289–296. doi: 10.1016/j.gie.2008.04.022

Nyman, S., Lindhe, J., Karring, T., and Rylander, H. (1982). New attachment following surgical treatment of human periodontal disease. *J. Clin. Periodontol.* 9, 290–296. doi: 10.1111/j.1600-051X.1982.tb02095.x

Patino, M. G., Neiders, M. E., Andreana, S., Noble, B., and Cohen, R. E. (2002). Collagen as an implantable material in medicine and dentistry. *J. Oral Implantol.* 28, 220–225. doi: 10.1563/1548-1336(2002)028<0220:CAAIMI>2.3.CO;2

Pihlstrom, B. L., Michalowicz, B. S., and Johnson, N. W. (2005). Periodontal diseases. *Lancet* 366, 1809–1820. doi: 10.1016/S0140-6736(05)67728-8

Postlethwaite, A. E., Seyer, J. M., and Kang, A. H. (1978). Chemotactic attraction of human fibroblasts to type I, II, and III collagens and collagen-derived peptides. *Proc. Natl. Acad. Sci. U.S.A.* 75, 871–875. doi: 10.1073/pnas.75.2.871

Rothamel, D., Schwarz, F., Sculean, A., Herten, M., Scherbaum, W., and Becker, J. (2004). Biocompatibility of various collagen membranes in cultures of human PDL fibroblasts and human osteoblast-like cells. *Clin. Oral Implants Res.* 15, 443–449. doi: 10.1111/j.1600-0501.2004.01039.x

Seo, B. M., Miura, M., Gronthos, S., Bartold, P. M., Batouli, S., Brahim, J., et al. (2004). Investigation of multipotent postnatal stem cells from human periodontal ligament. *Lancet* 364, 149–155. doi: 10.1016/S0140-6736(04)16627-0

Slots, J., Macdonald, E. S., and Nowzari, H. (1999). Infectious aspects of periodontal regeneration. *Periodontol. 2000* 19, 164–172. doi: 10.1111/j.1600-0757.1999.tb00154.x

Tal, H., Kozlovsky, A., Artzi, Z., Nemcovsky, C. E., and Moses, O. (2008). Cross-linked and non-cross-linked collagen barrier membranes disintegrate following surgical exposure to the oral environment: a histological study in the cat. *Clin. Oral Implants Res.* 19, 760–766. doi: 10.1111/j.1600-0501.2008.01546.x

Timpl, R. (1996). Macromolecular organization of basement membranes. *Curr. Opin. Cell Biol.* 8, 618–624. doi: 10.1016/S0955-0674(96)80102-5

Voytik-Harbin, S. L., Brightman, A. O., Kraine, M. R., Waisner, B., and Badylak, S. F. (1997). Identification of extractable growth factors from small intestinal submucosa. *J. Cell. Biochem.* 67, 478–491. doi: 10.1002/(SICI)1097-4644(19971215)67:4<478::AID-JCB6>3.0.CO;2-P

Wang, Y. Y., Chatzistavrou, X., Faulk, D., Badylak, S., Zheng, L., Papagerakis, S., et al. (2015). Biological and bactericidal properties of Ag-doped bioactive glass in a natural extracellular matrix hydrogel with potential application in dentistry. *Eur. Cell Mater.* 29, 342–355. doi: 10.22203/eCM.v029a26

Zubery, Y., Goldlust, A., Alves, A., and Nir, E. (2007). Ossification of a novel cross-linked porcine collagen barrier in guided bone regeneration in dogs. *J. Clin. Periodontol.* 78, 112–121. doi: 10.1902/jop.2007.060055

Conflict of Interest Statement: The authors declare that the research was conducted in the absence of any commercial or financial relationships that could be construed as a potential conflict of interest.

frontiers in Physiology

ORIGINAL RESEARCH
published: 15 March 2017
doi: 10.3389/fphys.2017.00152

Iodixanol as a Contrast Agent in a Fibrin Hydrogel for Endodontic Applications

Gabriel Hertig[1], Matthias Zehnder[2], Anna Woloszyk[3], Thimios A. Mitsiadis[3], Anja Ivica[1] and Franz E. Weber[1]*

[1] Oral Biotechnology and Bioengineering, University of Zurich, Zurich, Switzerland, [2] Preventive Dentistry, Periodontology, and Cariology, University of Zurich, Zurich, Switzerland, [3] Orofacial Development and Regeneration, Institute of Oral Biology, University of Zurich, Zurich, Switzerland

The application of biomaterials used in regenerative endodontics should be traceable. In this study, we checked some basic effects of rendering a fibrin hydrogel radiopaque using an iodine-based contrast agent (iodixanol) approved for systemic application. Fibrin hydrogels were prepared from a fibrin sealant (Tisseel) using either an isotonic iodixanol solution (Visipaque 320, test) or Tris buffer (control) as a diluent. Gelation kinetics, radiopacity, and swelling of lyophilized hydrogels were tested using standard methods. Hydrogel structure was evaluated using scanning electron microscopy (SEM). Furthermore, iodixanol release from the test gels was assessed using spectrophotometry, and tissue compatibility was compared between test and control hydrogels using the chick chorioallantoic membrane (CAM) assay. Results were compared using pairwise *t*-test, $p < 0.05$. Iodixanol caused a 70-fold delay in gelation to 26 min in the test compared to the control hydrogels (22 ± 1 s). Radiopacity of the test gels was 1.9 ± 0.2 mm Al/mm, compared to zero in the control hydrogels. Lyophilized hydrogel swelling was strongly reduced when iodixanol was added to the hydrogel ($p < 0.05$). Test hydrogels had an altered SEM appearance compared to controls, and exhibited a reduced porosity. Iodixanol release from the test hydrogels reached 14.5 ± 0.5% after 120 h and then ceased. This release did not have any apparent toxic effect and neither affected the viability, nor the physiology or vascularization of the CAM of fertilized chicken eggs. Iodixanol can render a fibrin hydrogel radiopaque and maintains its tissue compatibility, yet impacts gelation kinetics and hydrogel porosity.

Keywords: fibrin gel, regenerative endodontics, iodixanol, contrast agent, tooth

OPEN ACCESS

Edited by:
David P. Rice,
University of Helsinki, Finland

Reviewed by:
Jean-Christophe Farges,
Claude Bernard University Lyon 1, France
Aránzazu Díaz-Cuenca,
Consejo Superior de Investigaciones Científicas (CSIC), Spain

****Correspondence:***
Matthias Zehnder
matthias.zehnder@zzm.uzh.ch

Specialty section:
This article was submitted to Craniofacial Biology and Dental Research, a section of the journal Frontiers in Physiology

Received: *11 January 2017*
Accepted: *27 February 2017*
Published: *15 March 2017*

Citation:
Hertig G, Zehnder M, Woloszyk A, Mitsiadis TA, Ivica A and Weber FE (2017) Iodixanol as a Contrast Agent in a Fibrin Hydrogel for Endodontic Applications. Front. Physiol. 8:152. doi: 10.3389/fphys.2017.00152

INTRODUCTION

An exciting new field has emerged in endodontic research over the recent years: Regenerative Endodontics (Hargreaves, 2016). While attempts to attract soft tissues into the necrotic root canal space are not necessarily new (Nygaard Ostby, 1963), the systematic approach in the context of current tissue engineering concepts surely is. Different paths are followed that vary from pure basic science to translational medicine with the development and improvement of clinically applicable protocols. However, the passage to the clinics necessitates specific precautions for tissue engineering concepts and related products (Mao et al., 2012). These include issues such as treatment costs, safety, and also the regulation of medical devices by local administrative bodies.

Currently, in the context of pulp tissue engineering, a so-called cell-free or cell-homing approach is seen as favorable (Kim et al., 2010; Lee et al., 2010). This approach involves the conditioning of the root canal wall by EDTA to release molecular cues for the attraction and differentiation of invading pluripotent cells, followed by the application of a scaffold in the pulp space (Galler, 2016). In the current clinical protocol, this scaffold is a blood clot, which is generated by controlled bleeding through the apical foramen (Trope, 2010). Clinical outcomes with this technique vary (Chen et al., 2012), and negative reports have curbed the initial enthusiasm (Nosrat et al., 2012). Discoloration of the crown is a frequent observation, and continued growth of the root is not predictably achieved (Kahler et al., 2014; Simon et al., 2014).

The procedure of "controlled bleeding" *per se* is problematic from a clinical point of view, mainly for two reasons: Hemorrhage has a negative effect on tooth color (Marin et al., 1997), and the whole procedure and its state-of-the-art execution are hard if not impossible to be monitored. Proper case documentation, however, is the core of good clinical practice. Recent approaches to replace the controlled bleeding step in regenerative endodontics involved the application of a fibrin hydrogel into the empty pulp space in order to create a synthetic, non-staining blood clot (Ruangsawasdi et al., 2014). The fibrin hydrogel could be placed in a controlled manner using a micro-cannula or a lentulo spiral. However, it would be desirable to obtain a radiopaque hydrogel for better controlling and monitoring of the procedure. In the current study we investigated the effects of a biocompatible iodinated X-ray contrast agent systemically used in angiography on some basic properties of a fibrin hydrogel intended for endodontic applications.

MATERIALS AND METHODS

Preparation of Hydrogels

Hydrogels were prepared from a commercially available fibrin sealant (Tisseel, Baxter; Deerfield, IL). The two components of the sealant were diluted to obtain a control fibrin hydrogel as previously described (Ruangsawasdi et al., 2017). To prepare the control hydrogels, the thrombin component and the fibrinogen component were diluted in Tris-buffered saline (TBS) and then mixed as described below. In the test hydrogels, the TBS was replaced by an aqueous isotonic contrast agent (Visipaque 320, GE Healthcare, Cork, Ireland) containing 652 mg of iodixanol per mL of liquid, which equals 320 mg/mL of iodine. The pH of the two solutions was measured using a calibrated electrode (Metrohm, Herisau, Switzerland). The pH of TBS was 7.6, while the pH of Visipaque 320 equaled 7.1.

Gelation Kinetics

Fibrin hydrogels gelate via fibrin clotting. Clotting time was tested according to the method described by Vermylen et al. (1963). The two hydrogel components were prepared separately in micro-centrifugation tubes in a water bath at 37°C. For 250 μL of the thrombin solution 2 μL of thrombin were added to 248 μL of TBS or Visipaque; 250 μL of fibrinogen solution were prepared by adding 44 μL of fibrinogen to 206 μL of TBS or Visipaque. Pre-warmed thrombin solution was transferred to the fibrinogen counterpart using this pipette. The agents were mixed using a pipette. The micro-centrifugation tubes were kept in the water bath at 37°C during the whole experiment. A platinum loop was moved in and out of the clotting mixture until the appearance of the fibrin web, which marked the end point (hydrogelation). The time to reach this point was recorded using a stopwatch. These experiments were performed in triplicates with freshly prepared solutions.

Assessment of Radiopacity

Test and control hydrogels were filled into polycarbonate molds 10 mm in diameter and 1 mm thick. Three molds were filled per experiment. Slices with a thickness of 1 mm from the crowns of bovine teeth served as control for the clear distinction between material and the surrounding tissue in clinical situations. Specimens were placed on a radiographic sensor (Digora, Soredex, Tuusula, Finland) together with an aluminum step-wedge with a thickness from 0.5 to 6 mm (0.5 and 1 mm increments, **Figures 1a,b**). A Trophy Irix (Trophy, Paris, France) X-ray unit operating at 65 kV, 8 mA, and 0.22 s with a focus-film distance of 25 cm was used. Hydrogels were prepared immediately prior to use. These triplicate measurements were performed three times each with freshly prepared hydrogels. Digital radiographic images were imported with the Digora system, using Digora software version 1.51 for Windows without gray scale correction. Optimas image analysis software (Meyer Instruments Inc., Houston, TX) was used to determine the gray value of the samples and convert these to mm of aluminum equivalent (mm Al). To assess the relative radiopacity of the test fibrin hydrogel in human teeth, the root canals of premolars extracted for orthodontic reasons were prepared using

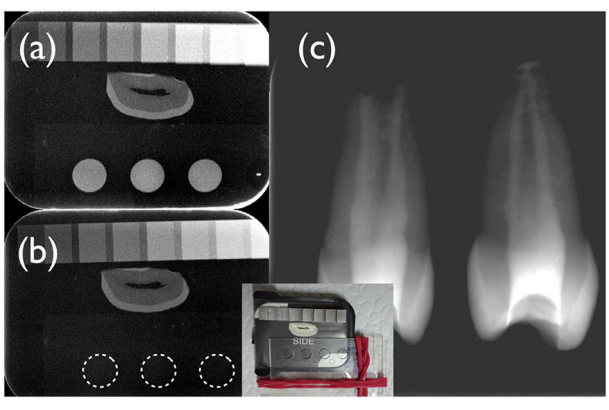

FIGURE 1 | Digital radiographs of the test (a,c) and the control fibrin hydrogel **(b)** under investigation. A cross-section of a human incisor crown was used as a reference. A photograph of the set-up is depicted in the insert. The aluminum step-wedge had a thickness of 0.5, 1, 1.5, 2, and then 3 mm Al, followed by 1 mm steps. As can be appreciated from this figure, the test hydrogel **(a)** had a radiopacity of ∼2 mm Al/mm, whilst the control hydrogel **(b)** displayed no radiopacity (dotted lines). Freshly mixed test hydrogel containing iodixanol was placed in the root canal system of immature human premolars using a lentulo spiral **(c)**. This test hydrogel apparently filled the whole canal space and could be clearly discerned from root dentin.

the ProTaper system (Sirona Dentsply Endodontics, Ballaigues, Switzerland) and filled with freshly mixed hydrogel using a lentulo spiral. The teeth were radiographed as described above.

Swelling of Hydrogels

The water-absorbing capacity (swelling) was calculated gravimetrically according to the formula:

$$\text{Swelling ratio} = (w_s - w_d)/w_d$$

where w_s is the weight of the swollen hydrogel and w_d is the weight of the dry hydrogel. The hydrogels were prepared with TBS or Visipaque, frozen at −80°C overnight and freeze-dried under vacuum for 24 h until constant weight in a lyophilization apparatus (Christ, Osterode am Harz, Germany). The dry hydrogels were pre-weighed in a precision balance (PE360; Mettler Toledo, Greifensee, Switzerland) and were immersed in 5 mL of TBS at 37°C for 5 min, 1, 8, and 24 h. After removing them from the TBS at each time point, the hydrogels were gently wiped with a filter paper and weighted again. Subsequently, the hydrogels were immersed in fresh TBS. The swelling ratio was measured by comparing the weight of hydrogels before and after immersing in TBS according to the equation. These experiments were performed in triplicates.

Scanning Electron Microscopy

To visualize the microstructure of the test and the control hydrogels under investigation, triplicates of lyophilized specimens were inspected using scanning electron microscopy (SEM). To this end, the freeze-dried hydrogels were attached to sticky carbon pads (Plano, Wetzlar, Germany) on SEM pin stubs. Specimens were sputtered with an 8 nm gold layer (Safematic, Bad Ragaz, Switzerland). Images were obtained at 5 mV acceleration voltage and 12 mm working distance using a secondary electron detector (Zeiss Supra 50VP, Oberkochen, Germany).

Release of Iodixanol from Test Hydrogels

The UV spectrum of an iodixanol solution in water shows a maximum at 244 nm and a specific absorption coefficient of 320 $\text{l g}^{-1}\ \text{cm}^{-1}$ at that wavelength (Schroder et al., 1997). To test the release of iodixanol from the test hydrogels, 1 mL of hydrogel was mixed with 49 mL of TBS in 50 mL polypropylene centrifugation tubes (Falcon, Thermo Fisher Scientific, Waltham, MA). These tubes were rotated at room temperature (25°C) at 6 rpm in an overhead rotator with a radius of 10 cm (Bibby Scientific, Staffordshire, UK). 100 μL of the solution were removed (and not replenished) to be assessed spectrophotometrically for their iodixanol content after 30 min, 1, 3, 8, 24, 48, 72, 120, and finally after 168 h. Experiments were done in triplicates. Iodixanol that washed out from the hydrogel was quantified at 244 nm in a spectrophotometer (Shimadzu, Kyoto, Japan) in quartz cuvettes against a standard curve. Iodixanol wash out is presented as % of total iodixanol originally present in the hydrogel in solution.

Chick Chorioallantoic Membrane (CAM) Assay

CAM assays were performed to assess the impact of test and control hydrogels on tissue viability and vascularization of fertilized chicken eggs (Beckers et al., 1997). A total of 14 fertilized Lohman white LSL chicken eggs (Animalco AG, Staufen AG, Switzerland) were used for these experiments, seven in the control and seven in the test hydrogel group. According to the local animal care guidelines (Canton of Zurich, Switzerland), no approval was necessary to perform these experiments, as they were executed only until embryonic day (ED) 14. Detailed procedures have been published (Woloszyk et al., 2016). Eggs were pre-incubated for 3 days at 38°C at a rotational speed of 360°/4 h (Bruja 3,000, Brutmaschinen-Janeschitz GmbH, Hammelburg, Germany). On ED 3, the eggs were processed for *in ovo* cultivation. The eggshell was wiped with 70% ethanol. To lower the developing embryo before opening of the shell using Scotch tape and scissors, 4 mL of albumen were removed through a small hole in the shell. The egg was stabilized in a 60 mm Petri dish base. The opening was covered with a second 60 mm Petri dish base, which was fixed to the bottom base using Scotch tape. Subsequently, the eggs were incubated at 37°C. On ED 7, hydrogel samples polymerized within a silicone O-ring (from Corning cryogenic vials, Sigma-Aldrich, St. Louis, MO) were gently placed on the CAM (1 per egg), and the eggs were incubated for further 7 days until ED 14. One egg in the test and one in the control group did not survive the 7 days pre-incubation, leaving 6 viable eggs in the control and the test group, respectively. On ED 14, the hydrogel probes together with the CAM were cut out and after fixing in 4% paraformaldehyde for 60 min at room temperature, the probes were washed and stored in PBS. Pictures were taken using a stereomicroscope (Leica Microsystems AG, Heerbrugg SG, Switzerland). Vascularization within the silicone O-ring was quantified on these images using ImageJ v1.50b.

Data Presentation

Numerical data is presented as means and standard deviations. Pair-wise comparisons between the test and the control hydrogel were performed using paired *t*-test. The alpha-type error was set at 5% ($p < 0.05$).

RESULTS

The control fibrin hydrogel prepared with TBS clotted quickly. The recorded mean gelation time was 22 ± 1 s. Gelation was strongly delayed by the presence of iodixanol; it occurred after 1,580 ± 75 s ($p < 0.05$), i.e., 26 min. The iodixanol solution (Visipaque) rendered the test hydrogel radiopaque with a mean radiopacity of 1.9 ± 0.2 mm Al/mm. The test hydrogel could clearly be distinguished from root dentin of human teeth radiographically (**Figures 1a,c**), while the control hydrogel had no detectable radiopacity (**Figure 1b**).

Results showed that swelling was strongly reduced when iodixanol was added to the hydrogel. Values decreased from 203% for control hydrogels prepared with TBS to only

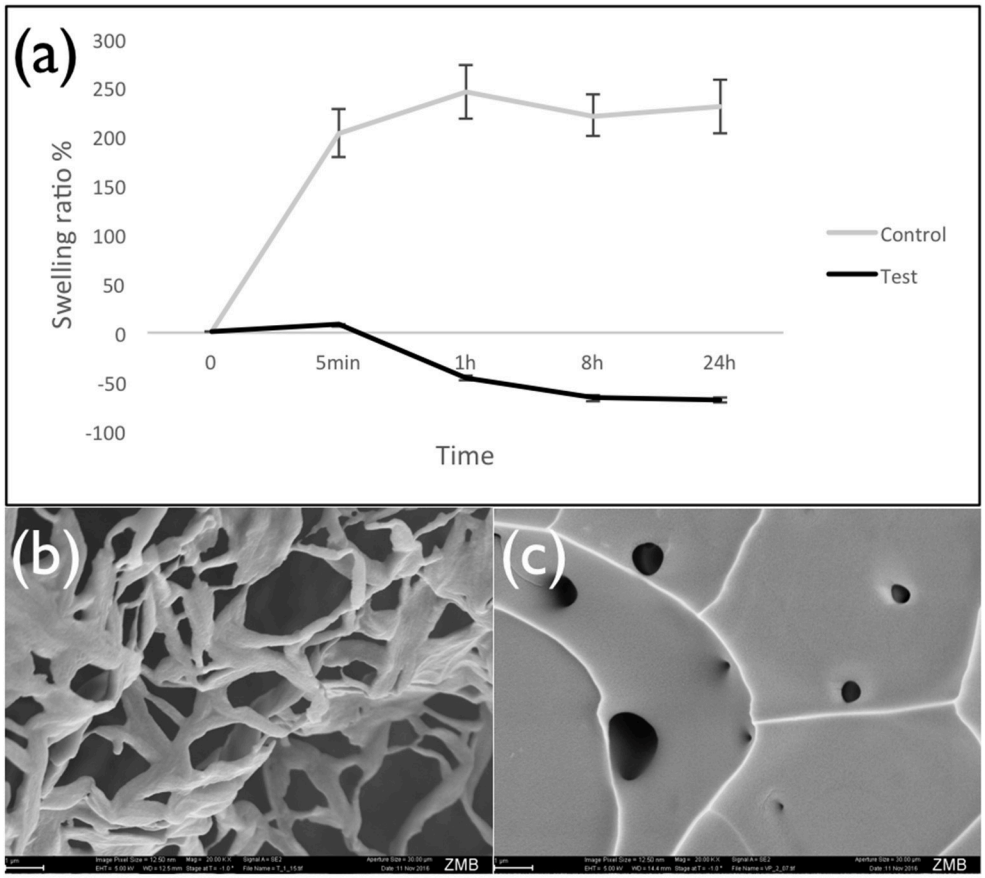

FIGURE 2 | Swelling of lyophilized hydrogels. Panel **(a)** presents the swelling ratio of lyophilized fibrin hydrogels prepared with TBS (control) and the iodixanol solution (Visipaque) after different time of incubation in TBS at 37°C, showing that iodixanol reduced the water sorption of hydrogel. As time passed, the amount of retained water in the test hydrogel decreased and caused the shrinking of the hydrogel structure. Panel **(b)** is a typical SEM image of the control hydrogel, panel **(c)** a corresponding image of the test hydrogel containing iodixanol.

8% for counterparts prepared with Visipaque (time point 5 min, $p < 0.05$) (**Figure 2a**). Inspection of the lyophilized hydrogels in a scanning electron microscope confirmed that iodixanol influenced their structure. While the control hydrogel showed the typical sponge-like porous structure (**Figure 2b**), the test hydrogel containing iodixanol had a more homogenous appearance with few internal openings (**Figure 2c**).

Iodixanol release from the hydrogels prepared with Visipaque reached 14.5 ± 0.5% after 120 h and then ceased (**Figure 3**). This release from test hydrogels did not have any apparent effect on the fertilized chicken eggs. All incubated eggs survived the exposure to either the test or the control hydrogel between embryonic day 7 and 14, and vascularization in the chorioallantoic membrane under the hydrogels looked similar (**Figure 4**). Quantification of the vascularization revealed no statistically significant difference between groups ($p = 0.34$).

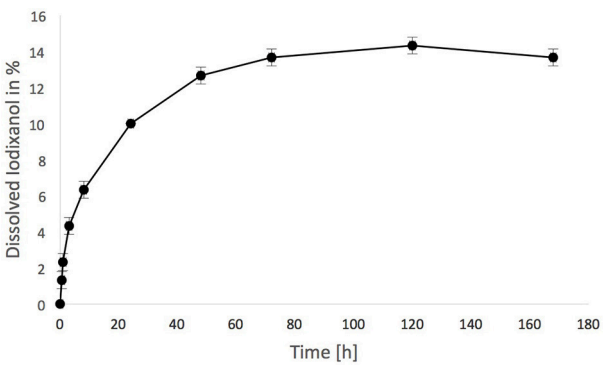

FIGURE 3 | Iodixanol release from test fibrin hydrogels. One milliliter was suspended in 49 mL of tris-buffered saline (TBS) over time, expressed in % of the total iodixanol that was present in the hydrogel initially.

DISCUSSION

This study showed that a radiopaque and tissue-compatible, yet slow setting and less porous fibrin hydrogel is obtained by diluting a commercially available fibrin sealant with an isotonic contrast agent containing iodixanol rather than TBS. Basic properties of this experimental hydrogel such as hydrogelation

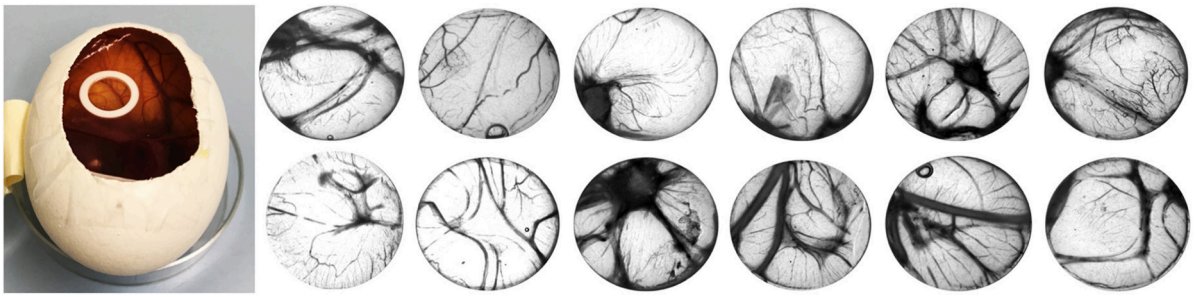

FIGURE 4 | Chick chorioallantoic membrane (CAM) assay used in this study (left). Control fibrin hydrogels (upper row) and radiopaque test counterparts spiked with iodixanol (lower row) were placed in o-rings on the CAM for 7 days (from embryonic day 7 to 14), and vascularization was quantified. There was no difference between the test and the control group.

kinetics, radiopacity, swelling, iodixanol release, and overall tissue compatibility were assessed. The current *in vitro* and *in ovo* results are preliminary observations and should be seen as such. At this point, it is not possible to draw conclusions regarding the suitability of the test hydrogel for pulp tissue engineering.

The fibrin sealant used in this study (Tisseel), which is designed to achieve hemostasis, to seal or glue tissue, and to support wound healing, has to be diluted in TBS to obtain a fibrin hydrogel that could be invaded by cells during the pulp regeneration process (Ruangsawasdi et al., 2014). This creates an opportunity to replace the TBS used for that purpose with a similar, isotonic product having enhanced contrast properties (Visipaque 320). Opacity of hydrogels by addition of the iodixanol that is contained in Visipaque has recently been tested in chitosan hydrogels for controlled blood vessel embolization (Fatimi et al., 2016). Iodixanol extends blood-clotting time (Bellemain-Appaix et al., 2012), which is concurrent with the results obtained here using a fibrin sealant. It is a non-ionic dimer (Jones and Goodall, 2003). In the current approach, we chose iodixanol because alternative contrast agents such as the non-ionic monomer iohexol (Omnipaque, Bayer Pharma AG, Berlin, Germany) and the ionic dimer ioxaglate (Hexabrix, Guerbet, Roissy, France) appear to have an even higher anticoagulant effect than iodixanol (Corot et al., 1996). It has also been shown that the slowing of the hydrogelation process in chitosan hydrogels by iodixanol is dose-dependent (Fatimi et al., 2016). Since teeth are inherently radiopaque structures, we used a high concentration of iodixanol compared to previous experiments on chitosan hydrogels for embolization. However, the radiopacity of permanent sealing materials requested by the ISO norm (2012), which is 3 mm Al/mm, was still not met. Nevertheless, the preliminary filling experiments with human teeth showed that the radiopacity should be sufficient for the intended purpose, i.e., the monitoring of the correct placement of the fibrin hydrogel (**Figure 1c**).

The extended clotting time, which resulted from the presence of iodixanol in the fibrin hydrogel, can be desirable in endodontic applications. The radiopaque fibrin hydrogel under investigation has a working time similar to endodontic sealers (Whitworth, 1999). It can be applied into the root canal system using for example a lentulo spiral. In contrast, the mere fibrin hydrogel diluted with TBS, which is commonly used as a control (Ruangsawasdi et al., 2014, 2017), is not easy to administer into the root canal system because of its immediate gelation.

The swelling of hydrogels is related to the crosslinking ratio in their polymeric network. Highly cross-linked hydrogels tend to swell less than counterparts with a lower crosslinking ratio (Peppas et al., 2000). The effect of iodixanol on swelling of lyophilized hydrogels and on the apparent hydrogel structure in SEM scans strongly suggests that hydrogel porosity is reduced. This is in line with previous studies showing reduction of chitosan hydrogel swelling by increasing their iodixanol concentration (Fatimi et al., 2016). The addition of iodixanol to fibrin-rich clots resulted in shorter, thinner, and more numerous fibrin fibers when compared to counterparts made with ioxaglate or buffer, leading to a much more compact 3D architecture with smaller pores and higher crosslinking of fibrin fibers (Bellemain-Appaix et al., 2012). Furthermore, there was an apparent negative swelling after 5 min with the test hydrogel under the current conditions. This might be indicative of a material degradation process. The iodixanol modified hydrogels hardly took up any TBS fluid, suggesting an important loss of hydrophilicty or material permeability. Both are important characteristics for a biomaterial scaffold in regenerative procedures. Incorporation of iodixanol seems to produce a fiber coalescence process leading to a tensional film-like morphology (**Figure 2**). It thus remains to be investigated how these iodixanol-induced alterations influence the permeability of fibrin hydrogels to migrating cells during regenerative processes.

We used the CAM assay as a measure of tissue compatibility of the new radiopaque hydrogel under investigation. Although this assay is relatively simple, it can be considered suitable for the pre-screening of scaffolds to determine whether they cause any adverse tissue reactions (Baiguera et al., 2012). Our results suggest good tissue compatibility of the test as well as the control hydrogel. However, it needs to be cautioned that the CAM assay is a non-mammalian organism that has not yet developed an immune system. This assay merely

determined the effect of the fibrin hydrogels on tissue viability and vascularization. Histological assessment of the hydrogels revealed that no blood vessels grew into the body of the hydrogels (data not shown). This is to be expected, as we did not embed any chemotactic molecules into the hydrogels (Anderson et al., 2011).

In conclusion, the current results revealed the possibility to elaborate radiopaque fibrin hydrogels for potential endodontic applications from materials that are already commercially available. Under the current conditions, tissue compatibility appeared not to be influenced by the addition of iodixanol to the hydrogel. Further *in vivo* studies should test the effects of different contrast agents on fibrin hydrogel structure combined with cell migration and attraction.

AUTHOR CONTRIBUTIONS

Study design: GH, MZ, TM, and FW. Data collection: GH, AW, and AI. Data analysis: MZ. Drafting manuscript: GH and MZ. Revising manuscript content: GH, MZ, AW, TM, AI, and FW. Approving final version of manuscript: GH, MZ, AW, TM, AI, and FW. MZ takes responsibility for the integrity of the data analysis.

FUNDING

This research was partly supported by the Swiss National Foundation (SNSF) grant 31003A_135633 (TM and AW), and a Swiss government scholarship (AI).

REFERENCES

Anderson, S. M., Siegman, S. N., and Segura, T. (2011). The effect of vascular endothelial growth factor (VEGF) presentation within fibrin matrices on endothelial cell branching. *Biomaterials* 32, 7432–7443. doi: 10.1016/j.biomaterials.2011.06.027

Baiguera, S., Macchiarini, P., and Ribatti, D. (2012). Chorioallantoic membrane for *in vivo* investigation of tissue-engineered construct biocompatibility. *J. Biomed. Mater. Res. B Appl. Biomater.* 100, 1425–1434. doi: 10.1002/jbm.b.32653

Beckers, M., Gladis-Villanueva, M., Hamann, W., Schmutzler, W., and Zwadlo-Klarwasser, G. (1997). The use of the chorio-allantoic membrane of the chick embryo as test for anti-inflammatory activity. *Inflamm. Res.* 46, 29–30. doi: 10.1007/s000110050039

Bellemain-Appaix, A., Beygui, F., Lesty, C., Gupta, S., Silvain, J., Le Feuvre, C., et al. (2012). Impact of anticoagulation on ionic and nonionic contrast media effect on thrombogenesis and fibrinolysis: the PEPCIT study. *Catheter Cardiovasc. Interv.* 79, 823–833. doi: 10.1002/ccd.23080

Chen, M. Y., Chen, K. L., Chen, C. A., Tayebaty, F., Rosenberg, P. A., and Lin, L. M. (2012). Responses of immature permanent teeth with infected necrotic pulp tissue and apical periodontitis/abscess to revascularization procedures. *Int. Endod. J.* 45, 294–305. doi: 10.1111/j.1365-2591.2011.01978.x

Corot, C., Chronos, N., and Sabattier, V. (1996). *In vitro* comparison of the effects of contrast media on coagulation and platelet activation. *Blood Coagul. Fibrinolysis* 7, 602–608.

Fatimi, A., Zehtabi, F., and Lerouge, S. (2016). Optimization and characterization of injectable chitosan-iodixanol-based hydrogels for the embolization of blood vessels. *J. Biomed. Mater. Res. B Appl. Biomater.* 104, 1551–1562. doi: 10.1002/jbm.b.33500

Galler, K. M. (2016). Clinical procedures for revitalization: current knowledge and considerations. *Int. Endod. J.* 49, 926–936. doi: 10.1111/iej.12606

Hargreaves, K. M. (2016). Adding regenerative endodontics to the table of contents. *J. Endod.* 42:1. doi: 10.1016/j.joen.2015.11.001

International Organization for Standardization ISO (2012). *Norm 6876. Dentistry—Root Canal Sealing Materials*. Vernier.

Jones, C. I., and Goodall, A. H. (2003). Differential effects of the iodinated contrast agents Ioxaglate, Iohexol and Iodixanol on thrombus formation and fibrinolysis. *Thromb. Res.* 112, 65–71. doi: 10.1016/j.thromres.2003.09.031

Kahler, B., Mistry, S., Moule, A., Ringsmuth, A. K., Case, P., Thomson, A., et al. (2014). Revascularization outcomes: a prospective analysis of 16 consecutive cases. *J. Endod.* 40, 333–338. doi: 10.1016/j.joen.2013.10.032

Kim, J. Y., Xin, X., Moioli, E. K., Chung, J., Lee, C. H., Chen, M., et al. (2010). Regeneration of dental-pulp-like tissue by chemotaxis-induced cell homing. *Tissue Eng. Part A* 16, 3023–3031. doi: 10.1089/ten.TEA.2010.0181

Lee, C. H., Cook, J. L., Mendelson, A., Moioli, E. K., Yao, H., and Mao, J. J. (2010). Regeneration of the articular surface of the rabbit synovial joint by cell homing: a proof of concept study. *Lancet* 376, 440–448. doi: 10.1016/S0140-6736(10)60668-X

Mao, J. J., Kim, S. G., Zhou, J., Ye, L., Cho, S., Suzuki, T., et al. (2012). Regenerative endodontics: barriers and strategies for clinical translation. *Dent. Clin. North Am.* 56, 639–649. doi: 10.1016/j.cden.2012.05.005

Marin, P. D., Bartold, P. M., and Heithersay, G. S. (1997). Tooth discoloration by blood: an *in vitro* histochemical study. *Endod. Dent. Traumatol.* 13, 132–138.

Nosrat, A., Homayounfar, N., and Oloomi, K. (2012). Drawbacks and unfavorable outcomes of regenerative endodontic treatments of necrotic immature teeth: a literature review and report of a case. *J. Endod.* 38, 1428–1434. doi: 10.1016/j.joen.2012.06.025

Nygaard Ostby, B. (1963). Nyere undersökelser over rotbehandlingsproblemet (recent investigations in endodontics). *Odontol. Tidskr.* 71, 467–478.

Peppas, N. A., Bures, P., Leobandung, W., and Ichikawa, H. (2000). Hydrogels in pharmaceutical formulations. *Eur. J. Pharm. Biopharm.* 50, 27–46.

Ruangsawasdi, N., Zehnder, M., and Weber, F. E. (2014). Fibrin gel improves tissue ingrowth and cell differentiation in human immature premolars implanted in rats. *J. Endod.* 40, 246–250. doi: 10.1016/j.joen.2013.09.022

Ruangsawasdi, N., Zehnder, M., Patcas, R., Ghayor, C., Siegenthaler, B., Gjoksi, B., et al. (2017). Effects of stem cell factor on cell homing during functional pulp regeneration in human immature teeth. *Tissue. Eng. Part A.* 23, 115–123. doi: 10.1089/ten.TEA.2016.0227

Schroder, M., Schafer, R., and Friedl, P. (1997). Spectrophotometric determination of iodixanol in subcellular fractions of mammalian cells. *Anal. Biochem.* 244, 174–176. doi: 10.1006/abio.1996.9861

Simon, S. R., Tomson, P. L., and Berdal, A. (2014). Regenerative endodontics: regeneration or repair? *J. Endod.* 40, S70–S75. doi: 10.1016/j.joen.2014.01.024

Trope, M. (2010). Treatment of the immature tooth with a non-vital pulp and apical periodontitis. *Dent. Clin. North. Am.* 54, 313–324. doi: 10.1016/j.cden.2009.12.006

Vermylen, C., De Vreker, R. A., and Verstaete, M. (1963). A rapid enzymatic method for assay of fibrinogen fibrin polymerization time (FPT test). *Clin. Chim. Acta* 8, 418–424.

Whitworth, J. (1999). Sealer selection: a considered approach. *Endod. Prac.* 2, 31–38.

Woloszyk, A., Liccardo, D., and Mitsiadis, T. A. (2016). Three-dimensional imaging of the developing vasculature within stem cell-seeded scaffolds cultured *in ovo*. *Front. Physiol.* 7:146. doi: 10.3389/fphys.2016.00146

Conflict of Interest Statement: The authors declare that the research was conducted in the absence of any commercial or financial relationships that could be construed as a potential conflict of interest.

frontiers in Physiology

ORIGINAL RESEARCH
published: 27 December 2016
doi: 10.3389/fphys.2016.00652

Spectroscopic and Mechanical Properties of a New Generation of Bulk Fill Composites

Riccardo Monterubbianesi[1], Giovanna Orsini[1], Giorgio Tosi[2], Carla Conti[2], Vito Librando[3], Maurizio Procaccini[1] and Angelo Putignano[1]*

[1] Department of Clinical Sciences and Stomatology, Polytechnic University of Marche, Ancona, Italy, [2] Department of Materials, Environmental Science and Urban Planning, Polytechnic University of Marche, Ancona, Italy, [3] Department of Chemical Sciences, University of Catania, Catania, Italy

Objectives: The aims of this study were to *in vitro* evaluate the degree of conversion and the microhardness properties of five bulk fill resin composites; in addition, the performance of two curing lamps, used for composites polymerization, was also analyzed.

Materials and Methods: The following five resin-based bulk fill composites were tested: SureFil SDR®, Fill Up!™ , Filtek™ , SonicFill™ , and SonicFill2™ . Samples of 4 mm in thickness were prepared using Teflon molds filled in one increment and light-polymerized using two LED power units. Ten samples for each composite were cured using Elipar S10 and 10 using Demi Ultra. Additional samples of SonicFill2, (3 and 5 mm-thick) were also tested. The degree of conversion (DC) was determined by Raman spectroscopy, while the Vickers microhardness (VMH) was evaluated using a microhardness tester. The experimental evaluation was carried out on top and bottom sides, immediately after curing (t0), and, on bottom, after 24 h (t24). Two-ways analysis of variance was applied to evaluate DC and VMH-values. In all analyses, the level of significance was set at $p < 0.05$.

Results: All bulk fill resin composites recorded satisfactory DCs on top and bottom sides. At t0, the top of SDR and SonicFill2 showed the highest DCs-values (85.56 ± 9.52 and 85.47 ± 1.90, respectively), when cured using Elipar S10; using Demi Ultra, SonicFill2 showed the highest DCs-values (90.53 ± 2.18). At t0, the highest DCs-values of bottom sides were recorded by SDR (84.64 ± 11.68), when cured using Elipar S10, and Filtek (81.52 ± 4.14), using Demi Ultra. On top sides, Demi Ultra lamp showed significant higher DCs compared to the Elipar S10 ($p < 0.05$). SonicFill2 reached suitable DCs also on bottom of 5 mm-thick samples. At t0, VMH-values ranged between 24.4 and 69.18 for Elipar S10, and between 26.5 and 67.3 for Demi Ultra. Using both lamps, the lowest VMH-values were shown by SDR, while the highest values by SonicFill2. At t24, all DC and VMH values significantly increased.

Conclusions: Differences in DC and VMH among materials are suggested to be material and curing lamp dependent. Even at t0, the three high viscosity bulk composites showed higher VMH than the flowable or dual curing composites.

Keywords: bulk fill resin composites, degree of conversion, surface microhardness, curing lamps, spectroscopy

OPEN ACCESS

Edited by:
Catherine Chaussain, Paris Descartes University, France

Reviewed by:
Natalina Quarto, University of Naples Federico II, Italy
Elisabeth Dursun, Paris Descartes University, France

****Correspondence:***
Giovanna Orsini
giovorsini@yahoo.com;
g.orsini@univpm.it

Specialty section:
This article was submitted to Craniofacial Biology and Dental Research, a section of the journal Frontiers in Physiology

Received: *09 October 2016*
Accepted: *12 December 2016*
Published: *27 December 2016*

Citation:
Monterubbianesi R, Orsini G, Tosi G, Conti C, Librando V, Procaccini M and Putignano A (2016) Spectroscopic and Mechanical Properties of a New Generation of Bulk Fill Composites. Front. Physiol. 7:652. doi: 10.3389/fphys.2016.00652

INTRODUCTION

In nowadays dentistry, resin-based composites have been and are widely used for dental restorations, even if with some disadvantages: shrinkage, shrinkage stress, micro cracks (in the dental structure or in the resin material), debonding, and secondary caries (Ilie et al., 2007; Ilie and Hickel, 2011; Tantbirojn et al., 2011; El-Saftya et al., 2012; Van Ende et al., 2012; Czasch and Ilie, 2013).

In the time, the multi-layer technique tried to reduce these drawbacks: the fact to place composites in dental cavities, using thin increments of 2 mm or less, allowed a good penetration of the light-curing, thus lowering the shrinkage stress (El-Saftya et al., 2012). Nevertheless, this procedure might afford air bubbles, no linkage between layers, troubles during composites placing, especially in the posterior areas, in which it is sometimes difficult to fill the deep cavities and it is often required a long chair time (Abbas et al., 2003; Sarrett, 2005).

To solve these problems, the manufacturers introduced bulk fill resin composites, consisting in new chemical monomers and fillers with an enhancement of their translucency and, consequently, with the potentiality of obtaining an optimal degree of conversion (DC), even in the bottom of the cavities, where it is more difficult to reach high DC. It has been demonstrated that there are several factors affecting the mechanical properties of a resin composite: chemical composition, amount of emitted radiation, distance from the tip of the light source, and photo-activation mode (Da Silva et al., 2008b). Recent improvements in nanotechnology have led to an optimal filler content of this new generation composites, by the addition of free nanosized spherical particles and clusters, which can act as a single unit, thus significantly improving their mechanical properties, also after finishing and polishing procedures (Beun et al., 2007; Jung et al., 2007; Czasch and Ilie, 2013). Furthermore, the benefit of these materials consists in the fact that they can be cured to a maximal increment thickness of 4–6 mm with a limited shrinkage, due to their high translucency, thus allowing the clinicians to rapidly fill the cavity, shortening the chair time (Van Ende et al., 2012). However, even if the first generation bulk filling materials (introduced by Dentsply with a product called SDR) presented a limited shrinkage stress, they showed unsatisfactory mechanical properties, due to the low percentage of fillers, thus requiring the use of a conventional resin composite, acting as an enamel-top capping layer (Campodonico et al., 2011; Ilie and Hickel, 2011; Van Dijken and Pallesen, 2014).

These limitations were improved with the introduction of high viscosity bulk fill composites, which can fill up the occlusal area in a unique step (as single bulk increment), cured and hence sculpted, without the need of an additional top capping layer. Indeed, innovative composites have been recently available on the market, such as SonicFill, which, for instance, uses the sonic energy to decrease viscosity; once the sonic energy has been removed, the resin composite gradually returns to the starting high viscosity status, assuring good mechanical properties (Ahmad, 2013).

The recent large use of high viscosity bulk fill composites have been due to the following positive factors: simplified procedures, increase of the filler percentage, high depth of cure, acceptable translucency, negligible shrinkage stress after polymerization, and satisfactory cavity adaptation (Ahmad, 2013).

As every modern resin-based system, also bulk fill composites necessitate the light curing process to be polymerized. It is noteworthy that clinicians have the tendency to overestimate the properties of bulk fill resin composites, giving an incorrect evaluation of the volumetric shrinkage, shrinkage stress, and DC. Moreover, other factors such as modulus of elasticity, rate of polymerization, polymerization kinetics, initiator chemistry, gel point, type of filler and monomer, development and intensity of the curing stress have to be taken into account (Ferracane et al., 2014). In fact, even if bulk filling restorations were recommended also in cavities up to 4 mm deep, it turned out that many practitioners are still improperly doubtful on their suitability in the clinical field (Czasch and Ilie, 2013).

The clinical performance of posterior resin-based composite restorations can be strongly affected by various parameters as DC and surface hardness. A high DC can determine good mechanical properties, chemical stability and longevity of the restoration (Da Silva et al., 2008a); it has been measured using different methods, such as Raman, NIR (near-infrared) and MIR (middle-infrared) spectroscopies, in order to evaluate changes of aliphatic/aromatic double bond ratio. A satisfactory polymerization degree is essential for the success of the restoration and can require even more than 24 h (Yoon et al., 2002; Miyazaki et al., 2003; Conti et al., 2005).

The surface hardness (measured as microhardness, by means of Vickers or Knoops tests) is defined as the resistance to permanent indentation or penetration on time, and it has to be evaluated in finishing and polishing phases, or when the resin composites are placed on large areas of masticatory force (Galvao et al., 2013; Tarle et al., 2015).

In order to evaluate the acceptable values of DC and surface microhardness, it is worldwide accepted to refer to the International Standard Test ISO 4049-2009, introduced for dental polymer-based restorative materials. In fact, to consider the suitability of a dental restoration (Flury et al., 2012), it is mandatory to take into account the determination of the depth of cure of a dental composite, referring to both DC and Vickers microhardness (VMH) as fundamental key tests (Flury et al., 2012; Leprince et al., 2012).

The primary aim of this study was to analyse the mechanical and spectroscopic properties of one low viscosity bulk fill composite (SDR), one medium viscosity/dual curing bulk fill composite (Fill Up!), and three high viscosity bulk fill composites (Filtek, SonicFill, SonicFill2), by means of DC and VMH measures. In addition, the potential correlation between DC and VMH was also evaluated.

The secondary aim was to evaluate the performance of two curing lamps in the photo-polymerization process of the different composite samples.

The null hypotheses were: (1) DC values and VMH values do not significantly change within the tested bulk fill composites and there is a correlation between DC and VMH; (2) there are no difference in the performance of the two tested curing lamps.

MATERIALS AND METHODS

Five commercial (shade 3) bulk fill composites for posterior restorations were tested (**Table 1**):

(1) SureFil® SDR® (from now on called SDR), a low viscosity flowable composite (Smart Dentin Replacement, Dentsply Caulk, Milford, DE, USA), which shows, in the manufacturer instructions, to need a final top capping layer.
(2) Fill Up!™(Coltène Whaledent AG, Altstätten, Switzerland), a medium-viscosity/dual curing bulk composite, which requires one step increment and no top capping layer, as shown in the manufacturer instructions.
(3) Filtek™ Bulk Fill Posterior Restorative (3M ESPE, St Paul MN, USA) a high viscosity bulk composite, which requires one step increment, no top capping layer as shown in the manufacturer instructions.
(4) SonicFill™ (Kerr Corp. Orange, CA, USA), and
(5) SonicFill2™ (Kerr Corp. Orange, CA, USA). Both SonicFill systems combine a flowable resin composite with an universal resin composite by using a hand piece which enables sonic activation. As shown by the manufacturer instructions, SonicFill2™ presents improved mechanical properties compared to SonicFill™.

The two light-curing lamps used for the polymerization of resin-composite samples presented the following technical details. Elipar S10 (3M ESPE) had an energy output 1200 mW/cm^2 and spectrum between 430 and 480 nm; on the other hand, Demi Ultra (Kerr Corp.) had variable energy output from 1100 to 1330 mW/cm^2 and spectrum between 450 and 470 nm, the energy intensity gradually changing from 1100 until 1330 mW/cm^2.

Degree of Conversion (DC)

To evaluate DC, homemade Teflon cylinders (of 4 mm in height and 6 mm of internal diameter) were used; for each curing lamp, 10 disk-shaped specimens of each of five resin composites were obtained and photo-polymerized in bulk for 20 s. During the photo-polymerization, to exclude oxygen contamination, each sample was covered with a mylar strip on both surfaces. It has to be noted that the sample mass simulates the amount of resin composite usually used to fill up a dental cavity of recurrent dimensions. All the samples were measured on top side (top) and on bottom side (bottom), immediately once cured (t0), and, only on bottom, after 24 h (t24), too. In addition, for SonicFill2, the DC measurements were performed also in 10 3 mm-thick and 10 5 mm-thick samples, and finally, a last measurement was performed after 240 h (t240) only in SonifFill2 4 mm-thick samples.

A DXR FT Raman spectrometer (Thermo Fischer Scientific, Zug, Switzerland) was used to obtain the Raman spectrum of bulk composites. In Raman determinations, DC was evaluated by comparing the ratio of the alkene carbon-carbon double bond (1638 cm^{-1}, reaction band B), which was formed during the polymerization, with the one of the aromatic benzene ring (1610 cm^{-1}), whose intensity does not change during the polymerization (reference band A). To evaluate the DC, calibration curves were plotted assuming that the ratio A/B on top of the no cured material may represent the 0% of polymerization, while the same ratio on the top at t24, may be taken as 100% of polymerization. For this reason, the top DC-values will not be described in the results. **Figure 1** shows a typical Raman spectrum with the decrease of olefinic C = C mode at 1635 cm^{-1} (reaction band) during the curing of both surfaces.

Vickers Microhardness

Vickers microhardness was determined with Leitz Micro-Hardness (Wetzal GMBH, Wetzlar, Germany) tester on the same samples used for the DC measurements. The method consisted in indenting the sample by a diamond indenter with the form of a right pyramid. In our case, a 50 g load was applied for

TABLE 1 | Chemical composition of the tested bulk fill composites.

Materials	Manufacturer	Type	Composition
SureFil® SDR®	Dentsply Caulk	Bulk-fill flowable composite	modified UDMA, TEGDMA, EBPDMA, pigment, photoinitiator, barium and strontium alumino-fluoro-silicate glasses, Silicon Dioxide—Amorphous, Strontium. Aluminosilicate Glass. Filler load: 68 wt%; 45 vol%.
Fill up!™	Coltène/Whaledent AG	Dual curing bulk composite	TMPTMA, UDMA, bis-GMA, TEGDMA, dibenzoyl peroxide; benzoyl peroxide, Zinc oxide coated. Filler load: 65 wt%; 49 vol%.
Filtek™ bulk fill posterior restorative	3M/ ESPE, St. Paul, MN, USA	Bulk-fill paste composite	Bis-GMA, bis-EMA, UDMA, zirconia, Filler load:76.5 wt%, 58.4 vol%.
SonicFill™	Kerr Corporation, CA, USA	Bulk-fill paste composite activated	Resin: EBADMA, BisphenolA-bis-(2-hydroxy-3-mehacryloxypropyl) ether, TEGDMA, 3-trimethoxysilylpropyl methacrylate, SiO_2, Glass, oxide, chemicals. Filler load: 83.5 wt%; 83 vol%.
SonicFill2™	Kerr Corporation, CA, USA	Bulk-fill paste composite activated	Poly(oxy-1,2-ethanediyl), α,α′-[(1-methylethylidene)di-4, 1-phenylene]bis[ω-[(2-methyl-1-oxo-2-propen-1-yl)oxy]-Not available. 2,2′-ethylenedioxydiethyl dimethacrylate. Filler load: 81.3% wt % unreported.

Bis-GMA, bisphenol-Aglycidyldimethacrylate; bis-EMA, ethoxylated bisphenol-A-dimethacrylate; UDMA, urethane dimethacrylate; TMPTMA, trimethylolpropane Trimethacrylate; TEGDMA, triethylene glycol dimethacrylate; TEGDMA, triethylene glycol dimethacrylate; EBADMA, ethoxylated bisphenol-A dimethacrylate; EBPDMA, ethoxylated Bis-GMA; SiO_2, silicon dioxide; wt%, weight percentage; vol%, volume percentage.

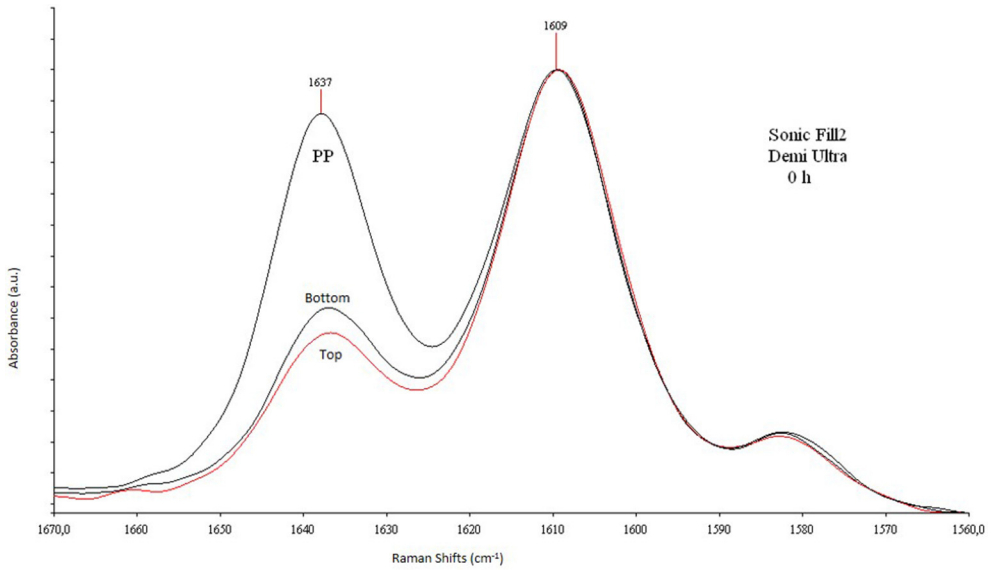

FIGURE 1 | Raman spectra between the reaction and reference bands. Raman spectra in the region 1670–1560 cm^{-1} of SonicFill2, 4 mm-thick, cured with Demi Ultra.

15 s. Once the load was removed, it was possible to evaluate (by using a microscope) the corresponding average value of the two indentation diagonals, to get the area of the sloping surface and, hence, to determine the corresponding hardness value.

The measurements of VMH were achieved at t0 and at t24 on the irradiated top surface of the samples. Three measurements were made for each sample: on the middle, on 0.15 mm and on 0.3 mm from the center. Calculations were made by using a computer software (Hardness-Course Vickers/Brinell/Rockwell copyright IBS 2012 version 10.4.4) (Fleming et al., 2008; Roberts et al., 2009; Nagi et al., 2015).

Statistical Analyses of DC and VMH Data

Statistical analyses were performed by means of R Project for Statistical Computing 3.3.0 (https://www.r-project.org/) and Microsoft Excel 2013. Normality of data distribution and homogeneity of group variances were verified by Kolmogorov-Smirnov test and Levene test, respectively. Differences of DC and VMH-values among groups and at different time intervals were evaluated by two-ways analyses of variance (Two-Ways ANOVA). The Tukey test was applied for *post-hoc* comparisons. In all analyses, the level of significance was set at $p < 0.05$.

RESULTS

Descriptive statistics of DC-values are reported in **Table 2**. Two different curing lamps were used in this study, Elipar S10 and Demi Ultra. At t0, they recorded statistically significant different DC-values between top and bottom sides ($p < 0.05$).

On top sides, at t0, DC-values of tested composites ranged between 70.40 and 85.56% using Elipar S10. On the other hand, using Demi Ultra lamp, top DC-values at t0 ranged between 82.30 and 90.53%. At t0, top DC-values obtained by Demi Ultra were significantly higher than the ones obtained using Elipar S10 ($p < 0.05$). SDR and SonicFill2 had higher DC-values than the other composites cured using Elipar S10; SonicFill2 recorded the highest DC-values when cured using Demi Ultra.

TABLE 2 | Degree of Conversion (DC).

Composites	*N*	t0 top		t0 bottom		t24 bottom	
		DC%	SD%	DC%	SD%	DC%	SD%
ELIPAR S10							
SDR	10	85.56	9.52	84.64	11.68	93.17	8.04
FILL UP!	10	82.79	3.20	65.03	6.57	94.71	7.96
FILTEK	10	78.27	3.95	74.32	7.30	92.20	9.01
SONICFILL	10	70.40	10.66	68.12	6.29	78.76	8.13
SONICFILL2	10	85.47	1.90	77.01	8.47	78.62	9.23
DEMI ULTRA							
SDR	10	84.93	2.26	75.67	2.20	91.94	10.02
FILL UP!	10	88.75	3.89	65.45	11.36	75.45	14.05
FILTEK	10	86.54	2.15	81.52	4.14	98.84	4.17
SONICFILL	10	82.30	6.03	78.78	5.90	90.95	8.92
SONICFILL2	10	90.53	2.18	75.44	3.53	80.25	7.32

N, number of samples; DC, Degree of Conversion; SD, Standard Deviation.
Mean of DC-values with Standard Deviation at t0, on top and bottom, together with t24 bottom values of samples cured using Elipar S10, and Demi Ultra lamps, respectively.

On bottom side, at t0, DC-values ranged between 65.03 and 84.64%, using Elipar S10. On the other hand, using Demi Ultra, they ranged between 65.45 and 81.52%. At t0, the highest bottom DC-values were recorded by SDR cured by Elipar S10 and Filtek cured by Demi Ultra ($p < 0.05$). After 24 h, all DC-values significantly increased ($p < 0.05$). Both at t0 and t24, the values recorded by the two curing lamps were not statistically different ($p > 0.05$). An additional DC evaluation was performed on

SonicFill2 samples of different thickness (3 and 5 mm-thick) at t0, using both lamps. **Figure 2** shows means of DC-values on top side of 3, 4, and 5 mm-thick samples, that were not statistically different ($p > 0.05$). On the other hand, on bottom side, the mean DC-values in the 3 mm (84.2%) and 5-thick samples (68.7%) were statistically different ($p < 0.05$). The last evaluation of SoniFill2 samples (4 mm-thick) after 240 h showed no significant difference of DC-values on top between t24 and t240 ($p > 0.05$).

The VMH-values recorded on the top of the different specimens by using the two curing lamps were statistically different (**Figure 3**). Demi Ultra showed higher VMH-values than Elipar S10 ($p < 0.05$). The mean of VMH measurements (from t0 to t24) showed the following significant increase ($p < 0.05$): 51.9 at t0 vs. 61.04 at t24 (using Elipar S10); 53.28 at t0 vs. 61.91 at t24 (using Demi Ultra). SonicFill2 had the highest VMH-values ($p < 0.05$): being 69.18 ± 3.15 at t0, using Demi Ultra, and 75.2 ± 1.69 at t24; using Elipar S10, 67.3 ± 3.7 at t0 and 71.12 ± 1.52, at t24. On the other hand, SDR showed the lowest VMH-values ($p < 0.05$): being 28.4 ± 2.34 at t0 and 35.28 ± 1.2 at t24, using Demi Ultra; using Elipar S10, 26.5 ± 3.71 at t0 and 36.73 ± 1.48 at 24.

Finally, Pearson's Test indicated that there is no correlation between DC and VMH, using both curing lamps (0.24 for Demi Ultra, 0.016 for Elipar S10).

DISCUSSION

Nowadays, it is becoming of growing tendency to use bulk fill resin composite materials because of their simplified procedures for filling in a single increment posterior restorations compared to the multi-increments techniques required by conventional

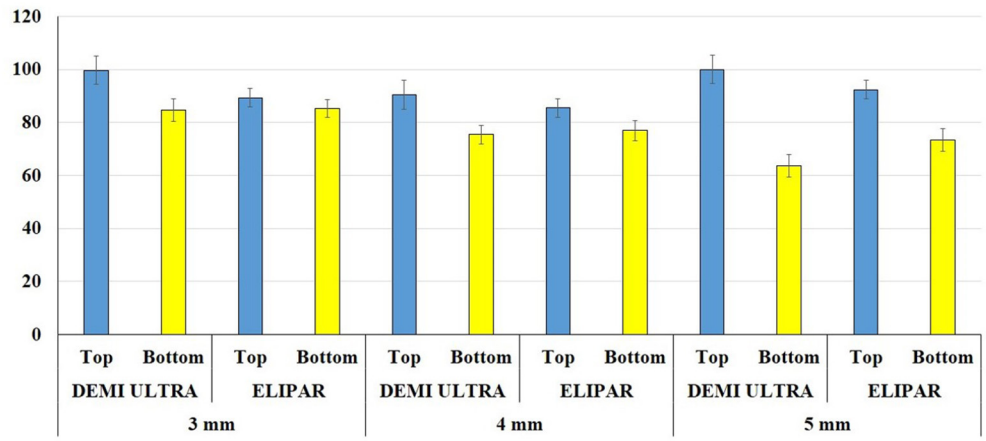

FIGURE 2 | Degree of Conversion (CD) comparison between top and bottom at different time. Mean of DC top and bottom values at t0 of SonicFill2 in 3, 4, and 5 mm-thick samples, cured using Demi Ultra and Elipar S10 lamps.

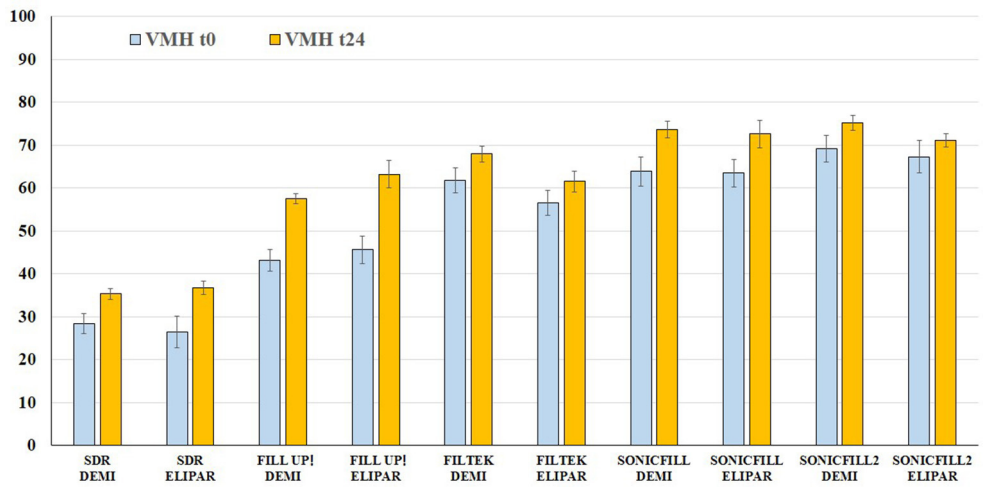

FIGURE 3 | Vickers microhardness (VMH) comparison on top at different time intervals. Mean and Standard Deviation of VMH-values of the five composites at t0 and t24 using Demi Ultra (DEMI) and Elipar S10 (ELIPAR) lamps.

resin composites. Indeed, manufacturers and recent scientific reports demonstrate that the main advantages of this restorative procedure consist in an increased depth of cure and a low polymerization shrinkage (Ilie et al., 2013; Leprince et al., 2014). Dental restorative composites polymerize to a certain depth, depending on the light beam penetration of the curing lamp inside the mass (Leloup et al., 2002), and a suitable polymerization of the whole composite mass remains one of the main important factors influencing the clinical success (Czasch and Ilie, 2013). In fact, high DC-values are important to assess optimal physical, mechanical and biological properties of resin composites; on the other hand, when there is not an optimal DC incomplete polymerization (unreacted—dangerous—monomer), marginal microleakage, discoloration, decrease of bonding strength and low mechanical properties can occur (Yap et al., 2004; Kusgoz et al., 2011; Alonso et al., 2013; Galvao et al., 2013). For a clinically acceptable restoration, some authors indicate that the DC-value should reach at least the 55% of it, however, even if resin-based dental materials are properly cured, they generally exhibit a significant amount of unreacted monomers (Soares et al., 2007; Galvao et al., 2013). High values of DC, up to 60%, can be due to improvements in the resin matrix (flexibility and viscosity of the starting monomer), to the composition and size of fillers and to the irradiance intensity (Dickens et al., 2003; Tursi et al., 2005).

In this study, in order to evaluate the DC-values of the tested bulk fill composites, which are based on the use of prepolymerized resins, it was assumed that the ratio 1635/1610 (described above) of the starting material, before the curing, may represent the 0% of polymerization, whereas the ratio of 100% of polymerization is assumed at t24 on the samples top sides (Ferracane, 1995; Blackham et al., 2009). For this reason, at t24, the DC-values on the top were not evaluated. Indeed, due to the overlapping of the reaction bands at 1635 cm^{-1} at t24 with the one at 240 h (e.g., SonicFill2), it has been hypothesized that after 24 h the polymerization process can be reasonably concluded. Therefore, these two reference points allow us to establish the evolution in time of the polymerization process: it was between t0 and t24, or between 0 and 100%. Raman spectroscopic evaluation shows that different DC-values are recorded between top and bottom at t0 for all composites, using the two curing lamps ($p < 0.05$). On top and at t0, Demi Ultra seems to cure better than Elipar S10 ($p < 0.05$), while on bottom and at t0, the two curing lamps are not statistically different to cure SDR and Filtek, which show the highest DC-values using Elipar S10 and Demi Ultra, respectively. After 24 h, bottom DC-values increase using both Elipar S10 and Demi Ultra, with no significant differences between the two curing lamps: once again SDR and Filtek show the best performance. In agreement with literature reports, all 4 mm-thick tested samples show high DC-values, mainly for t0 bottom determinations (Goracci et al., 2014; Leprince et al., 2014; Marovic et al., 2015). In the case of SDR, the high DC-values can be due to the high fluidity and transparency of this resin, even if, it is noteworthy again to remark, that a flowable resin composite, like SDR, needs an additional hardening top layer. Literature data concerning SonicFill and SDR evidence some discordance and, in general, lower DC-values than our data, mainly for t0 bottom determinations (57.9 and 50.3%, respectively, when using Demi Ultra lamp, with an output of 1100 mW/cm^2; see Goracci et al., 2014). Indeed some reports show that SDR DC-values on top ranged from the 77% (t0), using a light unit output of 1200 mW/cm^2 (Guimaraes et al., 2013), to the 67%, reported by other authors (Van Ende et al., 2013; Marovic et al., 2015). Among the high viscosity samples, SonicFill2 shows the highest DC-value with both curing lamps (at t0, on top), being Demi Ultra the best unit to polymerize it. However, both curing lamps result in a satisfactory performance, being Demi Ultra slightly superior than Elipar S10 in top surfaces curing ($p < 0.05$).

As mentioned above, DC-values of SonicFill2 have been determined also on 3 and 5 mm-thick samples at t0 (**Figure 2**). The bottom DC mean values of these samples at different thickness are statistically different, thus suggesting that the thickness of samples could condition the DC. However, it is noteworthy to underline that acceptable DC-values are registered even on the bottom side of 5 mm-thick samples.

Finally, the fact that there is no difference in DC SonicFill 2 values between t24 and t240 means that a satisfactory degree of polymerization can be reached after 24 h, in agreement with other literature reports (Ferracane, 1995; Blackham et al., 2009).

Hardness and microhardness measure the resistance to plastic deformation and indicates the resistance to indentation under functional stresses: a high value can be indicative of the ease of finishing and polishing of a restoration (Rahiotis et al., 2004; David et al., 2007). It has already been reported that hardness values may be related to the DC of carbon double bonds of a resin composite; even if with some divergence, it has been shown that a conversion around 90% of the resin may correspond to a bottom/top VMH ratio of 80% (Bouschlicher et al., 2004). Moreover, the microhardness of a resin composite depends also on the thickness: an increase in thickness causes a microhardness lowering.

In recent years, modulator interacting with camphorquinone (as in the case of the dual-curing composite Fill Up!), transparency enhancements and/or technological up grades (as in the case of high viscosity bulk fill composites) have been added to the resin composites, thus resulting in satisfactory microhardness values even in 4 mm-thick samples. Indeed, some authors reported that high viscosity bulk fill composites might exhibit high microhardness values because of the high percentage of fillers content (Barabanti et al., 2015; Nagi et al., 2015). **Figure 3** reports mean and SD of VMH top values at t0 and t24, using the two curing lamps. As expected, after 24 h, all samples show significant VMH increases ($p < 0.05$). Among the five materials, the lowest VMH mean value is shown by SDR, while a considerable increase is found for the medium viscosity dual curing Fill Up! (57 and 63 vs. 51 VMH, as claimed by the manufacturer Coltene); noteworthy is that at t0, SonicFill2 shows the highest VMH-value, using both curing lamps.

Several studies have tried to find a correlation between the DC and VMH for some authors no correlation may be drawn, while, for others, a negative trend occurs between the two parameters (Ferracane, 1985; De Wald and Ferracane, 1987; Santos et al.,

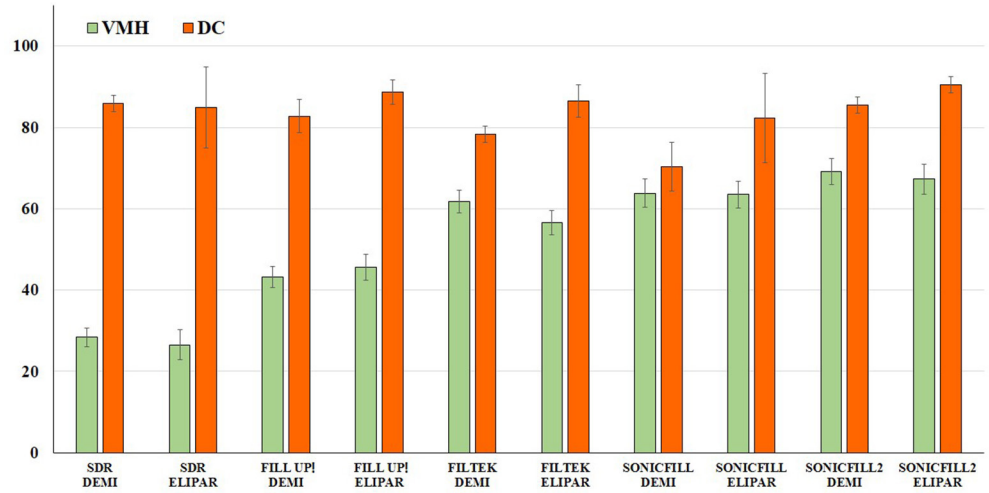

FIGURE 4 | Correlation between Vickers microhardness (VMH) and Degree of Conversion (DC). Comparison between mean VMH and DC-values (top t0) of the samples cured using Demi Ultra (DEMI) and Elipar S10 (ELIPAR) lamps.

2007; Da Silva et al., 2008a). In our case, the lack of any correlation is evident (Pearson's correlation coefficient: 0.24 for Demi Ultra, −0.016 for Elipar S10), meaning that, even if high values of two single parameters may point out a satisfactory dental curing, a linear correlation is lacking (**Figure 4**). This fact may be due to the different contents and viscosity of the five composites (**Table 1**).

In the attempt to analyse the behavior of a reasonable range of new bulk fill dental composites, a significant number of samples have been evaluated in the present work, however, other experiments are needed to make definitive remarks and, therefore, future analyses will aim to continue to analyse newly introduced materials. In definitive, differences in DC and VMH-values between our study and previous literature reports can be ascribed to improvements of fillers (composition and particles size distribution, percentage of filler load), of the resin matrix (monomer type and its chemical structure), and also to the enhanced performance of the new curing lamps. Indeed, it is important to underline the great impact that nanotechnology has produced in terms of development and progressing of dental materials science. Therefore, the present study can be considered relevant since there are no previous reports evaluating all the five bulk fill resin composites, using vibrational techniques, such as Raman spectroscopy, and also because this is the first time in which the performance of two new generation curing lamps have been analyzed.

CONCLUSIONS

In the light of the presented results, the two null hypotheses can be rejected: firstly, because there are differences in DC and VMH within the tested bulk fill composites, and no correlation can be drawn between DC and VMH; secondly, because the behavior of the two curing units is slightly different. Within the limits of the current study, it can be concluded that the five resin composites recorded satisfactory polymerization degree on both top and bottom sides.

To summarize, the flowable SDR shows high DC-values with both lamps, while, among high viscosity samples, SonicFill systems (and especially SonicFill2), combining the advantages of a flowable dental material with a universal resin composite, by using sonic activation, demonstrate excellent DC-values. In particular, SonicFill2 showed the highest DC-value using both curing lamps (at t0, on top), and an acceptable DC, even in case of 5 mm-thick samples.

Significant differences in VMH-values among the five tested materials are found: the lowest value has been evidenced by the flowable SDR, reinforcing the need of a top capping layer, while, in agreement with the literature, an appreciable increase has been found for the dual curing Fill Up!. Among the high viscosity resin composites, a satisfactory performance has been demonstrated by SonicFill and, mainly, by SonicFill2. Both DC and VMH determinations appear clinically significant to make a prevision of the future performances of restorations. The use of medium and, mainly, high viscosity bulk fill materials may also be important to avoid a further capping application. Moreover, this study can be useful to increase the knowledge of clinicians in understanding the curing performance of the tested lamps.

Our upcoming aim will be to increase the number of the tested dental composites, as well as to further study by means of vibrational techniques both dental and composites surfaces after finishing and polishing.

AUTHOR CONTRIBUTIONS

RM contributed to the research protocol, performed the experiments as part of his Ph.D. project, contributed to

the results analyses and writing. GO contributed to the idea, the research protocol, and the writing of the present manuscript. GT contributed to the correct developing of the research idea, the writing, the technical background of the entire manuscript. CC contributed to the technical idea and support all experimental phases. VL contributed to the Raman facilities use and data interpretation, and to the discussion finalization. MP contributed to the idea and the updated results organization of the manuscript. AP contributed to the idea, the findings interpretation, and the editing of the manuscript.

FUNDING

Dental materials were gently donated from the manufacturers.

ACKNOWLEDGMENTS

This work was supported by institutional funds from the Polytechnic University of Marche (GO, MP and AP). We would like to thank Prof. Luigi Ferrante for statistical advices. The authors are grateful also to Dr. Alberto Catellani and Dr. Gloria Altarocca for the precious experimental support.

REFERENCES

Abbas, G., Fleming, G. J., Harrington, E., Shortall, A. C., and Burke, F. J. (2003). Cuspal movement and microleakage in premolar teeth restored with a packable composite cured in bulk or in increments. *J. Dent.* 31, 437–444. doi: 10.1016/S0300-5712(02)00121-5

Ahmad, I. (2013). Deep resins, white fillings: a new technique for composite restorations. *Cosmet. Den.* 1, 12–18.

Alonso, A. C. B., De Souza-junior, E. J. C., Dressano, D., Araujo, G. A. S., Badriguez, J. M. C., and Hipolito, V. D. (2013). Effect of photointiator concentration on marginal and internal adaptation of experimental composite blends photo cured by modulated methods. *Eur. J. Dent.* 7, 1–8. doi: 10.4103/1305-7456.119056

Barabanti, N., Preti, A., Vano, M., Derchi, G., Mangani, F., and Cerutti, A. (2015). Indirect composite restorations luted with two different procedures: a ten years follow up clinical trial. *J. Clin. Exp. Dent.* 7, 54–59. doi: 10.4317/jced.51640

Beun, S., Glorieux, T., Devaux, J., Vreven, J., and Leloup, G. (2007). Characterization of nanofilled compared to universal and microfilled composites. *Dent. Mater.* 23, 51–59. doi: 10.1016/j.dental.2005.12.003

Blackham, J. T., Vandewalle, K. S., and Lien, W. (2009). Properties of hybrid resin composite systems containing prepolymerized filler particles. *Oper. Dent.* 34, 697–702. doi: 10.2341/08-118-L

Bouschlicher, M. R., Rueggeberg, F. A., and Wilson, B. M. (2004). Correlation of bottom-to-top surface microhardness and conversion ratios for a variety of resin composite compositions. *Oper. Dent.* 29, 698–704.

Campodonico, C., Tantbirojn, D., Olin, P., and Versluis, A. (2011). Cuspal deflection and depth of cure in resin-based composite restorations filled by using bulk, incremental and transtooth-illumination techniques. *J. Am. Dent. Assoc.* 152, 1176–1182. doi: 10.14219/jada.archive.2011.0087

Conti, C., Giorgini, E., Landi, L., Putignano, A., and Tosi, G. (2005). Spectroscopic and mechanical properties of dental resin composites cured with different light sources. *J. Mol. Struct.* 744, 641–646. doi: 10.1016/j.molstruc.2004.10.081

Czasch, P., and Ilie, N. (2013). *In vitro* comparison of mechanical properties and degree of cure of bulk fill composites. *Clin. Oral Investig.* 17, 227–235. doi: 10.1007/s00784-012-0702-8

Da Silva, E. M., Almeida, G. S., Poskus, L. T., and Guimarães, J. G. (2008a). Relationship between the degree of conversion, solubility and salivary sorption of a hybrid and nanofilled resin composite: influence of the light-activation mode. *J. Appl. Oral Sci.* 16, 161–166. doi: 10.1590/S1678-77572008000200015

Da Silva, E. M., Poskus, L. T., and Guimarães, J. G. (2008b). Influence of light-polymerization modes on the degree of conversion and mechanical properties of resin composites: a comparative analysis between a hybrid and a nanofilled composite. *Oper. Dent.* 33, 287–293. doi: 10.2341/07-81

David, J. R., Gomes, O. M., Gomes, J. C., Loguercio, A. D., and Reis, A. (2007). Effect of exposure time on curing efficiency of polymerizing unit equipped with light-emitting diodes. *J. Oral Sci.* 49, 19–24. doi: 10.2334/josnusd.49.19

De Wald, J. P., and Ferracane, J. L. (1987). A comparison of four modes of evaluating depth of cure of light-activated composites. *J. Dent. Res.* 66, 727–730. doi: 10.1177/00220345870660030401

Dickens, S. H., Stansbury, J. W., Choi, K. M., and Floyd, C. J. E. (2003). Photopolymerization kinetics of methacrylate dental resins. *Macromolecules* 36, 6043–6053. doi: 10.1021/ma021675k

El-Saftya, S., Silikas, N., and Watts, D. C. (2012). Creep deformation of restorative resin-composites intended for bulk-fill placement. *Dent. Mater.* 28, 928–935. doi: 10.1016/j.dental.2012.04.038

Ferracane, J. L. (1985). Correlation between hardness and degree of conversion during the setting reaction of unfilled dental restorative resins. *Dent. Mater.* 1, 11–14. doi: 10.1016/S0109-5641(85)80058-0

Ferracane, J. L. (1995). Current trends in dental composites. *Crit. Rev. Oral Biol. Med.* 6, 302–318. doi: 10.1177/10454411950060040301

Ferracane, J. L., Alex, G., and Margeas, R. (2014). Question: are bulk-fill composites a good idea? *Inside Dent.* 10, 42–44.

Fleming, G. J. P., Awan, M., Cooper, P. R., and Sloan, A. J. (2008). The potential of a resin-composite to be cured to a 4 mm depth. *Dent. Mater.* 24, 522–529. doi: 10.1016/j.dental.2007.05.016

Flury, S., Hayoz, S., Peutzfeldt, A., Hüsler, J., and Lussi, A. (2012). Depth of cure of resin composites: is the ISO 4049 method suitable for bulk fill materials? *Dent. Mater.* 28, 521–528. doi: 10.1016/j.dental.2012.02.002

Galvao, M. R., Caldas, S. G., Bagnato, V. S., de Souza Rastelli, A. N., and de Andrade, M. F. (2013). Evaluation of degree of conversion and hardness of dental composites photoactivated with different light guide tips. *Eur. J. Dent.* 7, 86–93.

Goracci, C., Cadenaro, M., Fontanive, L., Giangrosso, G., Juloski, J., Vichi, A., et al. (2014). Polymerization efficiency and flexural strength of low-stress restorative composites. *Dent. Mater.* 30, 688–694. doi: 10.1016/j.dental.2014.03.006

Guimaraes, T., Gushiken, N. O., and Braga, R. R. (2013). Degree of conversion, flexural modulus and polymerization stress of "Bulk Fill" composites. *Dent. Mater.* 29:43. doi: 10.1016/j.dental.2013.08.089

Ilie, N., and Hickel, R. (2011). Investigations on a methacrylate-based flowable composite based on the SDRTM technology. *Dent. Mater.* 27, 348–355. doi: 10.1016/j.dental.2010.11.014

Ilie, N., Jelen, E., Clementino-Luedemann, T., and Hickel, R. (2007). Low-shrinkage composite for dental application. *Dent. Mater. J.* 26, 149–155. doi: 10.4012/dmj.26.149

Ilie, N., Kebler, A., and Duner, J. (2013). Influence of various irradiation processes on the mechanical properties and polymerization kinetics of bulk-fill resin based composites. *J. Dent.* 41, 695–702. doi: 10.1016/j.jdent.2013.05.008

Jung, M., Sehr, K., and Klimek, J. (2007). Surface texture of four nanofilled and one hybrid composite after finishing. *Oper. Dent.* 32, 45–52. doi: 10.2341/06-9

Kusgoz, A., Ülker, M., Yesilyurt, C., Yoldas, O. H., Ozil, M., and Tanriver, M. (2011). Silorane-based composite: depth of cure, surface hardness, degree of conversion and cervical microleakage in class II cavities. *J. Esthet. Restor. Dent.* 23, 324–335. doi: 10.1111/j.1708-8240.2011.00411.x

Leloup, G., Holvoet, P. E., Bebelman, S., and Devaux, J. (2002). Raman Scattering Determination of the depth of cure of light activated composites. *J. Oral Rehabil.* 29, 510–515. doi: 10.1046/j.1365-2842.2002.00889.x

Leprince, J. G., Leveque, P., Nysten, B., Gallez, B., Devaux, J., and Leloup, G. (2012). New insight into the "depth of cure" of dimethacrylate-based dental composites. *Dent. Mater.* 28, 512–520. doi: 10.1016/j.dental.2011.12.004

Leprince, J. G., Palin, W. M., Vanacker, J., Sabbsgh, J., Devaux, J., and Leloup, G. (2014). Physico-mechanical characteristics of commercially available bulk-fill composites. *J. Dent.* 42, 993–1000. doi: 10.1016/j.jdent.2014.05.009

Marovic, D., Tauböck, T. T., Attin, T., Panduric, V., and Tarle, Z. (2015). Monomer conversion and shrinkage force kinetics of low-viscosity bulk-fill resin composites. *Acta Odontol. Scand.* 73, 474–480. doi: 10.3109/00016357.2014.992810

Miyazaki, M., Onose, H., Iida, N., and Kazama, H. (2003). Determination of residual double bonds in resin–dentin interface by Raman spectroscopy. *Dent. Mater.* 19, 245–251. doi: 10.1016/S0109-5641(02)00039-8

Nagi, S. M., Moharam, L. M., and Zaazou, M. H. (2015). Effect of resin thickness and curing time on the micro-hardness of bulk-fill resin composites. *J. Clin. Exp. Dent.* 7, 600–604. doi: 10.4317/jced.52536

Rahiotis, C., Kakaboura, A., Loukidis, M., and Vougiouklakis, G. (2004). Curing efficiency of various types of light-curing units. *Eur. J. Oral Sci.* 12, 89–94. doi: 10.1111/j.0909-8836.2004.00092.x

Roberts, H. W., Berzins, D. W., and Charlton, D. G. (2009). Hardness of three resin-modified glass ionomer restorative materials as a function of depth and a function of depth and time. *J. Esthet. Restor. Dent.* 21, 262–274. doi: 10.1111/j.1708-8240.2009.00273.x

Santos, G. P., Medeiros, I. S., Fellows, C. E., Muench, A., and Braga, R. R. (2007). Composite depth of cure obtained with QTH and LED units assessed by microhardness and micro-Raman Spectroscopy. *Oper. Dent.* 31, 79–83. doi: 10.2341/06-26

Sarrett, D. C. (2005). Clinical challenges and the relevance of materials testing for posterior composite restorations. *Dent. Mater.* 21, 9–20. doi: 10.1016/j.dental.2004.10.001

Soares, L. E., Liporoni, P. C., and Martin, A. A. (2007). The effect of soft-start polymerization by second generation LEDs on the degree of conversion of resin composite. *Oper. Dent.* 32, 160–165. doi: 10.2341/06-45

Tantbirojn, D., Pfeifer, C. S., Braga, R. R., and Versluis, A. (2011). Do low-shrink composites reduce polymerization shrinkage effects? *J. Dent. Res.* 90, 596–601. doi: 10.1177/0022034510396217

Tarle, Z., Attin, T., Marovic, D., Andermatt, L., Ristic, M., and Tauböck, T. T. (2015). Influence of irradiation time on subsurface degree of conversion and microhardness of high-viscosity bulk-fill resin composites. *Clin. Oral Investig.* 19, 831–840. doi: 10.1007/s00784-014-1302-6

Turssi, C. P., Ferracane, J. L., and Vogel, K. (2005). Filler features and their effects on wear and degree of conversion of particulate dental resin composites. *Biomaterials* 26, 4932–4937. doi: 10.1016/j.biomaterials.2005.01.026

Van Dijken, J. W., and Pallesen, U. (2014). A randomized controlled three year evaluation of 'bulk-filled' posterior resin restorations based on stress decreasing resin technology. *Dent. Mater.* 30, 245–251. doi: 10.1016/j.dental.2014.05.028

Van Ende, A., De Munck, J., Van Landuyt, K. L., Poitevin, A., Peumans, M., and Van Meerbeek, B. (2013). Bulk-filling of high C-factor posterior cavities: effect on adhesion to cavity-bottom dentin. *Dent. Mater.* 29, 269–277. doi: 10.1016/j.dental.2012.11.002

Van Ende, A., Mine, A., De Munck, J., Poitevin, A., and Van Meerbeek, B. (2012). Bonding of low-shrinking composites in high C-factor cavities. *J. Dent.* 40, 295–303. doi: 10.1016/j.jdent.2012.01.004

Yap, A. U., Soh, M. S., Han, T. T., and Siow, K. S. (2004). Influence of curing lights and modes on cross-link density of dental composites. *Oper. Dent.* 29, 410–415.

Yoon, T. H., Lee, Y. K., Lim, B. S., and Kim, C. W. (2002). Degree of polymerization of resin composite by different light sources. *J. Oral Rehabil.* 29, 1165–1173. doi: 10.1046/j.1365-2842.2002.00970.x

Conflict of Interest Statement: The authors declare that the research was conducted in the absence of any commercial or financial relationships that could be construed as a potential conflict of interest.

The reviewer ED and handling Editor declared their shared affiliation, and the handling Editor states that the process nevertheless met the standards of a fair and objective review.

frontiers in Physiology

MINI REVIEW
published: 29 September 2017
doi: 10.3389/fphys.2017.00769

Synchrotron Phase Tomography: An Emerging Imaging Method for Microvessel Detection in Engineered Bone of Craniofacial Districts

Alessandra Giuliani[1], Serena Mazzoni[1], Luigi Mele[2], Davide Liccardo[2], Giuliana Tromba[3] and Max Langer[4]*

[1] Sezione di Biochimica, Biologia e Fisica Applicata, Dipartimento di Scienze Cliniche Specialistiche e Odontostomatologiche, Università Politecnica delle Marche, Ancona, Italy, [2] Sezione di Biotecnologie, Istologia Medica e Biologia Molecolare, Dipartimento di Medicina Sperimentale, Università degli Studi della Campania "L. Vanvitelli", Naples, Italy, [3] Elettra Sincrotrone Trieste S.C.p.A, Trieste, Italy, [4] Centre de Recherche en Acquisition et Traitment d'Images pour la Santé (CREATIS), Centre National de la Recherche Scientifique (CNRS) UMR 5220, Institut national de la santé et de la recherche médicale (Inserm) U1206, Université de Lyon, INSA-Lyon, Villeurbanne, France

The engineering of large 3D constructs, such as certain craniofacial bone districts, is nowadays a critical challenge. Indeed, the amount of oxygen needed for cell survival is able to reach a maximum diffusion distance of ∼150–200 μm from the original vascularization vector, often hampering the long-term survival of the regenerated tissues. Thus, the rapid growth of new blood vessels, delivering oxygen and nutrients also to the inner cells of the bone grafts, is mandatory for their long-term function in clinical practice. Unfortunately, significant progress in this direction is currently hindered by a lack of methods with which to visualize these processes in 3D and reliably quantify them. In this regard, a challenging method for simultaneous 3D imaging and analysis of microvascularization and bone microstructure has emerged in recent years: it is based on the use of synchrotron phase tomography. This technique is able to simultaneously identify multiple tissue features in a craniofacial bone site (e.g., the microvascular and the calcified tissue structure). Moreover, it overcomes the intrinsic limitations of both histology, achieving only a 2D characterization, and conventional tomographic approaches, poorly resolving the vascularization net in the case of an incomplete filling of the newly formed microvessels by contrast agents. Indeed, phase tomography, being based on phase differences among the scattered X-ray waves, is capable of discriminating tissues with similar absorption coefficients (like vessels and woven bone) in defined experimental conditions. The approach reviewed here is based on the most recent experiences applied to bone regeneration in the craniofacial region.

Keywords: phase tomography, synchrotron radiation, microvessels, craniofacial bone engineering, X-ray phase-contrast imaging

OPEN ACCESS

Edited by:
Thimios Mitsiadis, University of Zurich, Switzerland

Reviewed by:
César Nombela Arrieta, University of Zurich, Switzerland
Jean-Christophe Farges, Claude Bernard University Lyon 1, France

****Correspondence:***
Alessandra Giuliani
a.giuliani@univpm.it

Specialty section:
This article was submitted to Craniofacial Biology and Dental Research, a section of the journal Frontiers in Physiology

Received: *27 June 2017*
Accepted: *20 September 2017*
Published: *29 September 2017*

Citation:
Giuliani A, Mazzoni S, Mele L, Liccardo D, Tromba G and Langer M (2017) Synchrotron Phase Tomography: An Emerging Imaging Method for Microvessel Detection in Engineered Bone of Craniofacial Districts. Front. Physiol. 8:769. doi: 10.3389/fphys.2017.00769

INTRODUCTION

Nowadays, craniofacial bone defects due to congenital conditions, disease, and injury cause major clinical issues, often solved with tissue replacement by autologous grafting. However, sometimes this procedure is hampered by an extensive donor site morbidity. In these cases, bone engineering protocols could support restoration of the function, or replace damaged or diseased tissues (Alsberg et al., 2001).

Since the long-term function of three-dimensional (3D) bone substitute biomaterials (BSB) is strongly dependent on adequate vascularization after grafting, research in craniofacial bone engineering has recently focused on approaches involving angiogenesis (Auger et al., 2013). These include the delivery of different growth factors to the defect site (Yoo and Kwon, 2013) or the engineering of microvascular networks by using endothelial cells and stem cells (Liu et al., 2013). Nevertheless, current vascularization methods are often not sufficiently rapid for an adequate cellular oxygen supply. Therefore, it is necessary to create microvascular networks within 3D tissue constructs *in vitro* before grafting (Laschke et al., 2006).

However, full comprehension of the bone vascularization pathways is still hampered by limitations in the use of imaging techniques to monitor these processes *in-vivo*. Nowadays, new and interesting imaging modes are available. Upputuri et al. (2015) recently classified the vascular imaging approaches into three groups: non-optical techniques (X-ray, magnetic resonance, ultrasound, and positron emission imaging), optical techniques (optical coherence, fluorescence, multiphoton, and laser speckle imaging), and hybrid techniques (photoacoustic imaging). Physical origin of the contrast, levels of resolution achieved, imaging depth and structures resolved (microvessels, bone, etc.) have been described and summarized for each group.

Inside the non-optical group, great interest is focused on X-ray imaging methods. They are based on X-ray attenuation of the different tissues and have been successfully used over the past few years to visualize large blood vessels.

In this regard, high resolution tomography (microCT) (Arkudas et al., 2010; Barbetta et al., 2012) is able to provide much higher resolution ($\sim$1 μm) imaging, than ultrasound ($\sim$30 μm) and MRI ($\sim$100 μm), allowing the visualization and quantification of microvasculature. This procedure is normally achieved with the use of contrast agents, which are radio opaque and radio dense fillers. It was recently proved by this approach that the 10 μm medium resolution microCT is able to image with success medium and large blood vessels (Nebuloni et al., 2014). Moreover, Langer et al. (Langer et al., 2011) successfully imaged the microvasculature with contrast agent in rat and mouse bone. While they proved that parts of the connectivity were not preserved (due to partial volume effect), a very large part of the contrast agent volume was retrieved.

Also, in recent years, a new method for combined 3D imaging and analysis of microvascularization and bone microstructure has emerged. It is based on the use of synchrotron phase microtomography (PhC-microCT) and it allows, as opposed to conventional 2D techniques like histology, to simultaneously identify in 3D multiple tissue features without using contrast agents. This is due to the increased sensitivity of phase sensitive X-ray imaging techniques. Indeed, due to increased sensitivity, this technique also overcomes the intrinsic limitations of conventional tomographic approaches, often unable to reliably reconstruct the full vascularization network in case of incomplete filling of microvessels by contrast agents (Fei et al., 2010).

In this mini-review, we briefly discuss the very recent advances in synchrotron phase tomography aiming at high-resolution imaging of engineered bone vasculature in craniofacial districts.

APPROACHING SYNCHROTRON PHASE TOMOGRAPHY METHODS

Differently from the conventional (attenuation-based) microCT in which the contrast is due to attenuation differences within the sample, in PhC-microCT the contrast originates from the phase shift of the X-ray beam passing through the matter (Snigirev et al., 1995; Bravin et al., 2013). This phase shift in non-mineralized biological tissues can be up to three orders of magnitude larger than attenuation (Momose et al., 1996; Lewis et al., 2003), explaining the highly increased contrast that has been observed with PhC-microCT imaging in investigating esophagus (Lewis et al., 2003), brain (Connor et al., 2009; Pinzer et al., 2012; Marinescu et al., 2013), liver (Lewis et al., 2003; Herzen et al., 2014), kidney (Velroyen et al., 2014), lung (Lewis et al., 2003), cartilage (Coan et al., 2010; Marenzana et al., 2012; Horng et al., 2014) and breast tissues (Arfelli et al., 2000; Stampanoni et al., 2011).

At least three methods have been studied for phase contrast X-ray imaging: X-ray grating interferometry (Momose, 1995, 2003; Momose et al., 1996), diffraction enhanced imaging (Davis et al., 1995; Ingal and Beliaevskaya, 1995; Chapman et al., 1997, 1998) and propagation-based imaging (Snigirev et al., 1995; Wilkins et al., 1996; Cloetens et al., 1999).

The first two methods are often confined to synchrotron sources because they require a monochromatic and highly collimated x-ray beam. Indeed, when coherence grating is used at conventional x-ray sources, a detrimental flux reduction is experienced. In turn, this flux reduction would require longer exposure times than at synchrotrons, hampering, as a consequence, the translation of the method to clinical settings (Nesch et al., 2009).

Very recently, grating-based (GB) Talbot interferometry (Weitkamp et al., 2005; Momose et al., 2009) was successfully applied, combined to conventional polychromatic x-ray sources. A third grating (Pfeiffer et al., 2007) was used to study weakly absorbing samples and, using synchrotron facilities, to excellently discriminate soft-tissues in cancerous human liver tissue (Noel et al., 2013) and in atherosclerotic plaques (Hetterich et al., 2013). Other studies performed with polychromatic x-ray sources allowed to achieve an improved imaging of parenchymal lung disease (Yaroshenko et al., 2013), breast lesions (Hauser et al., 2013; Sztrokay et al., 2013), cartilage (Tanaka et al., 2013), atherosclerotic plaques (Saam et al., 2013), and renal ischemia (Velroyen et al., 2014).

Unlike X-ray interferometry, the diffraction enhanced imaging method exploits the benefits of a μrad angular resolution achieved by filtering X-rays deflected by refraction. This is made possible using an analyzer crystal after the sample to select refracted X-rays from the sample.

Instead, the propagation-based method generates contrast by Fresnel or Fraunhofer diffraction: the first is achieved by placing the detector and the sample at a moderate distance.

In practice, at lower resolutions, the X-ray interferometric imaging is thus the preferential approach for revealing soft structures, being able to also sense the shallower phase gradients,

compared to the diffraction enhanced and propagation-based imaging methods. This is due to the principles of contrast generation; stronger contrast is generated at structural boundaries where the variations of refractive index are larger due to rapid phase gradients (Momose, 2003).

On the other hand, the propagation-based imaging method is of great advantage in high-resolution imaging because no optical components are needed when a coherent X-ray source is available, like at synchrotron facilities. The chance to get high resolutions has made propagation-based imaging the technique of choice in the study of both human bone ultrastructure and vasculature, with focused pre-clinical and clinical studies on vessels of medium and small thickness.

Concerning the investigation of human bone ultrastructure, X-ray phase nano-tomography, based on the propagation method, was recently shown to provide the appropriate spatial resolution and sensitivity to efficiently visualize and quantify the 3D organization of the lacuno-canalicular pattern (Langer et al., 2012). The study was performed considering several cells in osteonal and interstitial tissue: nanoscale density variations revealed that the cement line separating these tissues is hypermineralized. Moreover, the organization of the collagen fibers was reconstructed in 3D, showing a twisted plywood structure.

Imaging brain microvasculature is crucial for plasticity studies of cerebrovascular diseases. Traditionally, in the brain, absorption-based microCT and microMRI methods are applied, using contrast agents for a better visualization of the vasculature.

Very recently, propagation-based synchrotron PhC-microCT was applied to visualize the whole mouse brain microvasculature. It was carried out at high resolution ($\sim$3.7 μm) and without contrast agents (Miao et al., 2016). Microvasculature changes in C57BL/6 mice brain ($n = 14$) after 14-day reperfusion from transient middle cerebral artery occlusion (tMCAO) were observed. PhC-microCT demonstrated that the branching radius ratio (post- to pre-injury) of small vessels (radius $< 7.4\,\mu$m) in the injury group was significantly smaller than in the sham group. This result revealed active angiogenesis in brain recovery after stroke.

In another recent study, Fratini et al. (2015) showed that PhC-microCT allows the simultaneous visualization of three-dimensional micro-vascular network and neuronal systems of *ex-vivo* mouse spinal cord. This experiment was carried out at scales spanning from millimeters to hundreds of nanometers, without contrast agents and destructive sample preparation. Images of both the 3D distribution of micro-capillary network and the micrometric nerve fibers, axon-bundles and neuron soma, were obtained, confirming the efficiency of this technique also in pre-clinical studies of neurodegenerative pathologies and spinal-cord-injuries.

ASSESSMENT OF BONE MICROVESSELS DETECTION BY PHASE TOMOGRAPHY

Conventional X-ray microCT is a technique that allows a good visualization of the structure of mineralized bone and biomaterials, but it fails when attempting to discern soft tissues at high resolutions. On the contrary, PhC-microCT, based on propagation-based settings, was demonstrated to present, at high resolution, a better soft tissue contrast than conventional CT, clearly discriminating ligamentous, muscular, neural, and vascular structures (Horng et al., 2014).

These findings led some authors to investigate the 3D vascularization of engineered-bone tissue. Detailed imaging and a quantitative description of the complete vascular network in such constructs is crucial for monitoring the relation between bone formation and vascularization and phase tomography was shown to efficiently discriminate tissues with similar absorption coefficients (Langer et al., 2009).

However, the previous study was still limited by the use of a contrast agent. Indeed, although a new phase-contrast medium—the micro-bubble—was recently successfully applied to angiography applications (Tang et al., 2011), different authors

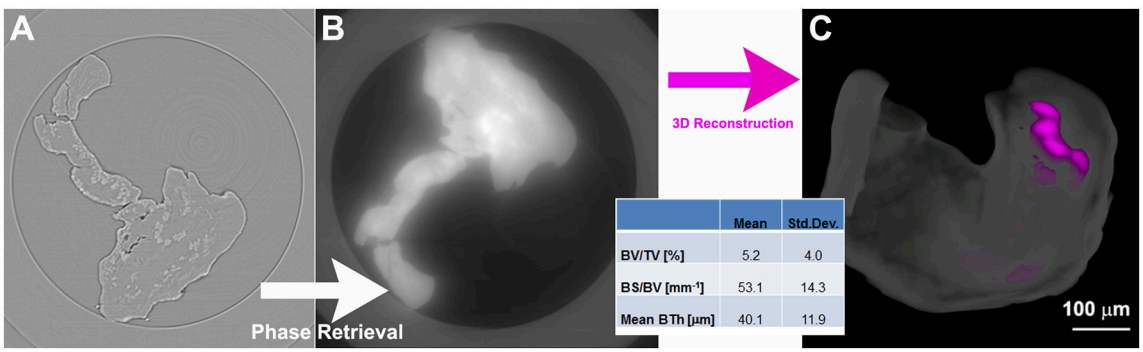

FIGURE 1 | Phase-contrast microCT analysis of woven bone (WB). **(A)** 2D slice before phase-retrieval processing: the edge-enhancement signal prevents a reliable discrimination and quantification of the two phases (WB and newly mineralized bone). **(B)** The same 2D slice as in **(A)** after phase-retrieval processing; and **(C)** 3D reconstruction of a WB sample after processing by phase retrieval: the woven structure is shown in translucent white, whereas the newly formed mineralized bone is depicted in magenta; (bottom inset) morphometric analysis of the mineralized bone. This figure was originally published in Paino et al. (2017; www.clinsci.org/content/early/2017/02/16/CS20170047).

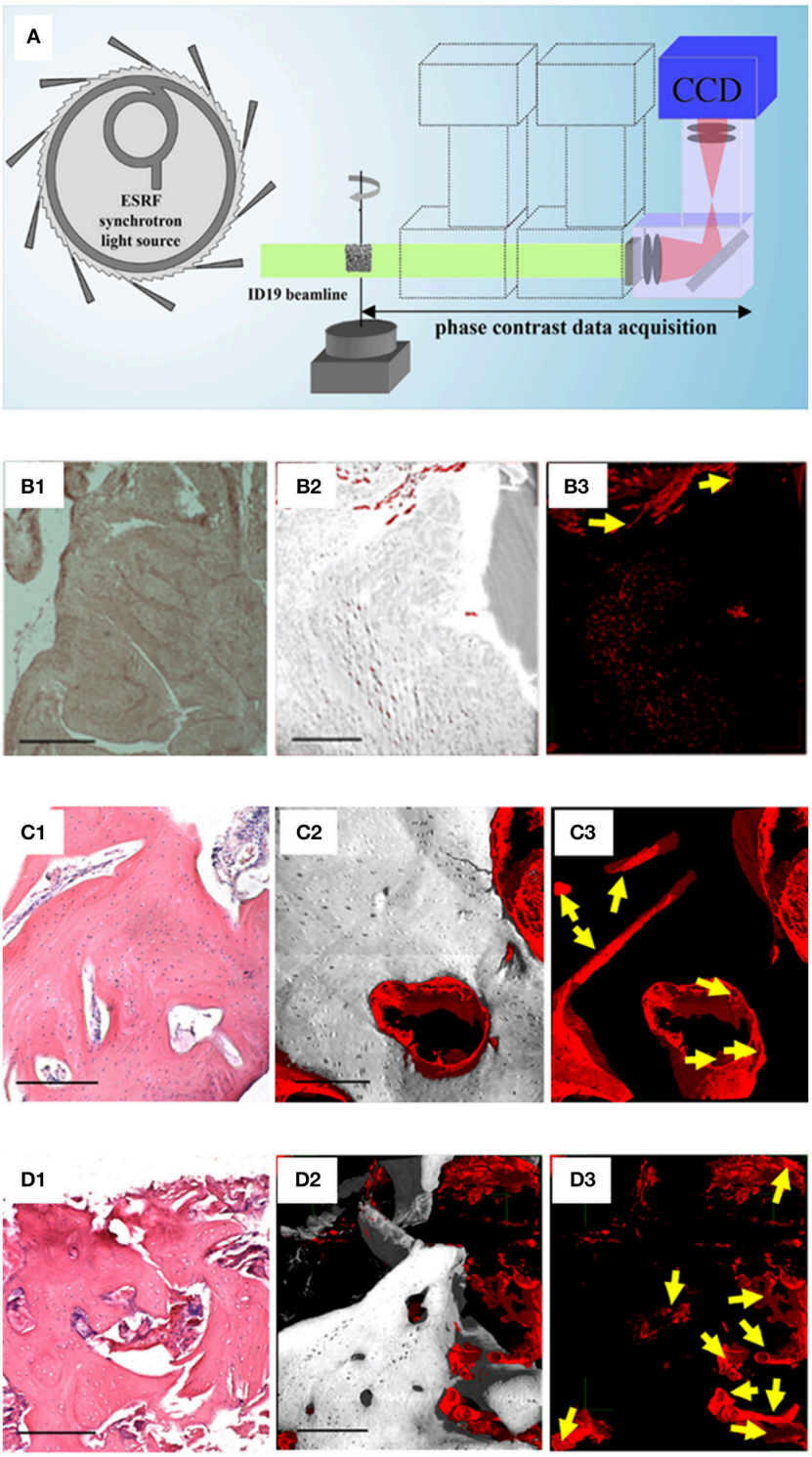

FIGURE 2 | Phase-contrast Holotomography (HT). **(A)** HT set-up at the ID19 beamline of the European Synchrotron Radiation Facility. Histological and HT analysis of the WB **(B)**, of a human *in vivo* stem cell-treated mandible **(C)**, and of a human mandible control **(D)**. For each group **(B–D)**, the panels on the left (1) represent histological sections with H&E staining, as reference; the central (2), and the right (3) panels are subvolumes of the 3D HT reconstructions where, to improve visualization, all phases were virtually deleted except for bone and vessels (2), or exclusively except for vessels (3). Yellow arrows indicate portions of vessels to discriminate them from possible artifacts. Scale bars = 250 μm. Panel **(A)** was originally published in Giuliani (2016; https://doi.org/10.1016/B978-0-08-100287-2.00012-4); Panels of the group-B were originally published in Paino et al. (2017; www.clinsci.org/content/early/2017/02/16/CS20170047); Panels of the group-C and of the group-D were originally published in Giuliani et al. (2013; http://onlinelibrary.wiley.com/doi/10.5966/sctm.2012-0136/epdf).

TABLE 1 | Summary of high resolution tomography (microCT) imaging modalities for vascular imaging in tissue engineering. Image resolution up to 600 nm (in propagation-based settings).

	Modality	Anatomical structures resolved	Advantages/disadvantages
Attenuation based	Without contrast agents	Mineralized tissues (bone, enamel, dentin, etc.)	Good 3D imaging of the mineralized structures/non-mineralized tissues not discriminated*
	With contrast agents	Blood vessels, cells/stem cells	Successful imaging of medium and large blood vessels/part of connectivity lost (no detection of small vessels)**
Phase-contrast based	Grating interferometry	Cancerous human liver tissue, atherosclerotic plaques, parenchymal lung, breast lesions, cartilage and renal ischemia§	Contrast-agent-free method, excellent for weakly absorbing samples imaging§/detrimental flux reduction and longer exposure times§§
	Diffraction enhanced	Breast tissues, cartilage, brain#	Contrast-agent-free method, μrad angular resolution/confined to synchrotron sources, not effective in sensing shallow phase gradients##
	Propagation-based (single distance)	First phases of bone mineralization, blood vessels, ligamentous and muscular structures nerve fibers, axon-bundles and neuron soma+	Contrast-agent-free method, high-resolution imaging/confined to synchrotron sources, not effective in sensing shallow phase gradients##
	Propagation-based (multiple distance)	Bone ultrastructure, small blood vessels++	Contrast-agent-free method, very high-resolution imaging, successful imaging of small blood vessels/confined to synchrotron sources##

* *Arkudas et al., 2010; Barbetta et al., 2012.*
***Fei et al., 2010; Langer et al., 2011; Nebuloni et al., 2014.*
§*Hauser et al., 2013; Hetterich et al., 2013; Noel et al., 2013; Saam et al., 2013; Sztrokay et al., 2013; Tanaka et al., 2013; Yaroshenko et al., 2013; Velroyen et al., 2014.*
§§*Nesch et al., 2009.*
#*Chapman et al., 1998; Connor et al., 2009; Coan et al., 2010.*
##*Momose, 2003.*
+*Horng et al., 2014; Bukreeva et al., 2015; Fratini et al., 2015; Manescu et al., 2016; Miao et al., 2016; Mazzoni et al., 2017.*
++*Langer et al., 2012; Giuliani et al., 2013; Paino et al., 2017.*

agree that PhC-microCT is able to perform a 3D visualization of the smallest capillaries (Momose et al., 2000; Fratini et al., 2015) in mice, without the use of any contrast agent.

This fact was confirmed in another recent study (Bukreeva et al., 2015), where synchrotron PhC-microCT was applied to visualize and analyze the 3D micro-vascular networks in bone-engineered constructs, made of porous ceramic scaffolds loaded with bone marrow stromal cells (BMSC), in an ectopic bone formation mouse-model. Samples seeded and not seeded with BMSC were compared, with or without the use of contrast agents. The authors achieved the 3D distribution of both vessels and collagen matrix and obtained quantitative information for the different samples, even for those not stained.

Experience in Craniofacial Districts

Nowadays, autologous bone is still considered the ideal grafting material in the craniofacial district (Yamanichi et al., 2008; Iezzi et al., 2017). Autologous grafts are vascularized and contain viable osteoblasts, organic and inorganic matrices, and growth factors that allow remodeling and structural integration with the host site. However, there are significant limitations associated with the use of autologous grafts, including the availability of donor tissue (since it has to be obtained intraorally), the need of additional surgical procedures and, consequently, increased operating times and costs (Tsigkou et al., 2010; Iezzi et al., 2017). When directly using synthetic and allogeneic grafts, only the periphery of the graft is efficiently vascularized. As a consequence, a central zone of necrosis frequently occurs, resulting in a shell of ossification at the surface, but with low level penetration, due to the limited transport of oxygen and metabolic requirements to the inner cell mass (Tsigkou et al., 2010). Thus, a rapid vascularization of bone grafts is a clinical challenge, based on the fact that the development of a mature and functional vasculature not only depends on migration and proliferation of endothelial cells but also requires cooperation and symbiosis between them and perivascular cells, acting as a potent stabilizer of the engineered blood vessels formed in the porous bone scaffold (Tsigkou et al., 2010).

Therefore a major task is to find advanced imaging techniques that could verify and quantify the mineralization process and neovascularization of grafts, at the early stages of bone formation (Paino et al., 2017). Third-generation synchrotron facilities produce brilliant X-ray photon beams, having high spatial coherence properties. They have been demonstrated to be suitable for several tissue engineering studies, detecting *in-vitro* the newly formed extracellular matrix (Albertini et al., 2009), the early colonies of endothelial cells (Giuliani et al., 2014), and the early phases of bone mineralization (Manescu et al., 2016;

Mazzoni et al., 2017), by introducing X-ray imaging methods based on phase-contrast.

Very recently, some authors (Paino et al., 2017) showed that human dental pulp stem cells (hDPSCs) can lead to a bone tissue ready to be grafted for clinical application. They demonstrated that hDPSCs proliferate *in-vitro*, differentiate into osteoblasts and express genes associated with angiogenesis factors, such as VEGF and PDGFA. Synchrotron-based X-ray phase-contrast imaging proved that, after 40 days of culture in standard medium, hDPSCs formed woven bone (WB), i.e., fibrous bone with a low level of mineralization. In particular, the PhC-microCT analysis was performed using a polychromatic beam, with a sample-to-detector distance of 150 mm, corresponding to a single-distance phase-contrast set-up. The osteogenic potential of WB fabricated after *in vitro* hDPSC culture was validated by the quantitative data extracted from the 3D PhC-microCT analysis (**Figure 1**). However, it was not possible to detect any vascularization using this technique.

In this regard, the holotomography (HT) technique added fundamental information (Paino et al., 2017). The HT approach differs from the PhC-microCT method based on a single distance in that the acquisition consists of tomographic scans at four different propagation distances, followed by a different reconstruction algorithm (**Figure 2A**). The HT analysis allowed to achieve a 3D reconstruction of the WB (**Figures 2B1,B2**), assessing the presence of new vessels (**Figure 2B3**). Indeed, because of their low attenuation coefficient, these new vessels are transparent in conventional attenuation-based tomographic reconstructions and the PhC-microCT method based on a single distance was still found to be not sufficiently sensitive. Indeed, this HT evidence confirmed deductions derived from the fact that hDPSCs strongly expressed high levels of VEGF and PDGF-A, which explains the vessel formation in the WB. This last finding is of paramount interest for physiology of the bone in craniofacial districts, because it satisfies the need of neoangiogenesis in the engineered site. Thus, these results strongly support the rationale that hDPSCs possess significant differentiation capabilities toward osteoangiogenesis, matching the gold standard for obtaining well-vascularized bone (Paino et al., 2017).

Moreover, some studies (d'Aquino et al., 2009) demonstrated that hDPSCs differentiate into osteoblasts and, when seeded on collagen I scaffolds, efficiently contribute to repair human mandible defects. In this context, another study (Giuliani et al., 2013) showed, by synchrotron HT, the stability and quality of both the regenerated bone and the vessel network 3 years after grafting. It was found that the regenerated tissue in grafted sites was unexpectedly constituted by compact bone, structurally different and denser compared to the healthy native alveolar bone of the same patient. However, in both the human mandible control and the human *in vivo* SC-treated mandible biopsies analyzed, in agreement with histological analyses, after 3 years the regenerated bone was well structured and vascularized. Two subvolumes of the human *in vivo* SC-treated mandible are shown in **Figures 2C1,C2**: one, referring to a representative histological slice, was used as a reference (**Figure 2C1**); the other, referring to the 3D reconstruction of the HT scan and the subsequent data analysis (**Figures 2C2,C3**). The unmineralized phases, with the exception of the one representing vessels, were virtually suppressed for a better visualization of bone (gray) and its vascularization (red). As confirmed histologically (**Figure 2C1**) these 3D reconstructions demonstrate that after 3 years bone tissue was well structured and vascularized. In particular, in **Figure 2C3**, only densities compatible with the vessel phase have been visualized, clearly showing a good vascularization. The same information is represented in **Figures 2D1–D3** for human mandible control. It is clearly shown that the bone is a well-structured cancellous structure (**Figures 2D1,D2**), with an homogeneous and fully organized vessel network (**Figure 2D3**): although here the vascularization is more structured than in the human *in vivo* SC-treated mandible, density signals compatible with neo-vessels were found in several areas of the biopsy retrieved from the treated site, confirming *in-vivo* that the hDPSCs have significant differentiation capabilities toward osteoangiogenesis (Giuliani et al., 2013).

CONCLUSIONS

While PhC-microCT was demonstrated to be capable of visualizing the 3D vessel network in *in-vitro* and *ex-vivo* conditions and without any sample sectioning and preparation, the use of coherent and highly brilliant Synchrotron X-ray sources was mandatory in order to achieve a higher image quality with sub-micrometer spatial resolution. Indeed, as reported in the literature and summarized in **Table 1**, microvessel detection in engineered bone was carried out mainly in two ways: by attenuation-based microCT, with the use of contrast agents, or by propagation-based PhC-microCT, without any marker. However, the application of the last method has required, up to now, access to synchrotron facilities. This fact constitutes a relevant limitation for a possible future use of phase-contrast imaging in clinical practice, since the radiation dose would be too high. Therefore, we propose this approach as a fundamental tool for angiogenesis studies in preclinical research and bone post-extractive studies in craniofacial districts.

AUTHOR CONTRIBUTIONS

AG: Concept and design; revision of the whole literature; coordination of the work drafting; final version definition and approval. SM and GT: Design (phase-contrast tomography); data research in literature on PhC-microCT; work drafting; final version approval. LM and DL: Design (physiology concepts); data research in literature on physiological interpretation of data; work drafting; final version approval. ML: Concept and design; data research in literature on PhC-microCT; work drafting; final version definition and approval. All the authors agreed to be accountable for all aspects of the work in ensuring that questions related to the accuracy or integrity of any part of the work are appropriately investigated and resolved.

REFERENCES

Albertini, G., Giuliani, A., Komlev, V., Moroncini, F., Pugnaloni, A., Pennesi, G., et al. (2009). Organization of extracellular matrix fibers within polyglycolic acid-polylactic acid scaffolds analyzed using X-ray synchrotron-radiation phase-contrast micro computed tomography. *Tissue Eng. C Methods* 15, 403–411. doi: 10.1089/ten.tec.2008.0270

Alsberg, E., Hill, E. E., and Mooney, D. J. (2001). Craniofacial tissue engineering. *Crit. Rev. Oral Biol. Med.* 12, 64–75. doi: 10.1177/104544110101200 10501

Arfelli, F., Bonvicini, V., Bravin, A., Cantatore, G., Castelli, E., Palma, L. D., et al. (2000). Mammography with synchrotron radiation: phase-detection techniques. *Radiology* 215, 286–293. doi: 10.1148/radiology.215.1.r00ap10286

Arkudas, A. J., Beier, P., Pryymachuk, G., Hoereth, T., Bleiziffer, O., Polykandriotis, E., et al. (2010). Automatic quantitative micro-computed tomography evaluation of angiogenesis in an axially vascularized tissue-engineered bone construct. *Tissue Eng. C.* 16, 1503–1514. doi: 10.1089/ten.tec.2010.0016

Auger, F. A., Gibot, L., and Lacroix, D. (2013). The pivotal role of vascularization in tissue engineering. *Annu. Rev. Biomed. Eng.* 15, 177–200. doi: 10.1146/annurev-bioeng-071812-152428

Barbetta, A., Bedini, R., Pecci, R., and Dentini, M. (2012). Role of X-ray microtomography in tissue engineering. *Annali dell'Istituto Superiore di Sanità* 48, 10–18. doi: 10.4415/ANN_12_01_03

Bravin, A., Coan, P., and Suortti, P. (2013). X-ray phase-contrast imaging: from pre-clinical applications towards clinics. *Phys. Med. Biol.* 58, R1–R35. doi: 10.1088/0031-9155/58/1/R1

Bukreeva, I., Fratini, M., Campi, G., Pelliccia, D., Spanò, R., Tromba, G., et al. (2015). High-resolution X-ray techniques as new tool to investigate the 3D vascularization of engineered-bone tissue. *Front. Bioeng. Biotechnol.* 3:133. doi: 10.3389/fbioe.2015.00133

Chapman, D., Pisano, E., Thomlinson, W., Zhong, Z., Johnston, R. E., Washburn, D., et al. (1998). Medical applications of diffraction enhanced imaging. *Breast Dis.* 10, 197–207. doi: 10.3233/BD-1998-103-419

Chapman, D., Thomlinson, W., Johnston, R. E., Washburn, D., Pisano, E., Gmür, N., et al. (1997). Diffraction enhanced X-ray imaging. *Phys. Med. Biol.* 42, 2015–2025. doi: 10.1088/0031-9155/42/11/001

Cloetens, P., Luding, W., Baruchel, J., Van Dyck, D., Van Landuyt, J., Guigay, J. P., et al. (1999). Holotomography: quantitative phase tomography with micrometer resolution using hard synchrotron radiation x rays. *Appl. Phys. Lett.* 75:2912. doi: 10.1063/1.125225

Coan, P., Bamberg, F., Diemoz, P. C., Bravin, A., Timpert, K., Mützel, E., et al. (2010). Characterization of osteoarthritic and normal human patella cartilage by computed tomography X-ray phase-contrast imaging: a feasibility study. *Invest. Radiol.* 45, 437–444. doi: 10.1097/RLI.0b013e3181e193bd

Connor, D. M., Benveniste, H., Dilmanian, F. A., Kritzer, M. F., Miller, L. M., and Zhong, Z. (2009). Computed tomography of amyloid plaques in a mouse model of Alzheimer's disease using diffraction enhanced imaging. *Neuroimage* 46, 908–914. doi: 10.1016/j.neuroimage.2009.03.019

d'Aquino, R., De Rosa, A., Lanza, V., Tirino, V., Laino, L., Graziano, A., et al. (2009). Human mandible bone defect repair by the grafting of dental pulp stem/progenitor cells and collagen sponge biocomplexes. *Eur. Cell. Mater.* 18, 75–83. doi: 10.22203/eCM.v018a07

Davis, T. J., Gao, D., Gureyev, T. E., Stevenson, A. W., and Wilkins, S. W. (1995). Phase-contrast imaging of weakly absorbing materials using hard X-rays. *Nature* 373, 595–598. doi: 10.1038/373595a0

Fei, J., Peyrin, F., Malaval, L., Vico, L., and Lafage-Proust, M. H. (2010). Imaging and quantitative assessment of long bone vascularization in the adult rat using microcomputed tomography. *Anat. Rec.* 293, 215–224. doi: 10.1002/ar.21270

Fratini, M., Bukreeva, I., Campi, G., Brun, F., Tromba, G., Modregger, P., et al. (2015). Simultaneous submicrometric 3D imaging of the micro-vascular network and the neuronal system in a mouse spinal cord. *Sci. Rep.* 5:8514. doi: 10.1038/srep08514

Giuliani, A. (2016). "Analysis of bone response to dental bone grafts by advanced physical techniques," in *Bone Response to Dental Implant Materials*, ed A. Piattelli (Duxford: Elsevier Ltd.), 229–246.

Giuliani, A., Manescu, A., Langer, M., Rustichelli, F., Desiderio, V., Paino, F., et al. (2013). Three years after transplants in human mandibles, histological and in-line HT revealed that stem cells regenerated a compact rather than a spongy bone: biological and clinical implications. *Stem Cells Trans. Med.* 2, 316–324. doi: 10.5966/stemcells.2012-0136.

Giuliani, A., Moroncini, F., Mazzoni, S., Belicchi, M. L., Villa, C., Erratico, S., et al. (2014). Polyglycolic acid-polylactic acid scaffold response to different progenitor cell *in vitro* cultures: a demonstrative and comparative X-ray synchrotron radiation phase-contrast microtomography study. *Tissue Eng. Part C Methods* 20, 308–316. doi: 10.1089/ten.tec.2013.0213

Hauser, N., Wang, Z., Kubik-Huch, R. A., Trippel, M., Singer, G., Hohl, M. K., et al. (2013). A study on mastectomy samples to evaluate breast imaging quality and potential clinical relevance of differential phase contrast mammography. *Invest. Radiol.* 49, 131–137. doi: 10.1097/RLI.0000000000000001

Herzen, J., Willner, M. S., Fingerle, A. A., Noel, P. B., Koehler, T., Drecoll, E., et al. (2014). Imaging liver lesions using grating-based phase-contrast computed tomography with bi-lateral filter post-processing. *PLoS ONE* 9:e83369. doi: 10.1371/journal.pone.0083369

Hetterich, H., Fill, S., Herzen, J., Willner, M., Zanette, I., Weitkamp, T., et al. (2013). Grating-based X-ray phase-contrast tomography of atherosclerotic plaque at high photon energies. *Z. Med. Phys.* 23, 194–203. doi: 10.1016/j.zemedi.2012.12.001

Horng, A., Brun, E., Mittone, A., Gasilov, S., Weber, L., Geith, T., et al. (2014). Cartilage and soft tissue imaging using x-rays: propagation-based phase contrast computed tomography of the human knee in comparison with clinical imaging techniques and histology. *Invest. Radiol.* 49, 627–634. doi: 10.1097/RLI.0000000000000063

Iezzi, G., Piatelli, A., Giuliani, A., Mangano, C., Barone, A., Manzon, L., et al. (2017). Molecular, cellular and pharmaceutical aspects of bone grafting materials and membranes during maxillary sinus-lift procedures. Part 2: detailed characteristics of the materials. *Curr. Pharm. Biotechnol.* 18, 33–44. doi: 10.2174/1389201017666161202104002

Ingal, I. V., and Beliaevskaya, E. A. (1995). X-ray plane-wave topography observation of the phase contrast from a non-crystalline object. *J. Phys. D.* 28, 2314–2317. doi: 10.1088/0022-3727/28/11/012

Langer, M., Pacureanu, A., Suhonen, H., Grimal, Q., Cloetens, P., and Peyrin, F. (2012). X-ray phase nanotomography resolves the 3D human bone ultrastructure. *PLoS ONE* 7:e35691. doi: 10.1371/journal.pone.0035691

Langer, M., Prisby, R., Peter, Z., Boistel, R., Lafage-Proust, M. H., and Peyrin, F. (2009). Quantitative investigation of bone microvascularization from 3D synchrotron micro-computed tomography in a rat model. *Conf. Proc. IEEE Eng. Med. Biol. Soc.* 2009, 1004–1007. doi: 10.1109/IEMBS.2009.5333832

Langer, M., Prisby, R., Peter, Z., Guignandon, A., Lafage-Proust, M. H., and Peyrin, F. (2011). Simultaneous 3D imaging of bone and microstructure in a rat model. *IEEE Trans. Nucl. Sci.* 58, 139–145. doi: 10.1109/TNS.2010.2091282

Laschke, M. W., Harder, Y., Amon, M., Martin, I., Farhadi, J., Ring, A., et al. (2006). Angiogenesis in tissue engineering: breathing life into constructed tissue substitutes. *Tissue Eng.* 2, 2093–2104. doi: 10.1089/ten.2006.12.2093

Lewis, R. A., Hall, C. J., Hufton, A. P., Evans, S., Menk, R. H., Arfelli, F., et al. (2003). X-ray refraction effects: application to the imaging of biological tissues. *Br. J. Radiol.* 76, 301–308. doi: 10.1259/bjr/32889803

Liu, Y., Teoh, S. H., Chong, M. S., Yeow, C. H., Kamm, R. D., Choolani, M., et al. (2013). Contrasting effects of vasculogenic induction upon biaxial bioreactor stimulation of mesenchymal stem cells and endothelial progenitor cells cocultures in three-dimensional scaffolds under *in vitro* and *in vivo* paradigms for vascularized bone tissue engineering. *Tissue Eng. Part A* 19, 893–904. doi: 10.1089/ten.tea.2012.0187

Manescu, A., Giuliani, A., Mazzoni, S., Mohammadi, S., Tromba, G., Diomede, F., et al. (2016). Osteogenic potential of dual-blocks cultured with periodontal ligament stem cells: *in-vitro* and synchrotron microtomography study. *J. Periodont. Res.* 51, 112–124. doi: 10.1111/jre.12289

Marenzana, M., Hagen, C. K., Das Neves Borges, P., Endrizzi, M., Szafraniec, M. B., Ignatyev, K., et al. (2012). Visualization of small lesions in rat cartilage by means of laboratory-based x-ray phase contrast imaging. *Phys. Med. Biol.* 57, 8173–8184. doi: 10.1088/0031-9155/57/24/8173

Marinescu, M., Langer, M., Durand, A., Olivier, C., Chabrol, A., Rositi, H., et al. (2013). Synchrotron radiation X-ray phase micro-computed tomography as a new method to detect iron oxide nanoparticles in the brain. *Mol. Imaging Biol.* 15, 552–559. doi: 10.1007/s11307-013-0639-6

Mazzoni, S., Mohammadi, S., Tromba, G., Diomede, F., Piattelli, A., Trubiani, O., et al. (2017). Role of cortico-cancellous heterologous bone in human

periodontal ligament stem cell xeno-free culture studied by Synchrotron radiation phase-contrast microtomography. *Int. J. Mol. Sci.* 18:364. doi: 10.3390/ijms18020364

Miao, P., Wu, Z., Li, M., Ji, Y., Xie, B., Lin, X., et al. (2016). Synchrotron radiation X-ray phase-contrast tomography visualizes microvasculature changes in mice brains after ischemic injury. *Neural Plast.* 2016:3258494. doi: 10.1155/2016/3258494

Momose, A. (1995). Demonstration of phase-contrast X-ray computed tomography using an x-ray interferometer. *Nucl. Instrum. Methods A* 352, 622–628. doi: 10.1016/0168-9002(95)90017-9

Momose, A., Takeda, T., and Itai, Y. (2000). Blood vessels: depiction at phase-contrast X-ray imaging without contrast agents in the mouse and rat—feasibility study. *Radiology* 217, 593–596. doi: 10.1148/radiology.217.2.r00oc14593

Momose, A. (2003). Phase-sensitive imaging and phase tomography using X-ray interferometers. *Opt. Express* 11, 2303–2314. doi: 10.1364/OE.11.002303

Momose, A., Takeda, T., Itai, Y., and Hirano, K. (1996). Phase-contrast X-ray computed tomography for observing biological soft tissues. *Nat. Med.* 2, 473–475. doi: 10.1038/nm0496-473

Momose, A., Yashiro, W., Maikusa, H., and Takeda, Y. (2009). High-speed X-ray phase imaging and X-ray phase tomography with Talbot interferometer and white synchrotron radiation. *Opt. Express* 17, 12540–12545. doi: 10.1364/OE.17.012540

Nebuloni, L., Kuhn, G. A., Vogel, J., and Muller, R. (2014). A novel *in vivo* vascular imaging approach for hierarchical quantification of vasculature using contrast enhanced micro-computed tomography. *PLoS ONE* 9:e86562. doi: 10.1371/journal.pone.0086562

Nesch, I., Fogarty, D. P., Tzvetkov, T., Reinhart, B., Walus, A. C., Khelashvili, G., et al. (2009). The design and application of an in-laboratory diffraction-enhanced x-ray imaging instrument. *Rev. Sci. Instrum.* 80:093702. doi: 10.1063/1.3213621

Noel, P. B., Herzen, J., Fingerle, A. A., Willner, M., Stockmar, M. K., Hahn, D., et al. (2013). Evaluation of the potential of phase-contrast computed tomography for improved visualization of cancerous human liver tissue. *Z. Med. Phys.* 23, 204–211. doi: 10.1016/j.zemedi.2013.02.006

Paino, F., La Noce, M., Giuliani, A., De Rosa, A., Mazzoni, S., Laino, L., et al. (2017). Human DPSCs fabricate vascularized woven bone tissue: a new tool in bone tissue engineering. *Clin. Sci.* 131, 699–713. doi: 10.1042/CS20170047

Pfeiffer, F., Kottler, C., Bunk, O., and David, C. (2007). Hard x-ray phase tomography with low-brilliance sources. *Phys. Rev. Lett.* 98:108105. doi: 10.1103/PhysRevLett.98.108105

Pinzer, B. R., Cacquevel, M., Modregger, P., McDonald, S. A., Bensadoun, J. C., Thuering, T., et al. (2012). Imaging brain amyloid deposition using grating-based differential phase contrast tomography. *Neuroimage* 61, 1336–1346. doi: 10.1016/j.neuroimage.2012.03.029

Saam, T., Herzen, J., Hetterich, H., Fill, S., Willner, M., Stockmar, M., et al. (2013). Translation of atherosclerotic plaque phase-contrast CT imaging from synchrotron radiation to a conventional l-b X-ray source. *PLoS ONE* 8:e73513. doi: 10.1371/journal.pone.0073513

Snigirev, S., Snigireva, I., Kohn, V., Kuznetsov, S., and Schelokov, I. (1995). On the possibilities of X-ray phase contrast microimaging by coherent high-energy synchrotron radiation. *Rev. Sci. Instrum.* 66, 5486–5492. doi: 10.1063/1.1146073

Stampanoni, M., Wang, Z., Thuring, T., David, C., Roessl, E., Trippel, M., et al. (2011). The first analysis and clinical evaluation of native breast tissue using differential phase-contrast mammography. *Invest. Radiol.* 46, 801–806. doi: 10.1097/RLI.0b013e31822a585f

Sztrokay, A., Herzen, J., Auweter, S. D., Liebhardt, S., Mayr, D., Willner, M., et al. (2013). Assessment of grating-based X-ray phase-contrast CT for differentiation of invasive ductal carcinoma and ductal carcinoma *in situ* in an experimental *ex vivo* set-up. *Eur. Radiol.* 23, 381–387. doi: 10.1007/s00330-012-2592-1

Tanaka, J., Nagashima, M., Kido, K., Hoshino, Y., Kiyohara, J., Makifuchi, C., et al. (2013). Cadaveric and *in vivo* human joint imaging based on differential phase contrast by X-ray Talbot-Lau interferometry. *Z. Med. Phys.* 23, 222–227. doi: 10.1016/j.zemedi.2012.11.004

Tang, R., Xi, Y., Chai, W.-M., Wang, Y., Guan, Y., Yang, G. Y., et al. (2011). Microbubble-based synchrotron radiation phase contrast imaging: basic study and angiography applications. *Phys. Med. Biol.* 56, 3503–3512. doi: 10.1088/0031-9155/56/12/004

Tsigkou, O., Pomerantseva, I., Spencer, J. A., Redondo, P. A., Hart, A. R., O'Doherty, E., et al. (2010). Engineered vascularized bone grafts. *Proc. Natl. Acad. Sci. U.S.A.* 107, 3311–3316. doi: 10.1073/pnas.0905445107

Upputuri, P. K., Sivasubramanian, K., Mark, C. S. K., and Pramanik, M. (2015). Recent Developments in vascular imaging techniques in tissue engineering and regenerative medicine. *Biomed. Res. Int.* 2015:783983. doi: 10.1155/2015/783983

Velroyen, A., Bech, M., Zanette, I., Schwarz, J., Rack, A., Tympner, C., et al. (2014). X-Ray Phase-contrast tomography of renal ischemia-reperfusion damage. *PLoS ONE* 9:e109562. doi: 10.1371/journal.pone.0109562

Weitkamp, T., Diaz, A., David, C., Pfeiffer, F., Stampanoni, M., Cloetens, P., et al. (2005). X-ray phase imaging with a grating interferometer. *Opt. Express* 13, 6296–6304. doi: 10.1364/OPEX.13.006296

Wilkins, S. W., Gureyev, T. E., Gao, D., Pogany, A., and Stevenson, A. W. (1996). Phase-contrast imaging using polychromatic hard X-raays. *Nature* 384, 335–338. doi: 10.1038/384335a0

Yamanichi, N., Itose, T., Neiva, R., and Wang, H. L. (2008). Long-term evaluation of implant survival in augmented sinuses: a case series. *Int. J. Periodontics Restorative Dent.* 28, 163–169.

Yaroshenko, A., Meinel, F. G., Bech, M., Tapfer, A., Velroyen, A., Schleede, S., et al. (2013). Pulmonary emphysema diagnosis with a preclinical small-animal X-ray dark-field scatter-contrast scanner. *Radiology* 269, 427–433. doi: 10.1148/radiol.13122413

Yoo, S. Y., and Kwon, S. M. (2013). Angiogenesis and its therapeutic opportunities. *Mediators Inflamm.* 2013:127170. doi: 10.1155/2013/127170

Conflict of Interest Statement: The authors declare that the research was conducted in the absence of any commercial or financial relationships that could be construed as a potential conflict of interest.

The reviewer CA and handling Editor declared their shared affiliation.

frontiers in Physiology

MINI REVIEW
published: 25 October 2018
doi: 10.3389/fphys.2018.01510

An Overview on Current Non-invasive Diagnostic Devices in Oral Oncology

Marco Mascitti[1], Giovanna Orsini[1], Vincenzo Tosco[1], Riccardo Monterubbianesi[1], Andrea Balercia[2], Angelo Putignano[1], Maurizio Procaccini[1,3] and Andrea Santarelli[1,3]*

[1] Department of Clinical Sciences and Stomatology, Marche Polytechnic University, Ancona, Italy, [2] Department of Oral and Head-Neck Surgery, Umberto I General Hospital, Marche Polytechnic University, Ancona, Italy, [3] National Institute of Health and Science of Aging, INRCA, Ancona, Italy

Oral squamous cell carcinoma (OSCC) is the most common head and neck malignancy, and despite advances in cancer therapies, the overall 5-year survival rate has remained below 50% over the past decades. OSCC is typically preceded by potentially malignant disorders (PMD), but distinguishing high-risk from low-risk PMD is challenging. In the last years, several diagnostic methods as light-based detection systems (LBDS) have been proposed to facilitate the detection of OSCC and PMD. Furthermore, the recent evolution of nanotechnology may provide new opportunities to detect PMD and OSCC at an early stage. Indeed, several preclinical studies showed the potential of nanotechnology to enhance diagnostic accuracy. For these reasons, it is fundamental to conduct studies to evaluate the efficacy of nanotechnology implementation in LBDS. The aim of this article is to review the current literature on LBDS and to provide a summary of the sensitivity and specificity of each technique, and possible future applications of nanotechnologies. The LBDS showed great potential for screening and monitoring oral lesions, but there are several factors that hinder an extensive use of these devices. These devices seem to be useful in assessing lesion margins that must be biopsied. However, to date, conventional oral examination, and tissue biopsy remain the gold standard for OSCC diagnosis. The use of nanotechnologies could be the next step in the evolution of LBDS, thus providing devices that can help clinicians to detect and better monitor oral lesions.

Keywords: light-based detection system, early diagnosis, OSCC, chemiluminescence, autofluorescence, nanotechnology

OPEN ACCESS

Edited by:
Gianpaolo Papaccio, Università degli Studi della Campania Luigi Vanvitelli, Italy

Reviewed by:
Alessandra Pisciotta, Università degli Studi di Modena e Reggio Emilia, Italy
Luigi Mele, Università degli Studi di Napoli Federico II, Italy

****Correspondence:***
Marco Mascitti
marcomascitti86@hotmail.it

Specialty section:
This article was submitted to Craniofacial Biology and Dental Research, a section of the journal Frontiers in Physiology

Received: *30 July 2018*
Accepted: *08 October 2018*
Published: *25 October 2018*

Citation:
Mascitti M, Orsini G, Tosco V, Monterubbianesi R, Balercia A, Putignano A, Procaccini M and Santarelli A (2018) An Overview on Current Non-invasive Diagnostic Devices in Oral Oncology. Front. Physiol. 9:1510. doi: 10.3389/fphys.2018.01510

INTRODUCTION

Oral squamous cell carcinoma (OSCC) is the most common head and neck malignancy and the sixth most common tumour worldwide (Warnakulasuriya, 2009). Despite advances in therapies, the overall 5-year survival rate has remained unchanged during the past decades, mainly due to delayed diagnosis (Gomez et al., 2009). OSCC is typically preceded by potentially malignant disorders (PMD), a group of clinically suspicious lesions. Although the majority of PMD do not progress to OSCC, distinguishing high-risk PMD from low-risk PMD is challenging for dental practitioners (Yang et al., 2018). Furthermore, patients treated for OSCC are at risk of developing recurrences and secondary primary tumours, due to field cancerization and/or incomplete surgery (Day and Blot, 1992). Currently, conventional oral examination (COE), consisting in visual and tactile assessment of accessible oral structures, followed by tissue biopsy still constitutes the gold

standard for diagnosis of PMD and OSCC. However, there are some limitations of this procedure, such as sampling bias that can lead to underdiagnosis or misdiagnosis, particularly in multifocal lesions (Yang et al., 2018).

The possibility of making an early diagnosis is crucial for reducing high mortality rate and morbidity of OSCC patients. In the last years, several light-based detection systems (LBDS), based on optical properties of biological tissues, have emerged with claims of enhancing oral mucosal examinations and facilitating the detection of PMD and OSCC.

Furthermore, the recent evolution of nanotechnology may provide new opportunities to detect PMD and OSCC at an early stage (El-Sayed et al., 2005). Several preclinical studies showed the potential to enhance diagnostic accuracy of optical diagnostic technologies (e.g., Raman spectroscopy) or imaging techniques (e.g., Magnetic resonance imaging) (Chen et al., 2018). Among the latter techniques, reflectance confocal microscopy seems to improve the evaluation of oral lesions, by detecting backscattered light from illuminated tissue, producing high resolution tissue map. However, several technological limitations need to be resolved to validate diagnostic accuracy (Lucchese et al., 2016). LBDS showed several advantages compared to the aforementioned approaches, such as low cost and ease of use. For these reasons, it is fundamental to conduct studies to evaluate the efficacy of nanotechnology implementation in LBDS.

The aim of this article is to review the literature on LBDS currently on the market (**Tables 1**, 2), providing clinicians with a better understanding of their advantages and limits, and possible future applications of nanotechnologies.

ViziLite®

ViziLite® (Zila Pharmaceuticals, Phoenix, AZ, United States) is a chemiluminescence-based detection device designed to facilitate the early identification of PMD and OSCC. In 2002 ViziLite® became the first device approved by FDA for this purpose (Oh and Laskin, 2007). This is a disposable capsule formed by an outer shell of flexible plastic containing acetyl salicylic acid and an inner glass vial containing hydrogen peroxide. To activate it, the capsule is bent to break the inner glass vial, triggering the reaction of the chemicals contained in the two compartments. Consequently, a bluish-white light (430–580 nm) is produced,

TABLE 1 | Published studies on VELscope® for clinical detection of oral lesions.

Author and year	Patients	Type of lesion	Sens	Spec	PPV	NPV
Poh et al., 2006	20	OSCC	95%	–	100%	–
Lane et al., 2006	44	PMD, OSCC	98%	100%	100%	86%
Roblyer et al., 2009	65	OL	95.9%	96.2%	–	–
Jayaprakash et al., 2009	60	OL	72%	50%	76%	46%
Mehrotra et al., 2010	156	OL	50%	38.9%	6.4%	90.3%
Koch et al., 2011	78	PMD, OSCC	94%	16%	45%	77%
Paderni et al., 2011	175	PMD, OSCC	80.7%	97.5%	93.9%	91.3%
Awan et al., 2011a	126	PMD	84.1%	15.3%	37.8%	61.1%
Scheer et al., 2011	64	OSCC	100%	80.8%	54.5%	100%
Marzouki et al., 2012	85	OL	92%	77%	–	–
McNamara et al., 2012	130	OL	66.7%	6.0%	4.1%	75%
Farah et al., 2012	112	PMD	30%	63%	19%	75%
Rana et al., 2012	123	PMD	100%	74%	16.7%	100%
Hanken et al., 2013	60	PMD	97.9%	33.3%	85.5%	80%
Sawan and Mashlah, 2015	71	OL	100%	74.1%	46.4%	100%
Kaur and Jacobs, 2015	130	OL	67%	62%	29.8%	89%
Jane-Salas et al., 2015	60	OL	40%	80%	62.5%	66.7%
Elvers et al., 2015	20	PMD	–	–	–	–
Ayoub et al., 2015	30	Screening	–	–	–	–
Ohnishi et al., 2016	20	OSCC	91%	100%	100%	58.3%
Scheer et al., 2016	41	OSCC	33.3%	88.6%	33.3%	88.6%
Yamamoto et al., 2017	62	PMD, OSCC	85.9%	26.7%	83.3%	30.8%
Ganga et al., 2017	200	OL	76%	66.3%	24.4%	95.1%
Burian et al., 2017	90	OSCC	–	–	–	–
Huang et al., 2017	140	PMD, OSCC	98.3%	77.6%	91.7%	93.8%
Amirchaghmaghi et al., 2018	21	PMD, OSCC	90%	15%	40%	71%
Farah et al., 2018	11	PMD	–	–	–	–
Canjau et al., 2018	18	OL	94.4%	100%	100%	50%

OL, oral lesions; PMD, potentially malignant disorders; OSCC, oral squamous cell carcinoma; Sens, sensitivity; Spec, specificity; PPV, positive predictive value; NPV, negative predictive value. Where possible, missing data were recalculated.

TABLE 2 | Published studies on light-based detection systems other than VELscope® for clinical detection of oral lesions.

Author and year	Device	Patients	Type of lesion	Sens	Spec	PPV	NPV
Huber et al., 2004	ViziLite	150	PMD	–	–	–	–
Ram and Siar, 2005	ViziLite	40	PMD, OSCC	100%	14.3%	80%	100%
Epstein et al., 2006	ViziLite	134	PMD	–	–	–	–
Kerr et al., 2006	ViziLite	501	OL	–	–	–	–
Farah and McCullough, 2007	ViziLite	55	OL	100%	0%	18.2%	–
Oh and Laskin, 2007	ViziLite	100	Screening	–	–	–	–
Epstein et al., 2008	ViziLite	84	PMD	100%	55%	37%	100%
Mehrotra et al., 2010	ViziLite	102	OL	0%	75.5%	0%	94.8%
Awan et al., 2011b	ViziLite	126	OL	87%	24%	15%	92%
Mojsa et al., 2012	ViziLite	30	PMD	57.6%	37.5%	79.2%	17.6%
Rajmohan et al., 2012	ViziLite	30	PMD, OSCC	85%	100%	100%	76.9%
Ujaoney et al., 2012	ViziLite	44	PMD	59%	78%	–	–
Vashisht et al., 2014	ViziLite	60	PMD, OSCC	95.5%	84.6%	91.3%	91.7%
Kammerer et al., 2015	ViziLite	44	PMD	100%	30%	26%	100%
Chaudhry et al., 2016	ViziLite	100	PMD	84.8%	41.2%	58.3%	70%
Sweeny et al., 2011	Identafi	88	PMD (white)	50%	98%	50%	98%
			(violet)	50%	81%	11%	97%
			(green)	0%	86%	0%	95%
Lane et al., 2012	Identafi	124	PMD	82%	87%	–	–
Messadi et al., 2014	Identafi	21	OL	–	–	–	–
Lalla et al., 2015	Identafi	342	screening	–	–	–	–
Lalla et al., 2016	Identafi	88	OL (white)	100%	100%	100%	100%
			(Violet)	27.5%	96.3%	61.1%	86.4%
			(Green)	40%	71.7%	22.9%	85.1%
McIntosh et al., 2009	Microlux/DL	50	PMD	77.8%	70.7%	36.8%	93.5%
Ibrahim et al., 2014	Microlux/DL	599	Screening	100%	32.4%	17.9%	100%
Moro et al., 2010	GOCCLES	32	PMD, OSCC	100%	93%	92%	100%
Moro et al., 2015	GOCCLES	61	PMD	96.9%	3.1%	50%	50%

OL, oral lesions; PMD, potentially malignant disorders; OSCC, oral squamous cell carcinoma; Sens, sensitivity; Spec, specificity; PPV, positive predictive value; NPV, negative predictive value. Where possible, missing data were recalculated.

lasting for 10 min (Liu et al., 2016). A modified version (ViziLite® PLUS) consists of a combination of chemiluminescence and toluidine blue (TB) marking system, an acidophilic dye that selectively stains acidic substances such as DNA. Furthermore, an accessory eyewear has been developed, to allow better isolation of chemiluminescent light (Sambandham et al., 2013). Its clinical use requires a 1-min rinse of 1% acetic acid solution, to desiccate oral tissues, followed by oral examination with 430–580 nm wavelength light. The altered epithelial cells, due to higher nuclear/cytoplasmic ratio, reflect the light and cause the appearance of an "aceto-white" lesion, whereas normal cells appear blue (Nagi et al., 2016).

The first studies regarding ViziLite®, published in 2004–2007, were conducted on subjects with different clinical conditions, ranging from normal mucosa to diagnosed OSCC, with the aim to explore the diagnostic utility of chemiluminescence-based strategies (**Table 2**). In the first reported study, ViziLite® identified a subclinical lesion, suggesting its utility in identifying occult epithelial abnormalities (Huber et al., 2004). In a small cohort of patients with oral lesions, ViziLite® appears to be a better diagnostic tool than TB in detection of OSCC and PMD (Ram and Siar, 2005). Another study highlights the ability of ViziLite® to show brighter and better demarcated lesions than using incandescent light, aiming to enhance the identification of lesions that could be biopsied (Epstein et al., 2006). Unfortunately, these results have not been confirmed, which failed to demonstrate significant improvement in identification and evaluation of oral lesions (Farah and McCullough, 2007; Oh and Laskin, 2007). Interestingly, a cross-sectional study compared ViziLite® and VELscope® to evaluate their clinical utility in diagnosing oral lesions, but the authors failed to demonstrate any superiority to COE (Mehrotra et al., 2010).

For this reason, a new version of this device has been developed (ViziLite® PLUS), aiming to improve the diagnostic power of TB marking system. First results were encouraging, showing that TB reduced the number of false positive cases leaving the false negative rate unchanged (Epstein et al., 2008). On the contrary, ViziLite® PLUS does not seems to be useful to detect malignancies in patients with clearly visible lesions (Mojsa et al., 2012). In fact, some authors described the better diagnostic accuracy of ViziLite® with respect to TB staining alone (Rajmohan et al., 2012; Vashisht et al., 2014), justifying the combined use of these two techniques.

Recently, the results of a clinical study suggested that, although the adjunct of TB to ViziLite® reduced the false positive cases without increasing the number of false negatives, there are little benefits in using this device in general dental practise (Chaudhry et al., 2016).

In conclusion, despite the fact that ViziLite® facilitates the identification of hyperkeratotic areas and may increase the visibility of mucosal lesions, the main limitation is currently the high proportion of false positive and false negative tests, regarding the identification of dysplastic areas rather than hyperkeratosis (Chhabra et al., 2015).

VELscope®

VELscope® (LED Medical Diagnostics, White Rock, BC, Canada) is a hand-held non-magnifying device for direct visualisation of oral mucosa autofluorescence that became commercially available after FDA approval in 2006 (Ayoub et al., 2015). No need of technical measures, such as the use of dimmed light, pre-rinse or lesion-marking solutions, make VELscope® easy to use. It uses a 120 W arc-lamp and a series of philtres and reflectors optimised for producing 400–460 nm wavelength light. The light emitted reaches oral mucosa and excites endogenous autofluorescence substances, called fluorophores (Yamamoto et al., 2017). Preliminary studies, regarding small groups of patients, gave encouraging results (**Table 1**). In the first reported study, 44 patients with confirmed oral dysplasia or OSCC were evaluated with both COE and VELscope®. The results showed that the device can differentiate PMD and OSCC from normal oral mucosa, with high sensitivity and specificity levels (Lane et al., 2006). These results were confirmed in a small OSCC cohort study, in which the use of autofluorescence-guided examination was able to identify subclinical high-risk fields with cancerous changes (Poh et al., 2006). In a study conducted on 60 patients using a semi-quantitative grading system for autofluorescence, VELscope® demonstrate good sensitivity and a better ability to recognise high-grade lesions than COE (Jayaprakash et al., 2009). Another study evaluated 65 subjects with VELscope®, using a specific algorithm based on the ratio of red-to-green fluorescence. The authors found that 405 nm wavelength light was able to discriminate neoplastic and non-neoplastic tissue with high sensitivity and specificity (Roblyer et al., 2009).

In a cross-sectional study, 175 patients with at least one clinical lesion were evaluated using VELscope®. However, despite the good results, the authors warned that this device could lead to overdiagnosis if used by non-specialists (Paderni et al., 2011). In fact, in the following years several studies on patients with PMD or OSCC reported low specificity values, highlighting this as the primary limitation of VELscope® (Awan et al., 2011a; Koch et al., 2011; Scheer et al., 2011). For these reason, other authors concluded that VELscope® examination alone does not provide significant diagnostic benefit beyond COE in screening for PMD and OSCC, also due to interobserver variability (Farah et al., 2012; McNamara et al., 2012). These results were confirmed by a study on 200 patients, limiting the utility of autofluorescence for OSCC screening (Ganga et al., 2017).

One effort to overcome these shortcomings consists of adding the VELscope® exam to the COE. Indeed, as reported by several authors, the combination of COE and VELscope® examination in patients with oral lesions could provide a significative diagnostic yield (Marzouki et al., 2012; Rana et al., 2012; Hanken et al., 2013). However, these results must be interpreted carefully due to the different inclusion and exclusion criteria used to select the patient cohorts, which can influence both sensitivity and specificity.

Other studies focused on combining VELscope® and other diagnostic tests, aiming to find out better approaches to improve detection of PMD and OSCC. For example, the combination approaches of tissue autofluorescence and salivary protoporphyrin IX levels seems to be effective to distinguish between normal mucosa and high-risk lesions (Kaur and Jacobs, 2015). The use of quantitative analysis of autofluorescence were developed to solve the problem of interobserver variability. Novel methods such as quadratic discriminant analysis or luminance ratio were promising, showing a strong concordance with histopathological diagnosis (Huang et al., 2017; Yamamoto et al., 2017). Recently, a retrospective study based on oral photograph was conducted to find colour distribution patterns related to neoplastic lesions. The fluorescence analysis showed differences in the red-to-green ratios of neoplastic areas, suggesting its clinical utility to detect early OSCC (Burian et al., 2017).

Recently, tissue autofluorescence was used to investigate biological aspects of oral carcinogenesis. In the first *in vitro* study, VELscope® was used to investigate the autofluorescence in a rat tongue carcinogenesis model. The results showed significant changes in autofluorescence pattern during progression to dysplasia and carcinoma (Ohnishi et al., 2016). In another study, RNA sequencing technique was used to identify molecular differences related to autofluorescence patterns. Results were encouraging, demonstrating that the autofluorescence-based excision was successful in achieving a clear molecular margin when excising PMD (Farah et al., 2018). These results confirmed those previously reported in literature, in which VELscope® demonstrated that the actual sizes of some lesions are significantly larger than they look clinically (Elvers et al., 2015).

In conclusion, several criticisms have been made about VELscope®, mainly focused to the limited capacity to extend the use of this device in general dental practise. Future research directions are aimed at improving the specificity of this device, allowing wider clinical use of VELscope® in routine general practise (Bhatia et al., 2013).

Identafi®

Identafi® (StarDental - DentalEZ, Lancaster, PA, United States) is a probe-like device designed for multispectral screening of PMD, approved by FDA in 2009 as oral screening device (Vigneswaran et al., 2009). Identafi® has three light sources of different wavelengths: white, violet (405 nm), and green-amber (545 nm) lights, that can be sequentially used in oral examination. While white light provides classical visualisation of oral mucosa, violet light excites endogen fluorophores, enabling the assessment of mucosa autofluorescence, like VELscope®. Green-amber

light, through the reflectance spectroscopy, excites haemoglobin molecules in the blood, with the aim to visualise the vasculature (Messadi et al., 2014). A mirror is attached to the probe to help visualise relatively obscure areas in oral cavity.

The first clinical trial with Identafi® was conducted on 88 patients who were treated previously for OSCC (**Table 2**). Screening results with white, violet, and green lights were compared to each other, showing limited benefits of tissue reflectance and autofluorescence in detecting high-risk lesions (Sweeny et al., 2011). In 2012, was reported a case series of PMD patients with the aim to evaluate the efficacy of Identafi®. Although the results are not clearly described, this device seems to be helpful in identifying characteristics not otherwise visible to the COE (Lane et al., 2012).

In a pilot study, Identafi® was used to evaluate tissue vascularity of PMD and to compare with the histological grading of the lesions using a vascular marker (CD34). The results found a correlation between tissue reflectance and histological assessment of vascular structure, in both OSCC and non-cancerous lesions (Messadi et al., 2014).

Two studies on the effectiveness of Identafi® were conducted on Australian population. In the first one, 342 urban Indigenous community members were screened for oral lesions using reflectance spectroscopy and autofluorescence imaging. Identafi® improved the visibility of oral cavity lesions and was capable to find new lesions not seen during COE, although the prevalence of oral pigmentation in this community could hamper the use of autofluorescence screening systems (Lalla et al., 2015). In the second study, 88 patients were evaluated with Identafi®, showing good specificity, negative predictive value, and accuracy (Lalla et al., 2016).

Taken together, the use of Identafi provide the clinician with more data than COE. Unfortunately, the results interpretation requires high level of experience and clinical training in oral pathology, suggesting that its usage should be limited to reference centres for oral pathology (Lalla et al., 2016).

OTHER DEVICES

Microlux/DL™ (AdDent Inc., Danbury, CT, United States) is a chemiluminescence-based device which became commercially available after FDA approval in 2005. This device has a diffused blue-white LED light source and a fibre optic light guide (McIntosh et al., 2009). It uses the same principles of ViziLite®: after 1-min rinse with 1% acetic acid, oral examination is performed with 460–555 nm wavelength light. Altered epithelial cells cause the appearance of "aceto-white" lesions, and LED light source makes the lesion more easily recognisable. Furthermore, the use of TB can be used in conjunction with Microlux/DL™, to enhance the visualisation of dysplastic areas (Ibrahim et al., 2014). In 2009 was conducted a study on 50 patients with oral white lesions to evaluate the efficacy of Microlux/DL™. The results showed that this device can enhance visualisation of oral mucosa, but no clinical improvement was observed, due to poor ability to distinguish between benign and malignant lesions (McIntosh et al., 2009). Another trial that evaluated the effectiveness of Microlux/DL™ was carried out in 2014. 599 patients were examined with COE and Microlux/DL™ with and without TB, showing high sensitivity but low specificity, indicating that this device is not effective to distinguish between benign and malignant lesions, although seems to be a promising screening test for oral lesions (Ibrahim et al., 2014).

GOCCLES® is a medical device (Pierrel S.p.A, Italy) approved by FDA in 2015. This is a low cost and easy-to-use device consisting in a pair of glasses equipped with special optical philtres that allows autofluorescence detection. Indeed, GOCCLES® was created to provide an easy and low cost mean of identification of autofluorescence abnormalities in oral cavity with the use of any dental curing light (Moro et al., 2015). In 2010 was reported the first study on GOCCLES® in a small cohort of selected patients, showing high sensitivity and specificity (Moro et al., 2010). Five years later, a non-randomised multicentre trial was conducted on patients at risk for OSCC, suggesting the need for further researches to define the diagnostic performance of this device (Moro et al., 2015). Indeed, despite the low cost of GOCCLES® could encourage more careful examinations, its main limitation seems to be the interobserver variability, that could be overcome by proper training.

In recent years, other instruments have been developed and commercialised for facilitate the early identification of oral lesions. Their operating principle is equivalent to the devices described above, using either autofluorescence or chemiluminescence detection. However, their clinical effectiveness is currently hampered by the lack of published studies. For these reasons, they will only be mentioned briefly here. Bio/Screen® (AdDent Inc., Danbury, CT, United States), an instrument with five violet (390–430 nm) high-power LED, designed to enhance the visualisation of mucosal abnormalities through the use of tissue autofluorescence (Kahn et al., 2018).

Orascoptic DK™ system (Orascoptic, Middleton, WI, United States) is another chemiluminescence-based device, designed to improve the visualisation of oral lesions through the use of blue-white LED light and oral rinse of 1% acetic acid solution (Patton et al., 2008).

Sapphire® Plus LD (DenMat Holdings, Lompoc, CA, United States), DentLight DOE™ Oral Exam System (DentLight, Richardson, TX, United States), and OralID™ 2.0 (Forward Science Technologies, Stafford, TX, United States) are other tissue autofluorescence-based devices developed in order to detect oral lesions (Kahn et al., 2018).

CONCLUSION AND FUTURE PERSPECTIVES

The diagnostic techniques presented here showed great potential for screening and monitoring oral lesions (Liu et al., 2016). Unfortunately, to date several factors hinder an extensive use of these devices: (1) data do not demonstrate clear superiority of these methods compared to COE; (2) there remains the need for well-designed multicentre prospective studies; (3) these devices

exhibit a not-negligible interobserver variability, limiting their use to clinicians with significant experience in oral pathology (Patton et al., 2008; Carreras-Torras and Gay-Escoda, 2015).

However, the current evidence suggests that these devices: (1) seem to be useful in assessing lesion margins that must be biopsied and, therefore, may be useful in surgical management; (2) can be used to investigate biological aspects of oral carcinogenesis, leading to more accurate methods for interpreting data from LBDS; (3) can be enhanced with new approaches used to analyse optical imaging data, with the aim to quantify the results obtained; (4) lowering the costs of these devices could indirectly lead to greater attention for oral lesions among both patients and general dental practitioners, allowing in turn to promote a culture of oral cancer prevention (Carreras-Torras and Gay-Escoda, 2015; Moro et al., 2015); (5) finally, the possibility of implementing LBDS through the use of tissue-marking dyes can in principle allows to develop strategies for the use of nanoparticles. Indeed, nanoparticles can provide molecular targeted imaging, with higher image contrast and resolution. For example, a promising nanotechnology in oral diagnostic research is the quantum dots, consisting in nanometre-sized semiconductor crystals (Walling et al., 2009). The biophysical characteristics of these particles confer several advantages over conventional dyes and fluorescent proteins. The possibility to link the quantum dots to molecules with the ability to target cancer cells make them ideal for diagnostic applications in detecting PMD and OSCC (Chen et al., 2018). Therefore, the use of nanotechnologies could be the next step in the evolution of LBDS, providing devices that can help clinicians to detect and better monitor oral lesions.

AUTHOR CONTRIBUTIONS

MM, AS, and MP conceived the literature review. MM and VT described the VELscope® system. AS and RM described the ViziLite® system. AB and GO described the Identafi® system. AP, MP, and GO wrote the concluding remarks. All authors discussed and approved the final version of the manuscript.

REFERENCES

Amirchaghmaghi, M., Mohtasham, N., Delavarian, Z., Shakeri, M. T., Hatami, M., and Mosannen Mozafari, P. (2018). The diagnostic value of the native fluorescence visualization device for early detection of premalignant/malignant lesions of the oral cavity. *Photodiagnosis Photodyn. Ther.* 21, 19–27. doi: 10.1016/j.pdpdt.2017.10.019

Awan, K. H., Morgan, P. R., and Warnakulasuriya, S. (2011a). Evaluation of an autofluorescence based imaging system (VELscope) in the detection of oral potentially malignant disorders and benign keratoses. *Oral Oncol.* 47, 274–277. doi: 10.1016/j.oraloncology.2011.02.001

Awan, K. H., Morgan, P. R., and Warnakulasuriya, S. (2011b). Utility of chemiluminescence (ViziLite) in the detection of oral potentially malignant disorders and benign keratoses. *J. Oral Pathol. Med.* 40, 541–544. doi: 10.1111/j.1600-0714.2011.01048.x

Ayoub, H. M., Newcomb, T. L., Mccombs, G. B., and Bonnie, M. (2015). The use of fluorescence technology versus visual and tactile examination in the detection of oral lesions: a pilot study. *J. Dent. Hyg.* 89, 63–71.

Bhatia, N., Lalla, Y., Vu, A. N., and Farah, C. S. (2013). Advances in optical adjunctive AIDS for visualisation and detection of oral malignant and potentially malignant lesions. *Int. J. Dent.* 2013:194029. doi: 10.1155/2013/194029

Burian, E., Schulz, C., Probst, F., Palla, B., Troltzsch, M., Maglitto, F., et al. (2017). Fluorescence based characterization of early oral squamous cell carcinoma using the visually enhanced light scope technique. *J. Craniomaxillofac. Surg.* 45, 1526–1530. doi: 10.1016/j.jcms.2017.05.021

Canjau, S., Todea, D. C. M., Sinescu, C., Pricop, M. O., and Duma, V. F. (2018). Fluorescence influence on screening decisions for oral malignant lesions. *Rom. J. Morphol. Embryol.* 59, 203–209.

Carreras-Torras, C., and Gay-Escoda, C. (2015). Techniques for early diagnosis of oral squamous cell carcinoma: systematic review. *Med. Oral Patol. Oral Cir. Bucal* 20, e305–e315. doi: 10.4317/medoral.20347

Chaudhry, A., Manjunath, M., Ashwatappa, D., Krishna, S., and Krishna, A. G. (2016). Comparison of chemiluminescence and toluidine blue in the diagnosis of dysplasia in leukoplakia: a cross-sectional study. *J. Investig. Clin. Dent.* 7, 132–140. doi: 10.1111/jicd.12141

Chen, X. J., Zhang, X. Q., Liu, Q., Zhang, J., and Zhou, G. (2018). Nanotechnology: a promising method for oral cancer detection and diagnosis. *J. Nanobiotechnology* 16:52. doi: 10.1186/s12951-018-0378-6

Chhabra, N., Chhabra, S., and Sapra, N. (2015). Diagnostic modalities for squamous cell carcinoma: an extensive review of literature-considering toluidine blue as a useful adjunct. *J. Maxillofac. Oral Surg.* 14, 188–200. doi: 10.1007/s12663-014-0660-6

Day, G. L., and Blot, W. J. (1992). Second primary tumors in patients with oral cancer. *Cancer* 70, 14–19. doi: 10.1002/1097-0142(19920701)70:1<14::AID-CNCR2820700103>3.0.CO;2-S

El-Sayed, I. H., Huang, X., and El-Sayed, M. A. (2005). Surface plasmon resonance scattering and absorption of anti-EGFR antibody conjugated gold nanoparticles in cancer diagnostics: applications in oral cancer. *Nano Lett.* 5, 829–834. doi: 10.1021/nl050074e

Elvers, D., Braunschweig, T., Hilgers, R. D., Ghassemi, A., Mohlhenrich, S. C., Holzle, F., et al. (2015). Margins of oral leukoplakia: autofluorescence and histopathology. *Br. J. Oral Maxillofac. Surg.* 53, 164–169. doi: 10.1016/j.bjoms.2014.11.004

Epstein, J. B., Gorsky, M., Lonky, S., Silverman, S. Jr., Epstein, J. D., and Bride, M. (2006). The efficacy of oral lumenoscopy (ViziLite) in visualizing oral mucosal lesions. *Spec. Care Dentist.* 26, 171–174. doi: 10.1111/j.1754-4505.2006.tb01720.x

Epstein, J. B., Silverman, S. Jr., Epstein, J. D., Lonky, S. A., and Bride, M. A. (2008). Analysis of oral lesion biopsies identified and evaluated by visual examination, chemiluminescence and toluidine blue. *Oral Oncol.* 44, 538–544. doi: 10.1016/j.oraloncology.2007.08.011

Farah, C. S., Kordbacheh, F., John, K., Bennett, N., and Fox, S. A. (2018). Molecular classification of autofluorescence excision margins in oral potentially malignant disorders. *Oral Dis.* 24, 732–740. doi: 10.1111/odi.12818

Farah, C. S., and McCullough, M. J. (2007). A pilot case control study on the efficacy of acetic acid wash and chemiluminescent illumination (ViziLite) in the visualisation of oral mucosal white lesions. *Oral Oncol.* 43, 820–824. doi: 10.1016/j.oraloncology.2006.10.005

Farah, C. S., Mcintosh, L., Georgiou, A., and Mccullough, M. J. (2012). Efficacy of tissue autofluorescence imaging (VELScope) in the visualization of oral mucosal lesions. *Head Neck* 34, 856–862. doi: 10.1002/hed.21834

Ganga, R. S., Gundre, D., Bansal, S., Shirsat, P. M., Prasad, P., and Desai, R. S. (2017). Evaluation of the diagnostic efficacy and spectrum of autofluorescence of benign, dysplastic and malignant lesions of the oral cavity using VELscope. *Oral Oncol.* 75, 67–74. doi: 10.1016/j.oraloncology.2017.10.023

Gomez, I., Seoane, J., Varela-Centelles, P., Diz, P., and Takkouche, B. (2009). Is diagnostic delay related to advanced-stage oral cancer? A meta-analysis. *Eur. J. Oral Sci.* 117, 541–546. doi: 10.1111/j.1600-0722.2009.00672.x

Hanken, H., Kraatz, J., Smeets, R., Heiland, M., Assaf, A. T., Blessmann, M., et al. (2013). The detection of oral pre- malignant lesions with an autofluorescence based imaging system (VELscope) - a single blinded clinical evaluation. *Head Face Med.* 9:23. doi: 10.1186/1746-160X-9-23

Huang, T. T., Huang, J. S., Wang, Y. Y., Chen, K. C., Wong, T. Y., Chen, Y. C., et al. (2017). Novel quantitative analysis of autofluorescence images for oral cancer screening. *Oral Oncol.* 68, 20–26. doi: 10.1016/j.oraloncology.2017.03.003

Huber, M. A., Bsoul, S. A., and Terezhalmy, G. T. (2004). Acetic acid wash and chemiluminescent illumination as an adjunct to conventional oral soft tissue examination for the detection of dysplasia: a pilot study. *Quintessence Int.* 35, 378–384.

Ibrahim, S. S., Al-Attas, S. A., Darwish, Z. E., Amer, H. A., and Hassan, M. H. (2014). Effectiveness of the Microlux/DLTM chemiluminescence device in screening of potentially malignant and malignant oral lesions. *Asian Pac. J. Cancer Prev.* 15, 6081–6086. doi: 10.7314/APJCP.2014.15.15.6081

Jane-Salas, E., Blanco-Carrion, A., Jover-Armengol, L., and Lopez-Lopez, J. (2015). Autofluorescence and diagnostic accuracy of lesions of oral mucosa: a pilot study. *Braz. Dent. J.* 26, 580–586. doi: 10.1590/0103-6440201300181

Jayaprakash, V., Sullivan, M., Merzianu, M., Rigual, N. R., Loree, T. R., Popat, S. R., et al. (2009). Autofluorescence-guided surveillance for oral cancer. *Cancer Prev. Res.* 2, 966–974. doi: 10.1158/1940-6207.CAPR-09-0062

Kahn, M. A., Hall, J. M., and American Dental Association (2018). *The ADA Practical Guide to Soft Tissue Oral Disease*. Hoboken, NJ: Wiley. doi: 10.1002/9781119437277

Kammerer, P. W., Rahimi-Nedjat, R. K., Ziebart, T., Bemsch, A., Walter, C., Al-Nawas, B., et al. (2015). A chemiluminescent light system in combination with toluidine blue to assess suspicious oral lesions-clinical evaluation and review of the literature. *Clin. Oral Investig.* 19, 459–466. doi: 10.1007/s00784-014-1252-z

Kaur, J., and Jacobs, R. (2015). Combination of Autofluorescence imaging and salivary protoporphyrin in Oral precancerous and cancerous lesions: Non-invasive tools. *J. Clin. Exp. Dent.* 7, e187–e191. doi: 10.4317/jced.52100

Kerr, A. R., Sirois, D. A., and Epstein, J. B. (2006). Clinical evaluation of chemiluminescent lighting: an adjunct for oral mucosal examinations. *J. Clin. Dent.* 17, 59–63.

Koch, F. P., Kaemmerer, P. W., Biesterfeld, S., Kunkel, M., and Wagner, W. (2011). Effectiveness of autofluorescence to identify suspicious oral lesions–a prospective, blinded clinical trial. *Clin. Oral Investig.* 15, 975–982. doi: 10.1007/s00784-010-0455-1

Lalla, Y., Matias, M., and Farah, C. S. (2015). Oral mucosal disease in an Australian urban Indigenous community using autofluorescence imaging and reflectance spectroscopy. *Aust. Dent. J.* 60, 216–224. doi: 10.1111/adj.12320

Lalla, Y., Matias, M. A., and Farah, C. S. (2016). Assessment of oral mucosal lesions with autofluorescence imaging and reflectance spectroscopy. *J. Am. Dent. Assoc.* 147, 650–660. doi: 10.1016/j.adaj.2016.03.013

Lane, P., Follen, M., and Macaulay, C. (2012). Has fluorescence spectroscopy come of age? A case series of oral precancers and cancers using white light, fluorescent light at 405 nm, and reflected light at 545 nm using the Trimira Identafi 3000. *Gend. Med.* 9, S25–S35. doi: 10.1016/j.genm.2011.09.031

Lane, P. M., Gilhuly, T., Whitehead, P., Zeng, H., Poh, C. F., Ng, S., et al. (2006). Simple device for the direct visualization of oral-cavity tissue fluorescence. *J. Biomed. Opt.* 11:024006.

Liu, D., Zhao, X., Zeng, X., Dan, H., and Chen, Q. (2016). Non-Invasive Techniques for Detection and Diagnosis of Oral Potentially Malignant Disorders. *Tohoku J. Exp. Med.* 238, 165–177. doi: 10.1620/tjem.238.165

Lucchese, A., Gentile, E., Romano, A., Maio, C., Laino, L., and Serpico, R. (2016). The potential role of in vivo reflectance confocal microscopy for evaluating oral cavity lesions: a systematic review. *J. Oral Pathol. Med.* 45, 723–729. doi: 10.1111/jop.12454

Marzouki, H. Z., Tuong Vi Vu, T., Ywakim, R., Chauvin, P., Hanley, J., and Kost, K. M. (2012). Use of fluorescent light in detecting malignant and premalignant lesions in the oral cavity: a prospective, single-blind study. *J. Otolaryngol. Head Neck Surg.* 41, 164–168.

McIntosh, L., Mccullough, M. J., and Farah, C. S. (2009). The assessment of diffused light illumination and acetic acid rinse (Microlux/DL) in the visualisation of oral mucosal lesions. *Oral Oncol.* 45, e227–e231. doi: 10.1016/j.oraloncology.2009.08.001

McNamara, K. K., Martin, B. D., Evans, E. W., and Kalmar, J. R. (2012). The role of direct visual fluorescent examination (VELscope) in routine screening for potentially malignant oral mucosal lesions. *Oral Surg. Oral Med. Oral Pathol. Oral Radiol.* 114, 636–643. doi: 10.1016/j.oooo.2012.07.484

Mehrotra, R., Singh, M., Thomas, S., Nair, P., Pandya, S., Nigam, N. S., et al. (2010). A cross-sectional study evaluating chemiluminescence and autofluorescence in the detection of clinically innocuous precancerous and cancerous oral lesions. *J. Am. Dent. Assoc.* 141, 151–156. doi: 10.14219/jada.archive.2010.0132

Messadi, D. V., Younai, F. S., Liu, H. H., Guo, G., and Wang, C. Y. (2014). The clinical effectiveness of reflectance optical spectroscopy for the in vivo diagnosis of oral lesions. *Int. J. Oral Sci.* 6, 162–167. doi: 10.1038/ijos.2014.39

Mojsa, I., Kaczmarzyk, T., Zaleska, M., Stypulkowska, J., Zapala-Pospiech, A., and Sadecki, D. (2012). Value of the ViziLite Plus System as a diagnostic aid in the early detection of oral cancer/premalignant epithelial lesions. *J. Craniofac. Surg.* 23, e162–e164. doi: 10.1097/SCS.0b013e31824cdbea

Moro, A., De Waure, C., Di Nardo, F., Spadari, F., Mignogna, M. D., Giuliani, M., et al. (2015). The GOCCLES(R) medical device is effective in detecting oral cancer and dysplasia in dental clinical setting. Results from a multicentre clinical trial. *Acta Otorhinolaryngol. Ital.* 35, 449–454. doi: 10.14639/0392-100X-922

Moro, A., Di Nardo, F., Boniello, R., Marianetti, T. M., Cervelli, D., Gasparini, G., et al. (2010). Autofluorescence and early detection of mucosal lesions in patients at risk for oral cancer. *J. Craniofac. Surg.* 21, 1899–1903. doi: 10.1097/SCS.0b013e3181f4afb4

Nagi, R., Reddy-Kantharaj, Y. B., Rakesh, N., Janardhan-Reddy, S., and Sahu, S. (2016). Efficacy of light based detection systems for early detection of oral cancer and oral potentially malignant disorders: systematic review. *Med. Oral Patol. Oral Cir. Bucal* 21, e447–e455. doi: 10.4317/medoral.21104

Oh, E. S., and Laskin, D. M. (2007). Efficacy of the ViziLite system in the identification of oral lesions. *J. Oral Maxillofac. Surg.* 65, 424–426. doi: 10.1016/j.joms.2006.10.055

Ohnishi, Y., Fujii, T., Ugaki, Y., Yasui, H., Watanabe, M., Dateoka, S., et al. (2016). Usefulness of a fluorescence visualization system for the detection of oral precancerous and early cancerous lesions. *Oncol. Rep.* 36, 514–520. doi: 10.3892/or.2016.4776

Paderni, C., Compilato, D., Carinci, F., Nardi, G., Rodolico, V., Lo Muzio, L., et al. (2011). Direct visualization of oral-cavity tissue fluorescence as novel aid for early oral cancer diagnosis and potentially malignant disorders monitoring. *Int. J. Immunopathol. Pharmacol.* 24, 121–128. doi: 10.1177/03946320110240S221

Patton, L. L., Epstein, J. B., and Kerr, A. R. (2008). Adjunctive techniques for oral cancer examination and lesion diagnosis: a systematic review of the literature. *J. Am. Dent. Assoc.* 139, 896–905;quiz993–894. doi: 10.14219/jada.archive.2008.0276

Poh, C. F., Zhang, L., Anderson, D. W., Durham, J. S., Williams, P. M., Priddy, R. W., et al. (2006). Fluorescence visualization detection of field alterations in tumor margins of oral cancer patients. *Clin. Cancer Res.* 12, 6716–6722. doi: 10.1158/1078-0432.CCR-06-1317

Rajmohan, M., Rao, U. K., Joshua, E., Rajasekaran, S. T., and Kannan, R. (2012). Assessment of oral mucosa in normal, precancer and cancer using chemiluminescent illumination, toluidine blue supravital staining and oral exfoliative cytology. *J. Oral Maxillofac. Pathol.* 16, 325–329. doi: 10.4103/0973-029X.102476

Ram, S., and Siar, C. H. (2005). Chemiluminescence as a diagnostic aid in the detection of oral cancer and potentially malignant epithelial lesions. *Int. J. Oral Maxillofac. Surg.* 34, 521–527. doi: 10.1016/j.ijom.2004.10.008

Rana, M., Zapf, A., Kuehle, M., Gellrich, N. C., and Eckardt, A. M. (2012). Clinical evaluation of an autofluorescence diagnostic device for oral cancer detection: a prospective randomized diagnostic study. *Eur. J. Cancer Prev.* 21, 460–466. doi: 10.1097/CEJ.0b013e32834fdb6d

Roblyer, D., Kurachi, C., Stepanek, V., Williams, M. D., El-Naggar, A. K., Lee, J. J., et al. (2009). Objective detection and delineation of oral neoplasia using autofluorescence imaging. *Cancer Prev. Res.* 2, 423–431. doi: 10.1158/1940-6207.CAPR-08-0229

Sambandham, T., Masthan, K. M., Kumar, M. S., and Jha, A. (2013). The application of vizilite in oral cancer. *J. Clin. Diagn. Res.* 7, 185–186. doi: 10.7860/JCDR/2012/5163.2704

Sawan, D., and Mashlah, A. (2015). Evaluation of premalignant and malignant lesions by fluorescent light (VELscope). *J. Int. Soc. Prev. Commun. Dent.* 5, 248–254. doi: 10.4103/2231-0762.159967

Scheer, M., Fuss, J., Derman, M. A., Kreppel, M., Neugebauer, J., Rothamel, D., et al. (2016). Autofluorescence imaging in recurrent oral squamous cell carcinoma. *Oral Maxillofac. Surg.* 20, 27–33. doi: 10.1007/s10006-015-0520-7

Scheer, M., Neugebauer, J., Derman, A., Fuss, J., Drebber, U., and Zoeller, J. E. (2011). Autofluorescence imaging of potentially malignant mucosa lesions. *Oral*

Surg. Oral Med. Oral Pathol. Oral Radiol. Endod. 111, 568–577. doi: 10.1016/j.tripleo.2010.12.010

Sweeny, L., Dean, N. R., Magnuson, J. S., Carroll, W. R., Clemons, L., and Rosenthal, E. L. (2011). Assessment of tissue autofluorescence and reflectance for oral cavity cancer screening. *Otolaryngol. Head Neck Surg.* 145, 956–960. doi: 10.1177/0194599811416773

Ujaoney, S., Motwani, M. B., Degwekar, S., Wadhwan, V., Zade, P., Chaudhary, M., et al. (2012). Evaluation of chemiluminescence, toluidine blue and histopathology for detection of high risk oral precancerous lesions: a cross-sectional study. *BMC Clin. Pathol.* 12:6. doi: 10.1186/1472-6890-12-6

Vashisht, N., Ravikiran, A., Samatha, Y., Rao, P. C., Naik, R., and Vashisht, D. (2014). Chemiluminescence and toluidine blue as diagnostic tools for detecting early stages of oral cancer: an invivo study. *J. Clin. Diagn. Res.* 8, ZC35–ZC38. doi: 10.7860/JCDR/2014/7746.4259

Vigneswaran, N., Koh, S., and Gillenwater, A. (2009). Incidental detection of an occult oral malignancy with autofluorescence imaging: a case report. *Head Neck Oncol.* 1:37. doi: 10.1186/1758-3284-1-37

Walling, M. A., Novak, J. A., and Shepard, J. R. (2009). Quantum dots for live cell and in vivo imaging. *Int. J. Mol. Sci.* 10, 441–491. doi: 10.3390/ijms10020441

Warnakulasuriya, S. (2009). Global epidemiology of oral and oropharyngeal cancer. *Oral Oncol.* 45, 309–316. doi: 10.1016/j.oraloncology.2008.06.002

Yamamoto, N., Kawaguchi, K., Fujihara, H., Hasebe, M., Kishi, Y., Yasukawa, M., et al. (2017). Detection accuracy for epithelial dysplasia using an objective autofluorescence visualization method based on the luminance ratio. *Int. J. Oral Sci.* 9:e2. doi: 10.1038/ijos.2017.37

Yang, E. C., Tan, M. T., Schwarz, R. A., Richards-Kortum, R. R., Gillenwater, A. M., and Vigneswaran, N. (2018). Noninvasive diagnostic adjuncts for the evaluation of potentially premalignant oral epithelial lesions: current limitations and future directions. *Oral Surg. Oral Med. Oral Pathol. Oral Radiol.* 125, 670–681. doi: 10.1016/j.oooo.2018.02.020

Conflict of Interest Statement: The authors declare that the research was conducted in the absence of any commercial or financial relationships that could be construed as a potential conflict of interest.

frontiers in Physiology

REVIEW
published: 08 August 2018
doi: 10.3389/fphys.2018.01102

Novel Biological and Technological Platforms for Dental Clinical Use

*Giovanna Orsini[1,2], Pierfrancesco Pagella[1], Angelo Putignano[2] and Thimios A. Mitsiadis[1]**

[1] Orofacial Development and Regeneration, Institute of Oral Biology, Center of Dental Medicine, Faculty of Medicine, University of Zurich, Zurich, Switzerland, [2] Department of Clinical Sciences and Stomatology, Marche Polytechnic University, Ancona, Italy

Human teeth have a limited capacity to regenerate and thus biological reconstruction of damaged or lost dental tissues remains a significant challange in modern dentistry. Recent efforts focus on alternative therapeutic approaches for partial or whole tooth regeneration that complement traditional dental treatments using sophisticated materials and dental implants. These multidisciplinary approaches are based on the combination of stem cells with advanced tissue engineer products and computing technology, and they hold great promise for future applications in dentistry. The administration to patients of dynamic biological agents composed by stem cells and scaffolds will certainly increase the regenerative capacity of dental pathological tissues. The design of innovative materials for tissue restoration, diagnostics, imaging, and targeted pharmaceutical treatment will significantly improve the quality of dental care and will have a major societal impact. This review depicts the current challenges in dentistry and describes the possibilities for novel and succesful therapeutic applications in the near future.

Keywords: tooth, dental treatment, stem cells, organ-on-chip, organoids, dental implants, dental pulp, periodontium

OPEN ACCESS

Edited by:
Catherine Chaussain, Université Paris Descartes, France

Reviewed by:
Thomas G. H. Diekwisch, Texas A&M University, United States
Ivo Lambrichts, University of Hasselt, Belgium
Jean-Christophe Farges, Claude Bernard University Lyon 1, France

****Correspondence:***
Thimios A. Mitsiadis
thimios.mitsiadis@zzm.uzh.ch

Specialty section:
This article was submitted to Craniofacial Biology and Dental Research, a section of the journal Frontiers in Physiology

Received: *20 June 2018*
Accepted: *23 July 2018*
Published: *08 August 2018*

Citation:
Orsini G, Pagella P, Putignano A and Mitsiadis TA (2018) Novel Biological and Technological Platforms for Dental Clinical Use. Front. Physiol. 9:1102. doi: 10.3389/fphys.2018.01102

INTRODUCTION: THE TOOTH ORGAN

The tooth organ is composed by a unique combination of hard and soft tissues. The outermost layer is constituted by enamel, the most mineralized tissue of the human body, which guarantees protection to the inner elements of the tooth (**Figure 1**). Enamel displays unique physical characteristics, such as complex three-dimensional organization and extremely long hydroxyapatite crystallites, to resist large masticatory forces and continual attacks by acids from food and bacterial sources (Boyde, 1997). Ameloblasts, which are the epithelial cells responsible for enamel formation, and their precursors are lost upon tooth eruption, making human adult teeth inapt of enamel regeneration. The great complexity of enamel, together with the absence of appropriate cells in adult patients, make therapies aiming to enamel regeneration an exciting challenge.

Due to its extremely high mineral content, enamel is very brittle. This property is compensated by dentin, a less mineralized, elastic, avascular tissue (**Figure 1**). Dentin encloses the dental pulp, a soft connective tissue that conveys vascularization and innervation, representing the vital core of the tooth organ (**Figure 1**). The vascular system provides oxygen, nutrients and metabolites, while sensory innervation is fundamental for the perception of pain, heat/cold and mechanosensation that controls biting strength. In the peripheral boundary of the dental pulp

are situated mesenchymal-derived odontoblasts, which produce and maintain dentin. Dentin is characterized by closely packed tubules traversing its thickness and containing the cytoplasmatic extensions of odontoblasts, as well as sensory nerve terminals, which render dentin highly sensitive to external stimuli. More importantly, dentin can repair itself, due to the activation of the existing odontoblasts or the newly formed odontoblasts derived from pulp stem cells that produce a reactionary mineralized matrix upon injury. However, pulp reaction is not sufficient in case of severe tooth injury and/or extensive infection, and this healing failure often leads to pulp irreversible inflammation followed by necrosis (DeRosa, 2006).

The tooth is anchored to the alveolar bone by the roots, constituted by dentin and cementum. Roots are connected to the alveolar bone by a specialized connective tissue, the periodontal ligament, which ensures tooth stability, provides sensory information and absorbs mechanical stresses during chewing (**Figure 1**). Periodontal disease is the most frequent cause of tooth loss, making periodontal regeneration a pressing need for the dental field (Mitsiadis et al., 2015).

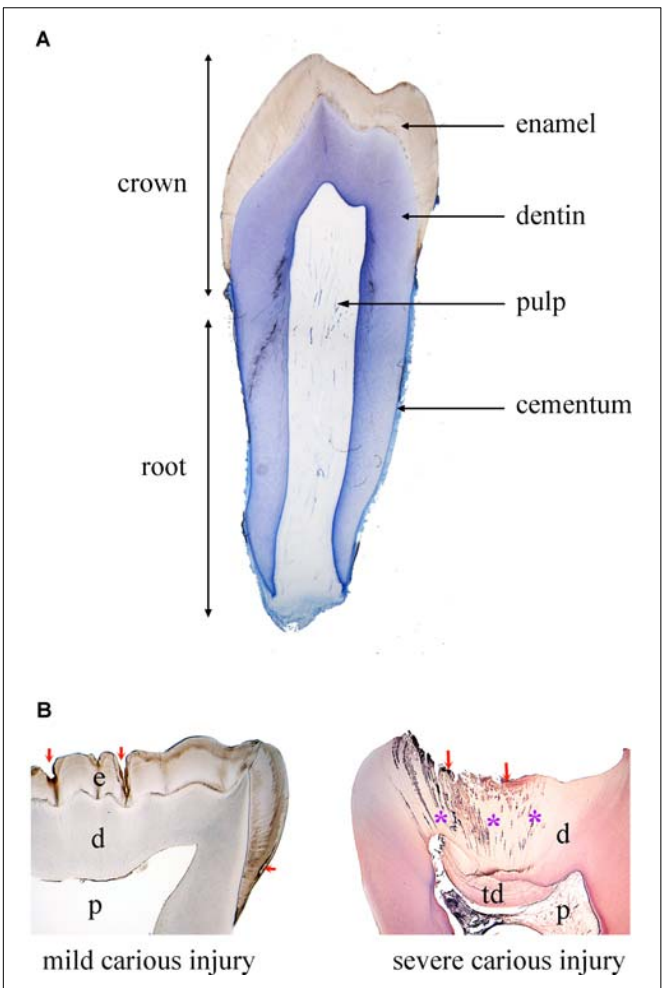

FIGURE 1 | Tooth structure in physiological and pathological conditions. **(A)** Histological section of a human premolar (blue color: toluidine blue). **(B)** Histological sections of human carious teeth. Left side: ground unstained section, showing mild carious injuries (red arrows) affecting only enamel. Right side: decalcified section stained with hematoxylin and eosin, showing a severe carious injury (red arrows) with bacterial invasion (asterisks: bacterial front within dentin). Abbreviations: d, dentin; e, enamel; p, pulp; td, tertiary dentin.

The structural hallmarks of dental hard tissues are strictly dependent on tightly regulated and long developmental processes that cannot be easily reproduced within acceptable therapeutic time frames. Moreover, the oral cavity constitutes a challenging environment for any regenerative approach, as it is constantly exposed to chemical, mechanical and bacterial insults. Despite these difficulties, recent technological advancements are becoming an inherent aspect of dental practice, improving effectiveness of treatments. Similarly, the continuous developments in stem cell research and nanotechnology are paving the way for regenerative approaches in dentistry.

INNOVATION IN CURRENT DENTAL TREATMENTS: FROM MATERIALS TO TOOTH REGENERATION

The great improvements in computing-related technologies and materials has widened the options to alternative and more precise dental treatments (Beuer et al., 2008; Hancocks, 2017), and helped in establishing more reliable diagnostic tools and therapeutic plans (Levato et al., 2015; Lynch, 2017). Numerous advancements have been made with the advent of novel imaging techniques such as computer-aided design and manufacturing (CAD/CAM) technology, optimized intraoral imaging, digital radiography, and computer aided implant surgery (Hammerle et al., 2009; Levato et al., 2015; Zhou et al., 2018). Apart from its use as a diagnostic tool, imaging contributed to the improvement of the daily dental practice, since treatments benefited from high definition microscopes that permit the detailed visualization of the operative dental field (Del Fabbro et al., 2015).

Material sciences have led the way for the development of therapeutic approaches aiming to substitute damaged or lost dental tissues. Despite limitations in functionality and longevity, biomaterials are still present in dental treatments since nanotechnology has remarkably improved their performance and the clinical outcome of certain procedures. The combination of nanomaterials with advanced technologies has upgraded prosthetic and aesthetic dentistry, which are fields aiming to optimize the functional and aesthetic appearance of dentition. 3D printing systems represent the most innovative next-step technology, aiming to manufacture customized products based on computer-designed digital tools (Yang et al., 2018). Pain management has also enormously benefited from the advent of these novel technologies (Banerjee et al., 2011). To minimize pain perception, low-level laser therapy and light emitting diode therapy (also known as photobiomodulation) have been used. These processes induce analgesia but also promote tissue healing and reduce inflammation and/or oedema by stimulating cell response (Carroll et al., 2014). Their efficacy has been already demonstrated for the treatment of trigeminal neuralgia, pain management during orthodontic treatment and

following surgeries within the orofacial complex, and dentin hypersensitivity (Kathuria et al., 2015).

However, the most important development of the last decade is the rise of a new dental discipline that is based on the capacity of stem cells to repair or regenerate various impaired tissues. Stem cell-based regenerative dentistry is linked to advanced tissue engineering products and nanotechnology, which have created an important clinical shift toward the functional repair and regeneration of damaged dental tissues.

Combining Stem Cell Biology and Nanotechnology for Regenerating Dental Tissues

Stem cells are characterized by their potential to self-replicate and their capacity to differentiate into a vast variety of cells populations (Mitsiadis and Graf, 2009). Epithelial and mesenchymal stem cell populations are present in almost all adult human tissues and organs, including teeth. A variety of dental mesenchymal stem cells (DMSCs) populations have been isolated from both deciduous and permanent teeth, characterized, and tested for their potential applications in regenerative dentistry (Gronthos et al., 2000; Gronthos et al., 2002; Miura et al., 2003). Adult DMSCs localized in the dental pulp and periodontal tissue ensure human tooth homeostasis and regeneration (Bluteau et al., 2008), and therefore represent optimal clinical tools for the repair of damaged dental tissues. Actual efforts are oriented toward pulp and periodontal tissue repair, where these tissues can be regenerated by transplantation of stem cells alone or in combination with functionalized scaffolds. More challenging and problematic is, however, the regeneration of tooth enamel using epithelial cells, since neither dental epithelial stem cells (DESCs) nor ameloblasts are present in the crown of adult functional teeth (Mitsiadis et al., 2015; Orsini et al., 2015). More exiting, but greatly perplexing, is the perspective to generate entire brand-new teeth by mixing DESCs and DMSCs. Although very difficult to be realized, several attempts toward this direction have been pursued in animal models (Oshima and Tsuji, 2014).

The success and efficacy of any stem cell-mediated therapy can be evaluated by a set of modern nanotechnology tools, since they allow tracking the migration, fate and regenerative impact of stem cells *in vivo*. For example, transplanted stem cells can be tracked for long periods with non-invasive imaging techniques using fluorescent dyes (Arbab et al., 2009; Gera et al., 2010), and with magnetic nanoparticles that can be traced by MRI and provide information about their kinetics and fate during dental tissue regeneration (Jimenez-Rojo et al., 2012). This knowledge could be used for designing appropriate scaffolds that will host stem cells before transplantation. Furthermore, it will allow evaluating the therapeutic efficacy of precise dental stem cell populations that have been exposed to specific microenvironments. Indeed, artificial microenvironments, which may direct stem cells toward a precise fate and function, can be achieved through nanotechnology (Bluteau et al., 2008). A big variety of nanoscale biodegradable structures with specific size, surface chemistry and shape can be used for the creation of microenvironments that are adapted for the needs of regenerative dentistry (Mitsiadis et al., 2012). Such biodegradable scaffolds, once transplanted, may act as temporary niches that control stem cell behavior and guide dental tissue repair (Iwatsuki et al., 2006).

It is obvious that the range of dental disciplines that can benefit from the recent advances of stem cell biology, material sciences and nanotechnology is extremely wide. The present mini-review covers current and future therapeutic approaches for managing the (1) damage of the tooth crown, including the harm of enamel and/or dentin-pulp tissues, (2) periodontal insults, and (3) tooth loss.

TOOTH CROWN DAMAGE

Current Restorative Treatments

Enamel and dentin of the tooth crown are most often the first tissues to be affected following traumatic injuries or carious lesions (**Figure 1**). Prompt and efficient repair of enamel and/or dentin is fundamental to prevent infection and damage extending toward dental soft tissues (i.e., dental pulp, periodontium) and alveolar bone. The most used approach for treating enamel and dentin harm is the substitution and restoration of the destroyed or lost dental hard tissues by sophisticated composite materials. However, traditional adhesive systems are unstable and fail over time, thus leading to marginal leakage and poor retention of the restoration in the tooth (Breschi et al., 2018). Therefore, a major task of nanotechnology in dentistry is to develop novel durable materials and adhesive systems with improved enamel- and/or dentin-bonding performance in order to increase the longevity of the restorations and prevent repeated treatments. Indeed, the introduction of novel materials such as phosphine oxide initiators and monomethacrylate diluents has led to dental composites with satisfactory and adequate properties (Kilambi et al., 2009). The introduction of nanofillers and nanomaterials led to even more significant advances in terms of optimizing the properties and performance of the composites (Ilie et al., 2013; Goracci et al., 2014; Monterubbianesi et al., 2016). These nanotechnology-based strategies using cross-linking agents and Ca- and P-releasing means, which mimic the process of natural dentin mineralization, have also reduced the degradation of the resin-dentin bonded interface (Mazzoni et al., 2018).

Ceramic-based materials are privileged by dentists for the restoration of damaged tooth crowns, mainly because of their superior aesthetic appearance and biocompatibility (Wittneben et al., 2017; Ozcan and Jonasch, 2018). To overcome the fact that ceramic materials are brittle and prone to cracks propagation, several transformation/toughening mechanisms have been developed, leading to higher aging resistant-ceramics (Zhang et al., 2017) such as zirconia with exceptional toughness and flexural strength (Guazzato et al., 2004).

Nanomodified materials could be also designed for controlling oral microbiota and the formation of dental plaque, and, furthermore, for enhancing the mineralization process in the cases of enamel wear and/or dentin hypersensitivity due to the extensive consumption of acidic drinks (Orsini et al., 2013; Lelli et al., 2014). Indeed, the use of synthetic nanohydroxyapatite particles and other Ca-based nanomodified

materials in dentifrices may offer a protective nanostructured coating on the tooth surface that simultaneously restores the lost minerals from enamel (Orsini et al., 2013; Lelli et al., 2014).

The preservation of the dental pulp, which is a living tissue ensuring tooth physiological function, is of prime importance during the treatment of a damaged tooth crown. In very severe tooth injury, the pulp is also affected and may lose its vitality. Therefore, the endodontic therapy (i.e., pulp tissue removal) is imposed in order to prevent further bacterial progression and damage of the surrounding alveolar bone. This is followed by disinfection of the dental root canals and the replacement of the pulp tissue with inorganic materials. Devitalized teeth are more fragile than normal teeth and consequently are predisposed to postoperative fractures (DeRosa, 2006).

Challenges in Dentin-Pulp Regeneration

Regenerative endodontics aims at reforming the original pulp tissue morphology and physiology based on tissue engineering principles (Murray and Garcia-Godoy, 2006; Diogenes and Hargreaves, 2017). Nanomaterials can be used either alone or implemented with growth factors and stem cells in order to stimulate and enhance the regenerative capacity of the pulp tissue. Adjustment of biomaterials for dental specific purposes would require adjustments at a nanoscale level, thus allowing multifunctionality within a given small surface, increasing the quality of targeting, and better controlling bioactive molecules delivery (Fioretti et al., 2011; Diogenes and Ruparel, 2017). Nanomaterials developed for endodontic purposes can deliver antibacterial and anti-inflammatory molecules, as well as growth factors that will guide the behavior (e.g., cell migration, proliferation, and differentiation) of the various dental pulp cell populations (e.g., pulp fibroblasts, endothelial cells, neuronal cells, immune cells). Biomimetic scaffolds composed of natural molecules, such as type I collagen, hyaluronic acid and chitosan, combined with nanoassembled materials possessing anti-inflammatory capabilities have been generated to stimulate pulp tissue regeneration and to prevent inflammation (Fioretti et al., 2011). Although such nanofibrous and microporous membranes have provided promising results, significant improvements are still needed to create scaffolds that promote proper pulp regeneration (Yamauchi et al., 2011; Albuquerque et al., 2014).

Numerous attempts using human DMSCs have been made in a variety of animal models in order to achieve complete dental pulp regeneration (**Figure 2A**), a process that also requires neovascularization and re-innervation of this tissue.

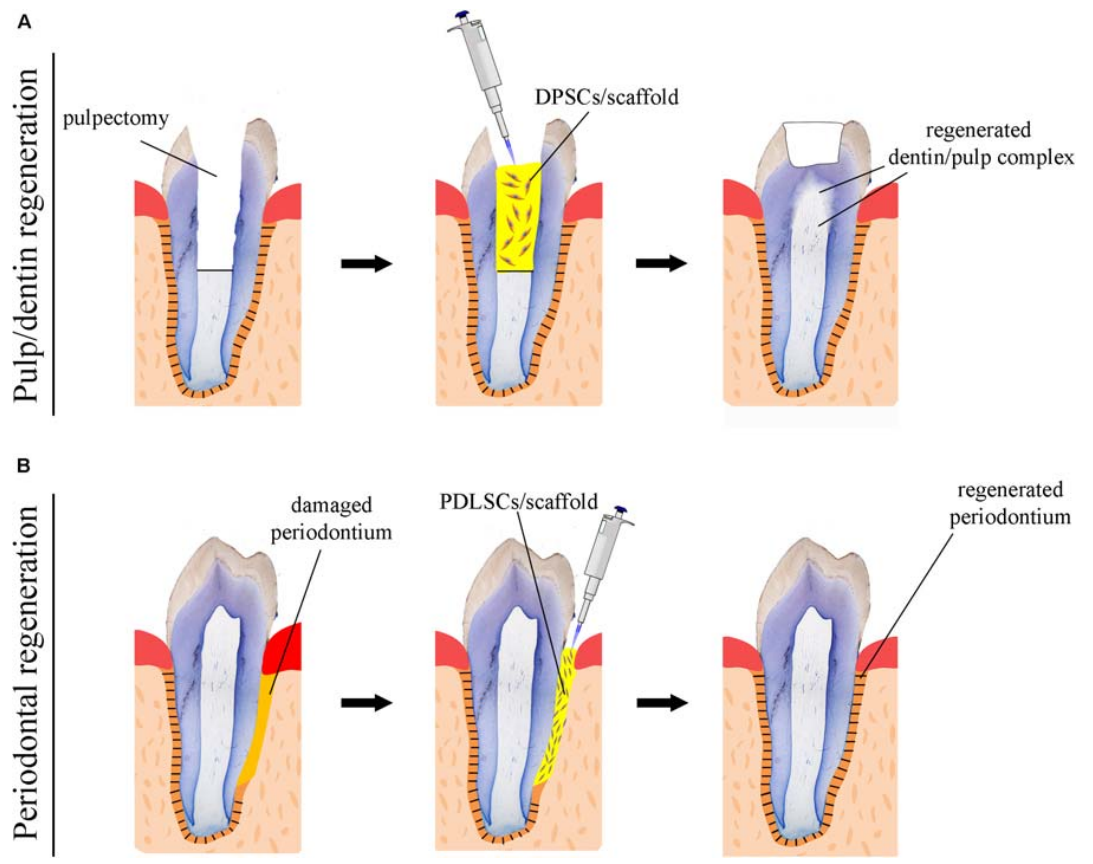

FIGURE 2 | Schematic representation of stem cell-based regenerative approaches in dentistry. **(A)** Use of scaffolds (yellow color) seeded with dental pulp stem cells (DPSCs) for the repair of the dentin-pulp complex. **(B)** Use of scaffolds (yellow color) seeded with periodontal ligament stem cells (PDLSCs) for the regeneration of the damaged periodontium.

Experiments have shown that human DMSCs are capable to differentiate into odontoblasts and to form dentin-like structures when transplanted together with a ceramic powder in immune-compromised mice *ex vivo* (Gronthos et al., 2000; Gronthos et al., 2002). Similar studies have revealed that human DMSCs seeded on poly-D, L-lactide/glycol scaffolds are able to regenerate vascularized pulp tissue when transplanted into an empty mouse tooth root canal (Volponi et al., 2010; Hayashi et al., 2015). Recently, new experimental strategies have been elaborated, where DMSCs-seeded scaffolds combined with bioactive molecules fulfill the empty pulp chamber immediately after pulp removal (Albuquerque et al., 2014; Piva et al., 2014). Pilot studies in humans have demonstrated the safety and efficacy of DMSCs for complete dental pulp regeneration and new dentin formation (Nakashima and Iohara, 2017; Nakashima et al., 2017). Bone morphogenetic proteins (BMPs) have been commonly used for accelerating and enhancing the production of dentin during dental pulp regeneration (Luiz De Oliveira Da Rosa et al., 2017). While these stem cell-based procedures appear to improve pulp tissue regeneration, their effectiveness for achieving accurate, precise and long-lasting therapies is still unclear. As a matter of fact, most approaches aiming at dental pulp regeneration led to the formation of fibrotic tissues that can undergo degeneration over time or be replaced with bone. The possibility to decellularise healthy human dental pulps (Song et al., 2017) opens new horizons in regenerative dentistry since these decellularised tissues could serve as natural scaffolds for supporting transplanted autologous DMSCs. Decellularised pulps represent ideal biomaterials for hosting stem cells and guiding neovascularization and re-innervation within the regenerating tissues. Moreover, novel 3D printing strategies has been developed to engineer prevascularized pulp-like hydrogel tissue constructs in full-length root canals (Athirasala et al., 2017).

While significant efforts have been produced so far, regenerative procedures have to be further investigated in order to ultimately provide evidence of functional dental pulp regeneration *in vivo* (**Figure 2A**; Torabinejad and Faras, 2012; Diogenes and Ruparel, 2017).

Challenges in Enamel Regeneration

De novo formation of enamel in humans is one of the greatest challenges in regenerative dentistry, since amelogenesis is a very complex process and DESCs that could regenerate enamel are very rare in adult human teeth. Very few dental epithelial cells with stem cell properties have been isolated from the periodontal tissue (i.e., epithelial rests of Malassez, ERM). Experiments using porcine ERM have demonstrated that these cells can differentiate into ameloblasts when co-cultured with dental pulp cells *in vitro* and can form enamel structures after their transplantation *in vivo* (Shinmura et al., 2008). Although ERM is a potential stem cell source for enamel regeneration, availability of these cells in human teeth is scarce, making thus necessary the identification of other epithelial stem cell populations of non-dental origin that could differentiate into enamel-producing ameloblasts.

Another key issue in generating new enamel is time. The accomplishment of proper enamel formation requires many years, a time frame clearly incompatible with clinical needs. Moreover, mild disturbances during this process could lead to the generation of defective enamel (Cantu et al., 2017). Therefore, any procedure and technique that will be able to considerably accelerate the process of amelogenesis will be of benefit to the patients and dental community.

PERIODONTAL DISEASES

Current Periodontal Therapies

Periodontium is a common site of pathologies that severely affect not only the structure of the surrounding tissues (i.e., dental root, alveolar bone) but also tooth functionality. Severe inflammation to the periodontium leads to significant alterations in both the structure and quantity of the alveolar bone, a process that ultimately may cause tooth loss (Lindhe et al., 1983). Contemporary, periodontal therapies include a wide range of surgical procedures along with use of bone grafts as tissue substitutes, barrier membranes for protecting the healing area from undesirable epithelial tissues (Howell et al., 1997; Aghaloo and Moy, 2007), and growth factors for enhancing the healing capacity of the harmed tissues (Lynch et al., 1991b). Bone grafting materials, aiming to stimulate bone augmentation and periodontal regeneration, include intraoral or extraoral autografts, freeze-dried and fresh-frozen bone allografts, animal-derived bone deproteinised xenografts, and hydroxyapatite and beta-tricalcium phosphate alloplasts (Pilipchuk et al., 2015; Sheikh et al., 2017). These grafting materials could be used alone or in association with various growth factors. It has been shown that application of these regenerative methods in clinics allowed the formation of novel osseous tissues with similar to the pre-existent native bone characteristics (Scarano et al., 2006; De Angelis et al., 2011; Danesh-Sani et al., 2016; Clark et al., 2018). Even though, these approaches do not always ensure a predictable and desirable outcome of periodontal regeneration and often result in healing with epithelial lining rather than new periodontal tissue formation (Lynch, 1992).

Challenges in Periodontal Regeneration

A fundamental goal in regenerative dentistry is to reconstruct a functional periodontium consisting of new cementum, alveolar bone and periodontal ligament around the tooth root damaged area (**Figure 2B**). DMSCs isolated from the periodontal space (i.e., periodontal ligament stem cells, dental follicle stem cells) of human teeth can differentiate into the various cell types of the periodontium *in vitro* when combined with different scaffolds or dentin matrix (Takahashi and Yamanaka, 2006; Washio et al., 2010; Arakaki et al., 2012; Yang et al., 2012). These stem cell populations have been shown to improve periodontal regeneration when transplanted into immunocompromised animals *ex vivo*, indicating their great potential for future stem cell-based therapies in dentistry (Seo et al., 2004; Caton et al., 2011). A variety of growth factors have been also used for improving the regenerative efficacy of stem cells in the periodontium. Diverse experiments have demonstrated that platelet-derived growth factors (PDGFs) stimulate periodontal

tissue regeneration (Lynch et al., 1991b; Howell et al., 1997; Clark et al., 2018), while BMPs enhance alveolar bone and cementum production (Lynch et al., 1989; Howell et al., 1997; Selvig et al., 2002). However, excessive bone formation that results in tooth ankylosis can be a frequent side effect following the use of BMPs, since these molecules favor and direct stem cells differentiation toward the osteogenic fate. An optimum way to ensure the delivery of a large amount of growth factors is to use blood constructs as platelet-rich plasma (PRP) integrated with different biological and synthetic grafts (Fernandes and Yang, 2016). It is expected that PRP will greatly promote tissue regeneration, since the healing process is triggered by the factors present in PRP. Indeed, clinical trials have shown that periodontal regeneration was promoted by the use of a combination of PRP and stem cells (Fernandes and Yang, 2016). However, there are still important issues to be addressed linked to the standardization of constructs preparations, the efficiency of their delivery and the patient-specific immune responses (Dhillon et al., 2012; Fernandes et al., 2016).

Clinical studies have demonstrated that enamel matrix derivatives also assist and promote periodontal tissue regeneration (Miron et al., 2016b, 2017). Advanced new bone grafting materials with improved physicochemical properties have been used as carriers of enamel protein derivatives in order to further improve their clinical performance (Miron et al., 2016a,b). Nevertheless, despite the very encouraging clinical outcomes, the mechanism of action of these enamel matrix molecules is not yet clear.

More recently, several attempts to achieve fast and effective periodontal regeneration have been performed using 3D printed and micropatterned biomaterials that provide architectural guidance for cell alignment and guidance during tissue repair (Pilipchuk et al., 2016).

TOOTH LOSS

Current Dental Implant Treatments

The use of dental implants has become a common and successful treatment for replacing missing teeth for pathologic, traumatic, and genetic causes (**Figure 3**; Esposito et al., 2014). A typical dental implant is composed of a metal screw part that interfaces and integrates within the alveolar bone, and another part where tooth crown substitutes are placed. The retention of a dental implant requires its close contact with the alveolar bone, a process termed osseointegration. Despite their large and regular usage in dental clinics, implants still need significant improvements, particularly in their capacity to stimulate cellular events at the implantation site that would guarantee their long-term integration and retention (Variola et al., 2009, 2011). The use of nanotechnology has improved the osseointegration of implants by modifying their surfaces, thus allowing the shortening of the healing period (Barbucci et al., 2003; Mendonca et al., 2008). Indeed, zinc-modified calcium silicate coatings, nanohydroxyapatite-blasted surfaces, nanotextured blasted titanium surfaces, as well as gold nanoparticles coated surfaces have considerably enhanced the adhesive properties of implants and therefore their osseointegration (Coelho et al., 2016; Heo et al., 2016; Bezerra et al., 2017; Yu et al., 2017). However, there is a major risk of infection of tissues surrounding the implant, a pathology termed peri-implantitis (Singh, 2011). *In vitro* and *in vivo* studies have shown that the incorporation of antibacterial agents to dental implants (e.g., silver nanoparticles) could partly prevent the growth of bacteria and therefore decrease the percentage of implant treatments failure (Godoy-Gallardo et al., 2016; Pokrowiecki et al., 2017). It has been also demonstrated that gallium-modified chitosan/poly (acrylic acid) bilayer coatings might improve titanium implant performances by limiting bacterial adhesion and proliferation (Bonifacio et al., 2017). Dental implants have also benefited from regenerative technologies using scaffolds, stem cells and growth factors that contribute to enhanced osseointegration and host tissue response (Pilipchuk et al., 2015). Despite a good number of preclinical studies in large animal models for guided bone and periodontal regeneration around implants using growth factors and protein delivery systems (Lynch et al., 1991a; Selvig et al., 2002; Sauerbier et al., 2011; Alvarez et al., 2012; Larsson et al., 2016), and the evident clinical advantages, well-conducted human randomized clinical studies that will definitively validate these approaches are still lacking (Seo et al., 2004; Caton et al., 2011; Rickert et al., 2011; Sauerbier et al., 2011). To date, only few randomized clinical trials have been performed and therefore it is absolutely necessary the realization of larger trials (Kaigler et al., 2013, 2015).

Challenges in Entire Tooth Regeneration

Regeneration of entire brand-new teeth for the replacement of missing or lost teeth is the most ambitious goal in dentistry and requires the use and recombination of dental mesenchymal and epithelial stem cells (Papagerakis and Mitsiadis, 2013; Otsu et al., 2014). DMSCs can form all mesenchymal components of the tooth organ and the surrounding tissues such as dentin, cementum, and alveolar bone, while DESCs are essential for the generation of enamel. Since most of the dental epithelial cell populations disappear shortly after tooth eruption and DESCs are limited in human adult teeth, current knowledge on DESCs has been obtained mainly from rodents, where they contribute to the renewal of the enamel in the continuously growing incisors (Mitsiadis and Harada, 2015).

Two main strategies have been elaborated for constructing whole new teeth (Mitsiadis and Papagerakis, 2011; Otsu et al., 2014; Mitsiadis and Harada, 2015). One approach consists in recombining and culturing DESCs and DMSCs *in vitro* until they will form a tooth germ that subsequently will be transplanted into the alveolar bone. It is expected that this tooth germ will further develop and grow, erupt and finally become a functional tooth. Another approach relies to tooth-shaped polymeric biodegradable scaffolds that are filled with both DESCs and DMSCs and implanted into the alveolar bone, expecting that will finally give rise to functional teeth. The three-dimensional structure of the scaffolds should drive the differentiation of the transplanted stem cells into odontoblasts and ameloblasts (Bluteau et al., 2008). Indeed, several experiments in mice using bioengineered approaches have revealed that functional teeth with appropriate crowns,

FIGURE 3 | Tooth replacement and correction of aesthetics in a patient. **(A)** Preoperative intraoral view of a young patient with a congenital missing tooth and compromised aesthetics of the other teeth. **(B)** Upon orthodontic, surgical and implant treatment, the teeth were prepared for aesthetic prosthetic rehabilitation. Asterisk indicates dental implant impression coping. **(C)** Postoperative intraoral view of the patient with the final ceramic restorations.

dental pulp, roots and periodontal ligament can be formed following their implantation in mandibles (Jimenez-Rojo et al., 2012; Oshima and Tsuji, 2014; Otsu et al., 2014; Mitsiadis and Harada, 2015). However, similar results have not yet been obtained with human cells, due mainly to the limited number of adult DESCs and the significantly elongated time period that is needed for proper human tooth development. Penury of DESCs within human adult teeth might be successfully addressed by differentiating patient-specific inducible pluripotent stem cells (iPSCs) into DESCs. Certain studies have shown that iPSCs technology could be successfully used in regenerative dentistry, since re-aggregation of human iPSC-derived mesenchymal cells and mouse dental epithelium resulted in the formation of entire teeth *ex vivo* (Takahashi and Yamanaka, 2006; Arakaki et al., 2012; Otsu et al., 2014; Mitsiadis and Harada, 2015). Although promising, this approach also needs further investigation, as effective protocols for the differentiation of human DESCs from iPSCs are not available yet.

NOVEL PLATFORMS FOR TOOTH MODELING, DRUG DISCOVERY AND DIAGNOSTICS

Use of Organoids and Organ-on-Chip Devices in Dentistry

Appropriate systems for modeling human organs and pathologies represent a constant need in all branches of biomedical research and practice, included dentistry. Animal models and two-dimensional (2D) human cell culture systems have been traditionally used for most pre-clinical studies aiming at the development of novel cell-based and pharmaceutical therapies. However, translation of preclinical results into effective treatments remains poor (Weeber et al., 2017), highlighting the need for accurate human-emulation systems (Skardal et al., 2016). In this context, great expectations are accompanying the recent developments on spheroids, organoids, microfluidics, and organ-on-chip technologies.

Spheroids and organoids are 3D culture systems, obtained by primary stem cells and tissues, which are increasingly used to model and understand tissue-specific physiology (**Figure 4**). The 3D structure of both systems allows establishment of complex cell–cell interactions and gradients of oxygen, nutrients and soluble signals that generate tissue-specific heterogeneous cell types. Organoids provide additional features compared to spheroids, as they are able of self-organization, exhibit similar architecture to the tissue of origin and exert tissue-specific complex functions (Yin et al., 2016).

Dental spheroids or dentospheres have been successfully generated from both mouse and human dental epithelial and mesenchymal (e.g., pulp and periodontium) tissues (Berahim et al., 2011; Bonnamain et al., 2011; Miquel, 2011; Natsiou et al., 2017). Epithelial dentospheres formed from mouse incisors and molars, upon modulation of their culture conditions, have either demonstrated strong stem cell capabilities or generated differentiation gradients (Natsiou et al., 2017). Human mesenchymal spheroids consistently displayed higher expression of odontoblast- and periodontal-specific differentiation markers when compared to 2D culture systems (Berahim et al., 2011; Bonnamain et al., 2011). These aspects make spheroids valuable tools for studying cytodifferentiation events in human dental tissues *in vitro*, and might be a source of stem cells for personalized dental regenerative approaches. Indeed, genetic diseases are often associated with dental anomalies (Mitsiadis and Luder, 2011; Klein et al., 2014), which could be properly modeled and investigated in patient-specific dental spheroids. Similarly, such spheroids represent novel tools for studying the behavior of definite human dental cell populations to novel materials and drugs. However, despite their incontestable advantages, it is not yet clear to what extent spheroids and organoids could faithfully represent the *in vivo* dental status. Organoids and spheroids in fact lack many features that are critical for the function of any organ, such as vasculature, innervation, mechanical cues, and immune responses (Ingber, 2016).

These limitations are the basis for the rise of microfluidic "organ-on-chip" systems. Organ-on-chips are microfluidic or nanofluidic devices composed of different chambers, where organ-specific elements such as epithelial, mesenchymal, endothelial, and neuronal cells and/or tissues are cultured (**Figure 4**; Bhatia and Ingber, 2014). Porous membranes allow the passage of molecular cues between the different chambers,

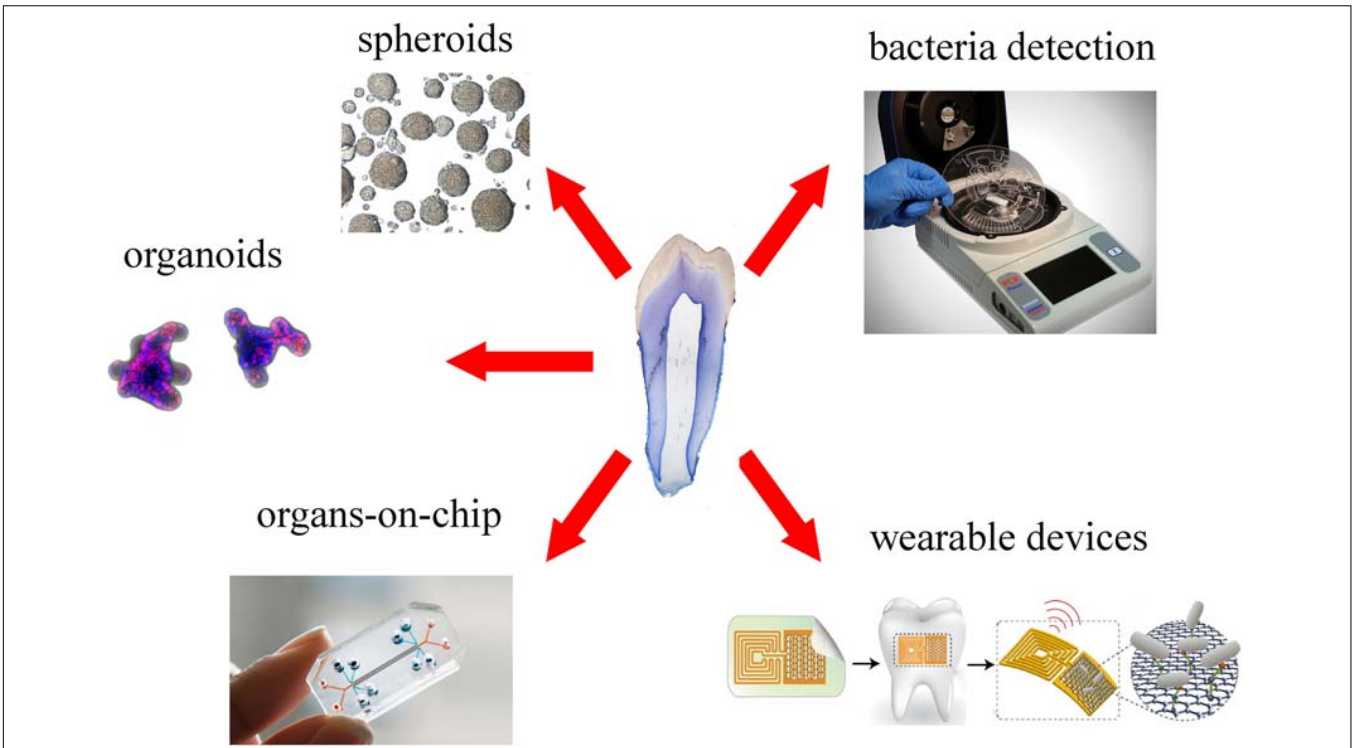

FIGURE 4 | Overview of new platforms for tooth modeling, drug discovery and diagnostics. From top right clockwise: LabDisk systems for bacteria detection (adapted from Czilwik et al., 2015) graphene-based wearable sensors (adapted from Mannoor et al., 2012), organ-on-chip (Emulate©), organoids (courtesy of Dr. T. Valenta, University of Zurich), spheroids (adapted from Natsiou et al., 2017).

while blood circulation is simulated by the regulated flow of enriched and specific media. These devices can incorporate mechanical forces to recreate physiological movements and stresses (Bhatia and Ingber, 2014), as well as electrical stimuli, allowing the modeling and analysis of complex organ-specific physiological and pathological processes. Importantly, circulating immune cells and even living microbiomes can be integrated in these devices to mimic complex organ-level responses (Bhatia and Ingber, 2014; Ingber, 2016). Microfluidic devices involving dental tissues have been used for the first time for analyzing the crosstalk of tooth germs and DMSCs with trigeminal innervation (Pagella et al., 2014, 2015). These pioneer studies have shown that microfluidics can faithfully imitate and reproduce the *in vivo* dental situation and thus reinforce the options to study dental tissues in "organ-on-chip" systems. Results obtained from these devices contribute to successfully emulate human- and patient-specific dental tissues *in vitro*. The most ambitious goal of these microfluidic devices consists in the modeling of the functional interconnection between different human organs, by the realization of so-called "bodies-on-chip." In fact, "organ-on-chip" devices can be interconnected via microfluidic tubes, which emulate systemic blood circulation. Via such emulated vasculature, molecular cues as well as immune responses can propagate to all organs, allowing the study of body-level responses to organ-specific events (Ingber, 2016). Such approach is already being used and optimized for modeling of pharmacokinetic and pharmacodynamics of systemic human drug responses (Prantil-Baun et al., 2018). With these platforms, it will be possible to study body-level responses to the various dental pathologies. While it is long known that oral diseases are strongly associated with a plethora of systemic disorders, including atherosclerosis, stoke, and systemic infections (Slavkin and Baum, 2000), the mechanisms underlying these connections and thus their therapeutic relevance are far from being understood. A human "body-on-chip" system would finally allow understanding how dental and systemic health are correlated, thus testing how the treatment of dental diseases affects general physiology.

Microfluidic devices could be also employed for the detection of both specific metabolites (Wu et al., 2017) and particular bacterial strains (Czilwik et al., 2015) that are involved in chronic diseases. Within the dental field, microfluidic devices have been used for the detection of pathogenic bacteria that lead to periodontitis and carious diseases. Recent technological developments allowed the significant shortening of this process via optimization of fully automated and integrated DNA extraction, multiplex PCR pre-amplification and species-specific real-time PCR (**Figure 4**; Chen et al., 2007; Czilwik et al., 2015). These systems allow a fast processing of samples, without loss of sensitivity and complex laboratory instrumentation.

Recent nanotechnology tools permitted the detection of single oral bacteria *in situ* via graphene-biosensors equipped with electrodes and antennae, which were printed onto enamel as "temporary-tattoos" (**Figure 4**) (Mannoor et al., 2012).

These wearable devices are thus capable of monitoring bacteria present in the mouth and more specifically on the tooth surface (Mannoor et al., 2012). The same principle has been applied very recently for detecting and identifying ingested food and liquids (Tseng et al., 2018). These mounted onto enamel nanodevices could be optimized to sense a wide variety of properties of drinks, such as alcohol content, salinity, sugars, pH, and temperature (Tseng et al., 2018). Although still in their experimental phase, such sensors represent excellent tools for the refined control and understanding of oral environment that will greatly help the field of preventive dentistry.

CONCLUDING REMARKS

The important advances in stem cells and materials sciences are driving innovative approaches in dentistry. These progresses hold a great promise for the development of efficient and personalized treatments in the near future. At the same time, optimization of sophisticated systems for the modeling and monitoring of human tissues is leading to unprecedented possibilities for the study of diseases, diagnostics, and drug testing. Although extremely exciting, most of these approaches are not yet applicable in dental clinics. Stem cell-based dental regenerative approaches still lack reliable techniques that allow controlling stem cell behavior upon transplantation. Similarly, state-of-the-art diagnostic systems still need to be validated in proper clinical settings. Nevertheless, these innovative approaches offer exciting perspectives to regenerative dentistry and might prove fundamental for the long-sought regeneration of fully functional dental tissues.

AUTHOR CONTRIBUTIONS

GO, PP, AP, and TM contributed to the writing, reading, and editing of the present review article.

FUNDING

This work was supported by institutional funds from University of Zurich.

REFERENCES

Aghaloo, T. L., and Moy, P. K. (2007). Which hard tissue augmentation techniques are the most successful in furnishing bony support for implant placement? *Int. J. Oral Maxillofac. Implants* 22(Suppl.), 49–70.

Albuquerque, M. T., Valera, M. C., Nakashima, M., Nor, J. E., and Bottino, M. C. (2014). Tissue-engineering-based strategies for regenerative endodontics. *J. Dent. Res.* 93, 1222–1231. doi: 10.1177/0022034514549809

Alvarez, P., Hee, C. K., Solchaga, L., Snel, L., Kestler, H. K., Lynch, S. E., et al. (2012). Growth factors and craniofacial surgery. *J. Craniofac. Surg.* 23, 20–29. doi: 10.1097/SCS.0b013e318240c6a8

Arakaki, M., Ishikawa, M., Nakamura, T., Iwamoto, T., Yamada, A., Fukumoto, E., et al. (2012). Role of epithelial-stem cell interactions during dental cell differentiation. *J. Biol. Chem.* 287, 10590–10601. doi: 10.1074/jbc.M111.285874

Arbab, A. S., Janic, B., Haller, J., Pawelczyk, E., Liu, W., and Frank, J. A. (2009). In vivo cellular imaging for translational medical research. *Curr. Med. Imaging Rev.* 5, 19–38. doi: 10.2174/157340509787354697

Athirasala, A., Lins, F., Tahayeri, A., Hinds, M., Smith, A. J., Sedgley, C., et al. (2017). A novel strategy to engineer pre-vascularized full-length dental pulp-like tissue constructs. *Sci. Rep.* 7:3323. doi: 10.1038/s41598-017-02532-3

Banerjee, A., Thompson, I. D., and Watson, T. F. (2011). Minimally invasive caries removal using bio-active glass air-abrasion. *J. Dent.* 39, 2–7. doi: 10.1016/j.jdent.2010.09.004

Barbucci, R., Pasqui, D., Wirsen, A., Affrossman, S., Curtis, A., and Tetta, C. (2003). Micro and nano-structured surfaces. *J. Mater. Sci. Mater. Med.* 14, 721–725. doi: 10.1023/A:1024919917969

Berahim, Z., Moharamzadeh, K., Rawlinson, A., and Jowett, A. K. (2011). Biologic interaction of three-dimensional periodontal fibroblast spheroids with collagen-based and synthetic membranes. *J. Periodontol.* 82, 790–797. doi: 10.1902/jop.2010.100533

Beuer, F., Schweiger, J., and Edelhoff, D. (2008). Digital dentistry: an overview of recent developments for CAD/CAM generated restorations. *Br. Dent. J.* 204, 505–511. doi: 10.1038/sj.bdj.2008.350

Bezerra, F., Ferreira, M. R., Fontes, G. N., Da Costa Fernandes, C. J., Andia, D. C., Cruz, N. C., et al. (2017). Nano hydroxyapatite-blasted titanium surface affects pre-osteoblast morphology by modulating critical intracellular pathways. *Biotechnol. Bioeng.* 114, 1888–1898. doi: 10.1002/bit.26310

Bhatia, S. N., and Ingber, D. E. (2014). Microfluidic organs-on-chips. *Nat. Biotechnol.* 32, 760–772. doi: 10.1038/nbt.2989

Bluteau, G., Luder, H. U., De Bari, C., and Mitsiadis, T. A. (2008). Stem cells for tooth engineering. *Eur. Cell Mater.* 16, 1–9. doi: 10.22203/eCM.v016a01

Bonifacio, M. A., Cometa, S., Dicarlo, M., Baruzzi, F., De Candia, S., Gloria, A., et al. (2017). Gallium-modified chitosan/poly(acrylic acid) bilayer coatings for improved titanium implant performances. *Carbohydr. Polym.* 166, 348–357. doi: 10.1016/j.carbpol.2017.03.009

Bonnamain, V., Neveu, I., and Naveilhan, P. (2011). In vitro analyses of the immunosuppressive properties of neural stem/progenitor cells using anti-CD3/CD28-activated T cells. *Methods Mol. Biol.* 677, 233–243. doi: 10.1007/978-1-60761-869-0_17

Boyde, A. (1997). Microstructure of enamel. *Ciba Found. Symp.* 205, 18–27; discussion 27–31.

Breschi, L., Maravic, T., Cunha, S. R., Comba, A., Cadenaro, M., Tjaderhane, L., et al. (2018). Dentin bonding systems: from dentin collagen structure to bond preservation and clinical applications. *Dent. Mater.* 34, 78–96. doi: 10.1016/j.dental.2017.11.005

Cantu, C., Pagella, P., Shajiei, T. D., Zimmerli, D., Valenta, T., Hausmann, G., et al. (2017). A cytoplasmic role of Wnt/beta-catenin transcriptional cofactors Bcl9, Bcl9l, and Pygopus in tooth enamel formation. *Sci. Signal.* 10:eaah4598. doi: 10.1126/scisignal.aah4598

Carroll, J. D., Milward, M. R., Cooper, P. R., Hadis, M., and Palin, W. M. (2014). Developments in low level light therapy (LLLT) for dentistry. *Dent. Mater.* 30, 465–475. doi: 10.1016/j.dental.2014.02.006

Caton, J., Bostanci, N., Remboutsika, E., De Bari, C., and Mitsiadis, T. A. (2011). Future dentistry: cell therapy meets tooth and periodontal repair and regeneration. *J. Cell Mol. Med.* 15, 1054–1065. doi: 10.1111/j.1582-4934.2010.01251.x

Chen, Z., Mauk, M. G., Wang, J., Abrams, W. R., Corstjens, P. L., Niedbala, R. S., et al. (2007). A microfluidic system for saliva-based detection of infectious diseases. *Ann. N. Y. Acad. Sci.* 1098, 429–436. doi: 10.1196/annals.1384.024

Clark, D., Rajendran, Y., Paydar, S., Ho, S., Cox, D., Ryder, M., et al. (2018). Advanced platelet-rich fibrin and freeze-dried bone allograft for ridge preservation: a randomized controlled clinical trial. *J. Periodontol.* 89, 379–387. doi: 10.1002/JPER.17-0466

Coelho, P. G., Zavanelli, R. A., Salles, M. B., Yeniyol, S., Tovar, N., and Jimbo, R. (2016). Enhanced bone bonding to nanotextured implant surfaces at a short healing period: a biomechanical tensile testing in the rat femur. *Implant Dent.* 25, 322–327. doi: 10.1097/ID.0000000000000436

Czilwik, G., Messinger, T., Strohmeier, O., Wadle, S., Von Stetten, F., Paust, N., et al. (2015). Rapid and fully automated bacterial pathogen detection on a centrifugal-microfluidic LabDisk using highly sensitive nested PCR with integrated sample preparation. *Lab Chip* 15, 3749–3759. doi: 10.1039/c5lc00591d

Danesh-Sani, S. A., Loomer, P. M., and Wallace, S. S. (2016). A comprehensive clinical review of maxillary sinus floor elevation: anatomy, techniques, biomaterials and complications. *Br. J. Oral Maxillofac. Surg.* 54, 724–730. doi: 10.1016/j.bjoms.2016.05.008

De Angelis, N., Felice, P., Pellegrino, G., Camurati, A., Gambino, P., and Esposito, M. (2011). Guided bone regeneration with and without a bone substitute at single post-extractive implants: 1-year post-loading results from a pragmatic multicentre randomised controlled trial. *Eur. J. Oral Implantol.* 4, 313–325.

Del Fabbro, M., Taschieri, S., Lodi, G., Banfi, G., and Weinstein, R. L. (2015). Magnification devices for endodontic therapy. *Cochrane Database Syst. Rev.* 8:CD005969. doi: 10.1002/14651858.CD005969.pub3

DeRosa, T. A. (2006). A retrospective evaluation of pulpotomy as an alternative to extraction. *Gen. Dent.* 54, 37–40.

Dhillon, R. S., Schwarz, E. M., and Maloney, M. D. (2012). Platelet-rich plasma therapy - future or trend? *Arthritis Res. Ther.* 14:219. doi: 10.1186/ar3914

Diogenes, A., and Hargreaves, K. M. (2017). Microbial modulation of stem cells and future directions in regenerative endodontics. *J. Endod.* 43, S95–S101. doi: 10.1016/j.joen.2017.07.012

Diogenes, A., and Ruparel, N. B. (2017). Regenerative endodontic procedures: clinical outcomes. *Dent. Clin. North Am.* 61, 111–125. doi: 10.1016/j.cden.2016.08.004

Esposito, M., Ardebili, Y., and Worthington, H. V. (2014). Interventions for replacing missing teeth: different types of dental implants. *Cochrane Database Syst. Rev.* 7:CD003815. doi: 10.1002/14651858.CD003815.pub4

Fernandes, G., Wang, C., Yuan, X., Liu, Z., Dziak, R., and Yang, S. (2016). Combination of controlled release platelet-rich plasma alginate beads and bone morphogenetic protein-2 genetically modified mesenchymal stem cells for bone regeneration. *J. Periodontol.* 87, 470–480. doi: 10.1902/jop.2016.150487

Fernandes, G., and Yang, S. (2016). Application of platelet-rich plasma with stem cells in bone and periodontal tissue engineering. *Bone Res.* 4:16036. doi: 10.1038/boneres.2016.36

Fioretti, F., Mendoza-Palomares, C., Avoaka-Boni, M. C., Ramaroson, J., Bahi, S., Richert, L., et al. (2011). Nano-odontology: nanostructured assemblies for endodontic regeneration. *J. Biomed. Nanotechnol.* 7, 471–475. doi: 10.1166/jbn.2011.1312

Gera, A., Steinberg, G. K., and Guzman, R. (2010). In vivo neural stem cell imaging: current modalities and future directions. *Regen. Med.* 5, 73–86. doi: 10.2217/rme.09.79

Godoy-Gallardo, M., Manzanares-Cespedes, M. C., Sevilla, P., Nart, J., Manzanares, N., Manero, J. M., et al. (2016). Evaluation of bone loss in antibacterial coated dental implants: an experimental study in dogs. *Mater. Sci. Eng. C Mater. Biol. Appl.* 69, 538–545. doi: 10.1016/j.msec.2016.07.020

Goracci, C., Cadenaro, M., Fontanive, L., Giangrosso, G., Juloski, J., Vichi, A., et al. (2014). Polymerization efficiency and flexural strength of low-stress restorative composites. *Dent. Mater.* 30, 688–694. doi: 10.1016/j.dental.2014.03.006

Gronthos, S., Brahim, J., Li, W., Fisher, L. W., Cherman, N., Boyde, A., et al. (2002). Stem cell properties of human dental pulp stem cells. *J. Dent. Res.* 81, 531–535. doi: 10.1177/154405910208100806

Gronthos, S., Mankani, M., Brahim, J., Robey, P. G., and Shi, S. (2000). Postnatal human dental pulp stem cells (DPSCs) in vitro and in vivo. *Proc. Natl. Acad. Sci. U.S.A.* 97, 13625–13630. doi: 10.1073/pnas.240309797

Guazzato, M., Albakry, M., Ringer, S. P., and Swain, M. V. (2004). Strength, fracture toughness and microstructure of a selection of all-ceramic materials. Part II. Zirconia-based dental ceramics. *Dent. Mater.* 20, 449–456. doi: 10.1016/j.dental.2003.05.002

Hammerle, C. H., Stone, P., Jung, R. E., Kapos, T., and Brodala, N. (2009). Consensus statements and recommended clinical procedures regarding computer-assisted implant dentistry. *Int. J. Oral Maxillofac. Implants* 24(Suppl.), 126–131.

Hancocks, S. (2017). What is digital about dentistry? *Br. Dent. J.* 223:305. doi: 10.1038/sj.bdj.2017.732

Hayashi, Y., Murakami, M., Kawamura, R., Ishizaka, R., Fukuta, O., and Nakashima, M. (2015). CXCL14 and MCP1 are potent trophic factors associated with cell migration and angiogenesis leading to higher regenerative potential of dental pulp side population cells. *Stem Cell Res. Ther.* 6:111. doi: 10.1186/s13287-015-0088-z

Heo, D. N., Ko, W. K., Lee, H. R., Lee, S. J., Lee, D., Um, S. H., et al. (2016). Titanium dental implants surface-immobilized with gold nanoparticles as osteoinductive agents for rapid osseointegration. *J. Colloid Interface Sci.* 469, 129–137. doi: 10.1016/j.jcis.2016.02.022

Howell, T. H., Fiorellini, J. P., Paquette, D. W., Offenbacher, S., Giannobile, W. V., and Lynch, S. E. (1997). A phase I/II clinical trial to evaluate a combination of recombinant human platelet-derived growth factor-BB and recombinant human insulin-like growth factor-I in patients with periodontal disease. *J. Periodontol.* 68, 1186–1193. doi: 10.1902/jop.1997.68.12.1186

Ilie, N., Kessler, A., and Durner, J. (2013). Influence of various irradiation processes on the mechanical properties and polymerisation kinetics of bulk-fill resin based composites. *J. Dent.* 41, 695–702. doi: 10.1016/j.jdent.2013.05.008

Ingber, D. E. (2016). Reverse engineering human pathophysiology with organs-on-chips. *Cell* 164, 1105–1109. doi: 10.1016/j.cell.2016.02.049

Iwatsuki, S., Honda, M. J., Harada, H., and Ueda, M. (2006). Cell proliferation in teeth reconstructed from dispersed cells of embryonic tooth germs in a three-dimensional scaffold. *Eur. J. Oral Sci.* 114, 310–317. doi: 10.1111/j.1600-0722.2006.00385.x

Jimenez-Rojo, L., Granchi, Z., Graf, D., and Mitsiadis, T. A. (2012). Stem cell fate determination during development and regeneration of ectodermal organs. *Front. Physiol.* 3:107. doi: 10.3389/fphys.2012.00107

Kaigler, D., Avila-Ortiz, G., Travan, S., Taut, A. D., Padial-Molina, M., Rudek, I., et al. (2015). Bone engineering of maxillary sinus bone deficiencies using enriched $CD90^+$ stem cell therapy: a randomized clinical trial. *J. Bone Miner. Res.* 30, 1206–1216. doi: 10.1002/jbmr.2464

Kaigler, D., Pagni, G., Park, C. H., Braun, T. M., Holman, L. A., Yi, E., et al. (2013). Stem cell therapy for craniofacial bone regeneration: a randomized, controlled feasibility trial. *Cell Transplant.* 22, 767–777. doi: 10.3727/096368912X652968

Kathuria, V., Dhillon, J. K., and Kalra, G. (2015). Low level laser therapy: a panacea for oral maladies. *Laser Ther.* 24, 215–223. doi: 10.5978/islsm.15-RA-01

Kilambi, H., Cramer, N. B., Schneidewind, L. H., Shah, P., Stansbury, J. W., and Bowman, C. N. (2009). Evaluation of highly reactive mono-methacrylates as reactive diluents for BisGMA-based dental composites. *Dent. Mater.* 25, 33–38. doi: 10.1016/j.dental.2008.05.003

Klein, C., Le Goff, C., Topouchian, V., Odent, S., Violas, P., Glorion, C., et al. (2014). Orthopedics management of acromicric dysplasia: follow up of nine patients. *Am. J. Med. Genet. A* 164A, 331–337. doi: 10.1002/ajmg.a.36139

Larsson, L., Decker, A. M., Nibali, L., Pilipchuk, S. P., Berglundh, T., and Giannobile, W. V. (2016). Regenerative medicine for periodontal and peri-implant diseases. *J. Dent. Res.* 95, 255–266. doi: 10.1177/0022034515618887

Lelli, M., Putignano, A., Marchetti, M., Foltran, I., Mangani, F., Procaccini, M., et al. (2014). Remineralization and repair of enamel surface by biomimetic Zn-carbonate hydroxyapatite containing toothpaste: a comparative in vivo study. *Front. Physiol.* 5:333. doi: 10.3389/fphys.2014.00333

Levato, C. M., Farman, A. G., and Miles, D. A. (2015). The "inevitability" of digital radiography in dentistry. *Compend. Contin. Educ. Dent.* 36, 238–240.

Lindhe, J., Haffajee, A. D., and Socransky, S. S. (1983). Progression of periodontal disease in adult subjects in the absence of periodontal therapy. *J. Clin. Periodontol.* 10, 433–442. doi: 10.1111/j.1600-051X.1983.tb01292.x

Luiz De Oliveira Da Rosa, W., Machado Da Silva, T., Fernando Demarco, F., Piva, E., and Fernandes Da Silva, A. (2017). Could the application of bioactive molecules improve vital pulp therapy success? A systematic review. *J. Biomed. Mater. Res. A* 105, 941–956. doi: 10.1002/jbm.a.35968

Lynch, C. (2017). Defining digital dentistry: a survey of recent literature. *J. Dent.* 59:1. doi: 10.1016/j.jdent.2017.01.005

Lynch, S. E. (1992). Methods for evaluation of regenerative procedures. *J. Periodontol.* 63, 1085–1092. doi: 10.1902/jop.1992.63.12s.1085

Lynch, S. E., Buser, D., Hernandez, R. A., Weber, H. P., Stich, H., Fox, C. H., et al. (1991a). Effects of the platelet-derived growth factor/insulin-like growth factor-I combination on bone regeneration around titanium dental implants. Results of a pilot study in beagle dogs. *J. Periodontol.* 62, 710–716.

Lynch, S. E., De Castilla, G. R., Williams, R. C., Kiritsy, C. P., Howell, T. H., Reddy, M. S., et al. (1991b). The effects of short-term application of a combination of platelet-derived and insulin-like growth factors on periodontal wound healing. *J. Periodontol.* 62, 458–467.

Lynch, S. E., Williams, R. C., Polson, A. M., Howell, T. H., Reddy, M. S., Zappa, U. E., et al. (1989). A combination of platelet-derived and insulin-like growth

factors enhances periodontal regeneration. *J. Clin. Periodontol.* 16, 545–548. doi: 10.1111/j.1600-051X.1989.tb02334.x

Mannoor, M. S., Tao, H., Clayton, J. D., Sengupta, A., Kaplan, D. L., Naik, R. R., et al. (2012). Graphene-based wireless bacteria detection on tooth enamel. *Nat. Commun.* 3:763. doi: 10.1038/ncomms1767

Mazzoni, A., Angeloni, V., Comba, A., Maravic, T., Cadenaro, M., Tezvergil-Mutluay, A., et al. (2018). Cross-linking effect on dentin bond strength and MMPs activity. *Dent. Mater.* 34, 288–295. doi: 10.1016/j.dental.2017.11.009

Mendonca, G., Mendonca, D. B., Aragao, F. J., and Cooper, L. F. (2008). Advancing dental implant surface technology–from micron- to nanotopography. *Biomaterials* 29, 3822–3835. doi: 10.1016/j.biomaterials.2008.05.012

Miquel, A. (2011). In the 11- M terrorist tragedy in Madrid. *Rev. Clin. Esp.* 211, 158–162. doi: 10.1016/j.rce.2010.11.012

Miron, R. J., Chandad, F., Buser, D., Sculean, A., Cochran, D. L., and Zhang, Y. (2016a). Effect of enamel matrix derivative liquid on osteoblast and periodontal ligament cell proliferation and differentiation. *J. Periodontol.* 87, 91–99. doi: 10.1902/jop.2015.150389

Miron, R. J., Sculean, A., Cochran, D. L., Froum, S., Zucchelli, G., Nemcovsky, C., et al. (2016b). Twenty years of enamel matrix derivative: the past, the present and the future. *J. Clin. Periodontol.* 43, 668–683. doi: 10.1111/jcpe.12546

Miron, R. J., Zucchelli, G., Pikos, M. A., Salama, M., Lee, S., Guillemette, V., et al. (2017). Use of platelet-rich fibrin in regenerative dentistry: a systematic review. *Clin. Oral Investig* 21, 1913–1927. doi: 10.1007/s00784-017-2133-z

Mitsiadis, T. A., and Graf, D. (2009). Cell fate determination during tooth development and regeneration. *Birth Defects Res. C Embryo Today* 87, 199–211. doi: 10.1002/bdrc.20160

Mitsiadis, T. A., and Harada, H. (2015). Regenerated teeth: the future of tooth replacement. *Regen. Med.* 10, 5–8. doi: 10.2217/rme.14.78

Mitsiadis, T. A., and Luder, H. U. (2011). Genetic basis for tooth malformations: from mice to men and back again. *Clin. Genet.* 80, 319–329. doi: 10.1111/j.1399-0004.2011.01762.x

Mitsiadis, T. A., Orsini, G., and Jimenez-Rojo, L. (2015). Stem cell-based approaches in dentistry. *Eur. Cell Mater.* 30, 248–257. doi: 10.22203/eCM.v030a17

Mitsiadis, T. A., and Papagerakis, P. (2011). Regenerated teeth: the future of tooth replacement? *Regen. Med.* 6, 135–139. doi: 10.2217/rme.10.101

Mitsiadis, T. A., Woloszyk, A., and Jimenez-Rojo, L. (2012). Nanodentistry: combining nanostructured materials and stem cells for dental tissue regeneration. *Nanomedicine* 7, 1743–1753. doi: 10.2217/nnm.12.146

Miura, M., Gronthos, S., Zhao, M., Lu, B., Fisher, L. W., Robey, P. G., et al. (2003). SHED: stem cells from human exfoliated deciduous teeth. *Proc. Natl. Acad. Sci. U.S.A.* 100, 5807–5812. doi: 10.1073/pnas.0937635100

Monterubbianesi, R., Orsini, G., Tosi, G., Conti, C., Librando, V., Procaccini, M., et al. (2016). Spectroscopic and mechanical properties of a new generation of bulk fill composites. *Front. Physiol.* 7:652. doi: 10.3389/fphys.2016.00652

Murray, P. E., and Garcia-Godoy, F. (2006). The outlook for implants and endodontics: a review of the tissue engineering strategies to create replacement teeth for patients. *Dent. Clin. North Am.* 50, 299–315, x. doi: 10.1016/j.cden.2005.11.009

Nakashima, M., and Iohara, K. (2017). Recent progress in translation from bench to a pilot clinical study on total pulp regeneration. *J. Endod.* 43, S82–S86. doi: 10.1016/j.joen.2017.06.014

Nakashima, M., Iohara, K., Murakami, M., Nakamura, H., Sato, Y., Ariji, Y., et al. (2017). Pulp regeneration by transplantation of dental pulp stem cells in pulpitis: a pilot clinical study. *Stem Cell Res. Ther.* 8:61. doi: 10.1186/s13287-017-0506-5

Natsiou, D., Granchi, Z., Mitsiadis, T. A., and Jimenez-Rojo, L. (2017). Generation of spheres from dental epithelial stem cells. *Front. Physiol.* 8:7. doi: 10.3389/fphys.2017.00007

Orsini, G., Jimenez-Rojo, L., Natsiou, D., Putignano, A., and Mitsiadis, T. A. (2015). In vivo administration of dental epithelial stem cells at the apical end of the mouse incisor. *Front. Physiol.* 6:112. doi: 10.3389/fphys.2015.00112

Orsini, G., Procaccini, M., Manzoli, L., Sparabombe, S., Tiriduzzi, P., Bambini, F., et al. (2013). A 3-day randomized clinical trial to investigate the desensitizing properties of three dentifrices. *J. Periodontol.* 84, e65–e73. doi: 10.1902/jop.2013.120697

Oshima, M., and Tsuji, T. (2014). Functional tooth regenerative therapy: tooth tissue regeneration and whole-tooth replacement. *Odontology* 102, 123–136. doi: 10.1007/s10266-014-0168-z

Otsu, K., Kumakami-Sakano, M., Fujiwara, N., Kikuchi, K., Keller, L., Lesot, H., et al. (2014). Stem cell sources for tooth regeneration: current status and future prospects. *Front. Physiol.* 5:36. doi: 10.3389/fphys.2014.00036

Ozcan, M., and Jonasch, M. (2018). Effect of cyclic fatigue tests on aging and their translational implications for survival of all-ceramic tooth-borne single crowns and fixed dental prostheses. *J. Prosthodont.* 27, 364–375. doi: 10.1111/jopr.12566

Pagella, P., Miran, S., and Mitsiadis, T. (2015). Analysis of developing tooth germ innervation using microfluidic co-culture devices. *J. Vis. Exp.* 102:e53114. doi: 10.3791/53114

Pagella, P., Neto, E., Jimenez-Rojo, L., Lamghari, M., and Mitsiadis, T. A. (2014). Microfluidics co-culture systems for studying tooth innervation. *Front. Physiol.* 5:326. doi: 10.3389/fphys.2014.00326

Papagerakis, P., and Mitsiadis, T. (2013). *Development and Structure of Teeth and Periodontal Tissues*. Hoboken, NJ: John Wiley & Sons, Inc. doi: 10.1002/9781118453926.ch109

Pilipchuk, S. P., Monje, A., Jiao, Y., Hao, J., Kruger, L., Flanagan, C. L., et al. (2016). Integration of 3D printed and micropatterned polycaprolactone scaffolds for guidance of oriented collagenous tissue formation in vivo. *Adv. Healthc. Mater.* 5, 676–687. doi: 10.1002/adhm.201500758

Pilipchuk, S. P., Plonka, A. B., Monje, A., Taut, A. D., Lanis, A., Kang, B., et al. (2015). Tissue engineering for bone regeneration and osseointegration in the oral cavity. *Dent. Mater.* 31, 317–338. doi: 10.1016/j.dental.2015.01.006

Piva, E., Silva, A. F., and Nor, J. E. (2014). Functionalized scaffolds to control dental pulp stem cell fate. *J. Endod.* 40, S33–S40. doi: 10.1016/j.joen.2014.01.013

Pokrowiecki, R., Zareba, T., Szaraniec, B., Palka, K., Mielczarek, A., Menaszek, E., et al. (2017). In vitro studies of nanosilver-doped titanium implants for oral and maxillofacial surgery. *Int. J. Nanomedicine* 12, 4285–4297. doi: 10.2147/IJN.S131163

Prantil-Baun, R., Novak, R., Das, D., Somayaji, M. R., Przekwas, A., and Ingber, D. E. (2018). Physiologically based pharmacokinetic and pharmacodynamic analysis enabled by microfluidically linked organs-on-chips. *Annu. Rev. Pharmacol. Toxicol.* 58, 37–64. doi: 10.1146/annurev-pharmtox-010716-104748

Rickert, D., Sauerbier, S., Nagursky, H., Menne, D., Vissink, A., and Raghoebar, G. M. (2011). Maxillary sinus floor elevation with bovine bone mineral combined with either autogenous bone or autogenous stem cells: a prospective randomized clinical trial. *Clin. Oral Implants Res.* 22, 251–258. doi: 10.1111/j.1600-0501.2010.01981.x

Sauerbier, S., Rickert, D., Gutwald, R., Nagursky, H., Oshima, T., Xavier, S. P., et al. (2011). Bone marrow concentrate and bovine bone mineral for sinus floor augmentation: a controlled, randomized, single-blinded clinical and histological trial–per-protocol analysis. *Tissue Eng. Part A* 17, 2187–2197. doi: 10.1089/ten.TEA.2010.0516

Scarano, A., Degidi, M., Iezzi, G., Pecora, G., Piattelli, M., Orsini, G., et al. (2006). Maxillary sinus augmentation with different biomaterials: a comparative histologic and histomorphometric study in man. *Implant Dent.* 15, 197–207. doi: 10.1097/01.id.0000220120.54308.f3

Selvig, K. A., Sorensen, R. G., Wozney, J. M., and Wikesjo, U. M. (2002). Bone repair following recombinant human bone morphogenetic protein-2 stimulated periodontal regeneration. *J. Periodontol.* 73, 1020–1029. doi: 10.1902/jop.2002.73.9.1020

Seo, B. M., Miura, M., Gronthos, S., Bartold, P. M., Batouli, S., Brahim, J., et al. (2004). Investigation of multipotent postnatal stem cells from human periodontal ligament. *Lancet* 364, 149–155. doi: 10.1016/S0140-6736(04)16627-0

Sheikh, Z., Hamdan, N., Ikeda, Y., Grynpas, M., Ganss, B., and Glogauer, M. (2017). Natural graft tissues and synthetic biomaterials for periodontal and alveolar bone reconstructive applications: a review. *Biomater. Res.* 21:9. doi: 10.1186/s40824-017-0095-5

Shinmura, Y., Tsuchiya, S., Hata, K., and Honda, M. J. (2008). Quiescent epithelial cell rests of Malassez can differentiate into ameloblast-like cells. *J. Cell. Physiol.* 217, 728–738. doi: 10.1002/jcp.21546

Singh, P. (2011). Understanding peri-implantitis: a strategic review. *J. Oral Implantol.* 37, 622–626. doi: 10.1563/AAID-JOI-D-10-00134

Skardal, A., Shupe, T., and Atala, A. (2016). Organoid-on-a-chip and body-on-a-chip systems for drug screening and disease modeling. *Drug Discov. Today* 21, 1399–1411. doi: 10.1016/j.drudis.2016.07.003

Slavkin, H. C., and Baum, B. J. (2000). Relationship of dental and oral pathology to systemic illness. *JAMA* 284, 1215–1217. doi: 10.1001/jama.284.10.1215

Song, J. S., Takimoto, K., Jeon, M., Vadakekalam, J., Ruparel, N. B., and Diogenes, A. (2017). Decellularized human dental pulp as a scaffold for regenerative endodontics. *J. Dent. Res.* 96, 640–646. doi: 10.1177/0022034517693606

Takahashi, K., and Yamanaka, S. (2006). Induction of pluripotent stem cells from mouse embryonic and adult fibroblast cultures by defined factors. *Cell* 126, 663–676. doi: 10.1016/j.cell.2006.07.024

Torabinejad, M., and Faras, H. (2012). A clinical and histological report of a tooth with an open apex treated with regenerative endodontics using platelet-rich plasma. *J. Endod.* 38, 864–868. doi: 10.1016/j.joen.2012.03.006

Tseng, P., Napier, B., Garbarini, L., Kaplan, D. L., and Omenetto, F. G. (2018). Functional, RF-trilayer sensors for tooth-mounted, wireless monitoring of the oral cavity and food consumption. *Adv. Mater.* 30:e1703257. doi: 10.1002/adma.201703257

Variola, F., Brunski, J. B., Orsini, G., Tambasco De Oliveira, P., Wazen, R., and Nanci, A. (2011). Nanoscale surface modifications of medically relevant metals: state-of-the art and perspectives. *Nanoscale* 3, 335–353. doi: 10.1039/c0nr00485e

Variola, F., Vetrone, F., Richert, L., Jedrzejowski, P., Yi, J.-H., Zalzal, S., et al. (2009). Improving biocompatibility of implantable metals by nanoscale modification of surfaces: an overview of strategies, fabrication methods, and challenges. *Small* 5, 996–1006. doi: 10.1002/smll.200801186

Volponi, A. A., Pang, Y., and Sharpe, P. T. (2010). Stem cell-based biological tooth repair and regeneration. *Trends Cell Biol.* 20, 715–722. doi: 10.1016/j.tcb.2010.09.012

Washio, K., Iwata, T., Mizutani, M., Ando, T., Yamato, M., Okano, T., et al. (2010). Assessment of cell sheets derived from human periodontal ligament cells: a pre-clinical study. *Cell Tissue Res.* 341, 397–404. doi: 10.1007/s00441-010-1009-1

Weeber, F., Ooft, S. N., Dijkstra, K. K., and Voest, E. E. (2017). Tumor organoids as a pre-clinical cancer model for drug discovery. *Cell Chem. Biol.* 24, 1092–1100. doi: 10.1016/j.chembiol.2017.06.012

Wittneben, J. G., Gavric, J., Belser, U. C., Bornstein, M. M., Joda, T., Chappuis, V., et al. (2017). Esthetic and clinical performance of implant-supported all-ceramic crowns made with prefabricated or CAD/CAM zirconia abutments: a randomized, multicenter clinical trial. *J. Dent. Res.* 96, 163–170. doi: 10.1177/0022034516681767

Wu, J., Dong, M., Santos, S., Rigatto, C., Liu, Y., and Lin, F. (2017). Lab-on-a-chip platforms for detection of cardiovascular disease and cancer biomarkers. *Sensors* 17:E2934. doi: 10.3390/s17122934

Yamauchi, N., Yamauchi, S., Nagaoka, H., Duggan, D., Zhong, S., Lee, S. M., et al. (2011). Tissue engineering strategies for immature teeth with apical periodontitis. *J. Endod.* 37, 390–397. doi: 10.1016/j.joen.2010.11.010

Yang, B., Chen, G., Li, J., Zou, Q., Xie, D., Chen, Y., et al. (2012). Tooth root regeneration using dental follicle cell sheets in combination with a dentin matrix - based scaffold. *Biomaterials* 33, 2449–2461. doi: 10.1016/j.biomaterials.2011.11.074

Yang, W. F., Choi, W. S., Leung, Y. Y., Curtin, J. P., Du, R., Zhang, C. Y., et al. (2018). Three-dimensional printing of patient-specific surgical plates in head and neck reconstruction: a prospective pilot study. *Oral Oncol.* 78, 31–36. doi: 10.1016/j.oraloncology.2018.01.005

Yin, X., Mead, B. E., Safaee, H., Langer, R., Karp, J. M., and Levy, O. (2016). Engineering stem cell organoids. *Cell Stem Cell* 18, 25–38. doi: 10.1016/j.stem.2015.12.005

Yu, J., Xu, L., Li, K., Xie, N., Xi, Y., Wang, Y., et al. (2017). Zinc-modified calcium silicate coatings promote osteogenic differentiation through TGF-beta/Smad pathway and osseointegration in osteopenic rabbits. *Sci. Rep.* 7:3440. doi: 10.1038/s41598-017-03661-5

Zhang, F., Chevalier, J., Olagnon, C., Batuk, M., Hadermann, J., Van Meerbeek, B., et al. (2017). Grain-boundary engineering for aging and slow-crack-growth resistant zirconia. *J. Dent. Res.* 96, 774–779. doi: 10.1177/0022034517698661

Zhou, W., Liu, Z., Song, L., Kuo, C. L., and Shafer, D. M. (2018). Clinical factors affecting the accuracy of guided implant surgery-a systematic review and meta-analysis. *J. Evid. Based Dent. Pract.* 18, 28–40. doi: 10.1016/j.jebdp.2017.07.007

Conflict of Interest Statement: The authors declare that the research was conducted in the absence of any commercial or financial relationships that could be construed as a potential conflict of interest.

Advantages of publishing in Frontiers

OPEN ACCESS
Articles are free to read for greatest visibility and readership

FAST PUBLICATION
Around 90 days from submission to decision

HIGH QUALITY PEER-REVIEW
Rigorous, collaborative, and constructive peer-review

TRANSPARENT PEER-REVIEW
Editors and reviewers acknowledged by name on published articles

Frontiers
Avenue du Tribunal-Fédéral 34
1005 Lausanne | Switzerland

Visit us: www.frontiersin.org
Contact us: info@frontiersin.org | +41 21 510 17 00

REPRODUCIBILITY OF RESEARCH
Support open data and methods to enhance research reproducibility

DIGITAL PUBLISHING
Articles designed for optimal readership across devices

FOLLOW US
@frontiersin

IMPACT METRICS
Advanced article metrics track visibility across digital media

EXTENSIVE PROMOTION
Marketing and promotion of impactful research

LOOP RESEARCH NETWORK
Our network increases your article's readership